

Branes and Supersymmetric Quantum Field Theories

Thesis by
Chan Youn Park

In Partial Fulfillment of the Requirements
for the Degree of
Doctor of Philosophy



California Institute of Technology
Pasadena, California

2014
(Defended November 19, 2013)

© 2014

Chan Youn Park

All Rights Reserved

Acknowledgments

First of all I want to express my gratitude to my advisor, John H. Schwarz, without whose guidance I would not have been able to pursue my graduate study. I also thank Sergei Gukov for advice and support during the earlier part of my doctoral study; Anton Kapustin for the reading courses I had when I started my study at Caltech; Frank Porter for helping me with getting TA positions; and Hirosi Ooguri for his help in several occasions during my study. And I thank them for being on my candidacy and defense committees.

I was indebted to my collaborators for their help during our projects. Yuji Tachikawa gave me advice not only about physics, but also about how to do physics. Kentaro Hori showed me the importance of both insight and rigor in doing physics. I thank both of them for their generous supports for my visits to Japan. I learned a lot from and had great fun working with Kazunobu Maruyoshi and Wenbin Yan.

I also thank many people I met on my travels. Andy Neitzke and Sungjay Lee shared their time to listen to me, as well as to read my drafts carefully and give precious comments. Keshav Dasgupta and Jihye Seo invited me to wonderful opportunities at McGill and supported my visits. Kimyeong Lee, Dongmin Gang, Eunkyung Koh, and Piljin Yi hosted my visits to KIAS and gave me opportunities to present my work there. It was great meeting Jungmin Kim, Sungjoon Park, Rakkyeoung Seong, and Peng Zhao during the travels and have a good time with them.

It was my pleasure meeting wonderful members and alumni of Caltech string theory group, including Tudor Dimofte, Abhijit Gadde, Lotte Hollands, Heejoong Jung, Christoph Keller, Stefan Leichenauer, Arthur Lipstein, Yu Nakayama, Tadashi Okazaki, Pavel Putrov, Sakura Schafer-Nameki, Piotr Sulkowski, Jaroslav Trnka, and Masahito Yamazaki. I especially thank Changsoon Park and Jaewon Song for giving me advice inside and outside physics as seniors. I also thank Carol Silverstein for her great help on many occasions.

I am grateful to Sangmin Lee, my undergraduate advisor, for his guidance throughout

my study. I thank Minseok Jang for being a wonderful roommate and friend. I also thank my family for their endless support from the beginning.

Most of all, my deepest gratitude goes to my beloved wife Heajin, who made everything possible and nothing impossible.

Abstract

Since the discovery of D-branes as non-perturbative, dynamic objects in string theory, various configurations of branes in type IIA/B string theory and M-theory have been considered to study their low-energy dynamics described by supersymmetric quantum field theories.

One example of such a construction is based on the description of Seiberg-Witten curves of four-dimensional $\mathcal{N} = 2$ supersymmetric gauge theories as branes in type IIA string theory and M-theory. This enables us to study the gauge theories in strongly-coupled regimes. Spectral networks are another tool for utilizing branes to study non-perturbative regimes of two- and four-dimensional supersymmetric theories. Using spectral networks of a Seiberg-Witten theory we can find its BPS spectrum, which is protected from quantum corrections by supersymmetry, and also the BPS spectrum of a related two-dimensional $\mathcal{N} = (2, 2)$ theory whose (twisted) superpotential is determined by the Seiberg-Witten curve. When we don't know the perturbative description of such a theory, its spectrum obtained via spectral networks is a useful piece of information. In this thesis we illustrate these ideas with examples of the use of Seiberg-Witten curves and spectral networks to understand various two- and four-dimensional supersymmetric theories.

First, we examine how the geometry of a Seiberg-Witten curve serves as a useful tool for identifying various limits of the parameters of the Seiberg-Witten theory, including Argyres-Seiberg duality and Argyres-Douglas fixed points. Next, we consider the low-energy limit of a two-dimensional $\mathcal{N} = (2, 2)$ supersymmetric theory from an M-theory brane configuration whose (twisted) superpotential is determined by the geometry of the branes. We show that, when the two-dimensional theory flows to its infra-red fixed point, particular cases realize Kazama-Suzuki coset models. We also study the BPS spectrum of an Argyres-Douglas type superconformal field theory on the Coulomb branch by using its spectral networks. We provide strong evidence of the equivalence of superconformal field theories from different string-theoretic constructions by comparing their BPS spectra.

Contents

Acknowledgments	iii
Abstract	v
1 Introduction	1
1.1 Supersymmetric quantum field theory	1
1.2 Branes from string/M-theory	4
2 4d $\mathcal{N} = 2$ theory	8
2.1 4d $\mathcal{N} = 2$ gauge theory	8
2.1.1 $\mathcal{N} = 2$ multiplets	8
2.1.2 Pure SU(2) gauge theory	9
2.1.3 Low-energy effective action of an $\mathcal{N} = 2$ gauge theory	10
2.2 Seiberg-Witten theory	11
2.2.1 BPS states in the Coulomb branch	11
2.2.2 Electric-magnetic duality	12
2.2.3 Seiberg-Witten curve and differential	13
2.2.4 Wall-crossing of a BPS spectrum	14
2.2.5 Argyres-Douglas fixed points	15
2.3 Seiberg-Witten theory as a toy model	17
2.4 Brane configuration of Seiberg-Witten theories	17
2.4.1 Type IIA description	18
2.4.2 M-theory description	18
2.4.3 Type IIA/B descriptions from a chain of string dualities	19
2.5 Theory of class \mathcal{S}	22
2.5.1 Gaiotto's description of a 4d $\mathcal{N} = 2$ SU(2) SCFT	22

2.5.2	Classification of punctures	24
3	Ramification points of a Seiberg-Witten curve	26
3.1	SU(2) SCFT and the ramification of the Seiberg-Witten curve	28
3.2	SU(2) \times SU(2) SCFT and the ramification point	37
3.3	SU(3) SCFT and Argyres-Seiberg duality	41
3.4	SU(3) pure gauge theory and Argyres-Douglas fixed points	46
3.5	SU(2) gauge theory with massive matter	51
3.5.1	SU(2) gauge theory with four massive hypermultiplets	52
3.5.2	SU(2) gauge theory with two massive hypermultiplets	55
3.6	Brane configuration around a puncture and a ramification point	60
4	2d $\mathcal{N} = (2, 2)$ theory	63
4.1	2d $\mathcal{N} = (2, 2)$ supersymmetry	63
4.1.1	SUSY algebra	63
4.1.2	Chiral and twisted chiral multiplets	64
4.1.3	Supersymmetric Lagrangians	65
4.2	2d $\mathcal{N} = (2, 2)$ Landau-Ginzburg model	65
4.3	2d $\mathcal{N} = (2, 2)$ Gauged linear sigma model	67
4.4	Wall-crossing of 2d $\mathcal{N} = (2, 2)$ BPS spectra	69
4.5	2d $\mathcal{N} = (2, 2)$ theories from branes	71
4.5.1	From 4d $\mathcal{N} = 2$ to 2d $\mathcal{N} = (2, 2)$	71
4.5.2	2d $\mathcal{N} = (2, 2)$ theory from 4d $\mathcal{N} = 2$ theory at the root of the Higgs branch	73
4.5.3	Parameters of the 2d $\mathcal{N} = (2, 2)$ theory from branes	76
4.5.4	BPS spectrum of a mass-deformed classical $\mathbb{C}P^{N-1}$ sigma model	78
4.5.5	BPS spectrum of a quantum supersymmetric $\mathbb{C}P^{N-1}$ sigma model	80
5	Spectral networks	84
5.1	Construction of spectral networks	84
5.1.1	\mathcal{S} -walls	84
5.1.2	Around a branch point of ramification index N	85
5.1.3	Around a regular puncture of ramification index N	87

5.1.4	BPS Joint of \mathcal{S} -Walls	89
5.2	BPS spectrum from spectral networks	90
5.2.1	2d BPS states from spectral networks	90
5.2.2	4d BPS states from spectral networks	91
5.2.3	Finite \mathcal{S} -walls, 1-cycles and intersection numbers	92
6	2d wall-crossing and spectral networks	96
6.1	1 irregular puncture at $z = \infty$	96
6.1.1	$N=2$	97
6.1.2	$N=3$	97
6.1.3	$N=4$	99
6.2	1 irregular puncture at $z = \infty$, 1 regular puncture at $z = 0$	101
6.2.1	$N = 2$	102
6.2.2	Monodromy of the 2d BPS spectrum	105
6.2.3	A light soliton in the 2d BPS spectrum	106
6.2.4	$N=3$	109
7	2d $\mathcal{N} = (2, 2)$ SCFT and spectral networks	112
7.1	2d SCFT from the IR limit of the 2d $\mathcal{N} = (2, 2)$ theory from M-branes	112
7.1.1	2d $\mathcal{N} = (2, 2)$ theory from 4d $\mathcal{N} = 2$ theory at an Argyres-Douglas fixed point	112
7.1.2	2d $\mathcal{N} = (2, 2)$ theory from multiple M2-branes ending on a ramification point	118
7.2	SCFT from the IR limit of 2d $\mathcal{N} = (2, 2)$ theories	123
7.3	Supersymmetric Vacua	127
7.3.1	Brane System	127
7.3.2	Gauge Theory	128
7.3.3	Landau-Ginzburg Model	130
7.4	Chiral Rings	131
7.5	BPS Solitons	134
7.5.1	A single M2-brane	134
7.5.2	k M2-branes	135
7.6	2d BPS spectrum from spectral networks	136

7.6.1	Deformation by μ_N	137
7.6.2	General deformations	141
7.7	S^2 partition functions	143
8	4d $\mathcal{N} = 2$ SCFT and spectral network	147
8.1	SCFTs at Argyres-Douglas fixed points	148
8.1.1	$\mathcal{N} = 2$ SCFTs of class \mathcal{S}	148
8.1.2	Study of Argyres-Douglas fixed points via spectral networks	152
8.2	4d SCFTs in A_n -class	153
8.2.1	$\mathcal{S}[A_1; \mathcal{D}_{n+5}]$ theories	153
8.2.2	$\mathcal{S}[A_{N-1}; \mathcal{D}_I]$ theories	160
8.3	4d SCFTs in D_n -class	168
8.3.1	$\mathcal{S}[A_1; \mathcal{D}_{\text{reg}}, \mathcal{D}_{n+2}]$ theories	168
8.3.2	$\mathcal{S}[A_{N-1}; \mathcal{D}_{\text{II}}]$ theories	179
8.3.3	$\mathcal{S}[A_2; \mathcal{D}_{\text{reg}}, \mathcal{D}_{\text{III}}]$ theories	190
A	Normalization of compactified Seiberg-Witten curves	194
A.1	Normalization of a singular algebraic curve	194
A.2	Calculation of local normalizations	196
A.2.1	SU(2) SCFT	196
A.2.2	SU(2) \times SU(2) SCFT	203
A.2.3	SU(3) SCFT	207
A.2.4	SU(3) pure gauge theory	212
B	On Kazama-Suzuki models and their Landau-Ginzburg descriptions	217
C	SCFTs of Argyres-Douglas type	219
C.1	$\mathcal{S}[A_{N-1}; \mathcal{D}_I]$ theories from SU(N) pure SYM	219
C.2	$\mathcal{S}[A_{N-1}; \mathcal{D}_{\text{II}}]$ from SU(N) with $N_f = 2$	221
C.3	$\mathcal{S}[A_2; \mathcal{D}_{\text{reg}}, \mathcal{D}_{\text{III}}]$ from SU(3) with $N_f = 3$	222
	Bibliography	224

Chapter 1

Introduction

In this chapter we briefly review various topics that appear in this thesis as a preparation for the main text. In Section 1.1 we review general properties of supersymmetric field theory, focusing on the description of BPS states. In Section 1.2, we review the properties of various branes from type IIA string theory and M-theory, and the relation between various branes under string dualities.

1.1 Supersymmetric quantum field theory

Why supersymmetric theory is interesting Supersymmetry is a symmetry that associates to every boson its fermionic partner and vice versa. Schematically, a scalar field ϕ will be related by supersymmetry to a fermionic field ψ as

$$\delta_\epsilon \phi \sim \epsilon \psi. \quad (1.1)$$

If supersymmetry exists and is broken not at the planck scale but at much lower scale Λ_{SUSY} , for example around 1 TeV where new physics beyond the standard model is expected, then it provides an answer to the hierarchy problem. The hierarchy problem can

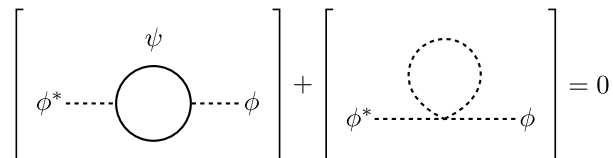


Figure 1.1: Loop cancellation from supersymmetry.

be illustrated by the two Feynmann diagrams shown in Figure 1.1, which contribute to the

mass renormalization of ϕ as quadratic divergence. Due to the divergence the scalar particle should have the quantum correction of the order of the UV cutoff, which should be the planck mass if we consider the standard model with gravity. If supersymmetry exists, then it makes the two diagrams cancel each other, thereby removing the quadratic divergence of the mass of ϕ . This mechanism tells us why the Higgs mass should be near Λ_{SUSY} , not near the planck scale.

Supersymmetry is also interesting theoretically because it is a new kind of symmetry different from the other symmetries we have observed so far from the nature in that supersymmetry has fermionic charges with anticommuting algebra. For example, the 4d Poincaré symmetry algebra can be represented as

$$\begin{aligned} [P_\mu, P_\nu] &= 0, \\ [P_\mu, M_{\rho\sigma}] &= i(\eta_{\mu\rho}P_\sigma - \eta_{\mu\sigma}P_\rho), \\ [M_{\mu\nu}, M_{\rho\sigma}] &= i(\eta_{\nu\rho}M_{\mu\sigma} - \eta_{\nu\sigma}M_{\mu\rho} - \eta_{\mu\rho}M_{\nu\sigma} + \eta_{\mu\sigma}M_{\nu\rho}), \end{aligned} \quad (1.2)$$

where P_μ generates translations and $M_{\mu\nu}$ generates rotations in the 4d spacetime with a metric $\eta_{\mu\nu}$. Note that the algebra involves only commutators. In comparison, a supersymmetry algebra with four real supercharges, which corresponds to the smallest supersymmetry algebra in a 4d spacetime, can be represented as

$$\{Q_\alpha, \bar{Q}_{\dot{\alpha}}\} = 2\sigma_{\alpha\dot{\alpha}}^\mu P_\mu, \quad \{Q_\alpha, Q_\beta\} = \{\bar{Q}_{\dot{\alpha}}, \bar{Q}_{\dot{\beta}}\} = 0, \quad (1.3)$$

where Q_α is a Weyl spinor. This helps us to overcome the Coleman-Mandula theorem, which states that the maximal Lie algebra of symmetries of the S -matrix of a unitary local relativistic quantum field theory is a direct product of the Poincaré algebra and the Lie algebra of a compact internal symmetry group. Since the Coleman-Mandula theorem is about bosonic symmetries, by incorporating fermionic charges we can enlarge the Poincaré algebra nontrivially to a Lie superalgebra.

Central extension of supersymmetry algebra If we have more than one Weyl spinor supercharge, it is possible to extend the supersymmetry algebra so that the anticommutation of one supercharge, Q^I , with another, Q^J , gives a nonvanishing result, the central charges

Z^{IJ} .

$$\{Q_\alpha^I, Q_\beta^J\} = 2\sqrt{2}\epsilon_{\alpha\beta}Z^{IJ}, \quad I, J = 1, \dots, \mathcal{N}. \quad (1.4)$$

Because Z^{IJ} is antisymmetric in its indices,

$$Z^{IJ} = -Z^{JI}, \quad (1.5)$$

we need $\mathcal{N} > 1$ to have a central charge in a supersymmetry algebra.

BPS states The existence of central charges provides a special kind of massive states that saturate the so-called Bogomolny-Prasad-Sommerfield bound,

$$M \geq \sqrt{2}|Z_i|, \quad (1.6)$$

where M is the mass of the state and Z_i is from Z^{IJ} in its canonical form

$$Z^{IJ} = \begin{pmatrix} 0 & Z_1 & 0 & 0 & \cdots \\ -Z_1 & 0 & 0 & 0 & \cdots \\ 0 & 0 & 0 & Z_2 & \cdots \\ 0 & 0 & -Z_2 & 0 & \cdots \\ \vdots & \vdots & \vdots & \vdots & \ddots \end{pmatrix}. \quad (1.7)$$

States that saturate the bound are called BPS states.

One important aspect of BPS states is that they are in general stable under the continuous changes of various parameters of the theory because the masses of the BPS states are tied to the central charges, which are topological in their origin and therefore invariant under such changes. The equality of the mass and the central charge(s) results in decoupling some of the components of the state, which makes the size of the representation of the state smaller. This representation is called a short representation, in contrast to a long representation that a general massive state belongs to. Because of the difference between the numbers of degrees of freedom of the two representations, a BPS state cannot evolve into a non-BPS state, which provides the stability under quantum corrections. The stability of a BPS state is useful when we try to extrapolate the study done in a weak coupling regime to a strong coupling regime.

Theories with different amount of supercharges 4d supersymmetric gauge theories can have various numbers of supercharges. As we have more supersymmetry, it becomes easier to study the theory because supersymmetry allows us to apply more powerful analytic techniques to study it. However, an increased amount of supersymmetry make it impossible for a theory to have certain features without breaking some or all of the supersymmetry, so by studying a theory with a large amount of supersymmetry we lose more freedom in building a model that displays a behavior of our interest. Therefore somewhere in the middle there can be a good place to find models that describe physical phenomena we want to study and at the same time is simple enough to understand.

Among various 4d supersymmetric gauge theories, $\mathcal{N} = 1$ supersymmetric theories are under the least constraints from supersymmetry, therefore they are good starting points to study the minimal supersymmetric extension of the standard model. $\mathcal{N} = 2$ supersymmetric theories have the smallest amount of supercharges to have BPS states, and they provide useful toy models to study strongly-coupled theories that lack perturbative methods applicable. We will discuss this in more detail while reviewing the Seiberg-Witten theory. $\mathcal{N} = 4$ supersymmetry provides a large amount of supersymmetry that provides more analytic control over a theory, and therefore it serves as a defining ground of various theories.

1.2 Branes from string/M-theory

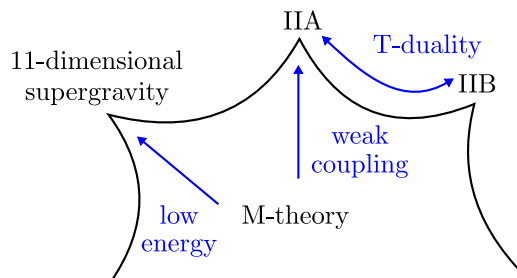


Figure 1.2

Various corners of M-theory String theories and 11d supergravity are believed to be different approximations of M-theory, which is a prospective theory of quantum gravity. The 11d supergravity describes the low-energy physics of M-theory. There are two types of string theories with 32 real supercharges, called type IIA and type IIB, which are related

by a perturbative duality called T-duality. Among the two theories, type IIA string theory can be understood as a weak coupling limit of M-theory.

Each theory contains various gauge fields. Both type IIA and type IIB string theories have an NS-NS 2-form gauge field B_2 that couples to fundamental strings. In addition to that, type IIA string theory contains RR 1- and 3-form gauge fields, C_1 , C_3 , and type IIB string theory contains RR 0-, 2-, and 4-form fields, C_0 , C_2 , C_4 . The 11d supergravity contains a 3-form gauge field A_3 . These gauge fields are coupled to extended objects of various dimensions and characteristics, called branes.

Branes in type IIA theory In type IIA theory, there are branes called Dp -branes and NS5-branes. A Dp -brane is defined as an object on which a fundamental string can end. It is an electric source of C_{p+1} for $-1 \leq p \leq 3$, and a magnetic source of C_{7-p} for $3 \leq p \leq 7$. Its tension is proportional to $1/g_s$, and therefore is massive when the coupling is small. It can end on a $D(p+2)$ -brane, thereby enabling us to construct an interesting configuration of intersecting D-branes. And it is a $\frac{1}{2}$ -BPS object, i.e., they preserve half of the supersymmetry of the theory such that the preserved supercharge is of the form $Q = \epsilon_+ Q_+ + \epsilon_- Q_-$ where

$$\Gamma^0 \cdots \Gamma^p \epsilon_- = \epsilon_+. \quad (1.8)$$

An NS5-brane couples magnetically to the NS-NS 2-form field B_2 . Its tension is proportional to $1/g_s^2$, and therefore is much heavier than D-branes in the weak string coupling regime. D2- and D4-branes can end on an NS5-brane. An NS5-brane is also a $\frac{1}{2}$ -BPS object, which preserves supercharge $Q = \epsilon_+ Q_+ + \epsilon_- Q_-$ where

$$\Gamma^0 \cdots \Gamma^5 \epsilon_{\pm} = \epsilon_{\pm}. \quad (1.9)$$

M-theory as a strong coupling limit of type IIA theory When we increase the string coupling g_s of type IIA theory, the theory grows the eleventh spacetime dimensional circle of radius $R_{10} = g_s l_s$, called an M-theory circle. Then M-theory, strong coupling limit of type IIA string theory, lives in the 11d spacetime containing the M-theory circle.

One piece of evidence of this picture is that the action of 10d type IIA supergravity, the low-energy effective theory of type IIA string theory, can be obtained from the dimensional

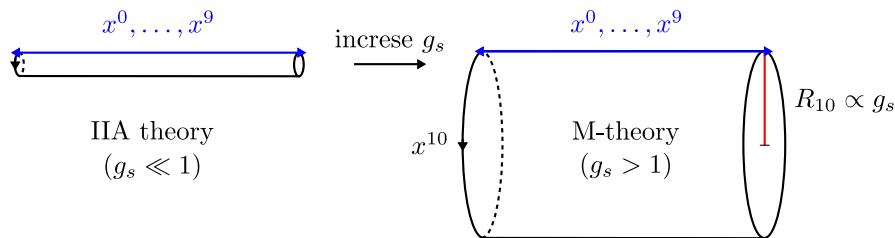


Figure 1.3

reduction of 11d supergravity on the M-theory circle. Another is that branes in type IIA string theory can be understood as coming from branes of M-theory.

Branes in M-theory In M-theory, there is one gauge field and two kinds of branes that couple to it electrically and magnetically, which are called M2-branes and M5-branes, respectively. An Mp -brane is a $\frac{1}{2}$ -BPS object: it preserves the supercharge ϵQ with

$$\Gamma^0 \Gamma^1 \dots \Gamma^p \epsilon = \epsilon. \quad (1.10)$$

An Mp -brane has tension $1/(l_P)^{p+1}$, where $l_P^3 = g_s(l_s)^3$.

Branes in IIA theory can be understood as M-branes wrapping the M-theory circle in various ways. When an M2-brane wraps the M-theory circle, it becomes a fundamental string in IIA, whereas when it is transverse to the M-theory circle, it reduces to a D2-brane. When an M5-brane wraps the M-theory circle, it becomes a D4-brane, and when it is not wrapping the M-theory circle, it becomes an NS5-brane.

Branes ending on branes There are various configurations of a brane ending on another brane, which enables us to build a network of branes whose low-energy effective world-volume theory provides a useful model to study a gauge theory in its strongly coupled regime.

First consider a configuration of a D2-branes filling (x^0, x^1) and $x^5 \geq 0$. When it ends at $x^5 = 0$ on a D4-brane filling $(x^0, x^1, x^2, x^3, x^4)$, from the D2-brane we get a 2d gauge theory (A_0, A_1) from its 3d world-volume theory with gauge field A_μ , and its last component, A_2 , combines with the three scalars corresponding to the fluctuation of the D2-brane along the D4-brane, (X^2, X^3, X^4) , to form a massless matter multiplet. When we increase the number of D2- and D4-branes, we can consider a nonabelian gauge theory and a nonabelian flavor

symmetry, respectively.

A D4-brane filling (x^0, \dots, x^3) and $x^6 \geq 0$ can end at $x^6 = 0$ on an NS5-brane filling (x^0, \dots, x^5) as a codimension two object. When lifted to M-theory, the two branes merge into a single, smooth M5-brane as shown in Figure 1.4. From the D4-brane we get a 4d

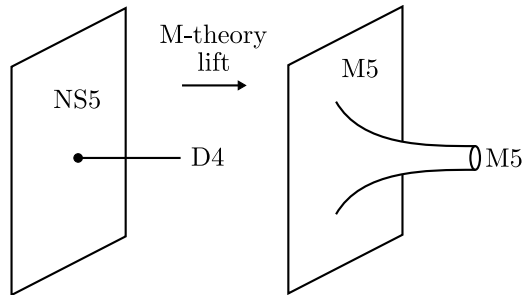


Figure 1.4: D4-brane ending on NS5-brane.

gauge theory from its worldvolume gauge field A_μ , where the last component A_4 combines with the fluctuation of the D4-brane (X^7, X^8, X^9) to form a matter multiplet.

Chapter 2

4d $\mathcal{N} = 2$ theory

Here we review Seiberg-Witten theory, putting emphasis on non-perturbative phenomena like wall-crossings and Argyres-Douglas fixed points. Then we describe type IIA brane configurations of 4d $\mathcal{N} = 2$ gauge theories, and observe how lifting such a configuration to M-theory provides the string theoretic origin of the Seiberg-Witten curve of the 4d theory. We also consider a chain of string dualities to obtain the description of Seiberg-Witten curves from type IIA/B string theory.

2.1 4d $\mathcal{N} = 2$ gauge theory

First we review basic facts of 4d $\mathcal{N} = 2$ gauge theory, mainly to set up the notation for the following discussion of Seiberg-Witten theory.

2.1.1 $\mathcal{N} = 2$ multiplets

The fields of $\mathcal{N} = 2$ supersymmetric theories can be expressed in terms of $\mathcal{N} = 1$ chiral fields Φ and W . Φ is an $\mathcal{N} = 1$ scalar multiplet satisfying

$$\bar{D}_{\dot{\alpha}}\Phi = 0, \tag{2.1}$$

which has as its components a fermionic field ψ_{α} and a complex scalar field ϕ . W is the field strength of a real superfield V that contains a gauge field A_{μ} and fermionic fields λ_{α} , $\bar{\lambda}_{\dot{\alpha}}$. From V we obtain the chiral field W defined by

$$W_{\alpha} = -\frac{1}{4}\bar{D}^2 D_{\alpha}V, \quad \bar{W}_{\dot{\alpha}} = -\frac{1}{4}D^2 \bar{D}_{\dot{\alpha}}V, \tag{2.2}$$

and it has as its components λ_α , $\bar{\lambda}_{\dot{\alpha}}$, and $F_{\mu\nu}$, the field strength of A_μ .

2.1.1.1 Vector multiplet

The gauge field of an $\mathcal{N} = 2$ supersymmetric theory is represented as an $\mathcal{N} = 2$ vector multiplet containing two $\mathcal{N} = 1$ chiral superfields, a scalar multiplet A and a field strength W . Both fields are in the adjoint representation of the gauge group of the theory, and the renormalizable Lagrangian of a 4d $\mathcal{N} = 2$ pure gauge theory with vector multiplet (A, W) is

$$\mathcal{L}_g = \frac{1}{4\pi} \text{Im Tr} \left[\tau \left(\int d^2\theta d^2\bar{\theta} A^\dagger e^{-2V} A + \frac{1}{2} \int d^2\theta W^\alpha W_\alpha \right) \right], \quad (2.3)$$

where τ is a complexified gauge coupling containing the theta angle θ and the gauge coupling constant g ,

$$\tau = \frac{\theta}{2\pi} + \frac{4\pi i}{g^2}, \quad (2.4)$$

and V is the $\mathcal{N} = 1$ gauge superfield, also in the adjoint representation.

2.1.1.2 Hypermultiplet

A matter field of an $\mathcal{N} = 2$ supersymmetric theory is called a hypermultiplet and contains one $\mathcal{N} = 1$ chiral multiplet Q and one $\mathcal{N} = 1$ anti-chiral multiplet \tilde{Q}^\dagger , both of which are in the same representation of the gauge group of the theory. When we have N_f number of $\mathcal{N} = 2$ hypermultiplets, each having mass m_i , the Lagrangian that provides the interaction of them with the gauge field is $\mathcal{L}_f + \bar{\mathcal{L}}_f$, where

$$\mathcal{L}_f = \int d^4\theta \left(Q_i^\dagger e^{-2V} Q_i + \tilde{Q}_i e^{-2V} \tilde{Q}_i^\dagger \right) + \int d^2\theta \left(\sqrt{2} \tilde{Q}_i \Phi Q_i + m_i \tilde{Q}_i Q_i \right). \quad (2.5)$$

2.1.2 Pure SU(2) gauge theory

We start from the renormalizable Lagrangian of a 4d $\mathcal{N} = 2$ pure SU(2) gauge theory, (2.3), which is asymptotically free. When the Lagrangian is expanded in components, it contains a scalar potential $V(a)$,

$$V(a) = \frac{1}{g^2} \text{Tr} \left([a, a^\dagger]^2 \right), \quad (2.6)$$

where a is the scalar component of the chiral superfield A in the $\mathcal{N} = 2$ vector multiplet. When a is in the Cartan of the gauge group, it gives a ground state. When the vacuum expectation value of a has a nonzero value, the gauge group is broken down to $U(1)$ and the theory is in the Coulomb branch. The continuum of inequivalent ground states, or the moduli space of the Coulomb branch, is parameterized by u . In the weak coupling regime of the gauge theory, u agrees with a gauge invariant classical variable,

$$u \equiv \text{Tr } a^2. \quad (2.7)$$

After the quantization of the theory, the quantum moduli space is parameterized by

$$u \equiv \langle \text{Tr } a^2 \rangle, \quad (2.8)$$

which is the expectation value of the classical quantity. When the theory has a nonzero value of u , we get massive gauge bosons W^\pm whose masses are proportional to u .

2.1.3 Low-energy effective action of an $\mathcal{N} = 2$ gauge theory

Now we describe the low-energy physics of the theory by finding out the effective action at a scale lower than the masses of massive states. In writing down the action there is a crucial fact that the low-energy effective action of an $\mathcal{N} = 2$ gauge theory, with terms with at most two derivatives and not more than four fermions, is determined by a holomorphic function \mathcal{F} , called a prepotential [1].

For $G = SU(2)$, when a acquires a vev the gauge group is spontaneously broken down to a $U(1)$ gauge group, the theory is in the Coulomb branch. We integrate out the massive W^\pm to get the low-energy effective Lagrangian

$$\mathcal{L}_{\text{eff}} = \frac{1}{4\pi} \text{Im} \left[\int d^4\theta \frac{\partial \mathcal{F}(A)}{\partial A} \bar{A} + \int d^2\theta \frac{1}{2} \frac{\partial^2 \mathcal{F}(A)}{\partial A^2} W^\alpha W_\alpha \right], \quad (2.9)$$

where now A and W_α are $U(1)$ -valued fields. When we compare (2.3) and (2.9), we find that the low-energy effective value of τ is

$$\tau_{\text{eff}}(a) = \frac{\partial^2 \mathcal{F}(a)}{\partial a^2}. \quad (2.10)$$

2.2 Seiberg-Witten theory

In [1] it is shown that we can determine the functional form of the prepotential \mathcal{F} , which is, including the perturbative 1-loop effect and the nonperturbative instanton corrections,

$$\mathcal{F} = \frac{i}{2\pi} A^2 \log \frac{A^2}{\Lambda^2} + \sum_{k=1}^{\infty} \mathcal{F}_k \left(\frac{\Lambda}{A} \right)^{4k} A^2, \quad (2.11)$$

where Λ is the dynamically generated scale of the theory. The work of Seiberg and Witten [2, 3] found every \mathcal{F}_k by determining the exact form of \mathcal{F} .

2.2.1 BPS states in the Coulomb branch

To find out the exact prepotential of a 4d $\mathcal{N} = 2$ pure gauge theory, we need to investigate the strong coupling regime of the gauge theory where the nonperturbative corrections are not negligible. For that purpose it is helpful to study the BPS states of the theory, because such a state that is found in the weak coupling regime is in general expected to persist even when the gauge coupling becomes strong.

When we define

$$a_{\text{D}}(u) = \frac{\partial \mathcal{F}}{\partial a}, \quad (2.12)$$

the central charge of a BPS state of a $\mathcal{N} = 2$ pure SU(2) gauge theory is

$$Z = a n_e + a_{\text{D}} n_m, \quad (2.13)$$

where the state has electric charge n_e and magnetic charge n_m of the U(1) IR gauge field, both of which are quantized to have integer values. In terms of a and a_{D} we can write down the mass of a BPS state with the U(1) charge (n_e, n_m) as

$$M = \sqrt{2}|Z|. \quad (2.14)$$

This mass formula can be a good hint to guess $a(u)$ and $a_{\text{D}}(u)$ in all u , including the strong coupling regime. If we can find $a(u)$ and $a_{\text{D}}(u)$ over all the Coulomb branch moduli space parametrized by u , we can determine the prepotential \mathcal{F} and then describe the low-energy

physics by the effective action \mathcal{L}_{eff} .

2.2.2 Electric-magnetic duality

The action (2.9) is invariant under an $\text{SL}(2, \mathbb{Z})$ duality. To see this, first consider taking

$$(a_{\text{D}}, a) \rightarrow (a, -a_{\text{D}}). \quad (2.15)$$

In order to see that this transformation leaves the action invariant under an appropriate redefinition of τ_{eff} , we first promote W to an independent field by implementing the Bianchi identity

$$\text{Im } DW = 0 \quad (2.16)$$

into the action using a vector superfield V_{D} as a Lagrange multiplier by adding the following term to the action,

$$\frac{1}{4\pi} \text{Im} \int d^4x d^4\theta V_{\text{D}} DW = -\frac{1}{4\pi} \text{Im} \int d^4x d^2\theta W_{\text{D}} W. \quad (2.17)$$

After integrating out W and taking

$$\tau_{\text{eff}} \rightarrow \tau_{\text{D,eff}} = -\frac{1}{\tau_{\text{eff}}}, \quad (2.18)$$

the action retains the original form in terms of the dual variables. It is easy to see that the action is invariant under another transformation,

$$(a_{\text{D}}, a) \rightarrow (a_{\text{D}} + a, a), \quad \tau_{\text{eff}} \rightarrow \tau_{\text{eff}} + 1. \quad (2.19)$$

These two transformations generate the full duality group $\text{SL}(2, \mathbb{Z})$. Note that the first transformation can be considered as an electric-magnetic duality.

2.2.3 Seiberg-Witten curve and differential

In two seminal papers [2, 3] Seiberg and Witten showed that by using a real two-dimensional surface, or a complex one-dimensional curve,

$$y^2 = (x - 1)(x + 1)(x - u), \quad (2.20)$$

and a first-order differential form,

$$\lambda = \frac{\sqrt{2}}{2\pi} \frac{\sqrt{x - u} dx}{\sqrt{x^2 - 1}}, \quad (2.21)$$

we can calculate $a(u)$ and $a_D(u)$,

$$a = \oint_{\gamma_1} \lambda, \quad a_D = \oint_{\gamma_2} \lambda, \quad (2.22)$$

where γ_1 and γ_2 are 1-cycles on the curve with a nonzero intersection

$$\gamma_1 \cdot \gamma_2 = 1. \quad (2.23)$$

The curve, called a Seiberg-Witten curve, is parametrized by u , the same variable that parametrizes the Coulomb branch moduli space. The differential, called a Seiberg-Witten differential, gives the mass of a BPS state when integrated along a 1-cycle of the curve. We can calculate $a(u)$ and $a_D(u)$ by finding out an appropriate set of 1-cycles of the curve, here γ_1 and γ_2 , respectively, and integrating λ along those cycles on the Seiberg-Witten curve. From that information we can calculate the prepotential \mathcal{F} and the low-energy effective action \mathcal{L}_{eff} .

The Seiberg-Witten curve (2.20) becomes singular when $u = \pm 1$. At each singularity a 1-cycle shrinks to vanish, signaling the appearance of a massless BPS state. Those BPS states start as massive ones when the U(1) gauge theory is weakly coupled, that is, when u is near ∞ . As we approach $u = \pm 1$ from $u = \infty$, the gauge theory becomes strongly coupled so that the perturbative description becomes less valid. When we finally meet one of the singularities, then a new massless state arises, which are not described by the previous low-energy effective action, revoking the validity of the action. Therefore we need a different low-energy effective action written in terms of the new massless state. Here the

$SL(2, \mathbb{Z})$ duality of the action plays a role. For example, at one of the two singularities the massless BPS states has $(n_e, n_m) = (0, 1)$. By taking the duality generated by

$$S = \begin{pmatrix} 0 & 1 \\ -1 & 0 \end{pmatrix}, \quad (2.24)$$

we can express the low-energy effective action in terms of a different charged field a_D , which couples electrically to the BPS state that becomes light at the singularity. Therefore this is the action that is valid perturbatively around the singularity.

2.2.4 Wall-crossing of a BPS spectrum

Because the Seiberg-Witten curve (2.20) has a vanishing 1-cycle at each singularity on the u -plane, there is a monodromy of 1-cycles around a path encircling $u = \pm 1$ which can be obtained from the Picard-Lefschitz formula,

$$\zeta \rightarrow \zeta + \langle \zeta, \gamma \rangle \gamma, \quad (2.25)$$

where γ is the vanishing 1-cycle and $\langle \zeta, \gamma \rangle$ is the intersection of the two 1-cycles. This in turn results in the monodromy of (a_D, a) around $u = \infty$, which can be calculated from the 1-loop formula of \mathcal{F} because in this region the nonperturbative corrections are negligible compared to the 1-loop contribution. The 1-loop β function of the low-energy effective $U(1)$ gauge theory gives

$$a_D = \frac{\partial \mathcal{F}}{\partial a} = \frac{2ia}{\pi} \log \left(\frac{a}{\Lambda} \right) + \frac{ia}{\pi}, \quad (2.26)$$

from which we get the monodromy matrix around $u = \infty$

$$M_\infty = \begin{pmatrix} -1 & 2 \\ 0 & -1 \end{pmatrix}, \quad (2.27)$$

and the BPS spectrum is invariant under this monodromy.

However, the monodromy around each singularity on the u -plane affects the BPS spectrum in a different manner. Each monodromy matrix can be calculated by identifying the corresponding vanishing 1-cycle (and therefore the $U(1)$ -charges of the BPS state that

becomes massless at the singularity),

$$M_1 = \begin{pmatrix} 1 & 0 \\ -2 & 1 \end{pmatrix}, \quad M_{-1} = \begin{pmatrix} -1 & 2 \\ -2 & 3 \end{pmatrix}. \quad (2.28)$$

These two matrices satisfy $M_1 M_{-1} = M_\infty$, consistent with the singularity structure on the u -plane. What is different about $M_{\pm 1}$ compared to M_∞ is that they generate a subgroup of $\text{SL}(2, \mathbb{Z})$, called $\Gamma(2)$. However, the BPS spectrum cannot be invariant under the action of these monodromies as they change the charge of a W-boson into a dyonic charge, which is impossible because a W-boson is a vector multiplet and a dyon is a hypermultiplet.

What is happening is that not all the BPS states that exist in the semi-classical regime are stable as u approach the strongly coupled regime $|u| < 1$. There is a real codimension-one curve on the u -plane going through $u = \pm 1$, on which $a_D(u)/a(u) \in \mathbb{R}$ is satisfied. The curve separates the u -plane, or the Coulomb branch moduli space of a pure $\text{SU}(2)$ gauge theory, into two regions. This curve is called a wall of marginal stability, or a BPS wall in short. For a pure $\text{SU}(2)$ gauge theory, inside the wall there are only two stable BPS states, a monopole with the $\text{U}(1)$ -charge $(n_e, n_m) = (0, +1)$ and a dyon with the $\text{U}(1)$ -charge $(+1, -1)$, and their anti-states. These are the states that become massless at the two singularities on the u -plane. Outside the wall, there are W-bosons with the $\text{U}(1)$ -charge $\pm(1, 0)$ and infinitely many dyons with the $\text{U}(1)$ -charge $\pm(n, 1)$, $n \in \mathbb{Z}$. As the value of u approaches the BPS wall from the outside and goes over it, a W-boson with the $\text{U}(1)$ -charge $(+1, 0)$ decays into a monopole with the $\text{U}(1)$ -charge $(0, +1)$ and a dyon with the $\text{U}(1)$ -charge $(+1, -1)$, and that is why there are only finitely many hypermultiplets inside the BPS wall.

2.2.5 Argyres-Douglas fixed points

In the complex two-dimensional Coulomb branch moduli space (u, v) of a 4d $\mathcal{N} = 2$ pure $\text{SU}(3)$ gauge theory, there is a choice of parameters that makes the low-energy effective theory an interacting superconformal field theory (SCFT), called an Argyres-Douglas fixed point [4]. When the theory is at the fixed point, there are two mutually nonlocal massless states. In other words, when there are two 1-cycles of the Seiberg-Witten curve of the

theory, γ_e and γ_m , such that their intersection is nonzero,

$$\langle \gamma_e, \gamma_m \rangle \neq 0, \quad (2.29)$$

and that they shrink to vanish as the theory approach the fixed point, the theory should be a nontrivial SCFT at the fixed point.

Studying the fixed point theory is a difficult task because it is strongly coupled and has no Lagrangian description. So we often consider a deformation of the theory from the fixed point by adding a relevant term. This can be achieved by considering a small change in the Coulomb branch parameters. For example, when $(u, v) = (u_1, v_1)$ is the location of an Argyres-Douglas fixed point of a pure SU(3) gauge theory, then we deform the parameter as

$$u = u_1 + \delta u. \quad (2.30)$$

Because the theory is at a nontrivial fixed point, the scaling dimension of the deformation $\Delta(\delta u)$ is greater than 1, and we have a deformation of

$$\delta \mathcal{L} = \frac{v_1}{\Lambda^{\Delta(\delta u)-1}} \int d^4\theta \delta u, \quad (2.31)$$

where Λ is the dynamically generated scale of the theory. If $1 < \Delta(\delta u) < 2$ this deformation is relevant, and if $\Delta(\delta u) > 2$ it is an irrelevant deformation from the fixed point. To find out the scaling dimension of a deformation, we can use the fact that by $\mathcal{N} = 2$ superconformal symmetry the scaling dimension of the scalar component u of a vector multiplet U is related to its U(1) R-symmetry charge as

$$\Delta(u) = \frac{1}{2}R(u). \quad (2.32)$$

When we can read out the R-charge of a deformation parameter from the Seiberg-Witten curve of the theory, we can tell if the corresponding deformation is relevant or not.

2.3 Seiberg-Witten theory as a toy model

In addition to the nonperturbative description of gauge theories, Seiberg-Witten theories provide interesting toy models for various physical phenomena.

Confinement and chiral symmetry breaking Seiberg-Witten theory provides an explicit example of the confinement of electric charge and the chiral symmetry breaking.

If we introduce a superpotential $m\text{Tr}A^2$, this breaks $\mathcal{N} = 2$ down to $\mathcal{N} = 1$. Near a singularity where a massless monopole occurs, the superpotential furnishes a vev to the monopole. Via the Higgs mechanism the unbroken $U(1)$ gauge field becomes massive, and the condensation of the monopoles leads to the confinement of electric charges by the dual Meissner effect.

The condensation also displays the chiral symmetry breaking when we have matter hypermultiplets, whose existence turns a monopole into a spinor of the global symmetry.

Electric-magnetic duality of BPS spectra Another phenomenon described by Seiberg-Witten theories is the electric-magnetic duality of the spectrum of BPS states.

The duality is conjectured by Montonen and Olive and is believed to hold for a 4d $\mathcal{N} = 4$ gauge theory. This is possible because for the theory a W -boson and a magnetic monopole live in the same multiplet. But a 4d $\mathcal{N} = 2$ pure gauge theory have the two in different multiplets and therefore the duality does not hold.

However, consider an $\mathcal{N} = 2$ gauge theory with four electric hypermultiplets. They are in a $\text{Spin}(8)$ vector multiplet, and magnetic monopoles are in a $\text{Spin}(8)$ spinor multiplet. Seiberg and Witten conjectured that the theory is invariant under $SL(2, \mathbb{Z})$ when the BPS spectrum transforms under the triality automorphism group of $\text{Spin}(8)$.

This S-duality is revisited by Gaiotto [5], whose study resulted in identifying various building blocks of strongly coupled 4d $\mathcal{N} = 2$ SCFTs.

2.4 Brane configuration of Seiberg-Witten theories

The centerpiece of Seiberg-Witten theory is that physics of the low-energy effective theory of a 4d $\mathcal{N} = 2$ gauge theory is encoded in a complex one-dimensional curve and a holomorphic 1-form on the curve. In [6, 7] the string-theoretic origin of the curve is discovered, which

shed a new light on the study of 4d $\mathcal{N} = 2$ theories and their BPS spectra. Here we review how to construct Seiberg-Witten curves from branes of type II string theories and M-theory.

2.4.1 Type IIA description

Figure 2.1 shows a brane configuration of type IIA string theory that describes a 4d $\mathcal{N} = 2$ $SU(2)$ gauge theory with four massless hypermultiplets, which is a superconformal field theory.

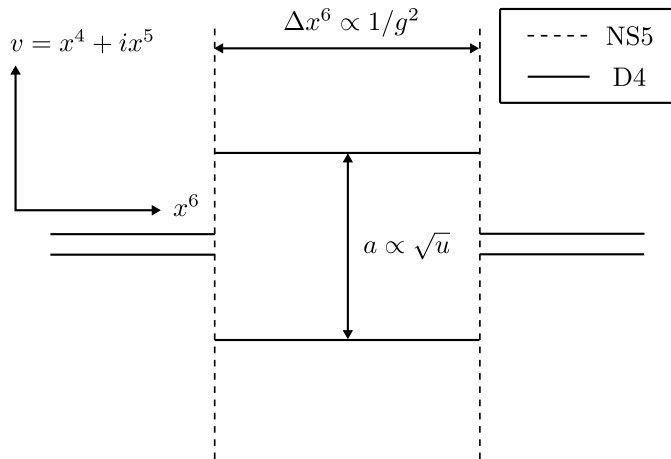


Figure 2.1: Type IIA brane configuration of a 4d $\mathcal{N} = 2$ $SU(2)$ SCFT.

There are two parallel NS5-branes that fill the 4d spacetime (x^0, \dots, x^3) and span the extra two-dimensional space (x^4, x^5) . And there are two parallel D4-branes that fill the same 4d spacetime and span the x^6 -direction. Each D4-brane is located at a point (x^4, x^5) on an NS5-brane.

The separation of the NS5-branes along the x^6 -direction is related to the 4d gauge coupling parameter, which is an exactly marginal parameter of this theory. The separation of the D4-branes along the (x^4, x^5) -plane is related to the expectation value of the scalar component of the vector multiplet of the 4d theory, or its Coulomb branch parameter.

2.4.2 M-theory description

Now we lift the IIA brane system to M-theory. Then we have an M-theory circle x^{10} and the two D4-branes become two M5-branes wrapping the M-theory circle. An NS5-brane becomes an M5-brane located at a point (x^6, x^{10}) on the M5-branes from the D4-branes.

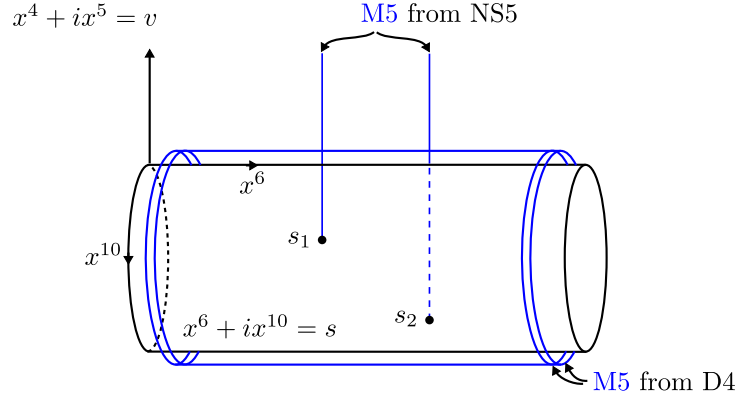


Figure 2.2: M-theory brane configuration of a 4d $\mathcal{N} = 2$ $SU(2)$ SCFT.

When the Coulomb branch parameter u is nonzero, these M5-branes merge into a single M5-brane. It fills the same 4d spacetime, and its configuration in the complex two-dimensional space (t, v) is described by a holomorphic equation $f(t, v) = 0$, where

$$f(t, v) = (t - t_1)(t - t_2)v^2 - ut, \quad t = \exp(x^6 + ix^{10}). \quad (2.33)$$

The subspace spanned by the single M5-brane is an algebraic curve, which can be identified with the Seiberg-Witten curve of the 4d $\mathcal{N} = 2$ gauge theory from the IIA brane system. The Seiberg-Witten differential is represented by

$$\lambda = \frac{v}{t} dt. \quad (2.34)$$

A BPS state corresponding to a 1-cycle of the Seiberg-Witten curve comes from an M2-brane whose boundary ends on the M5-brane along the 1-cycle. The mass of the BPS state is obtained by integrating λ along the 1-cycle, whose value corresponds to the area of the M2-brane [8, 9, 10].

2.4.3 Type IIA/B descriptions from a chain of string dualities

Here we will follow the chain of string dualities described in [11] to get type IIB description of a Seiberg-Witten curve. We start from the usual Hanany-Witten type IIA brane configuration of NS5-branes and D4-branes that fill the 4d spacetime as shown in Figure 2.3.

To follow the chain of string dualities, it is convenient to represent the directions that

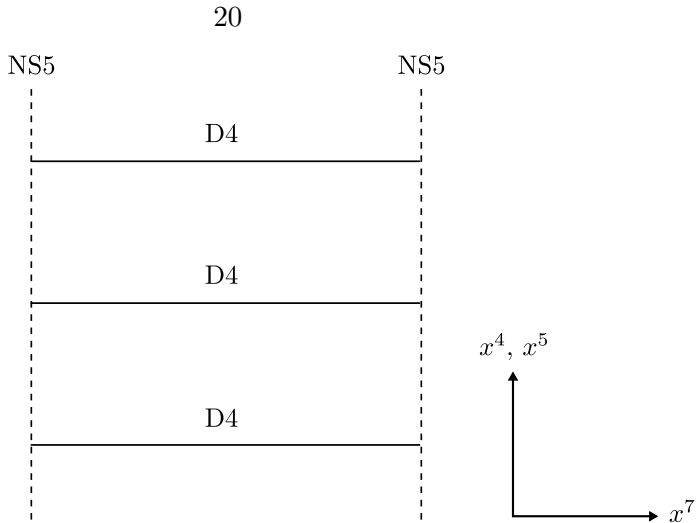


Figure 2.3: Type IIA brane configuration of a 4d $\mathcal{N} = 2$ pure $SU(3)$ gauge theory.

x^i	0	1	2	3	4	5	6	7	8	9
NS5	—	—	—	—	—	—	·	·	·	·
D4	—	—	—	—	·	·	·	—	·	·

Table 2.1

the branes span as in Table 2.1, where “—” means the corresponding brane spans the entire space along the direction and “·” means it is at a point along the direction.

x^i	0	1	2	3	4	5	6	7	8	9	10*
M5 from NS5	—	—	—	—	—	—	·	·	·	·	·
M5 from D4	—	—	—	—	·	·	·	—	·	·	○

Table 2.2

We lift this to M-theory. Then a D4-brane becomes an M5-brane wrapping the M-theory circle, which we will denote as x^{10} , and the NS5-D4-brane system becomes a single M5-brane wrapping the Seiberg-Witten curve. Note that x^{10} direction is marked with an asterisk, which implies that the corresponding direction is compact. “○” means a brane wraps the compact direction.

x^i	0	1	2	3	7	10*	4	5	6	8
NS5	—	—	—	—	t		v	·	·	

Table 2.3

Consider compactifying x^9 direction and switching the role of x^{10} and x^9 as the M-theory circle, which is the so-called “9-11 flip.” When the size of x^9 circle goes to zero, we are

moving toward another corner of the M-theory picture. As the M5-brane does not span any extent along the x^9 -direction, it becomes an NS5-brane wrapping the same Seiberg-Witten curve. Table 2.3 shows how this brane span the 10d spacetime.

To go from this type IIA picture to that of type IIB, we compactify one more direction, x^8 , and perform a T-duality along the direction. The result is shown in Table 2.4.

x^i	0	1	2	3	7	10*	4	5	6	8*
ALE over \mathbb{CP}^1	-	-	-	-	t	$v \in \text{ALE}$	\cdot	\cdot	\cdot	\cdot

Table 2.4

NS5 in the previous type IIA picture now becomes a pure geometry in type IIB string theory, which is an ALE fibration over \mathbb{CP}^1 [12, 6]. Note that the instanton effect [13, 14] is important in understanding the duality between the NS5-branes localized in the complex two-dimensional space of a fiber and the ALE space that spans the complex two-dimensional space and has the localized structures where the compact circle direction degenerates.

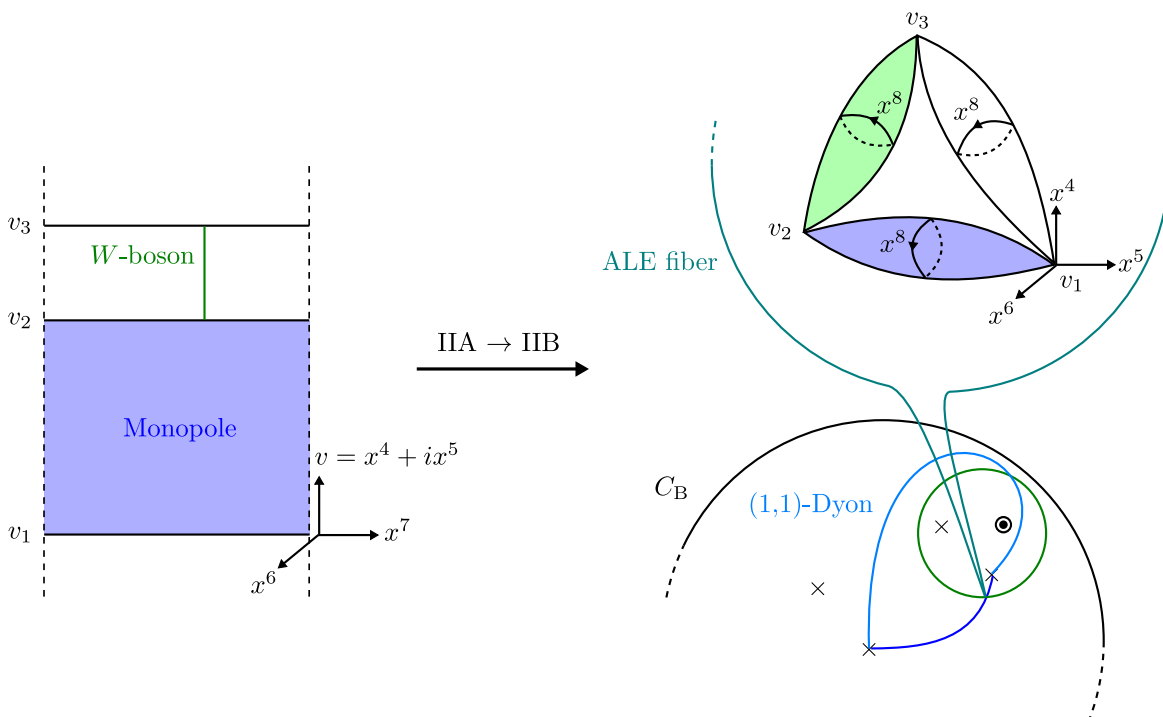


Figure 2.4

Figure 2.4 summarizes the result of the chain of dualities, where we start with a type IIA brane configuration of pure $SU(3)$ gauge theory. In this type IIA picture, there are three D4-branes located at v_1 , v_2 , and v_3 in the v -plane. Note that a fundamental string

stretched between two of the D4-branes corresponds to a W-boson, and that a D2-brane filling the two-dimensional space bounded by two of the D4-branes and the two NS5-branes gives us a magnetic monopole, both of them BPS states of the 4d theory.

Now at the end of the duality chain we get a type IIB geometry, ALE fibration over a Riemann sphere, C_B . Over a point of C_B there is an ALE fiber, which contains three 2-cycles. Now v_1 , v_2 , and v_3 are where the x^8 -circle shrinks, and therefore are the endpoints of the 2-cycles. The size of each 2-cycle varies as we move over C_B , because each v_i is a function of $t \in C_B$. There are four locations on C_B that two v_i 's coincide, which can be considered as branch points of $v(t)$, whose trivialization over C_B leads to $v_i(t)$. When we are at one of the four branch points, some of the 2-cycles shrink.

When we consider a line segment connecting two of the four branch points, shown in the right of Figure 2.4 as a blue curve on \mathcal{C} , and the fibration of the 2-cycles over the line segment, we can see that there is a compact 3-cycle with a topology of S^3 , and wrapping a D3-brane over this 3-cycle gives us a magnetic monopole. From a closed curve on \mathcal{C} shown as a green circle in Figure 2.4, we get a compact 3-cycle of the topology of $S^1 \times S^2$, and wrapping a D3-brane over this 3-cycle results in a W-boson. This is the familiar story of geometric engineering of a 4d $\mathcal{N} = 2$ gauge theory.

2.5 Theory of class \mathcal{S}

In [5] Gaiotto studied the dualities of 4d $\mathcal{N} = 2$ SCFTs from M5-branes wrapping punctured Riemann surfaces and unveiled building blocks out of which we can construct a family of $\mathcal{N} = 2$ theories, referred to as theories of class \mathcal{S} . Such a theory, including one corresponding to a building block, in general does not have a Lagrangian description and therefore is an interesting subject to study.

Here we will briefly review theories of class \mathcal{S} to gather some pieces of information needed to proceed to our main discussion.

2.5.1 Gaiotto's description of a 4d $\mathcal{N} = 2$ SU(2) SCFT

We can understand a 4d $\mathcal{N} = 2$ gauge theory as coming from multiple M5-branes wrapping a punctured Riemann surface. For an example, consider a 4d $\mathcal{N} = 2$ SU(2) SCFT, whose M-theory brane configuration is shown in Figure 2.5. This can be understood as two M5-

branes wrapping a Riemann sphere with four punctures, which we will call a Gaiotto curve C_G . When we use t as the coordinate of C_G , the Seiberg-Witten differential $\lambda = \frac{v}{t} dt$ of the

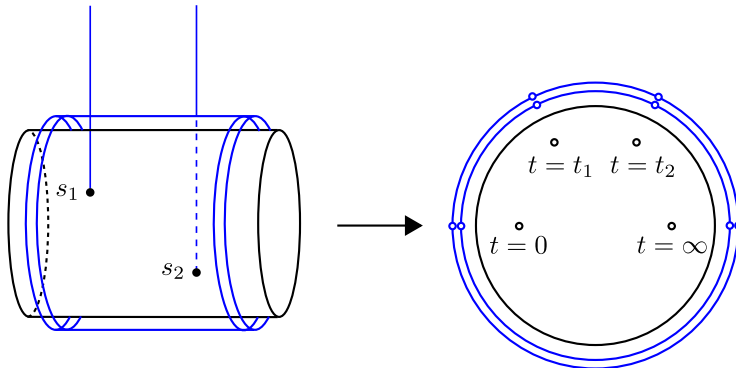


Figure 2.5

theory is in T^*C_G , the cotangent bundle of C_G . λ also has a dependence on the Coulomb branch parameter of the theory, which is interpreted as the deformations of the M5-branes along the fiber of T^*C_G . When we define $\lambda = x dt$, the Seiberg-Witten curve is

$$x^2 = \frac{u}{t(t-t_1)(t-t_2)}. \quad (2.35)$$

The locations of the punctures are where λ diverges, whose cross ratio encodes the gauge coupling constant of the 4d theory. There are interesting limits of τ . One is colliding the puncture at $t = t_1$ to $t = 0$. This corresponds to the weak coupling limit of the gauge theory, because this makes the separation of two M5-branes from the NS5-branes to be large. After taking this limit, λ has a simple pole at $t = 0$, whose residue is proportional to \sqrt{u} . This can be understood as the mass parameter of the weakly gauged $SU(2)$ flavor symmetry. Remembering that there is an $SL(2, \mathbb{Z})$ symmetry acting on the 4d $\mathcal{N} = 2$ SCFT, we should be able to understand the collision of any pair of punctures in the same way. What is suggested in [5] is that we can consider the C_G of a 4d $\mathcal{N} = 2$ SCFT as coming from two three-punctured spheres coupled by an $\mathcal{N} = 2$ vector multiplet as shown in Figure 2.6, where each puncture carries an $SU(2)$ flavor symmetry. The 4d $\mathcal{N} = 2$ theory obtained by compactifying two M5-branes on the three-punctured sphere is called \mathcal{T}_2 . By using \mathcal{T}_2 as a building block, we can build a family of 4d $\mathcal{N} = 2$ SCFTs. More generally, we can obtain other building blocks by considering compactifying multiple M5-branes on a punctured sphere, including \mathcal{T}_N from the compactification of N M5-branes on a sphere

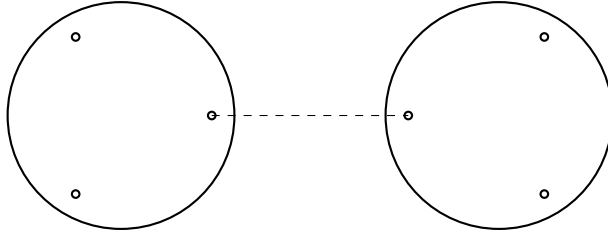


Figure 2.6: two \mathcal{T}_2 theories coupled by gauging an $SU(2)$ flavor symmetry.

with three punctures of $SU(N)$ flavor symmetry. A theory constructed out of such building blocks is called a theory of class \mathcal{S} .

2.5.2 Classification of punctures

A Gaiotto curve C_G of a 4d $\mathcal{N} = 2$ theories can have various kinds of punctures. When a Seiberg-Witten differential $\lambda = x dt$ has a singularity at a point on a Riemann surface of degree more than one, we call the point an irregular puncture. When the degree is equal to or less than one we call it a regular puncture, which are the punctures on the Gaiotto curves of SCFTs. A regular puncture can be used to couple two theories of class \mathcal{S} by gauging the flavor symmetry of a regular puncture of each theory and then couple the two by a vector multiplet.

Each regular puncture is characterized by a Young diagram. For example, the C_G of an

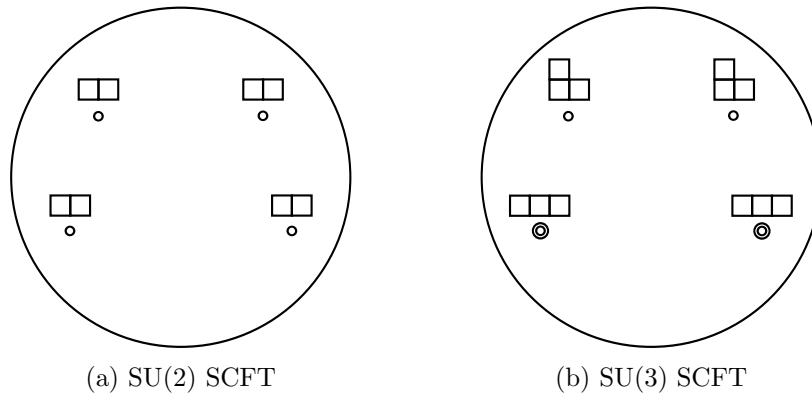


Figure 2.7: Punctures and their Young diagrams.

$SU(2)$ $N_f = 4$ SCFT has four punctures of the same type, as shown in Figure 2.7a, with all punctures having the same Young diagram. And the C_G of an $SU(3)$ $N_f = 6$ SCFT has four punctures of two different types, as shown in Figure 2.7b. We can easily expect that each puncture of the C_G of an $SU(N)$ $N_f = 2N$ SCFT can be decorated with a Young diagram of

N boxes, which represent a subgroup of the full $SU(N)$ flavor symmetry.

Chapter 3

Ramification points of a Seiberg-Witten curve

In [5] Gaiotto provided a description of 4d $\mathcal{N} = 2$ theories as coming from M5-branes wrapping punctured Riemann surfaces. In the description each puncture carries a flavor symmetry, through which two different theories of class \mathcal{S} can be coupled by gauging the flavor symmetry. Here we describe an alternative way [15] to explain the structure of the punctures from a topological consideration of Seiberg-Witten curve wrapping a Riemann surface.

In [7], it was shown that we can describe the Seiberg-Witten curve of a 4d $\mathcal{N} = 2$ supersymmetric field theory by a complex algebraic curve with various parameters of the theory as the coefficients of a polynomial that defines the curve. For example, an $\mathcal{N} = 2$ supersymmetric gauge theory with gauge group $SU(2)$ and four massless hypermultiplets is a superconformal field theory (SCFT) whose Seiberg-Witten curve C_{SW} is defined as the zero locus of

$$(t - 1)(t - t_1)v^2 - ut, \tag{3.1}$$

where (t, v) is a coordinate of $\mathbb{C}^* \times \mathbb{C}$ that contains C_{SW} , t_1 is related to the marginal gauge coupling parameter of the theory, and u is the Coulomb branch parameter.

In [5], Gaiotto showed that by wrapping N M5-branes over a Riemann surface with punctures, we can get a 4d gauge theory with $\mathcal{N} = 2$ supersymmetry. The locations of the punctures on the Riemann surface describe the gauge coupling parameters of the theory, and each puncture is characterized with a Young tableau of N boxes.

In much the same spirit, we can think of a Seiberg-Witten curve C_{SW} wrapping a Riemann surface C_{B} in the following way. For C_{SW} that (3.1) defines, consider t as a coordinate for a base C_{B} , which is a Riemann sphere in this case, and v as a coordinate normal to C_{B} . Then a projection $(v, t) \mapsto t$ gives us the required covering map from C_{SW} to C_{B} . When we generalize this geometric picture to the case of C_{SW} wrapping C_{B} N times, one natural way of thinking why each puncture has its Young tableau is to consider a puncture as a branch point of the projection π , which is now an N -sheeted covering map from C_{SW} onto C_{B} . Then the partition associated to the Young tableau of a puncture shows how the branching of the N sheets occurs there.

Now we can ask a question: for the Seiberg-Witten curve C_{SW} of a 4d $\mathcal{N} = 2$ supersymmetric gauge theory, can we identify every branch point on C_{B} of the covering map from C_{SW} to C_{B} with a puncture of [5]? To answer this question we will investigate several examples, which will lead us to the conclusion that, in addition to the branch points that are identified with the punctures, there are in general other branch points that are not directly related to the punctures. The locations of these additional branch points on C_{B} are related in general to every parameter of the theory, that is, not only gauge coupling parameters but also Coulomb branch parameters and mass parameters. This is not the case for the punctures whose positions on C_{B} are characterized by the gauge coupling parameters only. We will illustrate how these branch points can be utilized to explore interesting limits of the various parameters of the theory.

We start in Section 3.1 with SU(2) SCFT to explain how the covering map π provides the ramification of the Seiberg-Witten curve C_{SW} of the theory over a Riemann sphere C_{B} . In Section 3.2, we repeat the analysis of Section 3.1 to study SU(2) \times SU(2) SCFT, where we find a branch point that is not identified with a puncture of [5]. Its location on C_{B} depends on the Coulomb branch parameters of the theory, which enables us to investigate how the branch point behaves under various limits of the Coulomb branch parameters. In Section 3.3 we study SU(3) SCFT and how the branch points behave under the limit of the Argyres-Seiberg duality [16]. In Section 3.4, we extend the analysis to SU(3) pure gauge theory that is not a SCFT. There we will see how the branch points help us to identify interesting limits of the Coulomb branch parameters of the theory, the Argyres-Douglas fixed points [4]. In Section 3.5 we consider SU(2) gauge theories with massive hypermultiplets and illustrate how mass parameters are incorporated in the geometric description of the ramification of

C_{SW} . Appendix A contain the details of the mathematical procedures and the calculations of the main text.

3.1 SU(2) SCFT and the ramification of the Seiberg-Witten curve

The first example is a 4d $\mathcal{N} = 2$ superconformal SU(2) gauge theory. The corresponding brane configuration in type IIA string theory [7] is shown in Figure 3.1.

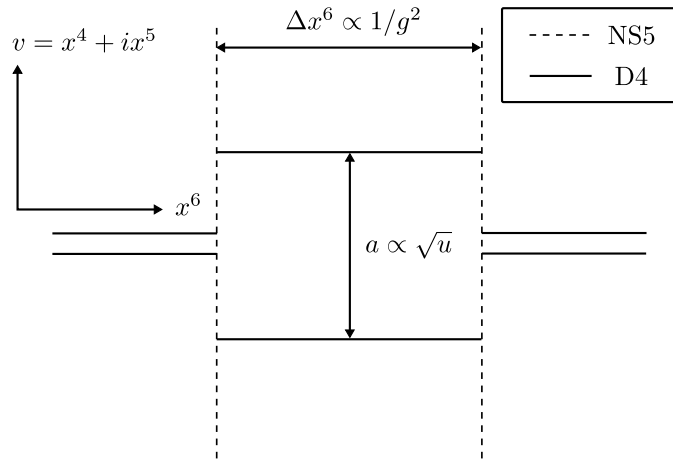


Figure 3.1: Brane configuration of SU(2) SCFT.

After the M-theory lift [7] this brane system becomes an M5-brane that fills the four dimensional spacetime, where the gauge theory lives, and wraps the Seiberg-Witten curve, which is the zero locus of

$$f(t, v) = (t - 1)(t - t_1)v^2 - ut. \quad (3.2)$$

This is a smooth, non-compact Riemann surface in \mathbb{C}^2 . Note that by construction the following four points

$$\mathcal{I} = \{(t, v) \in \mathbb{C}^2 \mid (0, 0), (1, \infty), (t_1, \infty), (\infty, 0)\},$$

are not included in C_{SW} .

It would be preferable if we can find a compact Riemann surface that describes the same

physics as C_{SW} . One natural way to compactify C_{SW} is embedding it into \mathbb{CP}^2 to get a compact algebraic curve \bar{C}_{SW} defined as the zero locus of

$$F(X, Y, Z) = (X - Z)(X - t_1 Z)Y^2 - uXZ^3,$$

which we will call \bar{C}_{SW} . The four points of \mathcal{I} are now mapped to

$$\{[X, Y, Z] \in \mathbb{CP}^2 \mid [0, 0, 1], [0, 1, 0], [1, 0, 0]\}.$$

\bar{C}_{SW} obtained this way is guaranteed to be smooth except at the points we added for the compactification, where it can have singularities [17]. Indeed \bar{C}_{SW} is singular at $[0, 1, 0]$ and $[1, 0, 0]$, which implies that \bar{C}_{SW} is not a Riemann surface. The singularity at $[0, 1, 0]$ corresponds to having two different tangents there. The other singularity at $[1, 0, 0]$ corresponds to a cusp.

Smoothing out a singular algebraic curve to find the corresponding Riemann surface can be done by normalization [17, 18]. This means finding a smooth Riemann surface \mathcal{C}_{SW} and a holomorphic map $\sigma : \mathcal{C}_{\text{SW}} \rightarrow \bar{C}_{\text{SW}}$. Appendix A.1 illustrates how we can get a normalization of a singular curve. After the normalization we can find, for every point $s_i \in \mathcal{C}_{\text{SW}}$, the local normalization map

$$\sigma_{s_i} : \mathcal{N}_{s_i} \rightarrow \mathbb{CP}^2, \quad s \mapsto [X(s), Y(s), Z(s)],$$

where $s \in \mathbb{C}$ is a local coordinate such that $s_i = 0$. Figure 3.2 illustrates how we get from the noncompact Seiberg-Witten curve C_{SW} its compactification \bar{C}_{SW} and the compact Riemann surface \mathcal{C}_{SW} , together the relations among them. Here we use the normalization map σ to build a map $\phi : \mathcal{C}_{\text{SW}} \rightarrow \{C_{\text{SW}} \cup \mathcal{I}\}$, whose local description near a point $s_i \in \mathcal{C}_{\text{SW}}$ is

$$\phi_{s_i} : \mathcal{N}_{s_i} \rightarrow \mathbb{C}^2, \quad s \mapsto (t(s), v(s)) = \left(\frac{X(s)}{Z(s)}, \frac{Y(s)}{Z(s)} \right),$$

where $s \in \mathbb{C}$ is a local coordinate such that $s_i = 0$.

The compactification of a Seiberg-Witten curve to a Riemann surface is discussed previously in [7]. It is also mentioned in [19] from the viewpoint of seeing a Seiberg-Witten

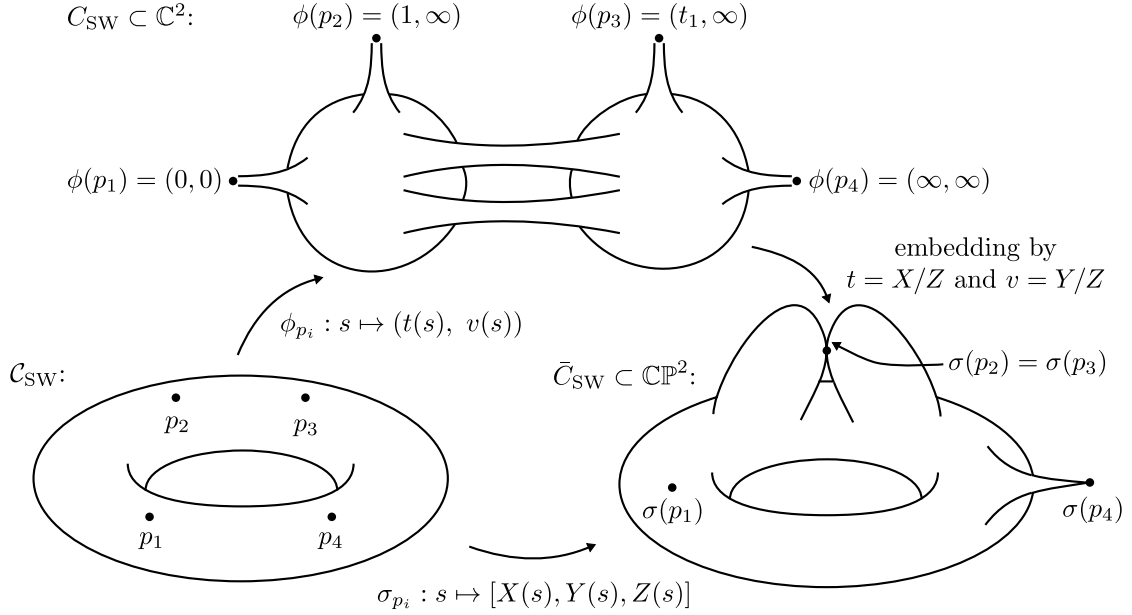


Figure 3.2: Schematic description of the compactification and the normalization of a Seiberg-Witten curve.

curve as a cycle embedded in the cotangent bundle T^*C_B of the base C_B .

Whether \mathcal{C}_{SW} gives the same physics as C_{SW} is a challenging question, whose answer will depend on what we mean by “the same physics.” For example, it is argued in [7] and is illustrated with great detail in [19] that the the low-energy effective theory of an M5-brane wrapping C_{SW} is described by the Jacobian of \mathcal{C}_{SW} . Extending those arguments is a very intriguing task, but we will not try to address it here.

Now that we have a smooth Riemann surface \mathcal{C}_{SW} , we want to wrap it over a Riemann surface, C_B . Note that for the current example we want C_B to be a Riemann sphere, or \mathbb{CP}^1 , because the corresponding 4d gauge theory comes from a linear quiver brane configuration [5]. To implement the wrapping, or the projection, from \mathcal{C}_{SW} to \mathbb{CP}^1 , we use ϕ to define a meromorphic function π on \mathcal{C}_{SW} such that its restriction to the neighborhood of $s_i \in \mathcal{C}_{\text{SW}}$ is

$$\pi_{s_i}(s) = t(s) = \frac{X(s)}{Z(s)},$$

where $t(s)$ is the value of the t -coordinate of $\{C_{\text{SW}} \cup \mathcal{I}\}$ at $\phi(s)$ and therefore has the range of \mathbb{CP}^1 .¹ This π is in general a many-to-one (two-to-one for the current example) mapping,

¹Note that $t : \mathcal{C}_{\text{SW}} \rightarrow \mathbb{CP}^1$ is well-defined over \mathcal{C}_{SW} , although $X/Z : \bar{\mathcal{C}}_{\text{SW}} \rightarrow \mathbb{CP}^1$ is not well-defined

therefore it realizes the required wrapping of \mathcal{C}_{SW} , or its ramification, over \mathbb{CP}^1 . Figure 3.3 summarizes the whole procedure of getting from \mathcal{C}_{SW} the normalization $\bar{\mathcal{C}}_{\text{SW}}$ and finding the ramification of \mathcal{C}_{SW} over C_{B} .

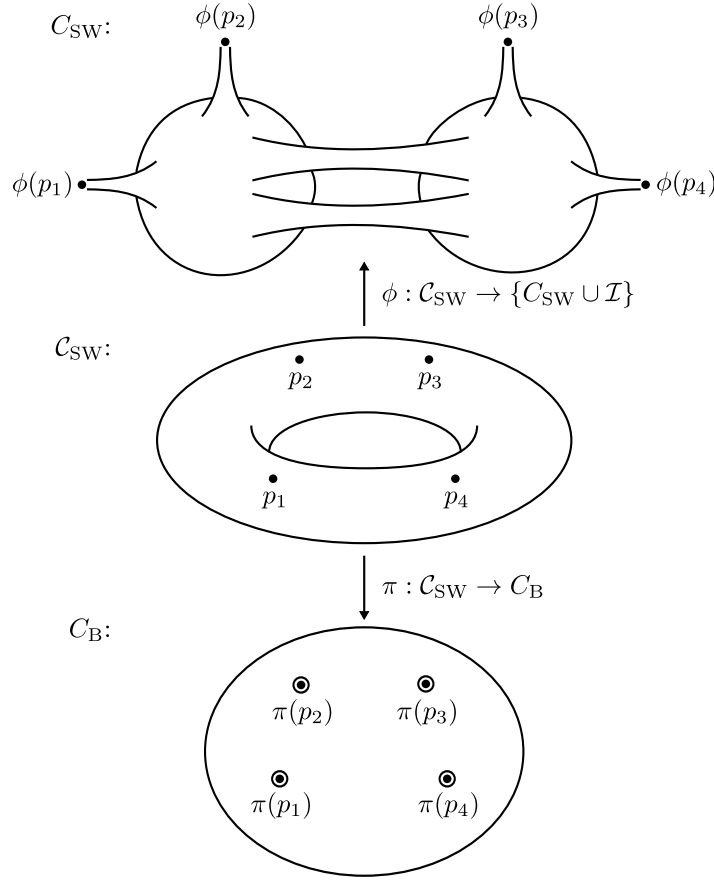


Figure 3.3: Summary of how to obtain \mathcal{C}_{SW} and C_{B} from \mathcal{C}_{SW} .

To analyze the ramification it is convenient to introduce a ramification divisor R_{π} [18],

$$R_{\pi} = \sum_{s \in \mathcal{C}_{\text{SW}}} (\nu_s(\pi) - 1)[s] = \sum_i (\nu_{s_i}(\pi) - 1)[s_i].$$

Here $\nu_s(\pi) \in \mathbb{Z}$ is the ramification index of $s \in \mathcal{C}_{\text{SW}}$, $s_i \in \mathcal{C}_{\text{SW}}$ is a point where $\nu_{s_i}(\pi) > 1$, and $[s_i]$ is the corresponding divisor² of \mathcal{C}_{SW} . In colloquial language, having a ramification at $[0, 1, 0] \in \bar{\mathcal{C}}_{\text{SW}}$ because it maps the point on $\bar{\mathcal{C}}_{\text{SW}}$ to two different points on \mathbb{CP}^1 , 1 and t_1 . This ill-definedness arises because we compactify \mathcal{C}_{SW} by embedding it into \mathbb{CP}^2 , which maps two different points on \mathcal{C}_{SW} , $(1, \infty)$ and (t_1, ∞) , to one point in \mathbb{CP}^2 , $[0, 1, 0]$, and therefore is the artifact of our embedding scheme. Normalization separates the two and resolves this difficulty, after which t is a well-defined function over all \mathcal{C}_{SW} .

²A divisor is a formal representation of a complex-one-codimension object, a point in this case.

index $\nu_s(\pi)$ at $s \in \mathcal{C}_{\text{SW}}$ means that $\nu_s(\pi)$ sheets over C_{B} come together at $\pi(s)$. When $\nu_s(\pi) > 1$ we say s is a ramification point on \mathcal{C}_{SW} , $\pi(s)$ is a branch point on C_{B} , and $\pi : \mathcal{C}_{\text{SW}} \rightarrow C_{\text{B}}$ has a ramification at $\pi(s)$.

The Riemann-Hurwitz formula [18] provides a relation between π , R_π , and the genus of \mathcal{C}_{SW} , $g(\mathcal{C}_{\text{SW}})$.

$$\chi_{\mathcal{C}_{\text{SW}}} = \deg(\pi) \cdot \chi_{\mathbb{CP}^1} - \deg(R_\pi) \Leftrightarrow \deg(R_\pi) = 2(g(\mathcal{C}_{\text{SW}}) + \deg(\pi) - 1). \quad (3.3)$$

Here χ_C is the Euler characteristic of C , and $\deg(\pi)$ is the number of intersections of \mathcal{C}_{SW} and $\pi^{-1}(t_0)$ for a general $t_0 \in \mathbb{CP}^1$. In the current example where \mathcal{C}_{SW} is the zero locus of (3.2), it is easy to see that $\deg(\pi) = 2$ because the equation is quadratic in v . Using this Riemann-Hurwitz formula, we can check if we have found all ramification points that are needed to describe the wrapping of \mathcal{C}_{SW} over C_{B} .

What we want to know is where the ramification points of \mathcal{C}_{SW} are and what ramification indices they have. We will try to guess where they are by investigating every point $s \in \mathcal{C}_{\text{SW}}$ that might have a nontrivial behavior under π . The candidates for such points are

- (1) $\{p_i \in \mathcal{C}_{\text{SW}} \mid \phi(p_i) \in \mathcal{I}\}$,
- (2) $\{q_i \in \mathcal{C}_{\text{SW}} \mid dt(q_i) = 0\} \Leftrightarrow \{q_i \in \mathcal{C}_{\text{SW}} \mid (\partial f / \partial v)(t(q_i), v(q_i)) = 0\}$.

We check the ramification of the points of (1) because at $t(p_i)$ some branches of $v(t)$ meet “at infinity.”³ Note that $\phi(p_i) = (t(p_i), v(p_i))$ is a point where $\lambda = \frac{v}{t} dt$, the Seiberg-Witten differential [8, 9, 10], is singular, and therefore each $\pi(p_i)$ corresponds to a puncture of [5]. The reason why the points of (2) correspond to nontrivial ramifications can be illustrated as in Figure 3.4, which shows the real slice of \mathcal{C}_{SW} near $\phi(q_i) = (t(q_i), v(q_i))$ when two branches of $v(t)$ meet each other at $\phi(q_i)$.

Using a local normalization map defined around each of these points, we can find the explicit form of π at the neighborhood of the point. If π is just a nice one-to-one mapping near the point, then we can forget about the point. But if π shows a nontrivial ramification at the point, we can describe the ramification of \mathcal{C}_{SW} near the point explicitly and calculate its ramification index.

³This qualification is because it is not true in t -coordinate. For example, $\phi(p_1)$ is not at infinity, because the t -coordinate is in fact the exponentiation of the spacetime coordinate, $t = \exp(-(x^6 + ix^{10}))$ [7]. By “at infinity” we imply that the point is at infinity of the 10d or 11d spacetime that contains the brane configuration.

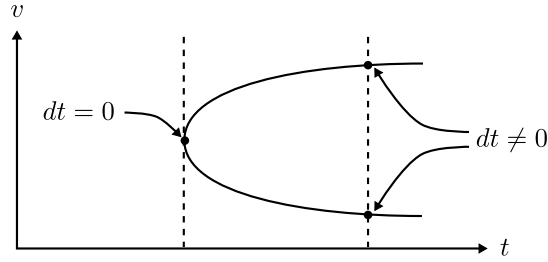


Figure 3.4: Why a nontrivial ramification occurs at $dt = 0$.

To represent what ramification structure each branch point on C_B has, we will decorate it with a Young tableau, which will be constructed in the following way: start with $N = \deg(\pi)$ boxes. Collect the ramification points that are mapped to the same branch point, and put as many boxes as the ramification index of a ramification point in a row. Repeat this to form a row of boxes for each ramification point. Then stack these rows of boxes in an appropriate manner. If we run out of boxes then we are done. If not, then each remaining box is a row by itself, and we stack them too. Figure 3.5 shows several examples of Young tableaux constructed in this way for various ramification structures.

For the example we are considering now, (1) gives us $\{p_1, \dots, p_4\}$ such that

$$\phi(p_1) = (0, 0), \quad \phi(p_2) = (1, \infty), \quad \phi(p_3) = (t_1, \infty), \quad \phi(p_4) = (\infty, 0),$$

and (2) does not give any new point other than (1) provides, so we have $\{p_i\}$ as the candidates to check if C_{SW} has nontrivial ramifications at the points. The local normalization near each p_i is calculated in Appendix A.2.1. From the local normalizations we get π , which maps $\{p_i\}$ to

$$\{\pi(p_1) = 0, \pi(p_2) = 1, \pi(p_3) = t_1, \pi(p_4) = \infty\}.$$

The ramification divisor of π is also calculated in Appendix A.2.1,

$$R_\pi = 1 \cdot [p_1] + 1 \cdot [p_2] + 1 \cdot [p_3] + 1 \cdot [p_4], \quad (3.4)$$

which shows that every p_i has a nontrivial ramification index of 2, and this is consistent

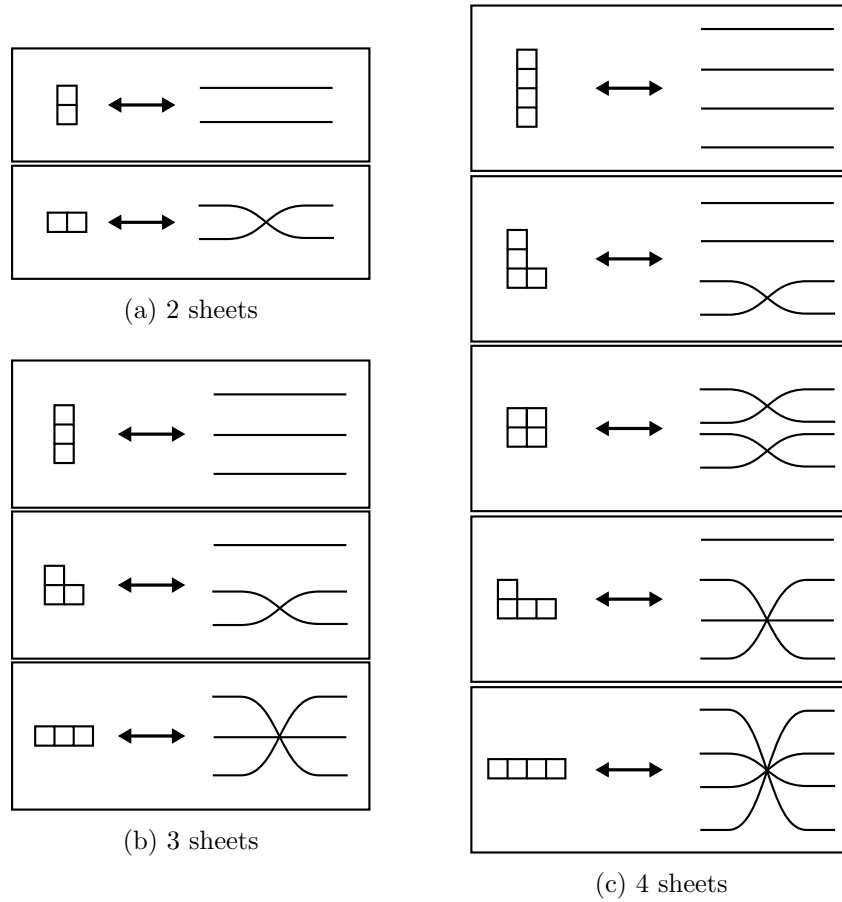


Figure 3.5: Young tableaux and the corresponding ramification structures.

with the Riemann-Hurwitz formula, (3.3),

$$\deg(R_\pi) = 1 + 1 + 1 + 1 = 4 = 2(g(\mathcal{C}_{\text{SW}}) + \deg(\pi) - 1),$$

considering $\deg(\pi) = 2$ and $g(\mathcal{C}_{\text{SW}}) = 1$. In the current example, where \mathcal{C}_{SW} is an elliptic curve, the result of (3.4) can be expected because an elliptic curve, when considered as a 2-sheeted cover over \mathbb{CP}^1 , has four ramification points of index 2. Figure 3.6 shows how π maps R_π of \mathcal{C}_{SW} to the branch points of C_B . For this example, all of the branch points are

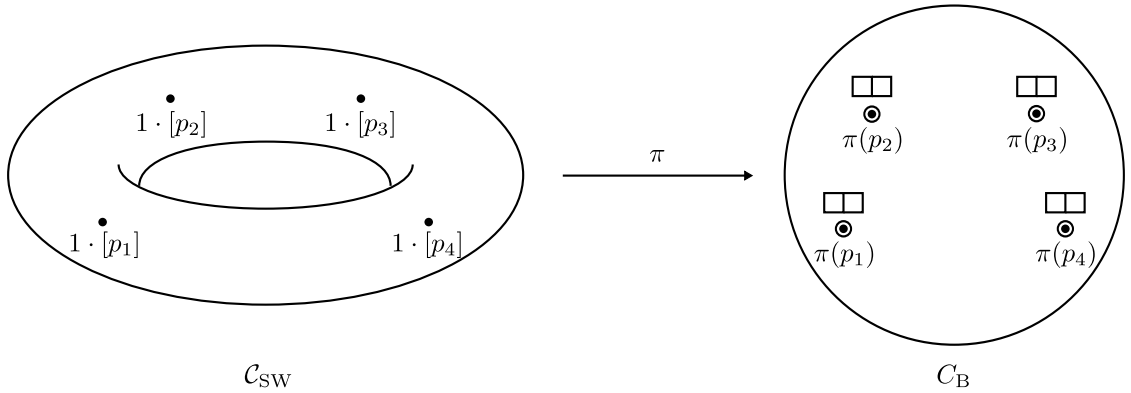


Figure 3.6: \mathcal{C}_{SW} and C_B for $\text{SU}(2)$ SCFT.

the images of the points $\{p_i\}$, therefore each branch point corresponds to a puncture of [5]. This example provides a geometric explanation of why each puncture can be labeled with its Young tableau.

The wrapping of the noncompact Seiberg-Witten curve C_{SW} over C_B is described by the composition of $\phi^{-1} : C_{\text{SW}} \rightarrow \mathcal{C}_{\text{SW}} \setminus \{p_i\}$ and π ,

$$\pi \circ \phi^{-1} : C_{\text{SW}} \rightarrow C_B \setminus \{\pi(p_i)\}, (t, v) \mapsto t.$$

Note that the noncompact Seiberg-Witten curve C_{SW} does not contain $\{\phi(p_i)\} = \mathcal{I}$. Therefore C_{SW} has no ramification point, unlike the compact Riemann surface \mathcal{C}_{SW} . That is, the two branches of C_{SW} only meet “at infinity,” and all branch points on C_B , $\{\pi(p_i)\}$, are from the points “at infinity.”

After embedding C_{SW} into \mathbb{CP}^2 , the Seiberg-Witten differential form λ ,

$$\lambda = \frac{v}{t} dt,$$

which is a meromorphic 1-form on C_{SW} , becomes⁴

$$\lambda = \frac{Y}{X} d\left(\frac{X}{Z}\right),$$

which defines a meromorphic 1-form on \bar{C}_{SW} . We pull λ back to $\omega = \sigma^*(\lambda)$, which defines a meromorphic 1-form on C_{SW} and therefore should satisfy the Poincaré-Hopf theorem [18]

$$\deg[(\omega)] = 2(g(C_{\text{SW}}) - 1), \quad (3.5)$$

where (ω) is a divisor of ω on C_{SW} , which is defined as

$$(\omega) = \sum_{s \in C_{\text{SW}}} \nu_s(\omega)[s],$$

where $\nu_s(\omega) \in \mathbb{Z}$ is the order⁵ of ω at s .

We want to see if (3.5) holds for this example as a consistency check. In order to do that, we need to find out every $s \in C_{\text{SW}}$ that has a nonzero value of $\nu_s(\omega)$. Considering that ω is a pullback of λ , the candidates for such points are

- (1) $\{p_i \in C_{\text{SW}} \mid \phi(p_i) \in \mathcal{I}\}$,
- (2) $\{q_i \in C_{\text{SW}} \mid dt(q_i) = 0\} \Leftrightarrow \{q_i \in C_{\text{SW}} \mid (\partial f / \partial v)(t(q_i), v(q_i)) = 0\}$,
- (3) $\{r_i \in C_{\text{SW}} \mid v(r_i) = 0\}$.

We check (1) because λ is singular at $\phi(p_i)$ and therefore ω may have a pole at p_i . We also check (2) and (3) because λ vanishes at $\phi(q_i)$ and $\phi(r_i)$ and therefore ω may have a zero at q_i or r_i . For this example (2) and (3) do not give us any additional point other than the points from (1). Therefore the candidates are $\{p_1, \dots, p_4\}$, the same set of points we have met when calculating R_π . Using the local normalizations near these points described

⁴Whether this embedding of λ is justifiable is a part of the question that the embedding of C_{SW} into \mathbb{CP}^2 gives the same physics as C_{SW} does or not.

⁵When ω has a pole at s , the pole is of order $-\nu_s(\omega)$; when ω has a zero at s , the zero is of order $\nu_s(\omega)$; otherwise $\nu_s(\omega) = 0$.

in Appendix A.2.1, we get

$$(\omega) = 0,$$

which means ω has neither zero nor pole over \mathcal{C}_{SW} . This is an expected result, since we can find a globally well-defined coordinate z of the elliptic curve \mathcal{C}_{SW} such that $\sigma^*(\lambda) = dz$.

The result is consistent with the Poincaré-Hopf theorem, (3.5),

$$\deg[(\omega)] = 0 = 2(g(\mathcal{C}_{\text{SW}}) - 1),$$

considering $g(\mathcal{C}_{\text{SW}}) = 1$.

3.2 $\text{SU}(2) \times \text{SU}(2)$ SCFT and the ramification point

In Section 3.1 we have studied the Seiberg-Witten curve of a 4d $\mathcal{N} = 2$ $\text{SU}(2)$ SCFT to identify how the wrapping of the curve over a Riemann sphere can be described by a covering map. In this section we apply the same analysis to the Seiberg-Witten curve of a 4d $\mathcal{N} = 2$ $\text{SU}(2) \times \text{SU}(2)$ SCFT. From this example, we will learn that on the curve there is a ramification point whose image under the covering map cannot be identified with one of the punctures of [5].

The brane configuration of Figure 3.7 gives a 4d $\mathcal{N} = 2$ $\text{SU}(2) \times \text{SU}(2)$ SCFT. The

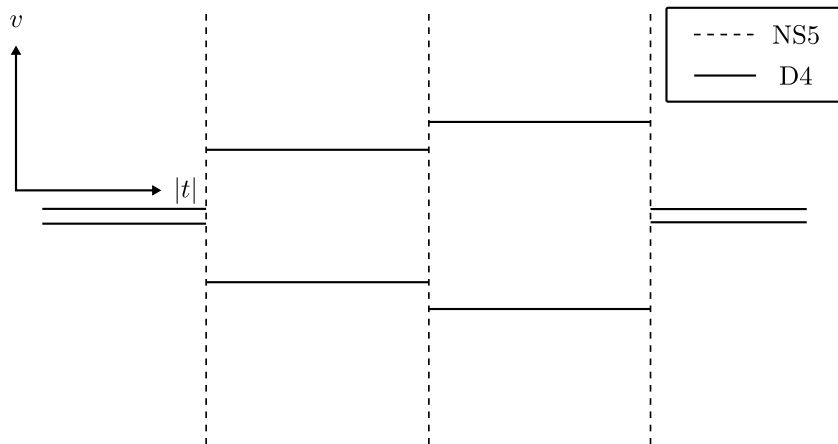


Figure 3.7: Brane configuration of $\text{SU}(2) \times \text{SU}(2)$ SCFT.

corresponding Seiberg-Witten curve C_{SW} is the zero locus of

$$f(t, v) = (t - 1)(t - t_1)(t - t_2)v^2 - u_1t^2 - u_2t. \quad (3.6)$$

Considering a normalization $\sigma : C_{\text{SW}} \rightarrow \bar{C}_{\text{SW}}$ and a meromorphic function $\pi : C_{\text{SW}} \rightarrow \mathbb{CP}^1$, we can introduce a ramification divisor $R_\pi = \sum_s (\nu_s(\pi) - 1)[s]$. Nontrivial ramifications may occur at

(1) $\{p_i \in C_{\text{SW}}\}$, where $\{\phi(p_i)\}$ are the points we add to C_{SW} to compactify it,

(2) $\{q_i \in C_{\text{SW}} \mid dt(q_i) = 0\} \Leftrightarrow \{q_i \in C_{\text{SW}} \mid (\partial f / \partial v)(t(q_i), v(q_i)) = 0\}$.

(1) gives us $\{p_1, \dots, p_5\}$ such that

$$\phi(p_1) = (0, 0), \quad \phi(p_2) = (1, \infty), \quad \phi(p_3) = (t_1, \infty), \quad \phi(p_4) = (t_2, \infty), \quad \phi(p_5) = (\infty, 0),$$

and from (2) we get $\{q\}$ such that

$$\phi(q) = (\rho, 0), \quad \rho = -u_2/u_1.$$

Using the local normalizations calculated in Appendix A.2.2, we get

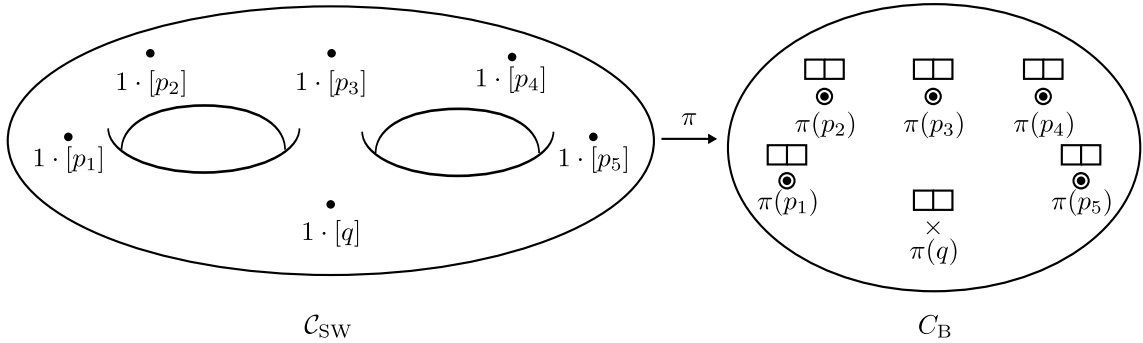
$$R_\pi = 1 \cdot [p_1] + 1 \cdot [p_2] + 1 \cdot [p_3] + 1 \cdot [p_4] + 1 \cdot [p_5] + 1 \cdot [q],$$

and

$$\deg(R_\pi) = 1 + 1 + 1 + 1 + 1 + 1 = 6,$$

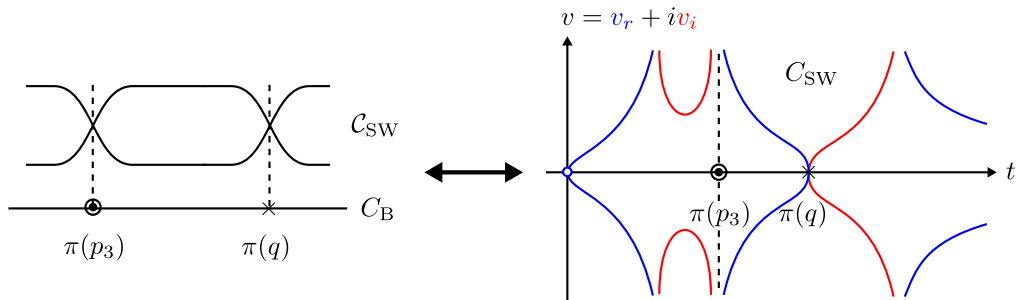
which is consistent with the Riemann-Hurwitz formula, (3.3), considering $\deg(\pi) = 2$ and $g(C_{\text{SW}}) = 2$. Figure 3.8 shows how π maps C_{SW} with its ramification points to C_{B} with its branch points.

Again R_π has a divisor $[p_i]$ whose image under π can be identified with a puncture of [5]. However, R_π also contains $[q]$, which means that ramification occurs also at q . The location of $\pi(q)$ on C_{B} depends on the Coulomb branch parameters u_1 and u_2 , unlike $\{\pi(p_i)\}$ whose locations depend only on the gauge coupling parameters t_1 and t_2 . In Figure 3.8 we denoted $\pi(q)$ with a symbol different from that of $\{\pi(p_i)\}$ to distinguish between the two. In this

Figure 3.8: \mathcal{C}_{SW} and \mathcal{C}_{B} for $\text{SU}(2) \times \text{SU}(2)$ SCFT.

example, two sheets are coming together at both $\{\pi(p_i)\}$ and $\pi(q)$, and therefore each of them has the same Young tableau corresponding to the ramification structure.

However, note that the noncompact Seiberg-Witten curve \mathcal{C}_{SW} does not contain $\{\phi(p_i)\}$ but contains $\phi(q)$ only, therefore it is the only ramification point that exists in \mathcal{C}_{SW} . That is, the branch point $\pi(q)$ comes from the ramification point of \mathcal{C}_{SW} , whereas the other branch points $\{\pi(p_i)\}$ that are identified with the punctures are from the points “at infinity.” Figure 3.9 shows the schematic cross-section of the compact Riemann surface \mathcal{C}_{SW} near p_3

Figure 3.9: Two branch points of different kinds: $\pi(p_3)$ from a point at $v = \infty$, $\pi(q)$ from the ramification point of \mathcal{C}_{SW} .

and q on the left side, and the real (and imaginary) slice of the noncompact Seiberg-Witten curve \mathcal{C}_{SW} on the right side. This illustrates the difference between the two kinds of branch points.

Taking various limits of the Coulomb branch parameters corresponds to moving $\pi(q)$ on \mathcal{C}_{B} in various ways, as shown in Figure 3.10. When $\pi(q)$ is infinitesimally away from one of $\{\pi(p_i)\}$, imagine cutting out a part of the Seiberg-Witten curve around the preimages of the two branch points. As there is no monodromy of $v(t)$ when going around a route that

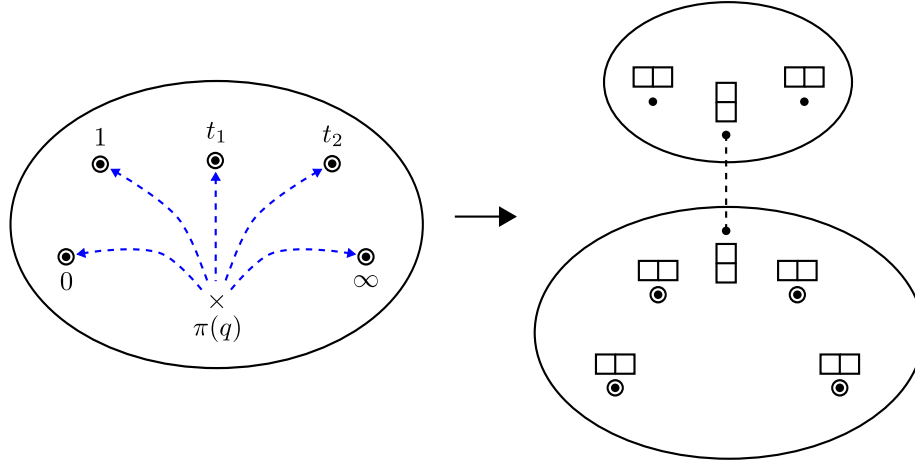


Figure 3.10: Branch point $\pi(q)$ under various limits of Coulomb branch parameters.

encircles the two branch points, we can fill the excised area topologically with two points, the result of which is shown in the lower right side of Figure 3.10. This corresponds to the Seiberg-Witten curve of $SU(2)$ SCFT that we have investigated in Section 3.1. The excised part of the Seiberg-Witten curve separates itself from the rest of the curve to form another curve which has the topology of a sphere. This is shown in the upper right side of Figure 3.10, where we represented only the ramification structure of each branch point. This can also be checked by taking the limits of the Coulomb branch parameters of (3.6), which will result in a reducible curve with two components, one being the curve of $SU(2)$ SCFT and the other a Riemann sphere.

Now we repeat the same analysis of the Seiberg-Witten differential $\lambda = \frac{v}{t} dt$ that we did in Section 3.1. The candidates for the points on \mathcal{C}_{SW} where ω has nonzero order are

- (1) $\{p_i \in \mathcal{C}_{SW}\}$, where $\{\phi(p_i)\}$ are the points we add to \mathcal{C}_{SW} to compactify it,
- (2) $\{q_i \in \mathcal{C}_{SW} | dt(q_i) = 0\} \Leftrightarrow \{q_i \in \mathcal{C}_{SW} | (\partial f / \partial v)(t(q_i), v(q_i)) = 0\}$,
- (3) $\{r_i \in \mathcal{C}_{SW} | v(r_i) = 0\}$.

From (3) we don't get any new point other than the points from (1) and (2) for this example, so the candidates are $\{p_1, \dots, p_5\}$ and $\{q\}$. Again we can analyze how ω behaves near those points by using the local normalizations calculated in Appendix A.2.2, which gives

$$(\omega) = 2 \cdot [q],$$

and

$$\deg[(\omega)] = 2 = 2(g(\mathcal{C}_{\text{SW}}) - 1).$$

This result is consistent with the Poincaré-Hopf theorem, (3.5), considering $g(\mathcal{C}_{\text{SW}}) = 2$.

3.3 SU(3) SCFT and Argyres-Seiberg duality

In Section 3.2 we have found a branch point on C_B that comes from the ramification point of the Seiberg-Witten curve and cannot be identified with a puncture. The location of this branch point on C_B depends on the Coulomb branch parameters, which enables us to use it as a tool to describe various limits of the parameters. In this section, we do the same analysis for the example of a 4d $\mathcal{N} = 2$ SU(3) SCFT to find the branch points from the ramification points of its Seiberg-Witten curve, this time their locations on C_B depending on both the gauge coupling parameter and the Coulomb branch parameters. And we will see how these branch points help us to illustrate the interesting limit of the theory studied by Argyres and Seiberg [16].

The starting point is a 4d $\mathcal{N} = 2$ SU(3) SCFT associated to the brane configuration of Figure 3.11.

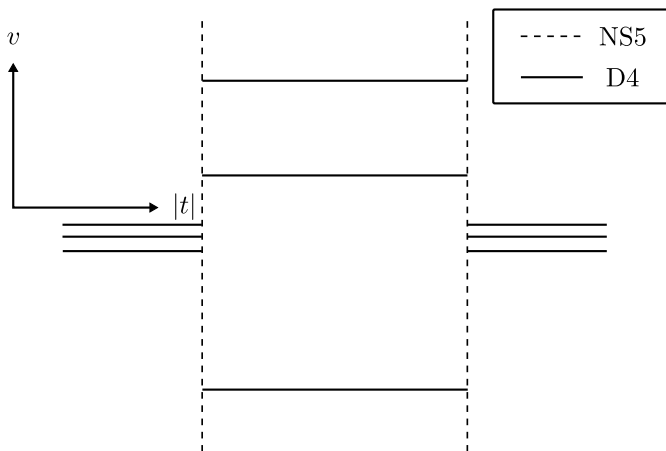


Figure 3.11: Brane configuration of SU(3) SCFT.

The corresponding Seiberg-Witten curve C_{SW} is the zero locus of

$$f(t, v) = (t - 1)(t - t_1)v^3 - u_2tv - u_3t. \quad (3.7)$$

Considering a normalization $\sigma : C_{\text{SW}} \rightarrow \bar{C}_{\text{SW}}$ and a meromorphic function $\pi : C_{\text{SW}} \rightarrow \mathbb{CP}^1$, we can introduce a ramification divisor $R_\pi = \sum_s (\nu_s(\pi) - 1)[s]$. Nontrivial ramifications may occur at

(1) $\{p_i \in C_{\text{SW}}\}$, where $\{\phi(p_i)\}$ are the points we add to C_{SW} to compactify it,

(2) $\{q_i \in C_{\text{SW}} \mid dt(q_i) = 0\} \Leftrightarrow \{q_i \in C_{\text{SW}} \mid (\partial f / \partial v)(t(q_i), v(q_i)) = 0\}$.

From (1) we get $\{p_1, \dots, p_4\}$ such that

$$\phi(p_1) = (0, 0), \quad \phi(p_2) = (1, \infty), \quad \phi(p_3) = (t_1, \infty), \quad \phi(p_4) = (\infty, 0).$$

(2) gives us $\{q_+, q_-\}$ such that

$$\phi(q_\pm) = (t_\pm, v_0),$$

where

$$v_0 = -\frac{(u_3/2)}{(u_2/3)}$$

and t_\pm are the two roots of $f(t, v_0) = 0$,

$$t_\pm = \frac{1 + t_1 + \rho}{2} \pm \sqrt{\left(\frac{1 + t_1 + \rho}{2}\right)^2 - t_1}, \quad \rho = \frac{(u_2/3)^3}{(u_3/2)^2}.$$

Calculations for the local normalizations near the points are given in Appendix [A.2.3](#), from which we get the ramification divisor of π as

$$R_\pi = 2 \cdot [p_1] + 1 \cdot [p_2] + 1 \cdot [p_3] + 2 \cdot [p_4] + 1 \cdot [q_+] + 1 \cdot [q_-],$$

and this satisfies

$$\deg(R_\pi) = 2 + 1 + 1 + 2 + 1 + 1 = 8 = 2(g(C_{\text{SW}}) + \deg(\pi) - 1),$$

which is consistent with the Riemann-Hurwitz formula, (3.3), considering $\deg(\pi) = 3$ and $g(\mathcal{C}_{\text{SW}}) = 2$. Figure 3.12 shows how π works.

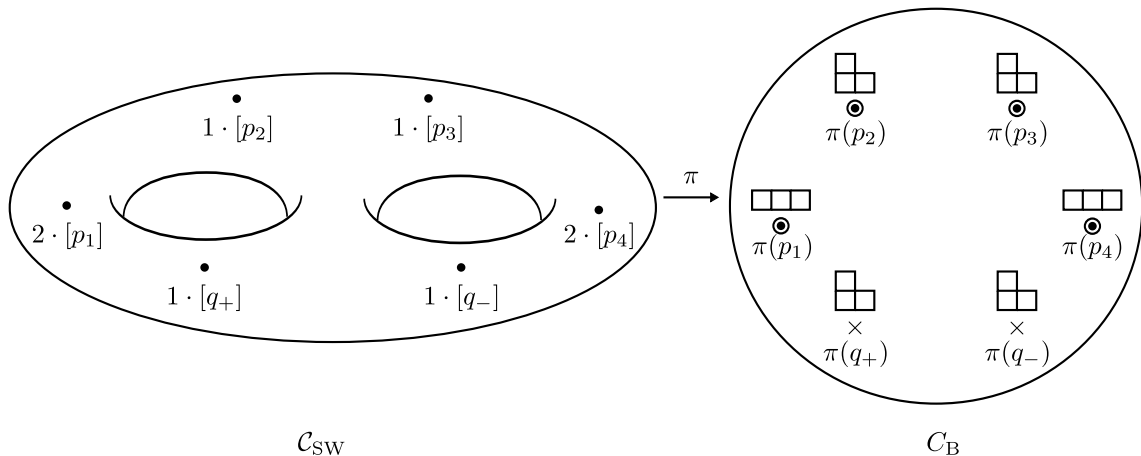


Figure 3.12: \mathcal{C}_{SW} and \mathcal{C}_{B} for SU(3) SCFT.

Considering that π is in general a three-to-one mapping, the fact that R_π has degree 2 at p_1 implies that the three sheets are coming together at $\pi(p_1)$, which corresponds to a Young tableau $\square\square\square$. And R_π having degree 1 at p_2 is translated into only two out of three sheets coming together at $\pi(p_2)$, which corresponds to a Young tableau $\begin{smallmatrix} \square & \square \\ \square & \square \end{smallmatrix}$. These $\{\pi(p_i)\}$ are identified with the punctures of [5].⁶

However, R_π also contains $[q_\pm]$, which means that ramifications of \mathcal{C}_{SW} occur also at q_\pm . These are the points of \mathcal{C}_{SW} where $dt = 0$ along \mathcal{C}_{SW} . The locations of $\pi(q_\pm)$ on \mathcal{C}_{B} depend on both the gauge coupling parameter t_1 and the Coulomb branch parameters u_2 and u_3 , unlike $\{\pi(p_i)\}$ whose locations depend only on t_1 . Therefore $\{\pi(q_\pm)\}$ are the branch points that are not identified with the punctures.

Again note that $\{\pi(q_\pm)\}$ are distinguished from $\{\pi(p_i)\}$ in that they are from the ramification points of the noncompact Seiberg-Witten curve \mathcal{C}_{SW} . That is, $\{\phi(q_\pm)\}$ are the only ramification points of \mathcal{C}_{SW} , whereas $\{\phi(p_i)\}$ are the points “at infinity.”

To see how the Argyres-Seiberg duality [16] is illustrated by the branch points, we take the corresponding limits for the Coulomb branch parameters and the gauge coupling parameter. When we take $u_2 \rightarrow 0$, $\pi(q_+)$ and $\pi(q_-)$ move toward $\pi(p_2) = 1$ and $\pi(p_3) = t_1$,

⁶Note that at $t = \pi(p_2)$ and at $t = \pi(p_3)$ only two among the three branches have the divergent $v(t)$, and therefore λ is divergent along only the two branches. This means that our analysis corresponds to that of [5] before making a shift of v . In [5] every branch has the divergence after the shift in v so that the flavor symmetry at the puncture is evident. Here we prefer not to shift v so that we can analyze the Seiberg-Witten curve as an algebraic curve studied in [7].

respectively. In addition we take the limit of $t_1 \rightarrow 1$, and the four branch points come together. Figure 3.13 shows the behavior of the branch points under the limit of the parameters. When we are near the limit of $u_2 = 0$ and $t_1 = 1$, the four branch points

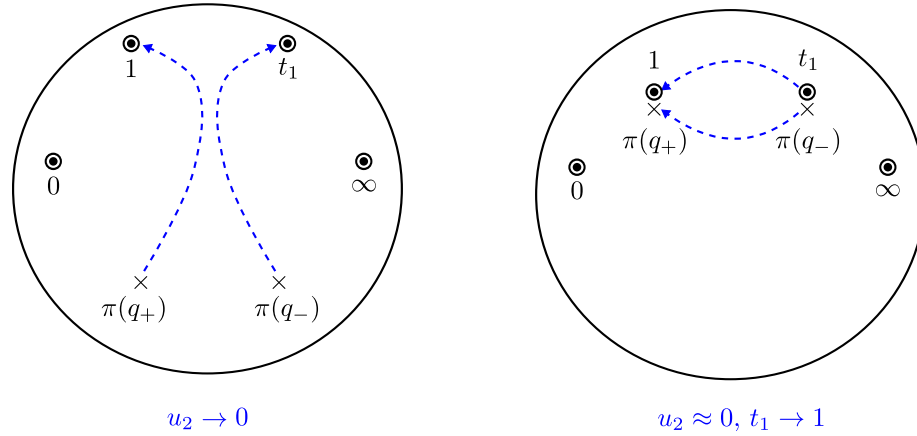


Figure 3.13: Behaviors of the branch points under the limit $u_2 \rightarrow 0$ and $t_1 \rightarrow 1$.

become infinitesimally separated from one another and we can imagine cutting out a part of the Seiberg-Witten curve around the preimages of the four branch points, separating the original curve into two parts. As the monodromy of $v(t)$ around the four branch points corresponds to a point of ramification index 3, we can see that one part becomes a genus 1 curve and the other becomes another genus 1 curve, considering the ramification structure of each of them. Figure 3.14 illustrates this. The genus 1 curve with three branch points of

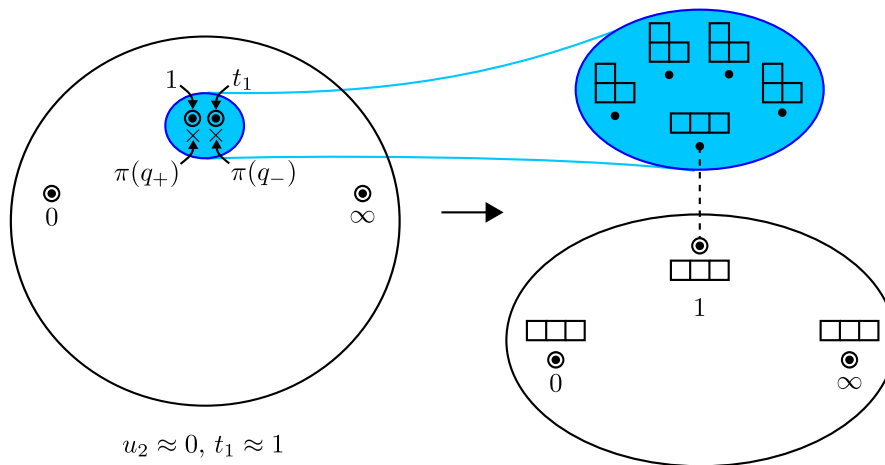


Figure 3.14: Appearance of E_6 curve under the limit $u_2 \rightarrow 0$ and $t_1 \rightarrow 1$.

ramification index 3 corresponds to the zero locus of

$$(t-1)^2 v^3 - u_3 t,$$

which is from (3.7) by setting $t_1 = 1$ and $u_2 = 0$. This curve can be identified with the Seiberg-Witten curve of E_6 theory [5, 16]. The other genus 1 curve is a small torus, which reminds us of the weakly gauged $SU(2)$ theory coupled to the E_6 theory that appears in [5, 16].

When we take $u_3 \rightarrow 0$ limit, $\pi(q_+)$ and $\pi(q_-)$ move toward $\pi(p_1) = 0$ and $\pi(p_4) = \infty$, respectively. The collision of $\pi(q_+)$ with $\pi(p_1)$ partially unravels the ramification over the two branch points, which results in one branch point with the corresponding ramification point having index 2, and the third sheet falling apart from the branch point. The same thing happens at $t = \infty$, so the result of the limit is a reducible curve with two components, one component being the same $SU(2)$ SCFT curve that we have investigated in Section 3.1 and the other a Riemann sphere. This can also be checked by setting $u_3 = 0$ in (3.7), which gives us an $SU(2)$ SCFT curve and a Riemann sphere. Figure 3.15 illustrates the limit and the partial unraveling of the ramification.

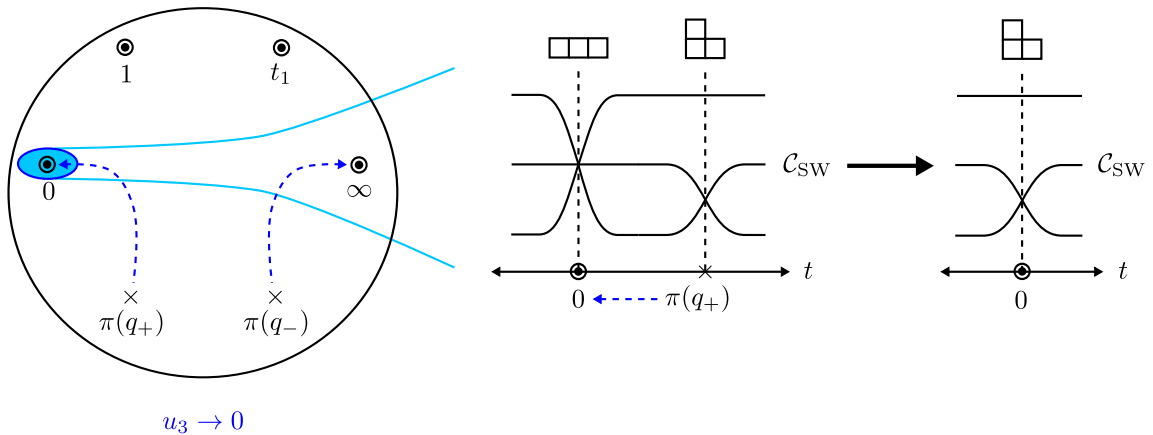


Figure 3.15: Behaviors of the branch points under the limit $u_3 \rightarrow 0$.

Let's proceed to the calculation of $(\omega) = \sum_s \nu_s(\omega)[s]$. The candidates for the points on \mathcal{C}_{SW} where ω has nonzero order are

- (1) $\{p_i \in \mathcal{C}_{\text{SW}}\}$, where $\{\phi(p_i)\}$ are the points we add to \mathcal{C}_{SW} to compactify it,
- (2) $\{q_i \in \mathcal{C}_{\text{SW}} | dt(q_i) = 0\} \Leftrightarrow \{q_i \in \mathcal{C}_{\text{SW}} | (\partial f / \partial v)(t(q_i), v(q_i)) = 0\}$,

(3) $\{r_i \in \mathcal{C}_{\text{SW}} | v(r_i) = 0\}$.

(1) and (2) give us $\{p_1, \dots, p_4\}$ and $\{q_{\pm}\}$, respectively. (3) does not result in any additional point. Using the local normalizations calculated in Appendix A.2.3, we can get

$$(\omega) = 1 \cdot [q_+] + 1 \cdot [q_-],$$

which is consistent with the Poincaré-Hopf theorem, (3.5),

$$\text{deg}[(\omega)] = 1 + 1 = 2 = 2(g(\mathcal{C}_{\text{SW}}) - 1),$$

considering $g(\mathcal{C}_{\text{SW}}) = 2$.

3.4 SU(3) pure gauge theory and Argyres-Douglas fixed points

What is interesting about the branch points we have found in Sections 3.2 and 3.3, the images of the ramification points of the Seiberg-Witten curve under the covering map, is that their locations on C_{B} depend in general on every parameter of the Seiberg-Witten curve, including both gauge coupling parameters and Coulomb branch parameters. Therefore they can be useful in analyzing how a Seiberg-Witten curve behaves as we take various limits for the parameters.

Furthermore, considering that branch points are important in understanding various noncontractible 1-cycles of a curve and that each such cycle on a Seiberg-Witten curve corresponds to a BPS state with its mass given by the integration of the Seiberg-Witten differential along the cycle [3, 2], the behaviors of branch points under the various limits of the parameters tell us some information regarding the BPS states.

To expand on these ideas, we will investigate in this section the case of a 4d $\mathcal{N} = 2$ SU(3) pure gauge theory, which has the special limits of the Coulomb branch parameters, the Argyres-Douglas fixed points [4]. We will describe how the branch points from the ramification points of the Seiberg-Witten curve of the theory help us to identify the small torus that arises at the fixed points.

Here the starting point is a 4d $\mathcal{N} = 2$ SU(3) pure gauge theory associated to the brane configuration of Figure 3.16. The corresponding Seiberg-Witten curve C_{SW} is the zero locus

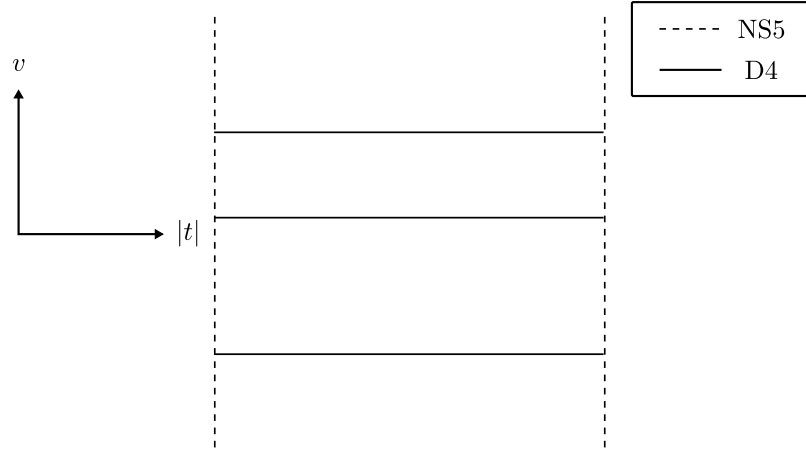


Figure 3.16: Brane configuration of SU(3) pure gauge theory.

of

$$f(t, v) = t^2 + (v^3 - u_2 v - u_3) t + \Lambda^6,$$

where Λ is the dynamically generated scale of the 4d theory. This is different from the previous examples, where the corresponding 4d theories are conformal and therefore are scale-free.

Considering a normalization $\sigma : \mathcal{C}_{\text{SW}} \rightarrow \bar{\mathcal{C}}_{\text{SW}}$ and a meromorphic function $\pi : \mathcal{C}_{\text{SW}} \rightarrow \mathbb{CP}^1$, we can introduce a ramification divisor $R_\pi = \sum_s (\nu_s(\pi) - 1)[s]$. Nontrivial ramifications may occur at

(1) $\{p_i \in \mathcal{C}_{\text{SW}}\}$, where $\{\phi(p_i)\}$ are the points we add to \mathcal{C}_{SW} to compactify it,

(2) $\{q_i \in \mathcal{C}_{\text{SW}} \mid dt(q_i) = 0\} \Leftrightarrow \{q_i \in \mathcal{C}_{\text{SW}} \mid (\partial f / \partial v)(t(q_i), v(q_i)) = 0\}$.

(1) gives us $\{p_1, p_2\}$ such that

$$\phi(p_1) = (0, \infty), \quad \phi(p_2) = (\infty, \infty),$$

and (2) gives us $\{q_{++}, q_{+-}, q_{-+}, q_{--}\}$ such that

$$\phi(q_{ab}) = (t_{2ab}, v_{2a}),$$

where $a, b = \pm 1$, $v_{2a} = a\sqrt{u_2/3}$, and t_{2ab} are the two roots of $f(t, v_{2a}) = 0$,

$$t_{2ab} = \left(v_{2a}^3 + \frac{u_3}{2}\right) + b\sqrt{\left(v_{2a}^3 + \frac{u_3}{2}\right)^2 - \Lambda^6}.$$

Using the local normalizations calculated in Section A.2.4, we get

$$R_\pi = 2 \cdot [p_1] + 2 \cdot [p_2] + 1 \cdot [q_{++}] + 1 \cdot [q_{+-}] + 1 \cdot [q_{-+}] + 1 \cdot [q_{--}],$$

and considering $\deg(\pi) = 3$ and $g(\mathcal{C}_{\text{SW}}) = 2$,

$$\deg(R_\pi) = 8 = 2(g(\mathcal{C}_{\text{SW}}) + \deg(\pi) - 1)$$

is consistent with the Riemann-Hurwitz formula, (3.3). Figure 3.17 illustrates how π works for this example. The appearance of the four branch points, $\{\pi(q_{\pm\pm})\}$, in addition to the branch points $\{\pi(p_i)\}$ that are identified with the punctures of [5], was previously observed in [20].

Again, $\{\phi(q_{\pm\pm})\}$ are the ramification points of the noncompact Seiberg-Witten curve \mathcal{C}_{SW} , whereas $\{\phi(p_i)\}$ are the points “at infinity,” therefore $\{\pi(q_{\pm\pm})\}$ are from the ramification points of \mathcal{C}_{SW} .

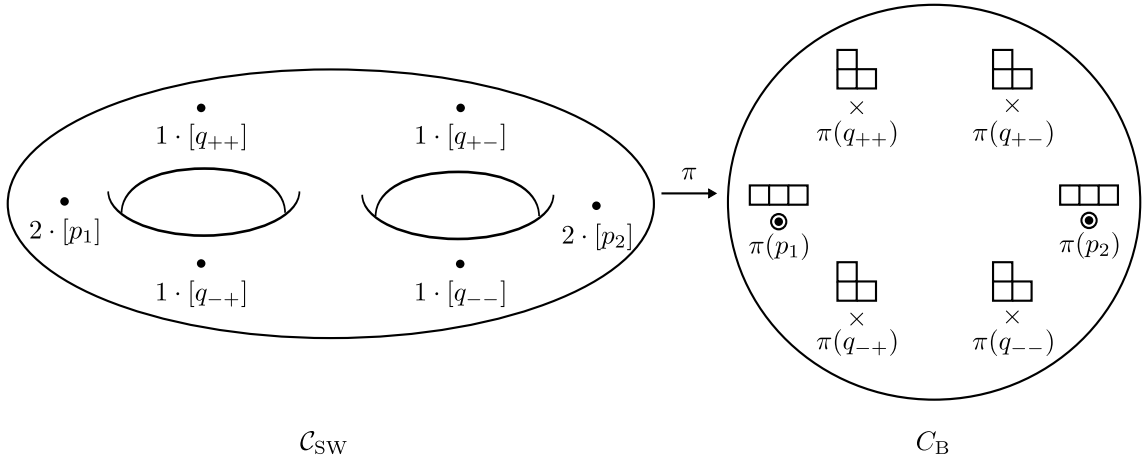


Figure 3.17: \mathcal{C}_{SW} and \mathcal{C}_{B} for SU(3) pure gauge theory.

The divisor of $\omega = \sigma^*(\lambda)$ is $(\omega) = \sum_s \nu_s(\omega)[s]$, and the candidates for the points on \mathcal{C}_{SW} where ω has nonzero order are

- (1) $\{p_i \in \mathcal{C}_{\text{SW}}\}$, where $\{\phi(p_i)\}$ are the points we add to \mathcal{C}_{SW} to compactify it,
- (2) $\{q_i \in \mathcal{C}_{\text{SW}} | dt(q_i) = 0\} \Leftrightarrow \{q_i \in \mathcal{C}_{\text{SW}} | (\partial f / \partial v)(t(q_i), v(q_i)) = 0\}$,
- (3) $\{r_i \in \mathcal{C}_{\text{SW}} | v(r_i) = 0\}$.
- (1) and (2) result in $\{p_1, p_2\}$ and $\{q_{ab}\}$, respectively. (3) gives us $\{r_{\pm}\}$ such that

$$\phi(r_{\pm}) = (t_{3\pm}, 0),$$

where $t_{3\pm}$ are the two roots of $f(t, 0) = 0$. Using the local normalizations calculated in Appendix A.2.4, we can get

$$(\omega) = -2 \cdot [p_1] - 2 \cdot [p_2] + 1 \cdot [q_{++}] + 1 \cdot [q_{+-}] + 1 \cdot [q_{-+}] + 1 \cdot [q_{--}] + 1 \cdot [r_+] + 1 \cdot [r_-],$$

which is consistent with the Poincaré-Hopf theorem, (3.5),

$$\deg[(\omega)] = 2 = 2(g(\mathcal{C}_{\text{SW}}) - 1),$$

considering $g(\mathcal{C}_{\text{SW}}) = 2$.

Now let's consider how the branch points behave as we approach the Argyres-Douglas fixed points. As the fixed points are at $u_2 = 0$ and $u_3 = \pm 2\Lambda^3$, let's denote the small deviations from one of the two fixed points by

$$u_2 = 0 + \delta u_2 = 3\epsilon^2 \rho, \tag{3.8}$$

$$u_3 = 2\Lambda^3 + \delta u_3 = 2\Lambda^3 + 2\epsilon^3, \tag{3.9}$$

where we picked $u_3 = 2\Lambda^3$. When $\epsilon \ll \Lambda$,

$$\pi(q_{ab}) = t_{2ab} \approx \Lambda^3 \left[1 + b \sqrt{2(1 + a\rho^{3/2}) \left(\frac{\epsilon}{\Lambda}\right)^3} \right]. \tag{3.10}$$

That is, $\{\pi(q_{ab})\}$ gather together near $t = \Lambda^3$, away from $\{\pi(p_i)\}$. The four values of t_{2ab} are away from $t = \Lambda^3$ by the distance of order $\Lambda^3 \cdot \mathcal{O}((\epsilon/\Lambda)^{3/2})$. Figure 3.18 illustrates this Coulomb branch limit.

From the viewpoint of the ramification structure of the Seiberg-Witten curve, this is a

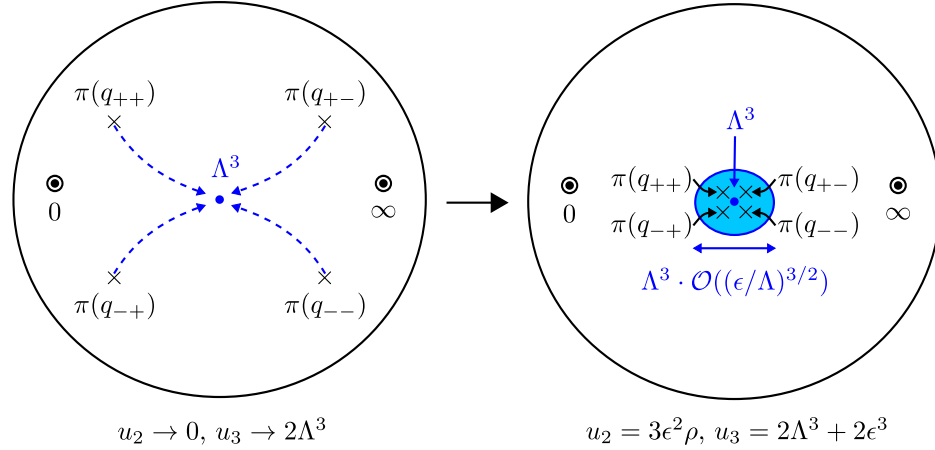


Figure 3.18: Behaviors of the branch points near the Argyres-Douglas fixed point.

similar situation to one that we have seen in Section 3.3, where we cut a Seiberg-Witten curve into two parts, giving each of them an additional point of ramification index 3. We do the same thing here, thereby getting a genus 1 curve, which is a small torus, and another genus 1 curve whose Seiberg-Witten curve is the zero locus of

$$v^3 t + (t - \Lambda^3)^2,$$

which is the curve with three branch points of ramification index 3. But this time we will try to find out the algebraic equation that describes the small torus. For that purpose it is tempting to zoom in on the part of C_B near $t = \Lambda^3$, in such a way that every parameter has an appropriate dependence on ϵ so that we can cancel out ϵ from all of them. Considering (3.8), (3.9), (3.10), and the dimension of each parameter, a natural way to scale out ϵ is to redefine the variables as

$$\begin{aligned} v &= \epsilon z, \\ u_2 &= 0 + 3\epsilon^2 \rho, \\ u_3 &= 2\Lambda^3 + 2\epsilon^3 \\ t &= \Lambda^3 + i(\epsilon\Lambda)^{3/2} w. \end{aligned}$$

Then $f(t, v)$ becomes

$$\begin{aligned} f(t, v) &= (t - \Lambda^3)^2 + \epsilon^3(z^3 - 3\rho z - 2)t \\ &\approx \Lambda^6(-w^2 + z^3 - 3\rho z - 2)(\epsilon/\Lambda)^3 + \mathcal{O}((\epsilon/\Lambda)^{9/2}), \end{aligned}$$

where we can identify a torus given by $w^2 = z^3 - 3\rho z - 2$, the same torus that appears at the Argyres-Douglas fixed points [4]. Figure 3.19 illustrates this procedure.

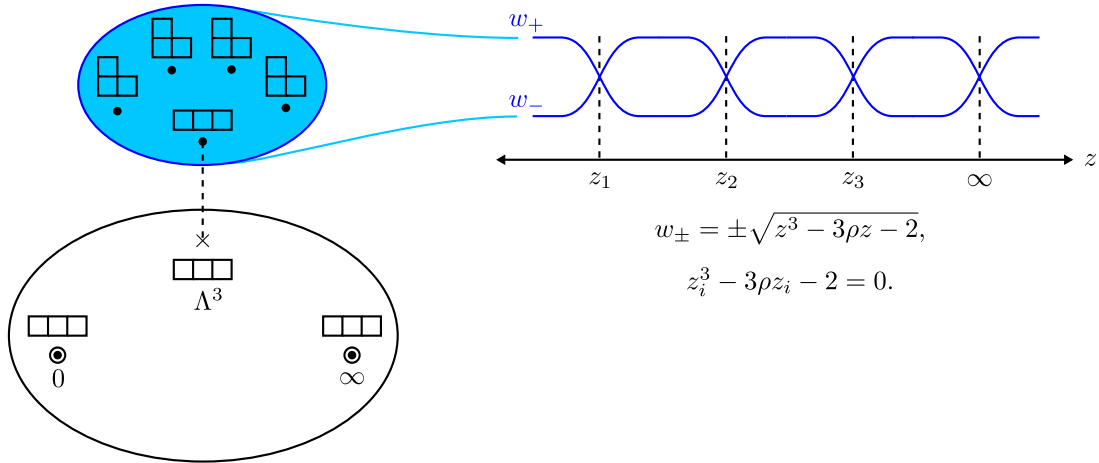


Figure 3.19: Appearance of a small torus at the Argyres-Douglas fixed points.

We can also calculate the Seiberg-Witten differential $\lambda = \frac{v}{t} dt$ on the small torus,

$$\lambda = \frac{v}{t} dt \approx \frac{\epsilon z}{\Lambda^3} \cdot i(\epsilon\Lambda)^{3/2} dw = i \frac{\epsilon^{5/2}}{\Lambda^{3/2}} z dw \propto \frac{\epsilon^{5/2}}{\Lambda^{3/2}} \frac{z(z^2 - \rho)}{w} dz,$$

which agrees with the Seiberg-Witten differential calculated in [4].

3.5 SU(2) gauge theory with massive matter

In this section we will take a look at the cases of 4d $\mathcal{N} = 2$ SU(2) gauge theories with massive hypermultiplets, where we can observe interesting limits of the Coulomb branch parameters and the mass parameters [21].

3.5.1 $SU(2)$ gauge theory with four massive hypermultiplets

In section 3.1 we analyzed a 4d $\mathcal{N} = 2$ $SU(2)$ SCFT, which has four massless hypermultiplets. Here we examine a gauge theory with the same amount of supersymmetry and the same gauge group but with massive hypermultiplets, and see how mass parameters change the ramification structure of the Seiberg-Witten curve.

This gauge theory is associated to the brane configuration of Figure 3.20. The corre-

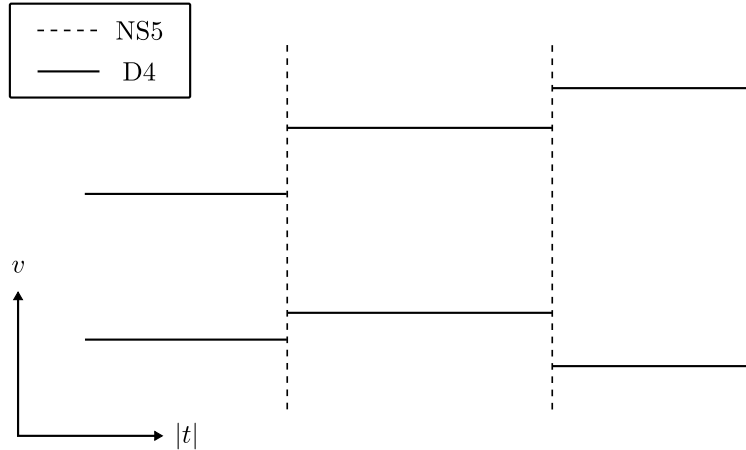


Figure 3.20: Brane configuration of $SU(2)$ gauge theory with four massive hypermultiplets.

sponding Seiberg-Witten curve C_{SW} is the zero locus of

$$f(t, v) = (v - m_1)(v - m_3)t^2 - (v^2 - u_2)t + (v - m_2)(v - m_4)c_4, \quad (3.11)$$

where m_1 and m_3 are the mass parameters of the hypermultiplets at $t = \infty$, m_2 and m_4 are the mass parameters of the hypermultiplets at $t = 0$, u_2 is the Coulomb branch parameter, and c_4 corresponds to the dimensionless gauge coupling parameter that cannot be absorbed by rescaling t and v [7].

From the usual analysis we get C_{B} as shown in Figure 3.21. Here $\{p_i\}$ are the points on C_{SW} such that

$$\begin{aligned} \phi(p_1) &= (0, m_2), \quad \phi(p_2) = (0, m_4), \quad \phi(p_3) = (t_-, \infty), \quad \phi(p_4) = (t_+, \infty), \\ \phi(p_5) &= (\infty, m_1), \quad \phi(p_6) = (\infty, m_3), \quad t_{\pm} = \frac{1}{2} (1 \pm \sqrt{1 - 4c_4}) \end{aligned}$$

are the points we add to C_{SW} to compactify it, and $\{q_i\}$ are where $dt = 0$ and whose images

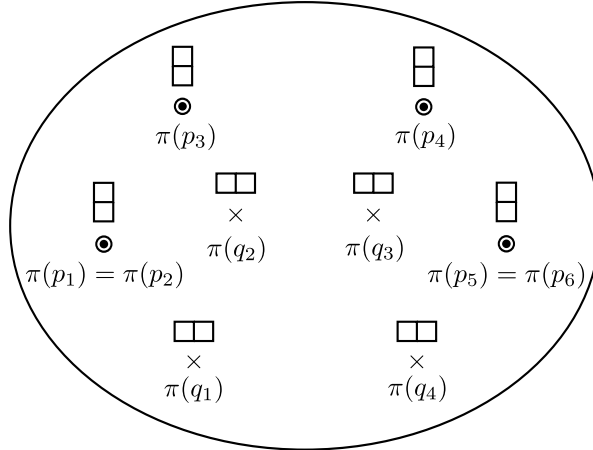


Figure 3.21: C_B for $SU(2)$ gauge theory with four massive hypermultiplets.

under π are the four roots of

$$\begin{aligned} & \frac{1}{4} (m_1 - m_3)^2 t^4 + (m_1 m_3 - u_2) t^3 + \\ & + \frac{1}{2} [c_4 (m_1 m_2 + m_2 m_3 + m_3 m_4 + m_4 m_1 - 2m_1 m_3 - 2m_2 m_4) + 2u_2] t^2 + \\ & + c_4 (m_2 m_4 - u_2) t + \frac{1}{4} c_4^2 (m_2 - m_4)^2. \end{aligned}$$

In [19] there also appears a similar picture of branch points in the analysis of the gauge theory from the same brane configuration. Note that we made a choice among the various brane configurations that give the same 4d $SU(2)$ gauge theory with four massive hypermultiplets, because each brane configuration in general results in a different ramification structure. So the choice does matter in our analysis and also when comparing our result with that of [19].

One notable difference from the previous examples is that $\{\pi(p_i)\}$ are not branch points. Instead we have four branch points $\{\pi(q_i)\}$ which furnish the required ramification structure. We can see that the locations of the branch points now depend also on the mass parameters in addition to the gauge coupling parameter and the Coulomb branch parameter. Note that all of the four branch points are from the ramification points of the noncompact Seiberg-Witten curve C_{SW} , because here the two branches of $v(t)$ do not meet “at infinity” with each other.

This theory has four more parameters, $\{m_i\}$, when compared to $SU(2)$ SCFT. In some

sense, these mass parameters represent the possible deformations of the Seiberg-Witten curve of $SU(2)$ SCFT. To understand what the deformations are, let's first see how $\{\pi(q_i)\}$ move when we take various limits of the mass parameters.

1. When $m_1 \rightarrow m_3$, one of $\{\pi(q_i)\}$, say $\pi(q_4)$, moves to $t = \infty = \pi(p_5) = \pi(p_6)$.
2. When $m_2 \rightarrow m_4$, one of $\{\pi(q_i)\}$, say $\pi(q_1)$, moves to $t = 0 = \pi(p_1) = \pi(p_2)$.
3. When $m_1 \rightarrow -m_3$ and at the same time $m_2 \rightarrow -m_4$, $\pi(q_2)$ moves to $t = t_- = \pi(p_3)$ and $\pi(q_3)$ moves to $t = t_+ = \pi(p_4)$.

The first limit corresponds to bringing the two points of \mathcal{C}_{SW} , p_5 and p_6 , together to one point, thereby developing a ramification point of index 2 there. The others can also be understood in a similar way. Figure 3.22 illustrates these limits.

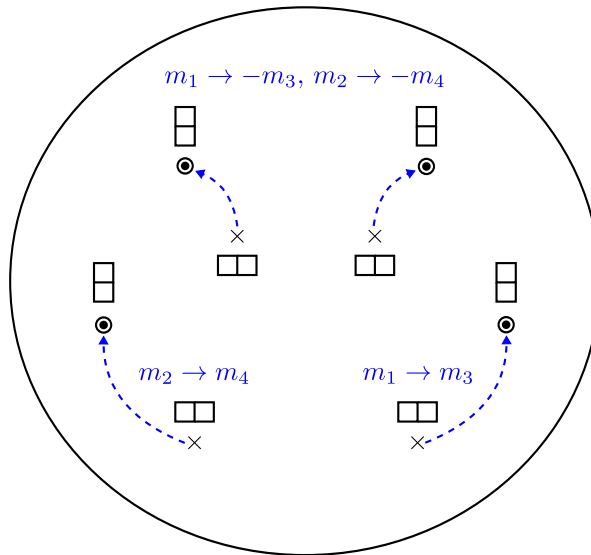


Figure 3.22: Behaviors of the branch points under various limits of mass parameters.

Note that we can get the Seiberg-Witten curve of $SU(2)$ SCFT by setting all the mass parameters of (3.11) to zero, which corresponds to taking all of the limits at the same time, thereby sending each $\pi(q_i)$ to one of $\{\pi(p_i)\}$ and turning $\{\pi(p_i)\}$ into four branch points as expected.

Now we turn the previous arguments on its head and see how we can deform the Seiberg-Witten curve of $SU(2)$ SCFT by turning on mass parameters. As an example, let's consider turning on $m_2 = -m_4 = m$. When $m = 0$, there is a branch point at $t = 0$. Now we turn

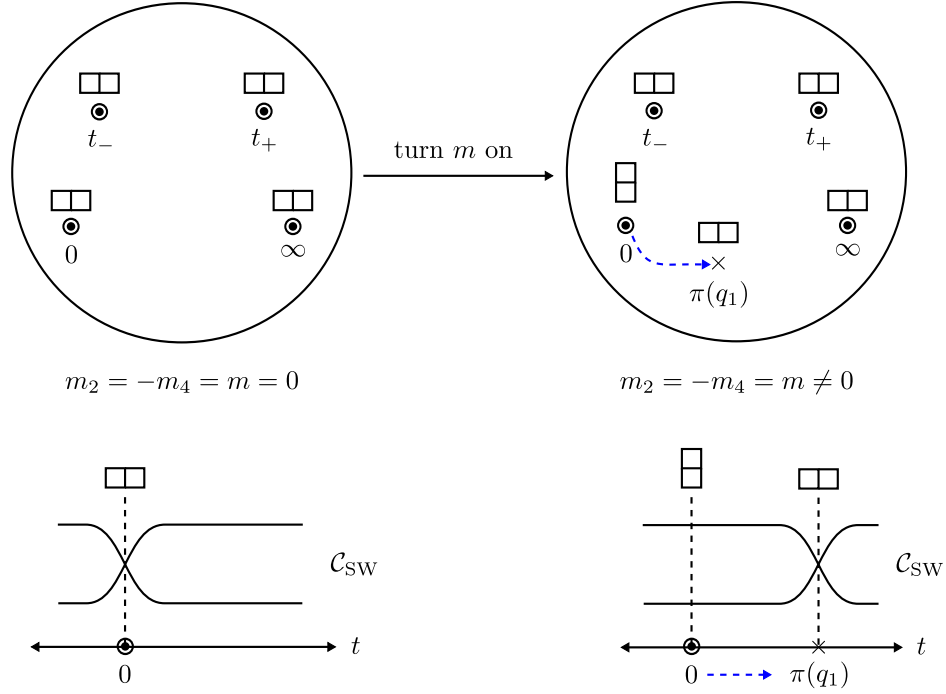


Figure 3.23: Removal of the branch point at $t = 0$ when we turn $m_2 = -m_4 = m$ on.

m on, then this separates the two sheets at $t = 0$, and $t = 0$ is no longer a branch point. But the topological constraint by the Riemann-Hurwitz formula requires four branch points to exist, and indeed a new branch point that corresponds to $\pi(q_1)$ develops. Figure 3.23 illustrates this deformation.

The other mass parameters can also be understood in a similar way as deformations that detach the sheets meeting at the branch points from each other, and the most general deformation will result in the Seiberg-Witten curve of $SU(2)$ gauge theory with four massive hypermultiplets, the theory we started our analysis here.

3.5.2 $SU(2)$ gauge theory with two massive hypermultiplets

Now we examine the example of a 4d $\mathcal{N} = 2$ supersymmetric $SU(2)$ gauge theory with two massive hypermultiplets. As mentioned earlier, there are various ways in constructing the brane configuration associated to the 4d theory. One possible brane configuration is shown in Figure 3.24, where two D4-branes that provide the massive hypermultiplets are distributed symmetrically on both sides.

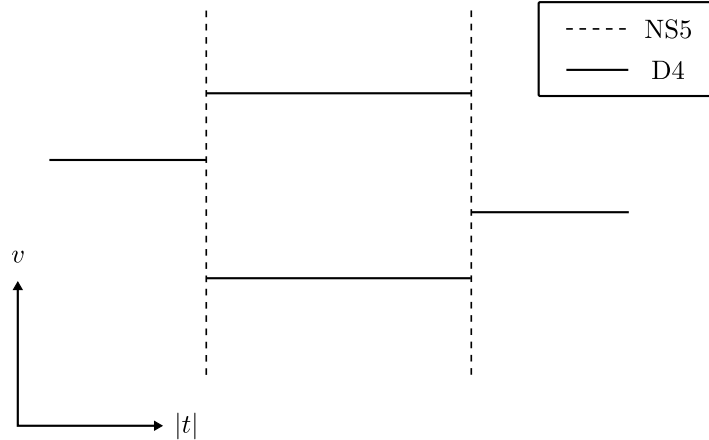


Figure 3.24: Brane configuration of $SU(2)$ gauge theory with two massive hypermultiplets, with symmetric distribution of D4-branes.

The corresponding Seiberg-Witten curve C_{SW} is the zero locus of

$$f(t, v) = (v - m_1)t^2 - (v^2 - u_2)t + (v - m_2)\Lambda^2, \quad (3.12)$$

where u_2 is the Coulomb branch parameter, m_1 and m_2 are the mass parameters, and Λ is the dynamically generated scale of the theory.

The usual analysis gives C_{B} as shown in Figure 3.25. $\{p_i\}$ are the points on C_{SW} such that

$$\phi(p_1) = (0, m_2), \quad \phi(p_2) = (0, \infty), \quad \phi(p_3) = (\infty, m_1), \quad \phi(p_4) = (\infty, \infty)$$

are the points we add to C_{SW} to compactify it. Note that here $\pi(p_1) = \pi(p_2) = 0$ and $\pi(p_3) = \pi(p_4) = \infty$ are not branch points. There are four branch points $\{\pi(q_i)\}$ whose locations on C_{B} are given by the four roots $\{t_i\}$ of the following equation.

$$\frac{1}{4}t^4 - m_1t^3 + \left(u_2 + \frac{\Lambda^2}{2}\right)t^2 - m_2\Lambda^2t + \frac{\Lambda^4}{4}.$$

We can see that the locations of $\{\pi(q_i)\}$ now depend also on the mass parameters in addition to the Coulomb branch parameter and the scale. Again the branch points come from the ramification points of the noncompact Seiberg-Witten curve C_{SW} . In [19] there also appears a similar picture of branch points in the analysis of the gauge theory from the same

symmetric brane configuration.

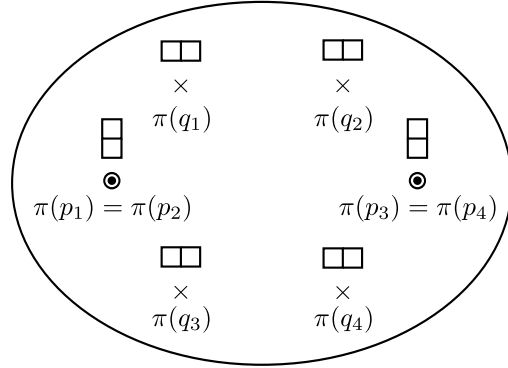


Figure 3.25: C_B for $SU(2)$ gauge theory with two massive hypermultiplets when the brane configuration is symmetric.

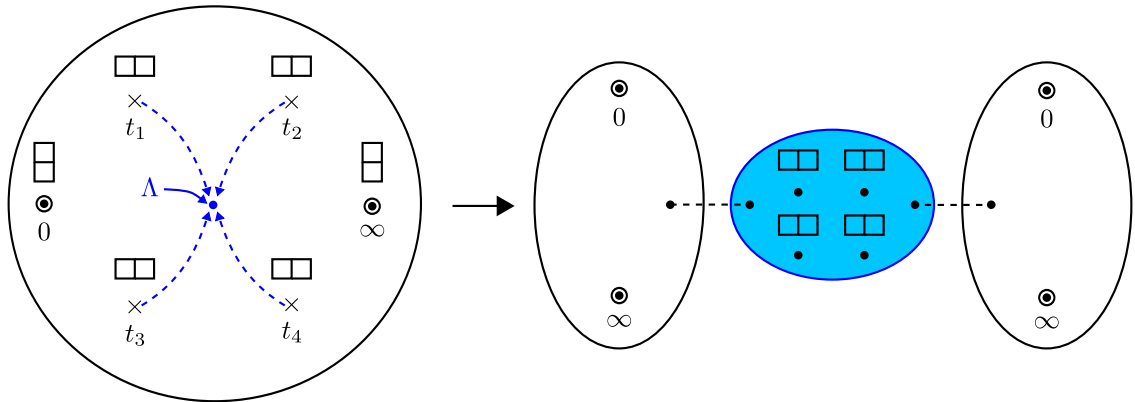


Figure 3.26: Behaviors of the branch points when $m_1 = m_2 \rightarrow \Lambda$, $u_2 \rightarrow \Lambda^2$.

When we take the limit of $m_1 = m_2 \rightarrow \Lambda$ and $u_2 \rightarrow \Lambda^2$, the four branch points approach $t = \Lambda$. Figure 3.26 illustrates the behavior of the branch points under the limit. This is a similar situation of four branch points of index 2 gathering together around a point as we have seen in Sections 3.3 and 3.4. Imagine cutting off a small region of the Seiberg-Witten curve around the preimages of the branch points when we are in the vicinity of the limit. Going around the four branch points makes a complete journey, that is, we can come back to the branch of $v(t)$ where we started, which implies that adding a point of ramification index 1 to each branch of the excised part of the curve gives us a compact small torus. After cutting off the region containing the preimages of the four branch points and adding a point to each branch, the two branches of the remaining part of the original Seiberg-Witten curve

become two Riemann spheres. This can also be seen by taking the Coulomb branch limit of the parameters in (3.12), which results in two components that have no ramification over t , that is, two Riemann spheres. Therefore we can identify a small torus and see nonlocal states becoming massless simultaneously as the cycles around the two of the four branch points vanish as we take the limit. It would be interesting to find out the explicit expression for the small torus as we did in Section 3.4, where we found the algebraic equation that describes the small torus of Argyres-Douglas fixed points, and to compare the small torus with the result of [21].

We have another brane configuration that gives us the same 4d physics, which is shown in Figure 3.27. Now the D4-branes that provide massive hypermultiplets are on one side only, thereby losing the symmetry of flipping t to its inverse and swapping m_1 and m_2 .

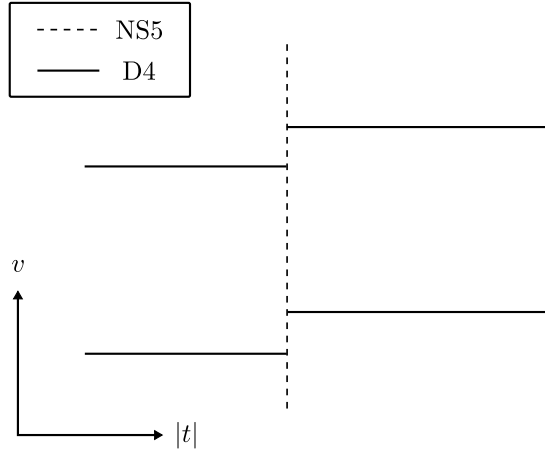


Figure 3.27: Brane configuration of $SU(2)$ gauge theory with two massive hypermultiplets, with asymmetric distribution of D4-branes.

The corresponding Seiberg-Witten curve C_{SW} is the zero locus of

$$f(t, v) = \Lambda^2 t^2 - (v^2 - u_2)t + (v - m_1)(v - m_2). \quad (3.13)$$

After the usual analysis, we can find C_{B} as shown in Figure 3.28. Here $\{p_i\}$ are the points on C_{SW} such that

$$\phi(p_1) = (0, m_1), \quad \phi(p_2) = (0, m_2), \quad \phi(p_3) = (1, \infty), \quad \phi(p_4) = (\infty, \infty),$$

are the points we add to C_{SW} to compactify it. Note that $\pi(p_1) = \pi(p_2) = 0$ and $\pi(p_3) = 1$

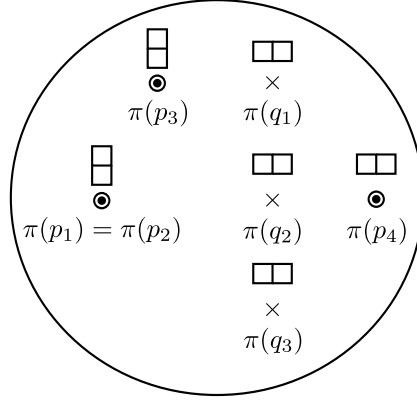


Figure 3.28: C_B for $SU(2)$ gauge theory with two massive hypermultiplets when the brane configuration is not symmetric.

are not branch points in this case, because each of them has a trivial ramification there as indicated with the corresponding Young tableau. $\pi(p_4) = \infty$ is a branch point. The locations of the other three branch points $\{\pi(q_i)\}$ are given by the three roots $\{t_i\}$ of (3.14).

$$\Lambda^2 t^3 + (u_2 - \Lambda^2) t^2 + (m_1 m_2 - u_2) t + \left(\frac{m_1 - m_2}{2} \right)^2 = 0. \quad (3.14)$$

Again we see that the locations of $\{\pi(q_i)\}$ depend on the mass parameters as well as the Coulomb branch parameters and the scale. $\{\pi(q_i)\}$ are distinguished from $\pi(p_4)$ in that they are from the ramification points of the noncompact Seiberg-Witten curve C_{SW} . In [19] there also appears a similar picture of branch points in the analysis of the gauge theory from the asymmetric brane configuration.

From (3.14), we can easily identify the limits of the parameters that send $\{\pi(q_i)\}$ to $t = 0$. That is,

- (1) When $m_1 = m_2 = m$, $t_1 \rightarrow 0$.
- (2) When $m^2 = u_2$, t_1 and $t_2 \rightarrow 0$.
- (3) When $m = \Lambda^2$, t_1 , t_2 , and $t_3 \rightarrow 0$.

The case of (3) is illustrated in the left side of Figure 3.29. Note that when we take the limit of $m_1 = m_2 \rightarrow \Lambda$ and $u_2 \rightarrow \Lambda^2$, the three branch points go to $t = 0$ and we can see that there are nonlocal states that become massless together in the limit. This is the same limit of the parameters as the one in the previous case of different brane configuration, a symmetric

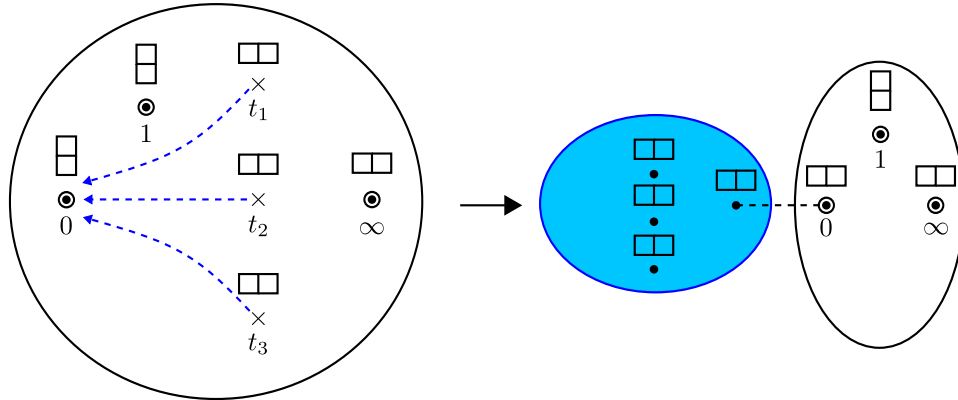


Figure 3.29: Behaviors of the branch points when $m_1 = m_2 \rightarrow \Lambda$, $u_2 \rightarrow \Lambda^2$.

brane configuration. Therefore, we observe the phenomenon of seemingly different brane configurations giving the same 4d physics.

However, unlike the previous case of symmetric brane configuration, where there are four branch points with ramification index 2 that are coming together under the limit, here there are only three of them moving toward a point as we take the limit. But note that while in the previous case going around the four branch points once gets us back to where we started, here going around the three branch points once does not complete a roundtrip and we need one more trip to get back to the starting point. This implies that, when excising the part of the Seiberg-Witten curve where the preimages of the three branch points come together, the monodromy around the region corresponds to a point of ramification index 2. After we cut the curve into two parts, we have one curve with four branch points of ramification index 2, which is a small torus, and the other curve with two branch points of ramification index 2, which is a Riemann sphere. This procedure is illustrated in the right side of Figure 3.29. This can also be seen by taking the Coulomb branch limit of the parameters of (3.13), which gives us a curve with two ramification points of index 2, the Riemann sphere.

3.6 Brane configuration around a puncture and a ramification point

Here we illustrated, through several examples, that when a Seiberg-Witten curve of an $\mathcal{N} = 2$ gauge theory has a ramification over a Riemann sphere C_B , some of the branch

points on C_B can be identified with the punctures of [5] but in general there are additional branch points from the ramification points of the Seiberg-Witten curve, whose locations on C_B depend on various parameters of the theory and therefore can be a useful tool when studying various limits of the parameters, including Argyres-Seiberg duality and the Argyres-Douglas fixed points.

Branch points have played a major role since the inception of the Seiberg-Witten curve. What is different here is that we change the point of view such that we can find branch points in a way that is compatible with the setup of [5], which enables us to complement and utilize its analysis. This change of the perspective can be illustrated as shown in Figure 3.30, which shows a brane configuration of an $SU(3)$ SCFT.

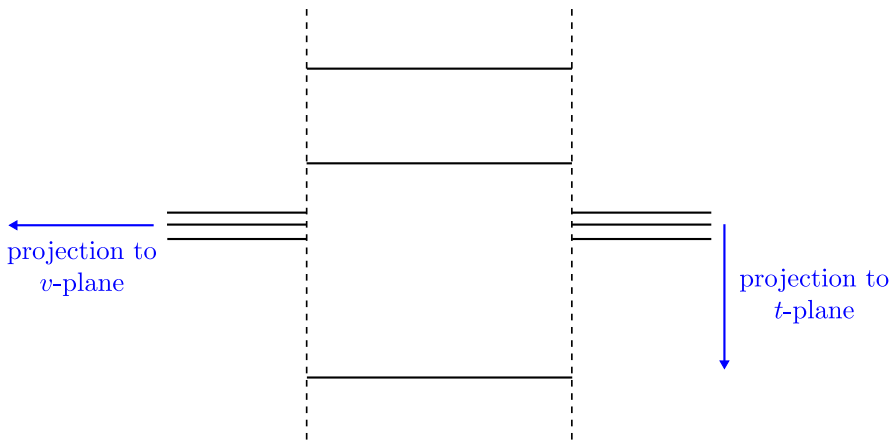


Figure 3.30: Two different ways of projecting a Seiberg-Witten curve onto a complex plane.

If we want to project the whole Seiberg-Witten curve onto a complex plane, there are two ways: one is projecting the curve onto the t -plane, and the other is projecting it onto the v -plane. In the original study of [3, 2] and in the following extensions of the analysis [22, 23, 24, 25, 26, 27, 28], the analyses of Seiberg-Witten curves have been done usually by projecting the curve onto the v -plane so that it can be seen as a branched two-sheeted cover over the complex plane. Then the branch points are such that the corresponding ramification points on the Seiberg-Witten curve have the same ramification index of 2, because a point on a Seiberg-Witten curve has the ramification index of either 2 or 1 when considering a two-sheeted covering map.

But here we project the Seiberg-Witten curve onto the t -plane such that the curve is a three-sheeted cover over the complex plane. This way of projection, which previ-

ously appeared in [29] and re-popularized by Gaiotto [5], makes it easier to understand the physical meaning of the branch points. When considering a Seiberg-Witten curve as a two-dimensional subspace of an M5-brane [6], the M5-brane can be described as a deformation of several coincident M5-branes wrapping a Riemann surface plus M5-branes meeting the coincident M5-branes transversely at the location of punctures. From the viewpoint of the coincident M5-branes, a transverse M5-brane is heavy and therefore can be considered as an operator when studying the theory living on the coincident M5-branes. See Figure 3.31a, which illustrates the configuration of M5-branes at a puncture and their projection onto C_B . Therefore when we project the Seiberg-Witten curve onto the t -plane, the branch points that are identified with the punctures can be related to the locations of the transverse M5-branes.

In comparison to that, the branch points that are not identified with the punctures come from the ramification points of the single noncompact M5-brane, which was the coincident M5-branes before turning on the Coulomb branch parameters of the theory. Figure 3.31b illustrates two ramification points of a ramified M5-brane and their projection onto C_B . If we consider the Seiberg-Witten curve as coming from several sheets of M5-branes, a ramification point of the curve is where those M5-branes come into a contact [19]. To investigate the local physics around these points, we can put an M2-brane near a ramification point, which leads to an interesting 2d theory from the configuration [30].

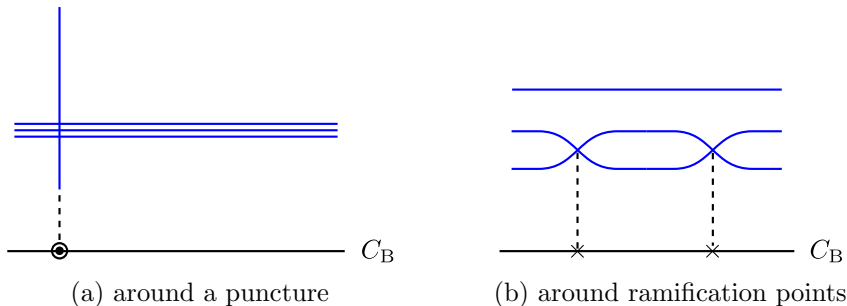


Figure 3.31: Configuration of M5-branes around a puncture and ramification points.

Chapter 4

2d $\mathcal{N} = (2, 2)$ theory

2d $\mathcal{N} = (2, 2)$ theories are similar to 4d $\mathcal{N} = 2$ theories in many respects, including the existence of BPS states that can be useful in understanding the 2d theories in their nonperturbative regimes. As it was helpful in understanding 4d $\mathcal{N} = 2$ theories to utilize brane configurations that provide the 4d theories as their low-energy effective world volume theories, it proved to be useful [31] to construct a brane configuration that describes a 2d $\mathcal{N} = (2, 2)$ theory. Here we first review the basics of 2d $\mathcal{N} = (2, 2)$ supersymmetry, and illustrate how to construct type IIA and M-theory brane configurations that can be used to understand the 2d theories.

4.1 2d $\mathcal{N} = (2, 2)$ supersymmetry

4.1.1 SUSY algebra

2d $\mathcal{N} = (2, 2)$ supersymmetry can be obtained via the dimensional reduction of 4d $\mathcal{N} = 1$ supersymmetry [32], which has four real supercharges that can be represented by two Weyl spinors $Q_\alpha, \bar{Q}_{\dot{\alpha}}$ with $U(1)_R$ -charge -1 and +1, respectively. After the dimensional reduction, this $U(1)$ symmetry is inherited to the 2d SUSY supercharges, which is called $U(1)_V$. The 2d SUSY has an additional internal symmetry from the rotational symmetry on the plane transverse to the 2d spacetime, which is called $U(1)_A$. We can organize the 2d supercharges according to the two $U(1)$ -charges as shown in Table 4.1.

From the dimensional reduction of the 4d $\mathcal{N} = 1$ SUSY algebra

$$\{Q_\alpha, \bar{Q}_{\dot{\alpha}}\} = 2\sigma_{\alpha\dot{\alpha}}^\mu P_\mu, \quad (4.1)$$

	U(1) _V = -1	U(1) _V = +1
U(1) _A = +1	Q_-	\bar{Q}_+
U(1) _A = -1	Q_+	\bar{Q}_-

Table 4.1

we obtain the 2d $\mathcal{N} = (2, 2)$ SUSY algebra

$$\{Q_{\pm}, \bar{Q}_{\pm}\} = 2(H \pm P), \{Q_+, Q_-\} = 2Z, \{Q_+, \bar{Q}_-\} = 2\tilde{Z}, \quad (4.2)$$

where H and P are the 2d Hamiltonian and momentum operators, and Z, \tilde{Z} are central charges.

4.1.2 Chiral and twisted chiral multiplets

A 2d $\mathcal{N} = (2, 2)$ chiral multiplet Φ contains one complex scalar field ϕ and a 2d Dirac fermion (ψ_+, ψ_-) . When we define 2d differential operators

$$D_{\pm} = \frac{\partial}{\partial\theta^{\pm}} - i\bar{\theta}^{\pm} \left(\frac{\partial}{\partial x^0} \pm \frac{\partial}{\partial x^1} \right), \quad \bar{D}_{\pm} = -\frac{\partial}{\partial\theta^{\pm}} + i\theta^{\pm} \left(\frac{\partial}{\partial x^0} \pm \frac{\partial}{\partial x^1} \right) \quad (4.3)$$

a chiral field satisfies $\bar{D}_{\pm}\Phi = 0$.

A 2d $\mathcal{N} = (2, 2)$ gauge field is represented by a 2d $\mathcal{N} = (2, 2)$ vector multiplet V that contains a 2d vector field A_{μ} , two Dirac fermions λ and $\bar{\lambda}$, and a complex scalar v , all in the same representation of the gauge group. Its field strength can be represented by a twisted chiral multiplet Σ , which is related to an abelian vector multiplet V by

$$\Sigma = \bar{D}_+ D_- V \quad (4.4)$$

and satisfies

$$\bar{D}_+ \Sigma = D_- \Sigma = 0. \quad (4.5)$$

The lowest component of Σ is a complex scalar field σ .

4.1.3 Supersymmetric Lagrangians

Using a 2d $\mathcal{N} = (2, 2)$ chiral field Φ we can obtain supersymmetric Lagrangians. One is a D-term Lagrangian,

$$\mathcal{L}_D = \int d^4\theta K(\Phi, \bar{\Phi}), \quad (4.6)$$

where K is a real function of Φ and $\bar{\Phi}$. This provides the kinetic term of the chiral fields, and is invariant under both $U(1)_V$ and $U(1)_A$. We can also construct an F-term Lagrangian \mathcal{L}_F ,

$$\mathcal{L}_F = \int d^2\theta W(\Phi) + (\text{h. c.}), \quad (4.7)$$

where W is a holomorphic function of Φ and is called a superpotential. This term is invariant under $U(1)_A$, but it is invariant under $U(1)_V$ only when $W(\Phi)$ is quasi-homogeneous of degree 2 with respect to the symmetry.

From a 2d $\mathcal{N} = (2, 2)$ twisted chiral field we can also construct similar Lagrangians. There is a D-term Lagrangian that is constructed in the same way as (4.6). However, instead of \mathcal{L}_F , we have a twisted F-term Lagrangian from

$$\tilde{\mathcal{L}}_F = \int d\theta^- d\bar{\theta}^+ \mathcal{W}(\Sigma), \quad (4.8)$$

where \mathcal{W} is a holomorphic function of Σ and is called a twisted superpotential. This is invariant under $U(1)_V$, but it is invariant under $U(1)_A$ only when $\mathcal{W}(\Sigma)$ is quasi-homogeneous of degree 2 with respect to the symmetry.

4.2 2d $\mathcal{N} = (2, 2)$ Landau-Ginzburg model

We can consider a supersymmetric extension of a 2d Landau-Ginzburg model. Using 2d $\mathcal{N} = (2, 2)$ chiral fields Φ_i , we can construct its Lagrangian as the sum of a D-term and an F-term,

$$\mathcal{L}_{LG} = \int d^4\theta K(\Phi_i, \bar{\Phi}_i) + \int d^2\theta W(\Phi_i) + \int d^2\bar{\theta} \bar{W}(\bar{\Phi}_i). \quad (4.9)$$

We are often interested in the infra-red (IR) fixed point of a Landau-Ginzburg model which is a conformal theory. Under a renormalization group flow toward the IR fixed point, the D-term adjusts itself so that the fixed point theory is superconformal. It is the superpotential of the F-term that defines the universality class of the fixed point theory, because the F-term is not renormalized under the renormalization group flow.

When the action of the Landau-Ginzburg model is expanded in its components, the potential energy is given by

$$U = g^{i\bar{j}} \frac{\partial W}{\partial \phi^i} \frac{\partial \bar{W}}{\partial \bar{\phi}^{\bar{j}}}, \quad g_{i\bar{j}} = \frac{\partial^2}{\partial \phi^i \partial \bar{\phi}^{\bar{j}}} K(\phi^k, \bar{\phi}^{\bar{k}}). \quad (4.10)$$

When the metric is positive definite, supersymmetric ground states of the Landau-Ginzburg model are found by solving

$$\frac{\partial W}{\partial \phi^i} = 0. \quad (4.11)$$

When we have more than one ground states that are separated from each other, there can be a soliton interpolating the two vacua. As an example, consider two ground states $\phi^i = \phi_1^i$ and $\phi^i = \phi_2^i$ and a time-independent configuration interpolating the two ground states,

$$\phi_i(x^1 = -\infty) = \phi_1^i, \quad \phi_i(x^1 = +\infty) = \phi_2^i. \quad (4.12)$$

Then the central charge Z_{12} of this configuration is [33]

$$Z_{12} = 2 (W(\phi_2^i) - W(\phi_1^i)), \quad (4.13)$$

and the mass of the soliton is [34]

$$M = \int dx^1 \left[g_{i\bar{j}} \frac{d\phi^i}{dx^1} \frac{d\bar{\phi}^{\bar{j}}}{dx^1} + g^{i\bar{j}} \frac{\partial W}{\partial \phi^i} \frac{\partial \bar{W}}{\partial \bar{\phi}^{\bar{j}}} \right] \quad (4.14)$$

$$= \int dx^1 \left| \frac{d\phi^i}{dx^1} - \alpha g^{i\bar{j}} \frac{\partial \bar{W}}{\partial \bar{\phi}^{\bar{j}}} \right|^2 + 2 \operatorname{Re} (\bar{\alpha} (W(\phi_2^i) - W(\phi_1^i))), \quad (4.15)$$

where $|\alpha| = 1$. When α is chosen such that

$$\alpha = \frac{W(\phi_2^i) - W(\phi_1^i)}{|W(\phi_2^i) - W(\phi_1^i)|}, \quad (4.16)$$

We have $M \geq Z_{12}$, the BPS bound of this solitonic configuration. A BPS soliton that saturates the bound satisfies

$$\frac{d\phi^i}{dx^1} = \alpha g^{i\bar{j}} \frac{\partial \bar{W}}{\partial \bar{\phi}^{\bar{j}}}, \quad (4.17)$$

which implies that the soliton is represented on the W -plane as a straight line connecting $W(\phi_{1,i})$ and $W(\phi_{2,i})$ [35], because

$$\frac{\partial W}{\partial x^1} = \frac{\partial W}{\partial \phi^i} \frac{d\phi^i}{dx^1} = \frac{W(\phi_2^i) - W(\phi_1^i)}{|W(\phi_2^i) - W(\phi_1^i)|} |\partial W|^2. \quad (4.18)$$

4.3 2d $\mathcal{N} = (2, 2)$ Gauged linear sigma model

Another example of 2d $\mathcal{N} = (2, 2)$ theory we will consider is a 2d $U(k)$ gauge theory with N_f chiral multiplets Q^i in the fundamental representation \mathbf{k} and $N_{\bar{f}}$ chiral multiplets $\tilde{Q}^{\bar{j}}$ in the anti-fundamental representation $\bar{\mathbf{k}}$. The kinetic terms of the gauge field and the chiral fields are given by their D-term Lagrangians,

$$\mathcal{L}_D = \int d^4\theta \left(Q^\dagger e^{2V} Q + \tilde{Q} e^{-2V} \tilde{Q}^\dagger - \frac{1}{2e^2} \text{tr}[\Sigma^\dagger \Sigma] \right), \quad (4.19)$$

where V is the 2d vector multiplet for the $U(k)$ gauge field, e is the coupling constant of the 2d gauge field, and Σ is its field strength twisted chiral multiplet.

The 2d gauge theory can have a twisted F-term Lagrangian containing the Fayet-Illiopoilos (FI) term and the theta term,

$$\mathcal{L}_F = \int d\theta^- d\bar{\theta}^+ \mathcal{W}(\Sigma) + (\text{h. c.}) \quad (4.20)$$

where the twisted superpotential is

$$\mathcal{W} = \frac{i\tau}{2} \Sigma, \quad \tau = ir + \frac{\theta}{2\pi}, \quad (4.21)$$

and r is the FI parameter.

In addition, the chiral fields can have twisted masses [31] that comes from gauging their flavor symmetry $U(N_f) \times U(N_{\bar{f}})$ and giving background values to the scalar components of the vector multiplets. Then the corresponding terms in the Lagrangian is

$$\mathcal{L}_{\tilde{m}} = \int d^4\theta \left(Q^\dagger e^{2V_1} Q + \tilde{Q} e^{-2V_2} \tilde{Q}^\dagger \right), \quad (4.22)$$

where V_1 and V_2 are background fields that are given by

$$V_1 = \theta^- \bar{\theta}^+ \tilde{m}_1 + (\text{h. c.}), \quad V_2 = \theta^- \bar{\theta}^+ \tilde{m}_2 + (\text{h. c.}). \quad (4.23)$$

Let's consider a 2d gauge theory without twisted masses, which is a gauged linear sigma model with a Lagrangian $\mathcal{L}_D + \mathcal{L}_F$. The potential energy of the theory is

$$U = \frac{e^2}{2} \text{tr} \left(qq^\dagger - \tilde{q}^\dagger \tilde{q} - r \right)^2 + \frac{1}{2e^2} \text{tr} [\sigma, \sigma^\dagger]^2 + q^\dagger \{ \sigma, \sigma^\dagger \} q, \quad (4.24)$$

where q, \tilde{q} is the scalar components of Q and \tilde{Q} , respectively. The space of classical vacua is obtained by solving $U = 0$, which requires σ to be diagonalizable in order for the second term in U to vanish. When $r > 0$, we need $\sigma = 0$ for the third term to vanish. In the limit of $e \rightarrow \infty$, corresponding to the IR limit of the 2d theory, massive modes decouple and the theory becomes a supersymmetric non-linear sigma model whose space of vacua is obtained by requiring the first term to be zero, which is the solution of

$$qq^\dagger - \tilde{q}^\dagger \tilde{q} = r \quad (4.25)$$

modulo $U(k)$ gauge transformations.

This theory is super-renormalizable with respect to the dimensionful gauge coupling parameter e . However, the dimensionless FI parameter r gets renormalized due to a 1-loop ultraviolet (UV) divergence when $N_f \neq N_{\bar{f}}$. The renormalized FI parameter at an energy scale μ is

$$r(\mu) = \frac{N_f - N_{\bar{f}}}{2\pi} \log \frac{\mu}{\Lambda}, \quad (4.26)$$

where Λ is the dynamically generated scale of the 2d theory. When μ is much large than Λ

such that $r(\mu) > 0$, in the limit of $e \rightarrow \infty$, $r(\mu)$ is interpreted as the size of the target space of the sigma model. Note that when $N_f = N_{\bar{f}}$ there is no running of r and the complexified FI parameter τ is an exactly marginal parameter.

Now consider including the twisted masses \tilde{m}_1 into the U(1) gauge theory with $N_f = N$ chiral fields Q (and no \tilde{Q} , i.e., $N_{\bar{f}} = 0$). In the limit of $e \rightarrow \infty$ the theory describes the supersymmetric \mathbb{CP}^{N-1} sigma model. When we integrate out Q , the effective Lagrangian is given by

$$\mathcal{L}_{\text{eff}} = \int d^4\theta \mathcal{K}_{\text{eff}}(\Sigma, \bar{\Sigma}) + \left(\int d\theta^- d\bar{\theta}^+ \mathcal{W}_{\text{eff}}(\Sigma) + \text{h.c.} \right), \quad (4.27)$$

and the exact form of the twisted superpotential $\mathcal{W}_{\text{eff}}(\Sigma)$ is calculated [35, 36, 31] to be

$$\mathcal{W}_{\text{eff}}(\Sigma) = \frac{1}{2} \left[i\tau\Sigma - \frac{1}{2\pi} \sum_{i=1}^N (\Sigma - \tilde{m}_i) \left(\log \left(\frac{\Sigma - \tilde{m}_i}{\mu} \right) - 1 \right) \right], \quad (4.28)$$

where $\tau = ir(\mu) + \theta/2\pi$. The potential energy from this Lagrangian is

$$U = g^{\sigma\bar{\sigma}} \frac{\partial\mathcal{W}}{\partial\sigma} \frac{\partial\mathcal{W}}{\partial\bar{\sigma}}, \quad g_{\sigma\bar{\sigma}} = \frac{\partial^2\mathcal{K}}{\partial\sigma\partial\bar{\sigma}}. \quad (4.29)$$

Therefore supersymmetric vacua are obtained by solving $\partial\mathcal{W}_{\text{eff}}/\partial\sigma = 0$, from which we get N_f vacua as the solutions of

$$\prod_{i=1}^N (\sigma - \tilde{m}_i) = \mu^N e^{2\pi i\tau}. \quad (4.30)$$

When $\tilde{m}_i = 0$, this theory becomes the supersymmetric \mathbb{CP}^{N-1} sigma model and it has $\binom{N}{2}$ number of solitons interpolating two among the N vacua. We will discuss later how the BPS spectrum changes when we introduce the twisted masses.

4.4 Wall-crossing of 2d $\mathcal{N} = (2, 2)$ BPS spectra

As is the case for 4d $\mathcal{N} = 2$ BPS states, the number of BPS states of a 2d $\mathcal{N} = (2, 2)$ theory does not change in general under continuous changes of the parameters of the theory, especially those of the superpotential W because it is W that determines the universality class of the theory. However, similarly to BPS spectra of 4d $\mathcal{N} = 2$ theories, a BPS spectrum

of a 2d $\mathcal{N} = (2, 2)$ theory can undergo a jump when the theory goes over a 2d BPS wall. Here we will briefly review the relevant formula [35], and later we will discuss examples of such phenomena in the context of spectral networks [37].

On the W -plane of a 2d $\mathcal{N} = (2, 2)$ Landau-Ginzburg model, consider a trajectory of a BPS state that is a straight line connecting two critical values of W , $w_a = W(\phi_a)$ and $w_b = W(\phi_b)$. When such a trajectory from w_a passes a point w on the W -plane, there is a preimage of the trajectory connecting w_a and w . This is a real $(n - 1)$ -dimensional homology cycle in the $(n - 1)$ -dimensional complex manifold defined by $W^{-1}(w)$, where n is the number of the chiral fields of the Landau-Ginzburg model, and we will call the cycle Δ_a . This is a vanishing cycle as it shrinks to zero when we take $w \rightarrow w_a$. Similarly we can think of another cycle Δ_b that is a preimage of the trajectory connecting w_b and w . Now the number of solitons between the two critical values of W that cannot disappear by deformations is given by the intersection of the two cycles [35],

$$A_{ab} = \langle \Delta_a, \Delta_b \rangle. \quad (4.31)$$

To understand how this formula can provide us information about the 2d wall-crossing, as an example consider a superpotential W that has three critical values $W = w_a, w_b$, and w_c , and that has a certain set of the parameters so that there is one soliton connecting w_a and w_b , another soliton connecting w_b and w_c , and no soliton connecting w_a and w_c . Suppose that W is changed such that the Δ_a is changed to a different cycle Δ'_a whose image on the W -plane passes through w_b , while the other cycles remain to be the same homology elements. Then from Picard-Lefschetz theory of vanishing cycles we get [35]

$$\Delta'_a = \Delta_a \pm \langle \Delta_a, \Delta_b \rangle \Delta_b, \quad (4.32)$$

which provides the number of solitons connecting the critical values w_a and w_c ,

$$A'_{ac} = A_{ac} \pm A_{ab}A_{bc}. \quad (4.33)$$

Then we see that the number of solitons connecting w_a and w_c has jumped from zero to nonzero, implying the 2d theory passed through a 2d BPS wall.

4.5 2d $\mathcal{N} = (2, 2)$ theories from branes

In this section we study IIA brane configurations and their M-theory lift that describe 2d $\mathcal{N} = (2, 2)$ theories [31, 38, 39, 40].

4.5.1 From 4d $\mathcal{N} = 2$ to 2d $\mathcal{N} = (2, 2)$

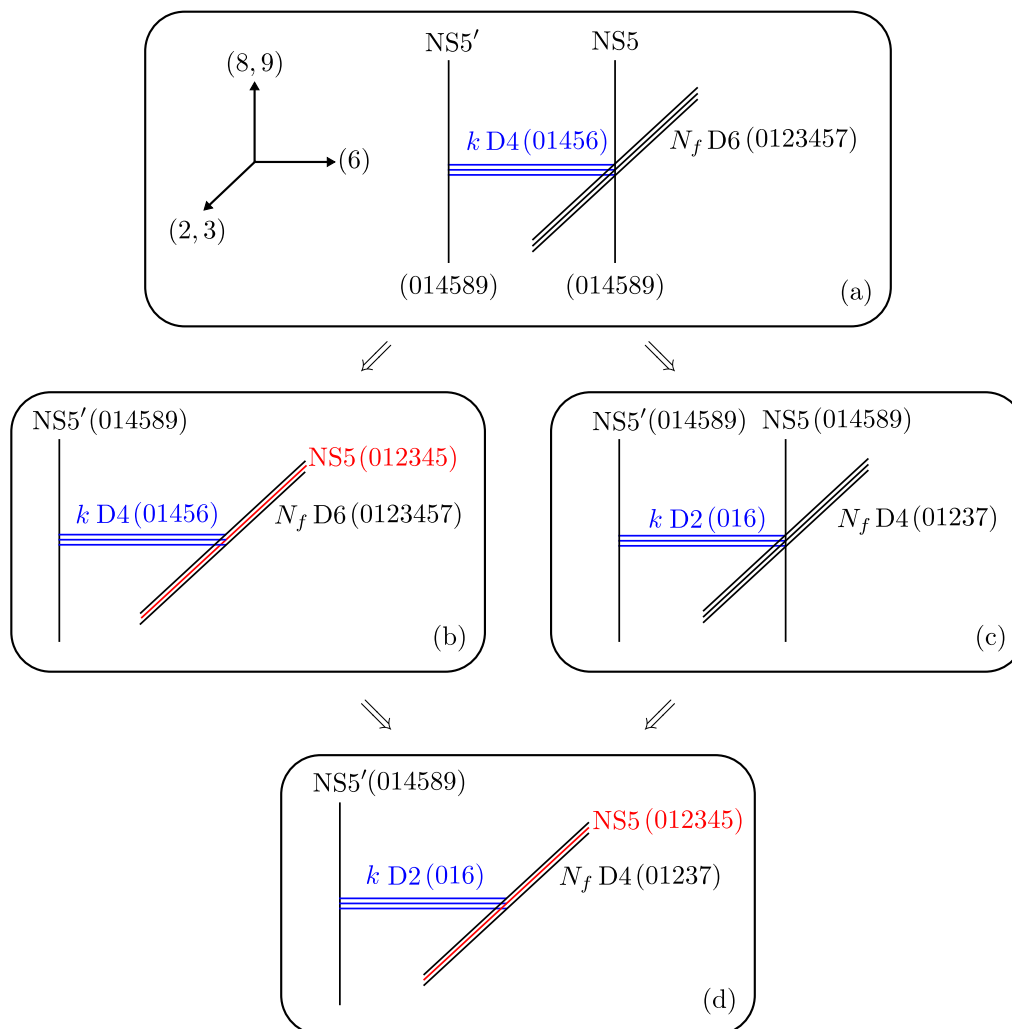


Figure 4.1

We can obtain the brane configuration of a 2d $\mathcal{N} = (2, 2)$ theory from that of a 4d $\mathcal{N} = 2$ theory shown in Figure 4.1a. Here N_f D6-brane, each of which provides an $\mathcal{N} = 2$ hypermultiplet Q_i in the fundamental representation of $U(k)$ for the 4d theory living on k D4-branes, are moved along x^6 to the location of one of the two NS5-branes. The mass of Q_i depends on the distance along the (x^8, x^9) -plane between the D4-branes and the D6-brane.

The 4d theory also has an $\mathcal{N} = 2$ vector multiplet, consisting of an $\mathcal{N} = 1$ chiral multiplet Φ that is in the adjoint representation of $U(k)$ and parametrizes the locations of the D4-branes on the (x^8, x^9) -plane, and an $\mathcal{N} = 1$ vector multiplet V giving the $U(k)$ gauge field of the 4d theory.

If we rotate the NS5-brane from (x^8, x^9) to (x^2, x^3) [41], denoting the other NS5-brane as NS5', we obtain the brane configuration shown in Figure 4.1b, which gives us a 4d $\mathcal{N} = 1$ theory [42, 43]. This rotation makes Φ massive [44], and integrating it out results in reducing the $\mathcal{N} = 2$ vector multiplet to the $\mathcal{N} = 1$ vector multiplet. The $\mathcal{N} = 2$ hypermultiplet Q_i in the fundamental representation of $U(k)$ becomes two $\mathcal{N} = 1$ chiral multiplets Q_i and \tilde{Q}^i , one in the fundamental representation of $U(k)$ and the other in the antifundamental representation. Because a D6-brane spans the x^7 -direction and the NS5-brane meets it at $x^7 = 0$, we can break the D6-brane into two, each of which furnishes either Q_i or \tilde{Q}^i , and by sending one of the two semi-infinite D6-brane to infinity along the NS5-brane, we can decouple either Q_i or \tilde{Q}^i . Here we will keep Q_i and decouple \tilde{Q}^i .

To sum up, at the end of the process from Figure 4.1a to Figure 4.1b we have a 4d $\mathcal{N} = 1$ vector multiplet, N_f $\mathcal{N} = 1$ chiral multiplets Q_i , and N_f $\mathcal{N} = 1$ chiral multiplets \tilde{Q}^i .

Now we take T-dualities twice, along x^4 and then along x^5 , to obtain the brane configuration of Figure 4.1d, which gives a 2d $\mathcal{N} = (2, 2)$ theory living on the (x^0, x^1) worldvolume of the k D2-branes from the D4-branes. To find out the field contents, consider the dimensional reduction of the 4d $\mathcal{N} = 1$ theory to a 2d $\mathcal{N} = (2, 2)$ theory [32]. Then the 4d chiral multiplets Q_i and \tilde{Q}^i become 2d chiral multiplets, and the 4d $\mathcal{N} = 1$ vector multiplet V becomes a 2d $\mathcal{N} = (2, 2)$ vector multiplet, which can be packaged into a 2d $\mathcal{N} = (2, 2)$ twisted chiral multiplet Σ ,

$$\Sigma = \sigma + \theta^+ \bar{\lambda}_+ + \bar{\theta}^- \lambda_- + \theta^+ \bar{\theta}^- (D - iF_{01}), \quad (4.34)$$

where we followed the notation of [45], see Chapter 12. This multiplet contains a scalar $\sigma = A_4 + iA_5$ as the lowest component, a 2d complex fermion with components λ_- and $\bar{\lambda}_+$, and $D - iF_{01}$ as the highest component, where D is an auxiliary real scalar field and F_{01} is the field strength of the 2d gauge field.

We can also take the T-dualities first and then rotate the NS5-brane. Starting from the 4d $\mathcal{N} = 2$ brane configuration of Figure 4.1a, we take the same T-dualities along x^4 and

x^5 as we did when we transformed 4.1b to 4.1d. The result is a IIA brane configuration that gives a 2d $\mathcal{N} = (4, 4)$ theory [46]. The 4d $\mathcal{N} = 2$ hypermultiplet Q_i becomes a 2d $\mathcal{N} = (4, 4)$ hypermultiplet (Q_i, \tilde{Q}^i) , which consists of two 2d $\mathcal{N} = (2, 2)$ chiral multiplets Q_i and \tilde{Q}^i . The 4d $\mathcal{N} = 2$ vector multiplet V becomes a 2d $\mathcal{N} = (4, 4)$ vector multiplet (Σ, Φ) , which consists of a 2d $\mathcal{N} = (2, 2)$ twisted chiral multiplet Σ containing a scalar $\sigma = A_4 + iA_5$ as the lowest component and a 2d $\mathcal{N} = (2, 2)$ chiral multiplet Φ containing a scalar $\phi = X^8 + iX^9$ as the lowest component [47].

Then we rotate the NS5-brane from (x^8, x^9) plane to (x^2, x^3) plane, obtaining the brane configuration shown in Figure 4.1d. The rotation of the NS5-brane breaks the half of the supersymmetry and makes the 2d $\mathcal{N} = (2, 2)$ chiral multiplet Φ massive. What we get from the original 4d $\mathcal{N} = 2$ vector multiplet V is the 2d $\mathcal{N} = (2, 2)$ twisted chiral multiplet Σ . After the rotation the 2d $\mathcal{N} = (2, 2)$ chiral multiplets Q_i and \tilde{Q}^i can have different masses because they are no longer in a single multiplet. Each mass correspond to the location of the semi-infinite D4-brane along the NS5-brane, and we can decouple one of the two to keep the other one only, see Figure 7.2e.

Note the similarity of the two brane configuration Figure 4.1b and Figure 4.1d, one giving us a 4d $\mathcal{N} = 1$ theory and the other a 2d $\mathcal{N} = (2, 2)$ theory. The two theories have the same number of supercharges and share many physical phenomena [48], although the qualitative aspects of a 2d $\mathcal{N} = (2, 2)$ theory more resembles that of a 4d $\mathcal{N} = 2$ theory. Later we will compare the brane configuration that provides a 4d $\mathcal{N} = 1$ theory with a Landau-Ginzburg type polynomial superpotential in the adjoint chiral multiplet Φ with a brane configuration that gives a 2d $\mathcal{N} = (2, 2)$ theory to identify the twisted superpotential of the 2d theory as Landau-Ginzburg type.

4.5.2 2d $\mathcal{N} = (2, 2)$ theory from 4d $\mathcal{N} = 2$ theory at the root of the Higgs branch

Using the rotation of an NS5-brane previously described, we can get a brane configuration of a 2d theory from that of a 4d theory at the root of its baryonic Higgs branch.

We start with a 4d $\mathcal{N} = 2$ $SU(N)$ gauge theory with $N_f = N$ hypermultiplets coming from the IIA brane configuration shown in the left of Figure 4.2, where we have two NS5-branes filling the 4d spacetime and $v = x^4 + ix^5$, and D4-branes filling the same 4d spacetime and spanning $|t| = x^7$. When we lift the brane configuration to M-theory, it becomes a

Seiberg-Witten curve described by [7]

$$f_N(t, v) = t^2 - \left(\sum_{j=0}^N u_j v^{N-j} \right) t + \Lambda^N \prod_{j=1}^N (v - m_j) = t^2 - U_N(v; u_j) t + \Lambda^N M_N(v; m_j), \quad (4.35)$$

where $u_0 = 1$ and $u_1 = 0$. Λ is the dynamically generated scale of the 4d theory, u_j are the Coulomb branch parameters of the 4d theory, and m_j are the masses of $N_f = N$ hypermultiplets.

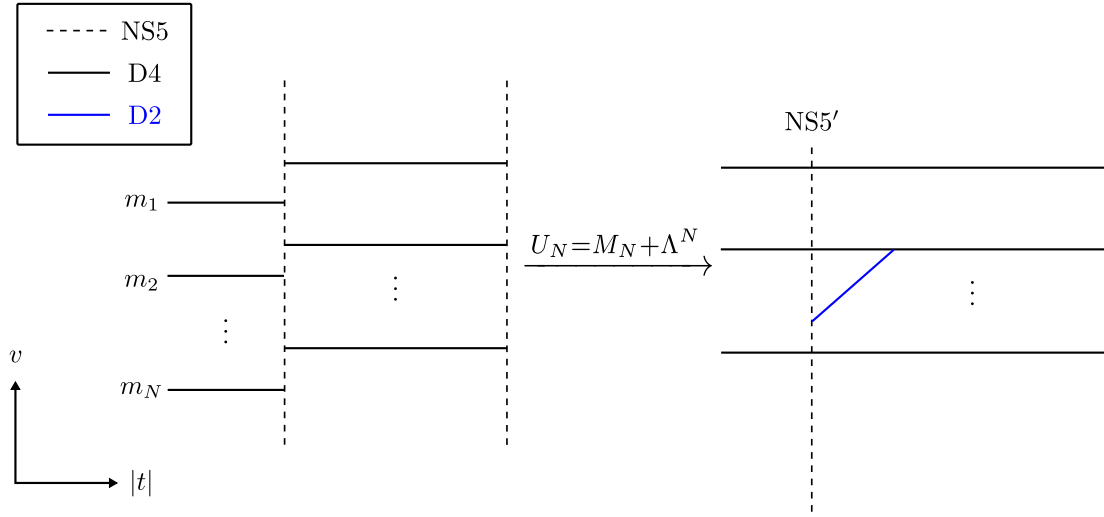


Figure 4.2

First we tune the mass parameters so that

$$U_N = M_N + \Lambda^N \quad (4.36)$$

is satisfied. This corresponds to moving the semi-infinite D4-branes along the v -direction so that each semi-infinite D4-brane aligns with each finite D4-brane between the NS5-branes. Then $f_N(t, v)$ is factorized into two curves,

$$f_N(t, v) = (t - \Lambda^N)(t - M_N), \quad (4.37)$$

and the 4d theory is at the root of the baryonic Higgs branch [38], where the Coulomb branch moduli space of the 4d theory meets the Higgs branch of the theory. As long as eq. (4.36) is satisfied, we can change u_j and m_j while keeping the 4d theory at the root of the

baryonic Higgs branch [49]. Let's assume that we have $SU(N_f) = SU(N)$ flavor symmetry so that $\sum m_j = 0$. Then we can think of u_j as being determined via eq. (4.36) when we fix m_j or vice versa.

The factorization of the original Seiberg-Witten curve implies that we can detach the NS5-brane at $t = \Lambda^N$, which we will call NS5', as shown in the right of Figure 4.2. Now the 4d theory is at its Higgs branch and we can put a D2-brane that fills the (x^0, x^1) -plane of the 4d spacetime and spans the x^6 -direction between NS5' and the rest of the Seiberg-Witten curve. This results in a brane configuration similar to Figure 4.1d, the difference being the orientation of NS5'. That is, NS5' of Figure 4.2 spans the same spacetime (012345) as the other NS5-brane.

This brane configuration results in a 2d $\mathcal{N} = (2, 2)$ U(1) gauge theory on the D2-brane [31]. The 2d theory has a free chiral multiplet Φ' having $\phi' = X^2 + iX^3$ as the lowest component, where (X^2, X^3) is the location of the D2-brane in the (x^2, x^3) -plane. It also has additional chiral multiplets Q_i , carrying U(1) gauge charge +1, from the fundamental strings between the D2-brane and the D4-branes.

Now we rotate NS5' such that the (x^2, x^3) -plane it fills rotates to the (x^8, x^9) -plane [41]. Then Φ' becomes massive and decouples from the 2d theory, and the brane configuration in the right of Figure 4.2 is the same as that of Figure 4.1d, if we relabel (23), (45), and (89) of Figure 4.1d to (45), (89), and (23), respectively. In addition to decoupling the chiral multiplet Φ' , the rotation of NS5' gives us an interesting constraint, the s-rule [50], which says that we cannot put more than one D2-brane between NS5' and a D4-brane if we want to get a supersymmetric configuration. This will be important when we consider multiple D2-branes.

So we obtained a 2d $\mathcal{N} = (2, 2)$ theory starting from a 4d theory at a special location of its moduli space. However, the final result, the brane configuration shown in the right of Figure 4.2, can be obtained from a general 4d $\mathcal{N} = 2$ theory. Consider a IIA brane configuration for a 4d $\mathcal{N} = 2$ pure $SU(N)$ gauge theory, and put a D2-brane between the brane configuration and another NS5-brane, denoted as NS5' in Figure 4.3, whose worldvolume fills $(x^0, x^1, x^4, x^5, x^8, x^9)$.

Now consider that we make the separation of the two NS5-branes at the two ends of D4-branes very large, corresponding to the UV gauge coupling of the 4d theory being very weak. When the D2-brane is moved near to one of the NS5-branes, then the brane configuration

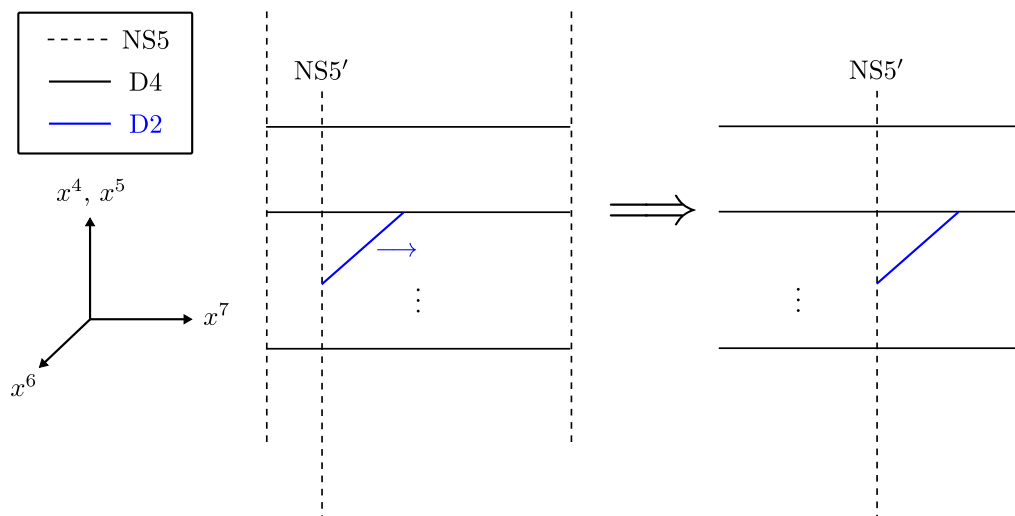


Figure 4.3

the D2 brane sees is effectively the same as that shown in the right of Figure 4.2. The Coulomb branch parameters of the 4d gauge theory from the brane configuration of Figure 4.3 become the mass parameters m_j of Figure 4.2, which make sense because when the 4d theory is weakly coupled, the Coulomb branch parameters can be understood as the mass parameters of the weakly gauged flavor symmetry [5].

4.5.3 Parameters of the 2d $\mathcal{N} = (2, 2)$ theory from branes

Figure 4.4 shows a IIA brane configuration that describes the 2d $\mathcal{N} = (2, 2)$ theory we studied in Section 4.5.2. There are various parameters describing the 2d theory, and they can be read off from the brane configuration [31, 51].

Δx^6 is the length of the D2-brane along x^6 , which is related to the dimensionful 2d gauge coupling parameter e as

$$\frac{1}{e^2} \sim \frac{\Delta x^6 l_s}{g_s}, \quad (4.38)$$

where l_s is the string length scale and g_s is the string coupling constant. When $\Delta x^6 \ll g_s l_s$ the 2d theory becomes strongly coupled, $e \rightarrow \infty$.

Δx^7 is the distance between the endpoint of the D2-brane and the NS5-brane, which is

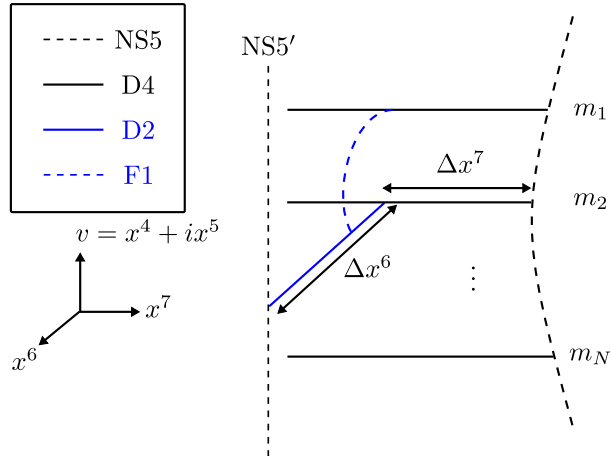


Figure 4.4

related to the 2d Fayet-Illiopoulos (FI) parameter r as

$$r \sim \frac{\Delta x^7}{g_s l_s}. \quad (4.39)$$

Note that this is not an exact relation, because there is the bending of the NS5-brane due to the D4-branes, so the notion of the distance Δx^7 is ambiguous. This and the introduction of a θ -angle to the 2d theory will be explained when we lift the brane configuration to M-theory, but for now we will consider $|r| \gg 1$, where we will disregard the ambiguity. Then the FI parameter is related to the 2d sigma model coupling parameter g as

$$r \sim \frac{1}{g^2}. \quad (4.40)$$

And there are m_j , which are related to the twisted masses of 2d chiral multiplets from the fundamental strings between the D2-brane and the D4-branes.

We will review the study of the BPS spectrum of the 2d theory from the D2-brane ending around $\Delta x^7 \ll 0$ in Section 4.5.4, which is described by a mass-deformed classical supersymmetric \mathbb{CP}^{N-1} sigma model [38], and from the D2-brane ending around $\Delta x^7 \gg 0$ in Section 4.5.5, which is described by a quantum supersymmetric \mathbb{CP}^{N-1} sigma model [31].

4.5.4 BPS spectrum of a mass-deformed classical $\mathbb{C}P^{N-1}$ sigma model

The 2d theory from a D2-brane in Figure 4.4, whose endpoint on a D4-brane is at far left from the NS5-brane, has the classical potential energy of

$$U = \sum_{i=1}^N |\sigma - m_i|^2 |q_i|^2 + \frac{e^2}{2} \left(\sum_{i=1}^N |q_i|^2 - r \right)^2, \quad (4.41)$$

where q_i is the scalar component of a 2d chiral superfield Q_i in the fundamental representation of $SU(N_f) = SU(N)$ with U(1) charge +1, and σ is the scalar component of the 2d twisted chiral superfield Σ .

When $\sigma = m_j$, the D2 brane ends on the j th D4-brane. Because we are considering $r \gg 1$ case here, for the 2d theory to be at the j th supersymmetric ground state we require $|q_j|^2 = r$ and $q_i = 0$ for $i \neq j$. Therefore there are $N_f = N$ supersymmetric ground states, and at each ground state, after eliminating Σ by its equation of motion, the 2d theory is described by the following effective Lagrangian [38],

$$\mathcal{L}_{\text{eff}} = r \int d^4\theta \log \left[1 + \sum_{i \neq j} \bar{W}_i^{(j)} \exp(2V_j - 2V_i) W_i^{(j)} \right], \quad (4.42)$$

where $W_i^{(j)}$ are chiral superfields, each of which comes from the fundamental string between the D2-brane ending on the j th D4-brane and the i th D4-brane and is defined such that its scalar component is

$$w_i^{(j)} = q_i/q_j, \quad q_j \neq 0, \quad i \neq j, \quad (4.43)$$

and V_i are background gauge superfields defined as

$$V_i = \theta^\alpha \sigma_{\alpha\dot{\alpha}}^\mu \bar{\theta}^{\dot{\alpha}} V_{\mu i} = \theta^- \bar{\theta}^+ m_i + \theta^+ \bar{\theta}^- (m_i)^*, \quad \hat{V}_{1i} = \text{Re}(m_i), \quad \hat{V}_{2i} = -\text{Im}(m_i), \quad \hat{V}_{0i} = \hat{V}_{3i} = 0. \quad (4.44)$$

The BPS spectrum of the 2d theory contains elementary quanta of $W_i^{(j)}$. In each of the

N vacua, there are $N - 1$ BPS multiplets from $W_i^{(j)}$, whose masses are

$$M_{ij} = |m_i - m_j| = \left| \sum_{i=1}^N m_i S_i \right| = |Z|, \quad (4.45)$$

where we defined the quantum number S_i corresponding to the flavor symmetry from m_i . $W_i^{(j)}$ carries $S_i = +1$, $S_j = -1$, and $S_k = 0$ for $k \neq i, j$.

The BPS spectrum also contains solitons. A soliton interpolating the i th ground state $\sigma = m_i$ at $x = -\infty$ and j th ground state $\sigma = m_j$ at $x = +\infty$ has the mass of

$$M_{ij} = r|m_i - m_j| = 2|\mathcal{W}(m_i) - \mathcal{W}(m_j)| = |Z|, \quad (4.46)$$

where $\mathcal{W}(\sigma) = \frac{i}{2}\tau\sigma$ is the classical twisted superpotential with the holomorphic quantity $\tau = r + i\frac{\theta_i}{2\pi}$ with the nonzero 2d θ -angle taking into account. There are $2\binom{N}{2} = N(N-1)$ solitons interpolating two among the N ground states.

The central charge Z is defined to be

$$Z = 2\Delta\mathcal{W} + i \sum_{i=1}^N m_i S_i, \quad (4.47)$$

and using this we can also get the masses of dyons in the BPS spectrum of the 2d theory.

The effect of quantum correction is that the naive definition of r as the distance from the NS5-brane to the endpoint of the D2-brane is not an exact description because of the bending of the NS5-brane. However, this can be addressed by adding quantum correction to the classical \mathcal{W} , and then the expression for Z still holds even after the quantum correction.

The result of the quantum correction is that r and θ are functions of m_i and Λ , the dynamically generated scale of the 2d theory. When $|m_i| \gg \Lambda$, we can express the FI parameter r as a function of $|m_i|/\Lambda$, and r is much greater than 1, which corresponds to the D2-brane ending at the far left of the IIA brane system and is consistent with the fact that the 2d theory is well described by a classical sigma model with coupling $g \propto 1/\sqrt{r}$.

As an example, let's consider the $N = 2$ case, that is we start with a 4d $\mathcal{N} = 2$ SU(2) theory with $N_f = 2$ hypermultiplets and get the 2d $\mathcal{N} = (2, 2)$ theory from it. In terms of $m = m_1 - m_2$, the running of the sigma model coupling under the 1-loop correction stops at the scale of m because the 2d chiral multiplets will be integrated out below the scale.

When $|m| \gg \Lambda$, we can express r as

$$r = \log \left(\frac{|m|^2}{\Lambda^2} \right) + c_0 + \sum_{k=1}^{\infty} c_k \left(\frac{|m|^2}{\Lambda^2} \right)^{-k}, \quad (4.48)$$

where the first term is a 1-loop contribution, c_0 is a renormalization-dependent finite contribution, and c_k is a k -instanton contribution. Indeed $r \gg 1$ when $|m| \gg \Lambda$, justifying our naive interpretation of r as the distance between the NS5-brane and the endpoint of the D2-brane. Note that we can redefine c_0 and c_k to be complex constants such that r is a holomorphic function of m .

4.5.5 BPS spectrum of a quantum supersymmetric \mathbb{CP}^{N-1} sigma model

So far we studied the 2d theory from the brane configuration of Figure 4.4 when $r \gg 1$, which can be described as a classical sigma model with the leading-order quantum correction from the 1-loop contribution. Because the classical potential energy of the 2d theory is given by (4.41), when $r \ll -1$ classically we cannot find a supersymmetric ground state that satisfies $U = 0$. From the perspective of the brane configuration, this means that classically we do not see the bending of the NS5-brane and therefore we cannot put a D2-brane between the NS5' and D4-NS5 brane system when NS5' is at $\Delta x^7 < 0$.

But we know that there is the bending of the NS5-brane due to the 1-loop quantum correction, and therefore we can put a D2-brane even when the NS5' is at $\Delta x^7 < 0$. In order to understand the 2d theory in this regime, we use the exact twisted superpotential of the 2d theory [36, 35].

To find the exact twisted superpotential, we start with a 2d $\mathcal{N} = (2, 2)$ U(1) gauge theory with N chiral multiplets Q_i , each having U(1) charge +1. This is the gauged linear sigma model we studied in Section 4.3, where we found that, after integrating out the chiral fields, the theory is described by an exact twisted superpotential

$$\mathcal{W}_{\text{eff}}(\Sigma) = \frac{1}{2} \left[i\tau\Sigma - \frac{1}{2\pi} \sum_{i=1}^N (\Sigma - \tilde{m}_i) \left(\log \left(\frac{\Sigma - \tilde{m}_i}{\mu} \right) - 1 \right) \right], \quad (4.49)$$

where

$$\tau = ir(\mu) + \theta/2\pi, \quad r(\mu) = \frac{N}{2\pi} \log \frac{\mu}{\Lambda}. \quad (4.50)$$

If we define

$$\tilde{\Lambda} = \Lambda e^{\frac{i\theta}{N}}, \quad (4.51)$$

then we can rewrite the twisted superpotential as

$$\mathcal{W}_{\text{eff}}(\Sigma) = \frac{1}{2} \sum_{i=1}^N (\Sigma - m_i) \left(\log \left(\frac{\Sigma - m_i}{\tilde{\Lambda}} \right) - 1 \right). \quad (4.52)$$

The ground states of this 2d theory can be found by solving [52]

$$\exp \left(2 \frac{\partial \mathcal{W}(\sigma)}{\partial \sigma} \right) = \exp \left[\sum_{i=1}^N \log \left(\frac{\sigma - m_i}{\tilde{\Lambda}} \right) \right] = \frac{\prod_i (\sigma - m_i)}{\tilde{\Lambda}^N} = 1. \quad (4.53)$$

Note that this equation is equivalent to

$$\sum_{i=1}^N \log \left(\frac{\sigma - m_i}{\tilde{\Lambda}} \right) = 2\pi i n, \quad n \in \mathbb{Z}, \quad (4.54)$$

and each choice of n can be absorbed into $\tilde{\Lambda}$ by the change of θ . n comes from the fact that F_{01} , the 2d gauge field strength in the imaginary part of the highest component of Σ ,

$$\Sigma = \sigma + \dots + \theta^+ \bar{\theta}^- (D - iF_{01}), \quad (4.55)$$

is subject to the constraint of the quantization of its magnetic flux [53],

$$\frac{1}{2\pi i} \int F = m \in \mathbb{Z}. \quad (4.56)$$

and by introducing n we make $D \pm iF_{01}$ two independent auxiliary fields [52].

When we focus on the case of $n = 0$, there are N ground states, $\sigma_1, \dots, \sigma_N$, each of which corresponds to a D2-brane ending on the IIA brane system in Figure 4.4. The mass of a 2d soliton interpolating two ground states $\sigma = \sigma_i$ and $\sigma = \sigma_j$ is

$$\left| 2 [\mathcal{W}(\sigma_i) - \mathcal{W}(\sigma_j)] + \sum_i m_i S_i \right|, \quad (4.57)$$

where S_i are the flavor charges. S_i result in the ambiguity of determining the mass of

the soliton, which can be resolved when we study a specific 2d theory from the brane configuration of Figure 4.4 [31].

As an example, let's consider how the case of $N = 2$ works out with the previous results. Assuming $m_1 + m_2 = 0$ to consider $SU(2)$ flavor symmetry, we have

$$\mathcal{W}(\sigma) = \frac{1}{2} \left[(\sigma - m_1) \left(\log \left(\frac{\sigma - m_1}{\tilde{\Lambda}} \right) - 1 \right) + (\sigma - m_2) \left(\log \left(\frac{\sigma - m_2}{\tilde{\Lambda}} \right) - 1 \right) \right] \quad (4.58)$$

$$= -\sigma + \frac{1}{2} \sigma \log \left(\frac{\sigma^2 - m_1^2}{\tilde{\Lambda}^2} \right) - \frac{1}{2} m_1 \log \left(\frac{\sigma - m_1}{\tilde{\Lambda}} \right) + \frac{1}{2} m_1 \log \left(\frac{\sigma + m_1}{\tilde{\Lambda}} \right), \quad (4.59)$$

from which we get the equation for the ground states for $n = 0$,

$$\frac{\partial \mathcal{W}}{\partial \sigma} = 0 \implies \sigma^2 = m_1^2 + \Lambda^2. \quad (4.60)$$

Then the difference of \mathcal{W} between the two ground states $\sigma_{\pm} = \pm \sqrt{m_1^2 + \Lambda^2}$ is

$$\mathcal{W}(\sigma_-) - \mathcal{W}(\sigma_+) = 2\sqrt{m_1^2 + \Lambda^2} + m_1 \log \left(\frac{m_1 - \sqrt{m_1^2 + \Lambda^2}}{m_1 + \sqrt{m_1^2 + \Lambda^2}} \right). \quad (4.61)$$

As previously mentioned, the mass of a soliton cannot be fixed due to the flavor charges. However, in the limit of $|m_1| \gg \Lambda$, the leading-order contribution to the mass comes from $\Delta \mathcal{W}$,

$$\Delta \mathcal{W} = m_1 \left[\log \left(\frac{m_1}{\Lambda} \right)^2 + c_0 + c_1 \left(\frac{m_1}{\Lambda} \right)^{-2} + \dots \right], \quad (4.62)$$

whereas the contribution from S_i to the mass is of the same order as the c_0 term. This limit is the regime where the classical analysis of the 2d theory is applicable, and the approximate value of the 2d FI parameter can be obtained using (4.46),

$$\Delta \mathcal{W} \simeq \frac{r}{2} |m_1 - m_2| \implies r = \log \left(\frac{m_1}{\Lambda} \right)^2 + \mathcal{O}(1) + \mathcal{O} \left(\frac{\Lambda^2}{m_1^2} \right) + \dots, \quad (4.63)$$

which corresponds to (4.48) and is indeed much larger than 1 when $|m_1| \gg \Lambda$.

In the opposite limit, $|m_1| \ll \Lambda$, (4.48) is not valid, which is indicated by the fact that $r \ll -1$ in this limit. But now we can see that this is because (4.48) corresponds to

expanding $\Delta\mathcal{W}$ in the other limit, $|m_1| \gg \Lambda$. If we do the correct expansion of $\Delta\mathcal{W}$, we get

$$\Delta\mathcal{W} = 2\Lambda \left(1 + \mathcal{O}\left(\frac{m_1}{\Lambda}\right) + \dots \right). \quad (4.64)$$

Again the contribution to the mass of a soliton from $\Delta\mathcal{W}$ is much larger than that from S_i in this limit, therefore we can find a good approximate value of the mass,

$$M \simeq 2|\Delta\mathcal{W}| = 4|\Lambda|, \quad (4.65)$$

which agrees with the result of [31] when $m_1 = 0$ up to a numerical factor. This completes the analysis of the BPS spectrum in this regime. That is, when $|m_1| \ll \Lambda$, the BPS spectrum consists of only solitons [48].

Here we analyzed the exact twisted superpotential of the 2d theory, and observed that in the limit of $|m_1| \gg \Lambda$ it reproduces the mass of BPS solitons of the classical supersymmetric \mathbb{CP}^1 sigma model, and that in the limit of $|m_1| \ll \Lambda$ it provides the mass of BPS solitons of the quantum supersymmetric \mathbb{CP}^1 sigma model. However, just analyzing the twisted superpotential does not lift the ambiguity of the flavor charges. Neither does it explain why we have different BPS spectra in the two limits — the classical sigma model has elementary quanta related to the flavor charges S_i and infinite number of dyons, whereas the quantum sigma model only has finite number of solitons. Therefore there should be a 2d wall-crossing phenomenon [38], which is nicely illustrated in [40].

Chapter 5

Spectral networks

Spectral networks are introduced in [37] as an extension of the analysis done in [6, 54], building on the previous related work of [19, 55, 40]. Here we will briefly review the topics of constructing a spectral network and using it to find the BPS spectra of 2d $\mathcal{N} = (2, 2)$ and 4d $\mathcal{N} = 2$ theories.

5.1 Construction of spectral networks

5.1.1 \mathcal{S} -walls

A spectral network consists of \mathcal{S} -walls, and each \mathcal{S} -wall carries two indices. One convenient picture to have in mind is that, when we consider the low energy effective theory of a 4d $\mathcal{N} = 2$ gauge theory on the Coulomb branch as coming from an M5-brane that wraps a punctured Riemann surface as an N -sheeted cover over it (8.1), these \mathcal{S} -walls correspond to the projections of the boundaries of M2-branes stretched between two sheets of the M5-brane onto the Riemann sphere, and the indices indicate which two sheets the boundaries are. This is not a precise statement, though, as pointed out in [10], but in some limit of the metric that the M-branes live the correspondence works. More precise statement is understanding an \mathcal{S} -wall as a self-dual string on the Riemann sphere, as explained in [6]. However, we expect both will give the same answer for the existence of a BPS state and the value of its central charge thanks to supersymmetry.

Each \mathcal{S} -wall follows the path described by the Seiberg-Witten curve and differential of the 4d theory. When we have a Seiberg-Witten curve $f(t, x) = 0$ as a multi-sheeted cover over the t -plane and the corresponding Seiberg-Witten differential $\lambda = xdt$, an \mathcal{S}_{jk} -wall of

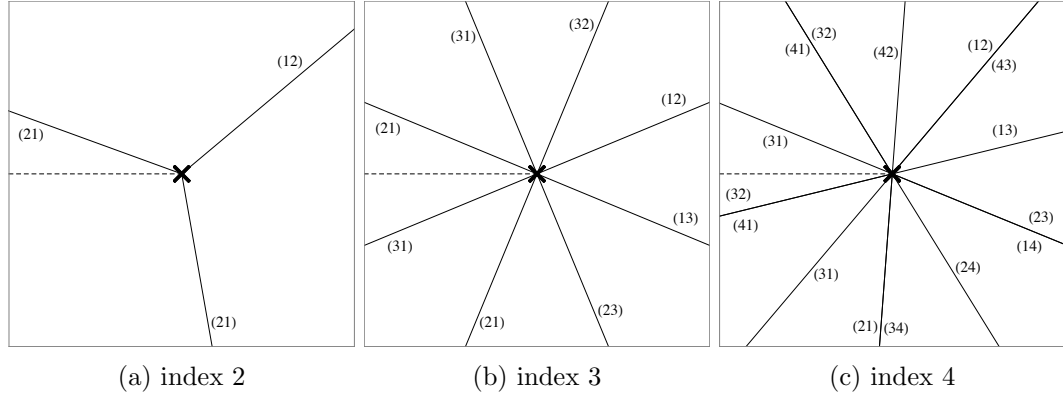


Figure 5.1: \mathcal{S} -walls around a branch point. \mathcal{S}_{jk} -walls are denoted by solid lines with (jk) . The broken line denotes the branch cut.

a spectral network satisfies

$$\frac{\partial \lambda_{jk}}{\partial \tau} = (\lambda_j(t, x) - \lambda_k(t, x)) \frac{dt}{d\tau} = e^{i\theta}, \quad (5.1)$$

where λ_j is the value of λ on the j -th sheet of x and τ is a real parameter along the \mathcal{S}_{jk} -wall.

An \mathcal{S} -wall starts either from a branch point or from a supersymmetric joint of \mathcal{S} -walls and flows in general into a puncture. In the following we will provide local descriptions of such cases. By patching the local pictures with the flow that (5.1) describes we construct a spectral network at a value of θ .

5.1.2 Around a branch point of ramification index N

First consider \mathcal{S} -walls on the curve $t = x^2$ around the branch point $t = 0$, with $\lambda = x dt$. On the t -plane, each \mathcal{S} -wall travels from the branch point along a real one-dimensional path defined by (5.1). For a fixed θ , each \mathcal{S} -wall starts at the branch point and goes to infinity as shown in Figure 5.5. Let us find out the equation that describes each \mathcal{S} -wall. We get two branches from the curve,

$$x_1 = \sqrt{t}, \quad x_2 = -\sqrt{t}, \quad (5.2)$$

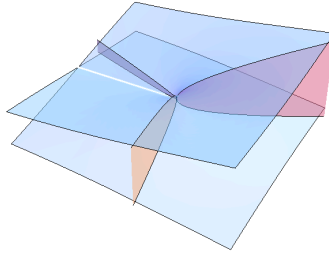


Figure 5.2: A Seiberg-Witten curve and \mathcal{S} -walls around a branch point of index 2.

which give us two differential equations for each θ ,

$$\lambda_{12}(t) \frac{dt}{d\tau} = 2\sqrt{t} \frac{dt}{d\tau} = \exp(i\theta), \quad (5.3)$$

$$\lambda_{21}(t) \frac{dt}{d\tau} = -2\sqrt{t} \frac{dt}{d\tau} = \exp(i\theta). \quad (5.4)$$

We will call the \mathcal{S} -walls obtained from the first equation \mathcal{S}_{12} , and the \mathcal{S} -walls from the second equation \mathcal{S}_{21} . By changing $\theta \rightarrow \theta + \pi$ we can also absorb the sign difference of λ_{12} and λ_{21} , which implies in practice we only need to solve the equation for $\theta \in [0, \pi)$ because the spectral network for $\theta + \pi$ can be obtained by flipping the indices of every \mathcal{S} -walls.

It is easy to solve the differential equations. We get, for \mathcal{S}_{12} ,

$$t(\tau) = \exp\left(\frac{2}{3}i\theta\right) \tau^{2/3}, \quad (5.5)$$

after an appropriate redefinition of τ . Now consider the cases when θ is changed by a multiple of 2π . When $\theta \rightarrow \theta + 2\pi$, the solution gets rotated around the branch point by $4\pi/3$, and it should be another \mathcal{S} -wall. However, there is a branch cut on the x -plane, and if the rotation by $4\pi/3$ makes the \mathcal{S}_{12} go through the branch cut, then the \mathcal{S} -wall becomes \mathcal{S}_{21} , otherwise it is another \mathcal{S}_{12} . When we change θ by π , the overall spectral network rotates by $\frac{2\pi}{3}$, which can be easily understood from (5.5), modulo the flip of the indices of the \mathcal{S} -walls as mentioned above. A spectral network around a branch point should be consistent under these monodromies, therefore we have three \mathcal{S} -walls as shown in Figure 5.5. Figure 5.2 illustrates the Seiberg-Witten curve and real two-dimensional surfaces that ends on the curve along the \mathcal{S} -walls. Here the Seiberg-Witten curve is represented by plotting the real part of x of the curve over the t -plane around a branch point of index 2.

Now let us generalize this analysis to the spectral network from a branch point of index

N [30]. When we have a branch point of ramification index N at $t = 0$, the corresponding curve is $t = x^N$, and the differential equation that governs the behavior of each \mathcal{S}_{ij} on the t -plane is

$$\omega_{ij} t^{1/N} \frac{\partial t}{\partial \tau} = \exp(i\theta), \quad (5.6)$$

where $\omega_{ij} = \omega_i - \omega_j$ and

$$\omega_k = \exp\left(\frac{2\pi i}{N} k\right), \quad k = 0, 1, \dots, N-1. \quad (5.7)$$

Then the solution for an \mathcal{S}_{ij} is

$$t_{ij}(\tau) = \left(\frac{\tau}{\omega_{ij}}\right)^{N/N+1} \exp\left(\frac{N}{N+1} i\theta\right) \quad (5.8)$$

after rescaling τ to absorb a real numerical coefficient. From the factor $1/\omega_{ij}$ we find $N(N-1)$ walls, and the exponent $\frac{N}{N+1}$ makes the angles between the walls to be multiplied by the factor $\frac{N}{N+1}$ from the differences of $\arg(1/\omega_{ij})$'s. As in the $N = 2$ case, the whole spectral network rotates by $\frac{2Nk\pi}{N+1}$ when we change θ from 0 to $2k\pi$. Consistency of a spectral network under this rotation requires $N-1$ additional walls and we have $N^2 - 1$ \mathcal{S} -walls around the branch point. The indices of \mathcal{S} -walls are determined by choosing the branch cut. Figures 5.1b, 5.1c shows spectral networks around a branch point of index 3 and 4, respectively.

5.1.3 Around a regular puncture of ramification index N

Let us first consider a regular puncture that carries an $SU(2)$ flavor symmetry in the A_1 theory. The residue of the Seiberg-Witten differential at the puncture is the Cartan of the flavor symmetry, in this case a mass parameter m . Consider such a regular puncture at $t = 0$, having $m \neq 0$. Then the corresponding (local) Seiberg-Witten curve is

$$t = (v - m)(v + m) = v^2 - m^2 \quad (5.9)$$

and the Seiberg-Witten differential is $\lambda = \frac{v}{t} dt$. When we project the curve on the t -plane, we have one branch point of index 2 at $t = -m^2$ and one puncture at $t = 0$.

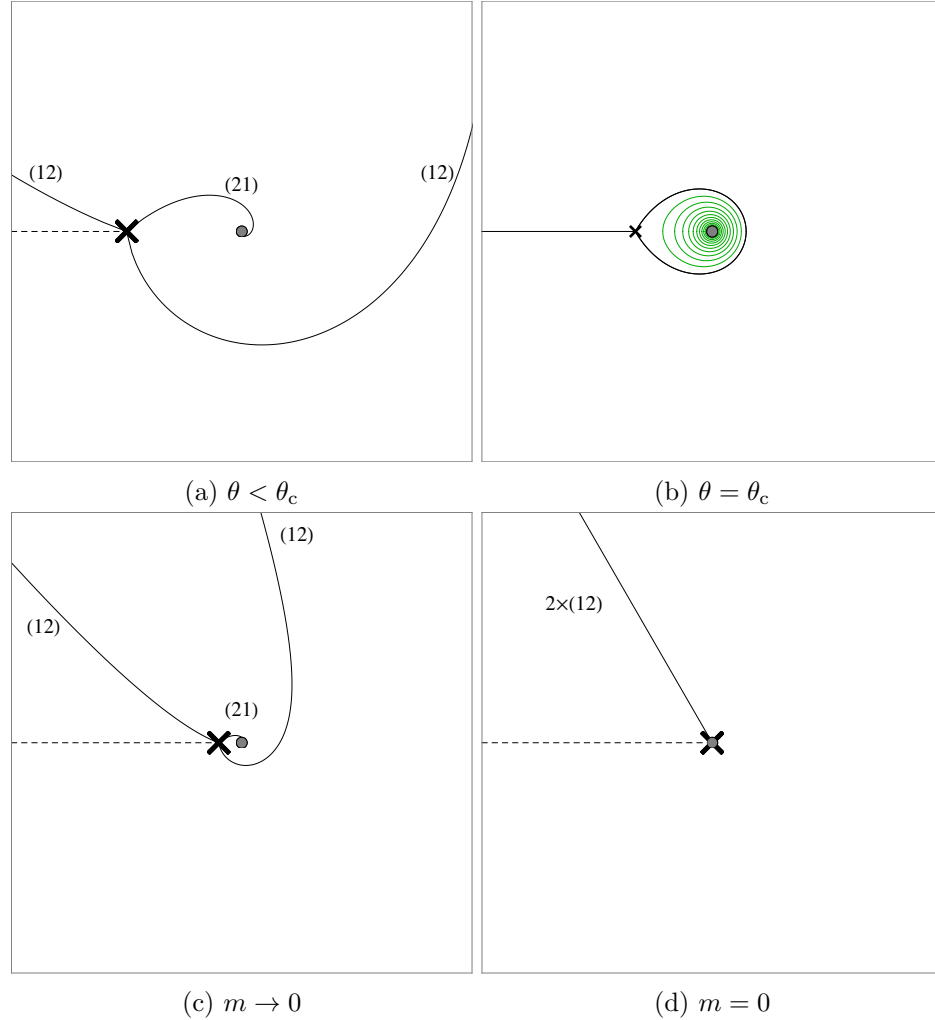
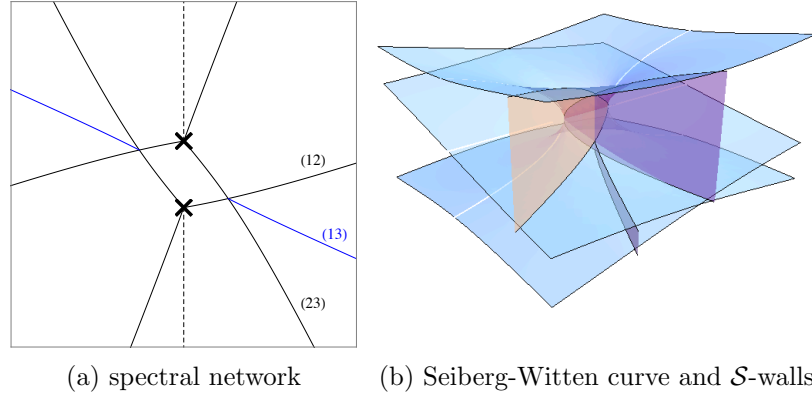


Figure 5.3: \mathcal{S} -walls around an $SU(2)$ puncture.

When $m \neq 0$, we can start with a spectral network from a branch point of index 2, as shown in Figure 5.3a. Note that one \mathcal{S} -wall flows into the puncture, while the other two escape to infinity [19]. When $\theta = \theta_c$, where $\theta_c = \arg(m_1 - m_2) + \pi/2 = \arg(2m) + \pi/2$, closed \mathcal{S} -walls can form around the puncture. This \mathcal{S} -wall has a topology of a cylinder, with its boundaries lying along the \mathcal{S} -walls on the two sheets. Therefore it corresponds to a BPS state carrying an $SU(2)$ flavor charge. This is consistent with the fact that an $\mathcal{N} = 2$ vector multiplet corresponds to an M2-brane with a topology of a cylinder, and when we gauge the flavor symmetry the \mathcal{S} -wall corresponds to a vector multiplet. Now consider the limit of $m \rightarrow 0$. Then the branch point moves toward the puncture as shown in Figure 5.3c, and when the two collide, we have a doublet of \mathcal{S} -walls emanating from the puncture.

Let us then consider the puncture with an $SU(N)$ flavor symmetry in the A_{N-1} theory.

Figure 5.4: \mathcal{S} -walls forming a joint.

The curve around the puncture is described by

$$t = \prod_{i=1}^N (v - m_i), \quad (5.10)$$

where $\sum_i m_i = 0$ and the Seiberg-Witten differential is $\lambda = \frac{v}{t} dt$. Let us focus on the massless limit where $t = 0$ becomes the branch point of index N , in addition to being the puncture. The asymptotic behavior of the \mathcal{S} -walls is obtained by solving

$$\int_0^t \omega_{ij} \frac{t'^{1/N}}{t'} dt' = e^{i\theta} \tau, \quad (5.11)$$

where we get $t(\tau) = \left(e^{iN\theta} / \omega_{ij}^N \right) \tau$ after rescaling real parameter τ . There are $N - 1$ sets of asymptotic directions for a value of θ due to the factor $1/\omega_{ij}^N$, and along each direction N \mathcal{S} -walls of same indices flow from the puncture. In total there are $N(N - 1)$ \mathcal{S} -walls from the massless puncture.

5.1.4 BPS Joint of \mathcal{S} -Walls

When we consider the spectral networks in (the compactification of) the A_{N-1} theory, $N > 2$, then there are more than two types of \mathcal{S} -walls. When there is a set of n \mathcal{S} -walls $\mathcal{S}_{i_1 i_2}, \mathcal{S}_{i_2 i_3}, \dots, \mathcal{S}_{i_n i_1}$, there can be a joint of the \mathcal{S} -walls. This is because $\lambda_{i_1 i_2} + \lambda_{i_2 i_3} + \dots + \lambda_{i_n i_1} = 0$ is satisfied at the joint such that it preserves supersymmetry.

Figure 5.4a shows the spectral network of the A_2 theory with two branch points of index 2, where we have \mathcal{S}_{13} coming from the joint of \mathcal{S}_{12} and \mathcal{S}_{23} . Figure 5.4b illustrates

the Seiberg-Witten curve and the three \mathcal{S} -walls that form a joint.

5.2 BPS spectrum from spectral networks

5.2.1 2d BPS states from spectral networks

We can construct a spectral network for the brane configuration and read out from it a 2d BPS spectrum of a 2d $\mathcal{N} = (2, 2)$ theory from an M2-brane ending at a point (t_0, v_j) on the Seiberg-Witten curve that spans 1 + 1-dimensional subspace of the 4d spacetime.

On which sheet of the covering space the endpoint lies determines the ground state of the 2d theory, and when an \mathcal{S}_{jk} -wall connects a (jk) -branch point to the endpoint $t = t_0$, it corresponds to a BPS soliton interpolating two 2d ground states corresponding to (t_0, v_j) and (t_0, v_k) [40]. The central charge of the BPS state is calculated by integrating λ_{jk} along the finite \mathcal{S} -wall,

$$Z = \int_{\tau_b}^{\tau_s} \lambda_{jk}(t) \frac{\partial t}{\partial \tau} d\tau = \int_{\tau_b}^{\tau_s} e^{i\theta} d\tau, \quad (5.12)$$

where $t(\tau_b)$ is the branch point and $t(\tau_s) = t_0$.

To find out all the BPS states, we change θ and see which \mathcal{S} -walls pass the M2-brane endpoint, where the value of θ that such an \mathcal{S} -wall exists gives the phase of the central charge of the BPS state. See Figure 5.5, where we have two 2d BPS states with $\arg(Z_{12}) = 0$ and $\arg(Z_{21}) = \pi$.

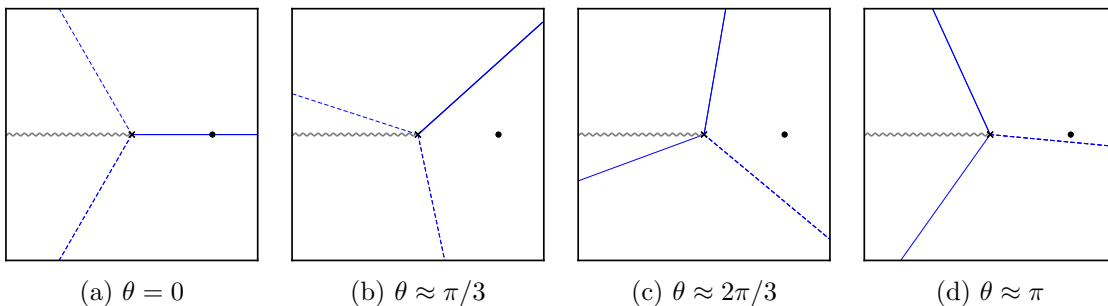


Figure 5.5

5.2.2 4d BPS states from spectral networks

Using spectral networks, we can identify a BPS state of the low energy effective theory, which corresponds to a cycle of the Seiberg-Witten curve, with a finite \mathcal{S} -walls [19, 37].

This is an \mathcal{S} -wall that has a finite value of

$$\int_{\mathcal{S}_{jk}} \lambda_{jk} = \int_{\tau_i}^{\tau_f} \lambda_{jk}(t) \frac{\partial t}{\partial \tau} d\tau = \int_{\tau_i}^{\tau_f} e^{i\theta_c} d\tau = Z, \quad (5.13)$$

where θ_c is the value of θ when such a finite \mathcal{S} -wall appears, as shown in Figure 5.6b, and Z is the central charge of the corresponding BPS state. To find out the whole set of BPS states, we evolve a spectral network from $\theta = 0$ to $\theta = 2\pi$ and identify finite \mathcal{S} -walls.

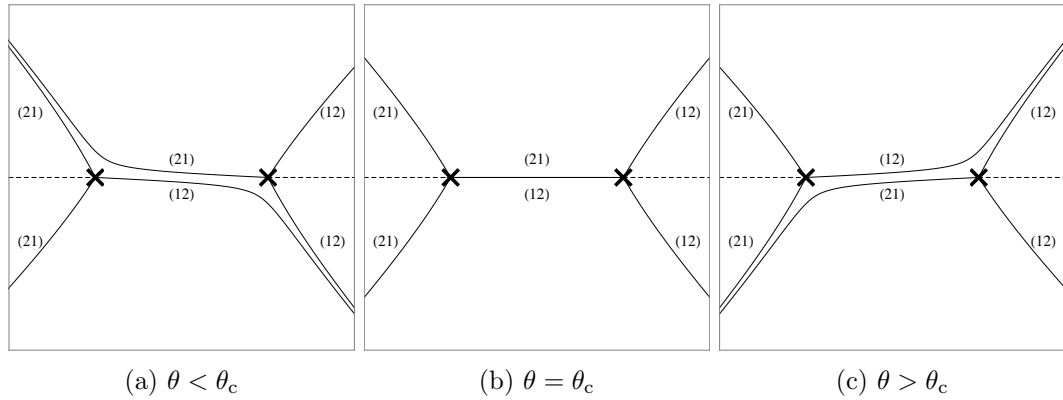


Figure 5.6: Appearance of a finite \mathcal{S} -wall.

Figure 5.6 shows how a finite \mathcal{S} -wall forms at $\theta = \theta_c$. When $\theta < \theta_c$, the corresponding spectral network, shown in Figure 5.6a, has two \mathcal{S} -walls of opposite indices that approach each other. When $\theta = \theta_c$, the two collide and this indicates that there is a finite \mathcal{S} -wall connecting the two branch points, forming a 1-cycle of the Seiberg-Witten curve. Figure 5.7 illustrates the Seiberg-Witten curve and the finite \mathcal{S} -wall.

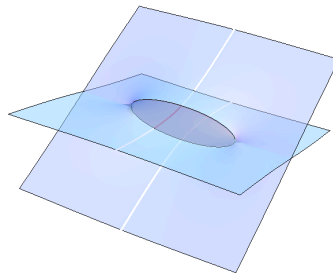


Figure 5.7: Seiberg-Witten curve from A_1 and a finite \mathcal{S} -wall.

Spectral networks provide more information than just the existence and the central charge of each BPS state: it also allows us to calculate the electric and the magnetic charges of the BPS state with respect to the IR gauge group. This is done by considering the intersections of the cycles corresponding to finite \mathcal{S} -walls, and in order to do that we need to put down the indices of every \mathcal{S} -wall of a spectral network.

We have already studied how to put indices to the \mathcal{S} -walls from a branch point and those from a joint, so the only question remaining is how to patch the \mathcal{S} -walls in the right way. The indices are changed only when an \mathcal{S} -wall crosses a relevant branch cut, which is from the trivialization of the covering map from the Seiberg-Witten curve to the base space. Suppose we have an \mathcal{S}_{ij} -wall crossing a (jk) -cut. Then after crossing the cut it becomes an \mathcal{S}_{ik} -wall [37], as shown in Figure 5.8.

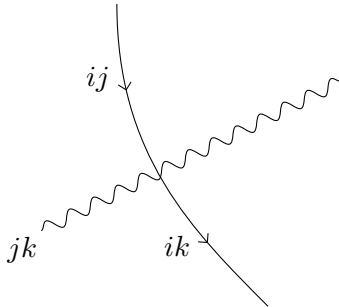


Figure 5.8: \mathcal{S} -wall crossing a branch cut.

We can give indices for all the \mathcal{S} -walls of a spectral network in a globally consistent manner, however local information around each intersection of finite \mathcal{S} -walls is enough for us to find out the IR charges of the corresponding BPS states. Appendix 5.2.3 explains how to calculate the intersections of the cycles from finite \mathcal{S} -walls of a spectral network.

5.2.3 Finite \mathcal{S} -walls, 1-cycles and intersection numbers

Here we review how to relate finite \mathcal{S} -walls to 1-cycles on the Seiberg-Witten curve, and how to calculate intersection numbers between the cycles from the finite \mathcal{S} -walls, which is crucial in calculating the U(1) IR charges of the corresponding BPS states.

The direction of a finite \mathcal{S}_{ij} -wall determines the orientation of the corresponding 1-cycle on the Seiberg-Witten curve. Figure 5.9a illustrates the case when one part of the cycle in the i -th sheet goes along the direction of the \mathcal{S}_{ij} -wall, while the other part in the j -th sheet goes along the opposite direction of the \mathcal{S} -wall. Figure 5.9b shows that when an \mathcal{S} -wall

is connected to a branch point, the corresponding 1-cycle goes across the branch cut and moves from the i -th sheet into the j -th sheet. The condition on a joint of multiple \mathcal{S} -walls guarantees that there is a consistent definition of the corresponding 1-cycle. See Figure 5.9c, where we have a joint of three \mathcal{S} -walls. In this way the direction of a 1-cycle from a finite \mathcal{S} -wall is completely determined. One can reverse the directions of the finite \mathcal{S} -wall to obtain a 1-cycle of the opposite orientation.

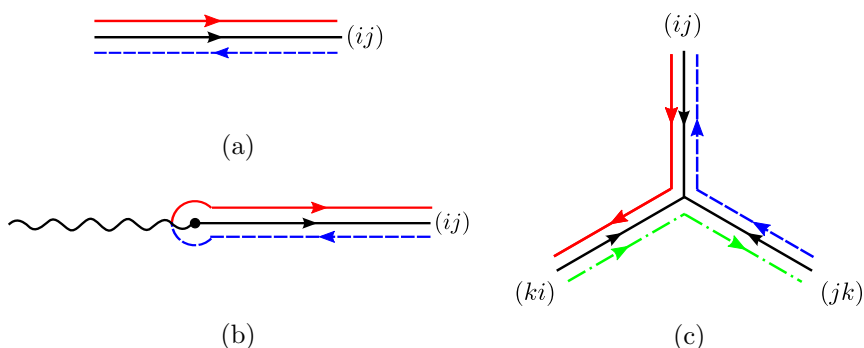


Figure 5.9: \mathcal{S} -walls and the corresponding 1-cycles. Black (solid) line: \mathcal{S} -walls. Red (solid) line: cycles on i -th sheet. Blue (dash) line: cycles on j -th sheet. Green (dash-dot) line: cycles on k -th sheet. Black dot: the branch point (ij) . Wiggled line: the branch cut separating i -th sheet and j -th sheet.

Examples of 1-cycles from finite \mathcal{S} -walls are shown in Figure 5.10, where the same colors and line shapes as those of Figure 5.9 are used to represent \mathcal{S} -walls, 1-cycles, and branch points/cuts. Figure 5.10a shows a finite \mathcal{S} -wall connecting two branch points, which gives a 1-cycle going from one sheet to the other. Figure 5.10b shows a finite \mathcal{S} -wall connecting three different branch points.

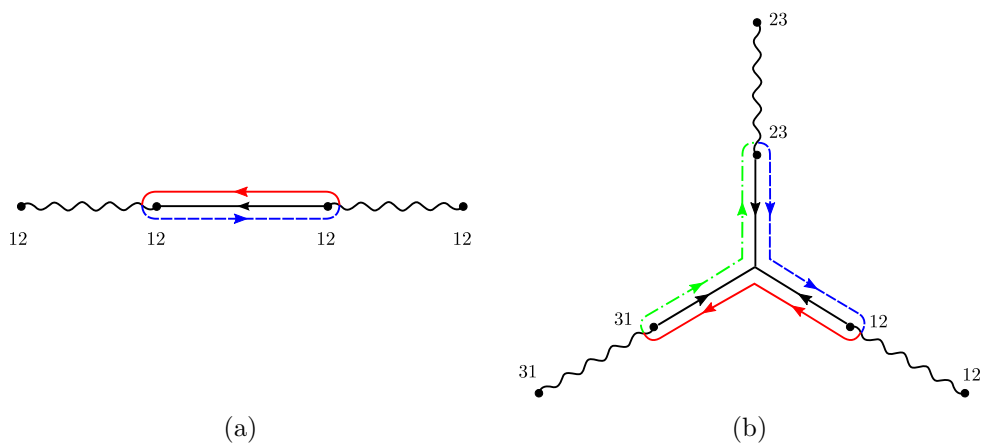


Figure 5.10: Finite \mathcal{S} -walls and corresponding 1-cycles

From the intersection number of two 1-cycles we can determine the U(1) IR charges of the corresponding BPS states. The convention for an intersection number is summarized in Figure 5.11. The intersection number is +1 if the first cycle goes across the second cycle from its left to its right, while the intersection number is -1 in the opposite case.

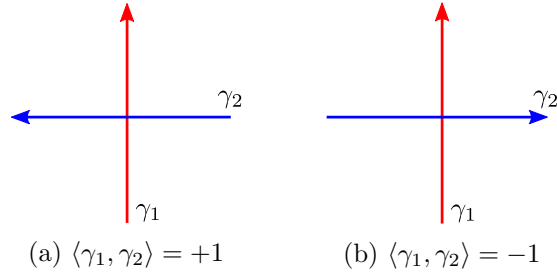


Figure 5.11: The convention for intersection number.

Since each finite \mathcal{S} -wall completely determines the corresponding 1-cycle, one can read off the intersection number between 1-cycles from the corresponding \mathcal{S} -walls. For example, if a finite \mathcal{S}_{ij} -wall crosses over another finite \mathcal{S}_{ik} -wall, the corresponding 1-cycles will have an intersection on the i -th sheet, and the direction of each cycle comes from the direction of each finite \mathcal{S} -wall. Figure 5.12a shows two finite \mathcal{S} -walls crossing over each other. Since one is an \mathcal{S}_{12} and the other is \mathcal{S}_{13} , the corresponding 1-cycles intersect only on the first sheet. If two \mathcal{S} -walls meet at the same branch point, they will again produce an intersection of the corresponding 1-cycles. Figure 5.12b shows two finite \mathcal{S} -walls meeting at the same branch point. The corresponding 1-cycles have intersection number ± 1 .

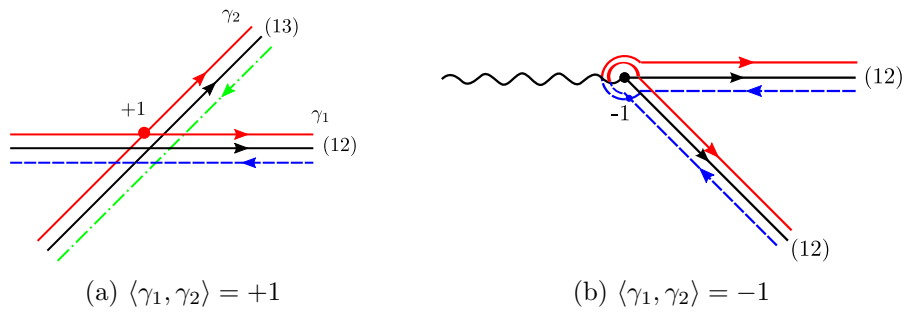


Figure 5.12: Local intersection number of 1-cycles

The intersection number of two 1-cycles is given by summing all the local intersection numbers of them. An example of calculating an intersection number of 1-cycles from finite \mathcal{S} -walls is shown in Figure 5.13.

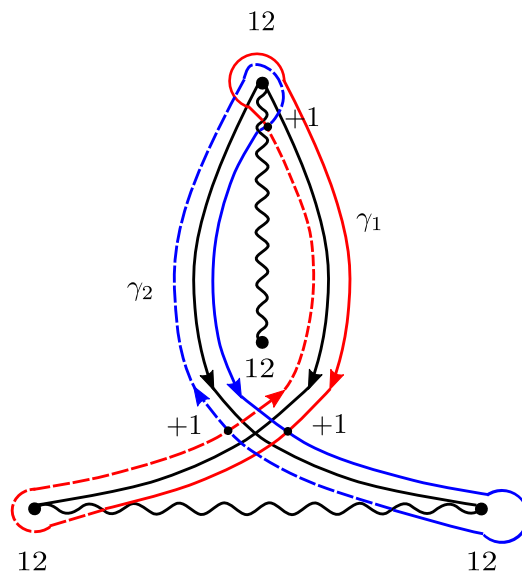


Figure 5.13: A 1-cycle γ_1 (red) intersects another 1-cycle γ_2 (blue) at three points (small black dots), and the intersection number is $\langle \gamma_1, \gamma_2 \rangle = +3$. Solid line: cycles on the first sheet. Dash line: cycles on the second sheet.

Chapter 6

2d wall-crossing and spectral networks

Here we examine several examples of spectral networks that exhibit 2d BPS wall-crossing phenomena. In Section 6.1 we consider spectral networks of Seiberg-Witten curves that wrap a sphere, which is a complex z -plane plus $z = \infty$, with one irregular puncture at $z = \infty$. In Section 6.2 we study spectral networks with one irregular puncture at $z = \infty$ and one regular puncture at $z = 0$.

6.1 1 irregular puncture at $z = \infty$

We studied in Section 4.5 that D2-branes ending on a IIA brane configuration that describes a 4d $\mathcal{N} = 2$ theory give a 2d $\mathcal{N} = (2, 2)$ theory. When we lift the whole brane system to M-theory, it becomes a configuration of M2-branes ending on a Seiberg-Witten curve that is wrapped by an M5-brane, which can be understood from what we have reviewed in Sections 2.4 and 4.5.

Consider a Seiberg-Witten curve

$$z = x^N + \mu_2 x^{N-2} + \cdots + \mu_N, \tag{6.1}$$

where z is the coordinate for the base space of sphere, and x is an N -sheeted cover over z . The Seiberg-Witten differential we consider is $\lambda = x dz$, which has an irregular puncture at $z = \infty$. The 4d theory from an M5-brane wrapping the Seiberg-Witten curve (6.1) is a deformation from an Argyres-Douglas fixed point theory [19], and the 2d theory from an M2-brane ending at $z = 0$ is claimed in [49, 30] to be equivalent to an $\mathcal{N} = (2, 2)$

Landau-Ginzburg model with superpotential

$$W(X) = \frac{1}{N+1}X^{N+1} + \sum_{j=2}^N \frac{\mu_j}{N+1-j}X^{N+1-j}. \quad (6.2)$$

6.1.1 $N=2$

Spectral networks of a Seiberg-Witten curve

$$z = x^2 + \mu_2. \quad (6.3)$$

at various values of θ are shown in Figure 6.1. As we change θ from 0 to π , the spectral network rotates by $N\pi/(N+1) = 2\pi/3$. To see the animated version, click [here](#).

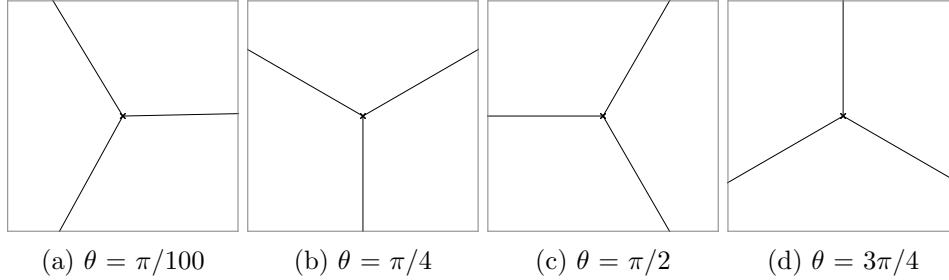


Figure 6.1: Spectral networks around a branch point of index $N = 2$.

This spectral network is a simple one that shows no 2d BPS wall-crossing phenomenon: wherever an M2-brane ends on the z -plane, the 2d theory has two BPS states. This is the same BPS spectrum as that of the deformed A_1 minimal model. When $\theta = \pi$, the spectral network looks the same as that of $\theta = 0$ except the indices of all the \mathcal{S} -walls are flipped, i.e., for an \mathcal{S}_{ij} at θ we have an \mathcal{S}_{ji} at $\theta + \pi$.

6.1.2 $N=3$

Here we study spectral networks from a Seiberg-Witten curve

$$z = x^3 + \mu_2x + \mu_3. \quad (6.4)$$

When $\mu_2 = 0$, we have one branch points of ramification index 3 on the z -plane. When $\mu_2 \neq 0$, there are two branch points of ramification index 2.

6.1.2.1 $\mu_2 = 0$

Figure 6.2 shows spectral networks at various values of θ when there is only one branch point of index 3. As we change θ from 0 to π , the spectral network rotates by $N\pi/(N+1) = 3\pi/4$. To see the animated version, click [here](#). There is no 2d BPS wall-crossing happening here,

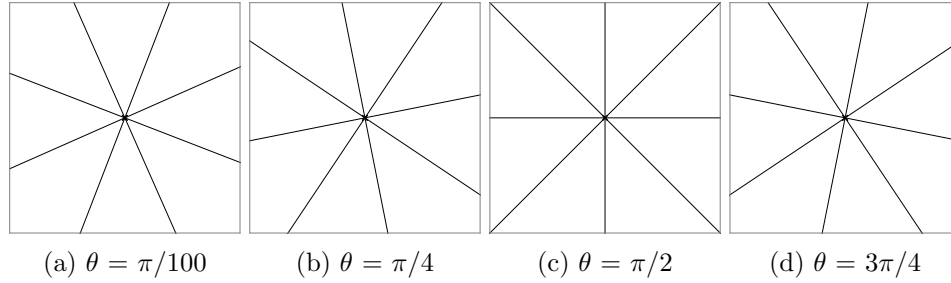


Figure 6.2: Spectral networks around a branch point of index $N = 3$, $\mu_2 = 0$.

and the 2d theory has six BPS states wherever the endpoint of the M2-brane lies on the z -plane. This is the same BPS spectrum as that of the deformed A_2 minimal model.

6.1.2.2 $\mu_2 \neq 0$

Spectral networks with two branch points of index 2 at various values of θ are shown in Figure 6.3. To see the animated version, click [here](#).

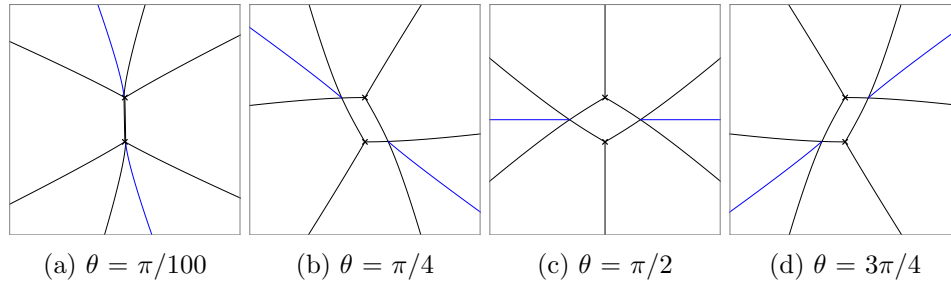


Figure 6.3: Spectral networks around a branch point of index $N = 3$, $\mu_2 \neq 0$.

Here we see the first, easiest example of a 2d BPS wall-crossing. Note that when the endpoint of a ground-state M2-brane is at $z = 0$, the blue \mathcal{S} -walls, each coming from a joint formed by two \mathcal{S} -walls from the branch points, cannot reach it, whereas when the endpoint is well away from $z = 0$ the blue \mathcal{S} -walls can hit the M2-brane endpoint. This illustrates the 2d BPS wall-crossing phenomenon we reviewed in Section 4.4.

Figure 6.4 shows the 2d BPS wall overlapped with a spectral network at a certain value of θ . The 2d BPS wall connects two branch points, and when the ground-state M2-brane

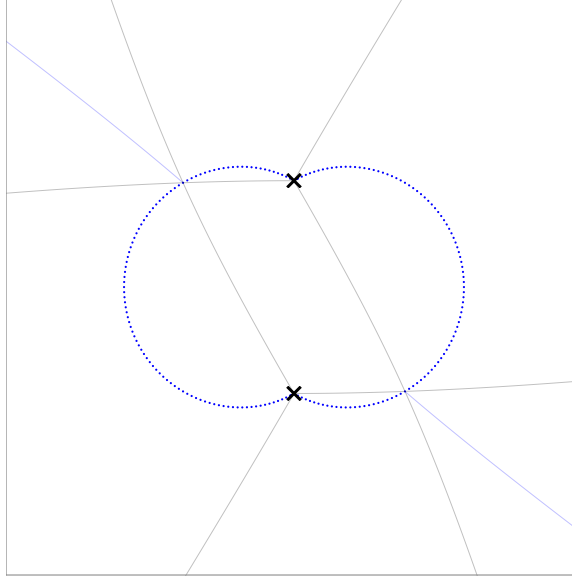


Figure 6.4: 2d BPS wall for $N = 3$.

ends inside the wall there are four 2d BPS states. When it ends outside the wall, the 2d theory has six BPS states. Therefore the moduli space of the 2d theory is divided by the 2d BPS wall into two BPS chambers, and the content of BPS spectra is consistent with what we studied in Section 4.4.

6.1.3 $N=4$

Consider a Seiberg-Witten curve

$$z = x^4 + \mu_2 x^2 + \mu_3 x + \mu_4. \quad (6.5)$$

In general there are three branch points of ramification index 2 on the z -plane. When $8\mu_2^3 + 27\mu_3^2 = 0$, we have one branch point of index 3 and another branch points of index 2. When $\mu_2 = \mu_3 = 0$, we have a single branch point of index 4, and as we have seen previously for $N = 2, 3$, there is no 2d BPS wall and there are $N(N - 1) = 12$ BPS states in the 2d theory, which is the same BPS spectrum as the deformed A_3 minimal model.

6.1.3.1 Two branch points

Spectral networks with two branch points on the z -plane at various values of θ are shown in Figure 6.5. To see the animated version, click [here](#).

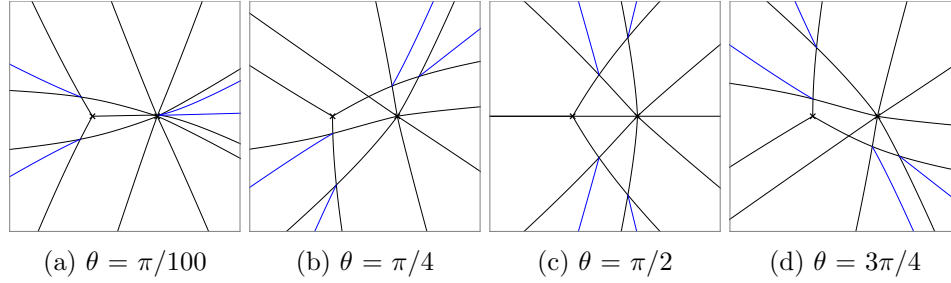


Figure 6.5: Spectral networks for $N = 4$ & two branch points.

Figure 6.6 shows the 2d BPS walls for this case. There are two walls, and when the M2-brane endpoint is outside of the two walls, the 2d theory still has twelve BPS states. As we cross a wall the 2d theory loses two BPS states from its spectrum, and when it ends at the region inside the inner wall the 2d theory has eight BPS states coming from the \mathcal{S} -walls from the branch points.

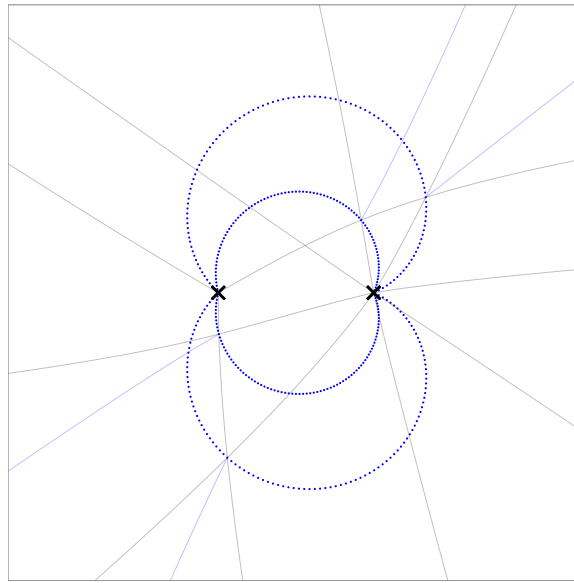


Figure 6.6: 2d BPS wall for $N = 4$ & two branch points.

6.1.3.2 Three branch points

Figure 6.7 shows the spectral networks for the case when we have three branch points of index 2, located symmetrically on the z -plane. To see the animated version, click [here](#).

Figure 6.8 shows the 2d BPS walls for this case. There are three walls located symmetrically around $z = 0$. Outside of all the walls, the 2d theory has a BPS spectrum with 12 states, and it loses 2 states as the endpoint goes across each wall. In the region that is the

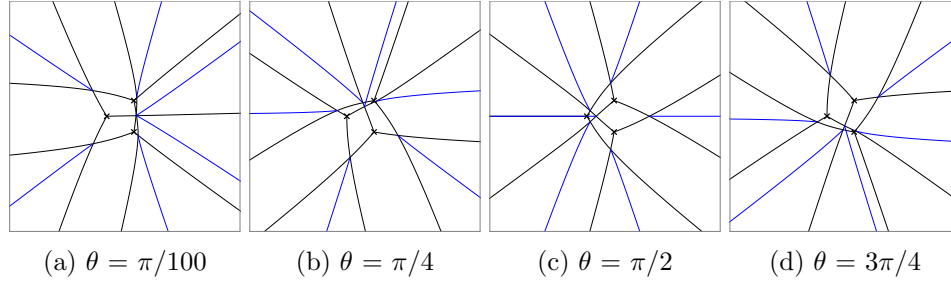


Figure 6.7: Spectral networks for $N = 4$ & three branch points.

intersection of the three regions inside each wall, the 2d theory loses $2 \times 3 = 6$ BPS states and the BPS spectrum has 6 states, all from the \mathcal{S} -walls from the branch points.

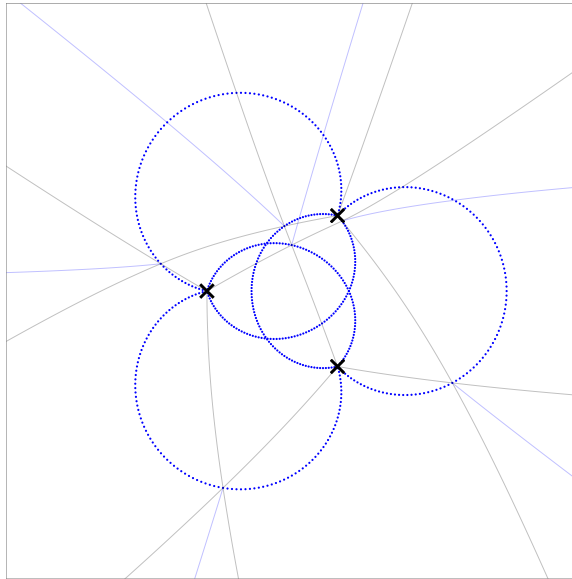


Figure 6.8: 2d BPS wall for $N = 4$ & three branch points.

6.2 1 irregular puncture at $z = \infty$, 1 regular puncture at $z = 0$

Now we consider adding a regular puncture at $z = 0$, meaning that the Seiberg-Witten differential has a simple pole at $z = 0$, giving a mass parameter. The Seiberg-Witten curve that we will consider here is

$$t = \prod_{i=1}^N (v + m_i) = v^N + \mu_2 v^{N-2} + \cdots + \mu_N, \quad (6.6)$$

where we will assume $\sum_i m_i = \mu_1 = 0$. The Seiberg-Witten differential is $\lambda = \frac{v}{t} dt$. For general μ_i we have $N - 1$ branch points of ramification index 2 on the t -plane.

If we rewrite the curve and the differential in terms of $x = v/t$ and $z = t$, we have

$$x^N + \frac{\mu_2}{z^2} x^{N-2} + \dots + \frac{\mu_N}{z^N} - \frac{1}{z^{N-1}} = 0 \quad (6.7)$$

as the Seiberg-Witten curve, and the Seiberg-Witten differential is $\lambda = x dz$. The 4d theory from this Seiberg-Witten curve is obtained from an Argyres-Douglas fixed point of a 4d $\mathcal{N} = 2$ $SU(N)$ theory with fine-tuned masses of N hypermultiplets [49], which we reviewed in Section 4.5.2. The 2d theory from an M2-brane ending on the Seiberg-Witten curve is what we have studied in Sections 4.5.3, 4.5.4, and 4.5.5.

6.2.1 $N = 2$

When $N = 2$, the Seiberg-Witten curve is a two-sheeted cover over the z -plane with a regular puncture at $z = 0$ and an irregular puncture at $z = \infty$. Figure 6.9 shows the spectral networks of the system when we have $m_1 = -m_2 = 1$. To see the animated version, click [here](#).

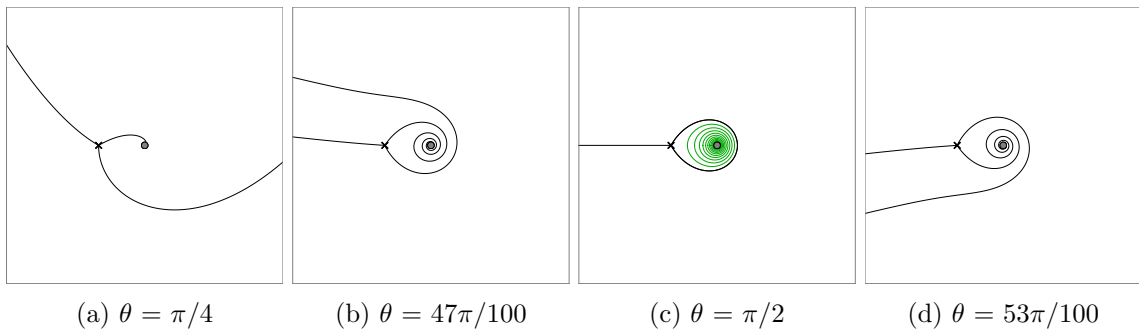


Figure 6.9: Spectral networks around a regular puncture, $N = 2$.

Note that we have a closed \mathcal{S} -wall when $\theta = \pi/2$. Around a regular puncture, a closed \mathcal{S} -wall appears at $\theta_c = \arg(m_i) \pm \frac{\pi}{2}$. In this case we have a single real mass parameter, and therefore we have a closed \mathcal{S} -wall at $\theta = \frac{\pi}{2}, \frac{3\pi}{2}$. At the value of θ where we find a closed \mathcal{S} -wall from a branch point, we have a family of closed \mathcal{S} -walls, a few of which is shown in Figure 6.9c. These closed \mathcal{S} -walls have the topology of a cylinder, and each of them corresponds to a 4d BPS state carrying the $SU(2)$ flavor charge, which becomes a vector multiplet when the flavor symmetry is gauged.

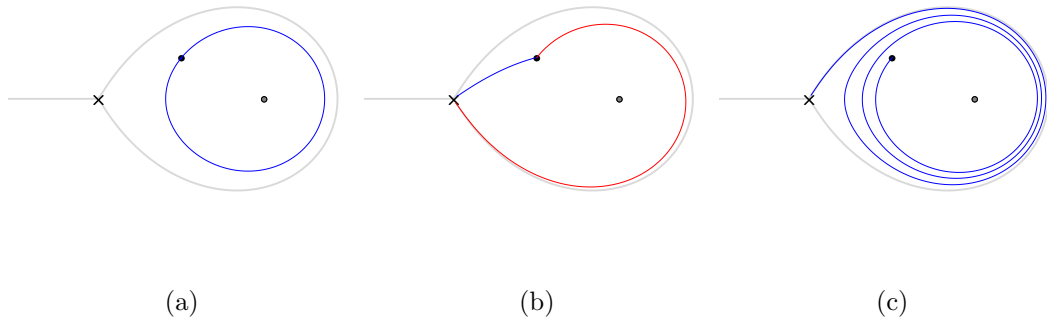


Figure 6.10

The closed \mathcal{S} -wall from the branch point behaves as a 2d BPS wall. To see how the 2d BPS spectrum changes as the M2-brane endpoint moves across the wall, we first consider the case when the endpoint is inside the wall, as shown in Figure 6.10. The corresponding 2d theory is the $\mathcal{N} = (2, 2)$ $\mathbb{C}P^1$ sigma model with twisted masses [38], which we studied in Section 4.5.4. There are three kinds of states in the BPS spectrum.

- Figure 6.10a shows a closed \mathcal{S} -wall [40]. There is a corresponding element of the first homology group of the Seiberg-Witten curve, which we denote as γ_f . The \mathcal{S} -wall corresponds to a 2d BPS state that has $Z[\gamma_f] = m_1 - m_2 = 2m_1$. The BPS state is identified with the elementary quantum state of the global $U(1)$ symmetry, which can be understood as coming from the 4d $SU(2)$ flavor symmetry that is broken into its Cartan subalgebra due to the twisted masses. There is one 2d BPS state of this kind at θ_c , $0 < \theta_c < \pi$, and there is another one from $-\gamma_f$, i.e., of the opposite orientation, at $\theta_c + \pi$.
- There are two solitons from γ_{s_1} and γ_{s_2} , as shown in Figure 6.10b, when $0 < \theta < \pi$. They satisfy $\gamma_{s_1} + \gamma_{s_2} = \gamma_f$, therefore each soliton carries a fraction of the flavor charge. They occur at different values of θ that are different from θ_c and $Z[\gamma_{s_1}] + Z[\gamma_{s_2}] \neq Z[\gamma_f]$. Again there are two additional 2d BPS states from $-\gamma_{s_1}$ and $-\gamma_{s_2}$ when $\pi < \theta < 2\pi$.
- There are “dyons” corresponding to $\gamma_{s_i} + n\gamma_f$ for $i = 1, 2$ and any integer n . Figure 6.10c shows the case of $\gamma_{s_1} + 3\gamma_f$.

Now let’s consider how the BPS spectrum changes as we move the M2-brane endpoint across the wall. Figure 6.11 illustrates the 2d wall-crossing phenomenon for this 2d theory.

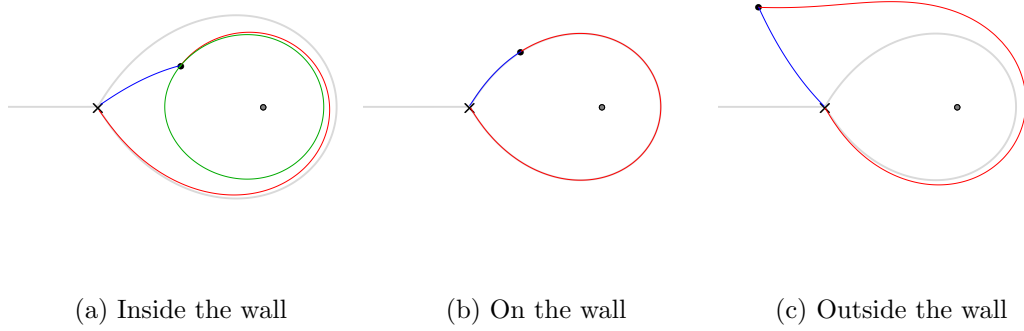


Figure 6.11

Let's start with three BPS states from γ_{s_1} , γ_{s_2} and γ_f that are inside the wall and satisfies $\gamma_{s_1} + \gamma_{s_2} = \gamma_f$, as shown in Figure 6.11a. As was previously mentioned, the sum of any two of the central charges $Z[\gamma_{s_1}]$, $Z[\gamma_{s_2}]$ and $Z[\gamma_f]$ is not equal to the third one, and the three 2d BPS states are stable.

Next we move the endpoint closer to the wall. When the ground state M2-brane ends exactly on the wall, as shown in Figure 6.11b, the three \mathcal{S} -walls occur at the same value of $\theta = \theta_c$. Now the central charges satisfy

$$Z[\gamma_{s_1}] + Z[\gamma_{s_2}] = Z[\gamma_f], \quad (6.8)$$

which shows that the 2d BPS state from a closed BPS string around the regular puncture is on the verge of decaying into two 2d BPS solitons.

Finally the endpoint of the ground state M2-brane is outside the wall in Figure 6.11c. Here we only have two solitons (and their anti-states) in the BPS spectrum, and there is no \mathcal{S} -wall corresponding to the other kinds of states. This is consistent with the fact that the exact supersymmetric $\mathbb{C}P^{N-1}$ sigma model with zero twisted masses contains in its BPS spectrum only the solitons interpolating N vacua [48, 31].

To see this, we take the limit of $m_1 \rightarrow 0$, colliding the branch point with the puncture at $z = 0$. Then we expect the two solitons to be equivalent, because their central charges only differ by one unit of the flavor charge, whose contribution to the central charge vanishes in the limit of $m_1 \rightarrow 0$. Therefore the two solitons will form a doublet for the $SU(2)$ global symmetry [31, 19, 40], which is illustrated in Figure 6.12 by taking m_1 to be very small and investigating the \mathcal{S} -walls corresponding to the solitons; compare this with Figure 6.11c

where m_1 is finite.

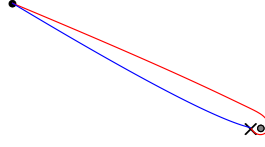


Figure 6.12: SU(2) doublet in the limit of $m_1 \rightarrow 0$.

6.2.2 Monodromy of the 2d BPS spectrum

In Section 4.5.5 we found the ground state of the 2d theory by solving

$$\exp\left(2\frac{\partial\mathcal{W}}{\partial\sigma}\right) = 1 \Leftrightarrow \frac{\partial\mathcal{W}}{\partial\sigma} = \pi in, \quad n \in \mathbb{Z}, \quad (6.9)$$

and we observed that n can be encoded in $\tilde{\Lambda}$ as

$$\tilde{\Lambda} = \mu \exp\left[\frac{-2\pi r(\mu) + i(\theta - 2\pi n)}{N}\right]. \quad (6.10)$$

When $N = 2$ and $m_1 + m_2 = 0$, we have, for the ground state equation,

$$\frac{(\sigma - m_1)(\sigma - m_2)}{\tilde{\Lambda}^2} = \frac{(\sigma^2 - m_1^2)}{\tilde{\Lambda}^2} = 1, \quad (6.11)$$

which is exactly the same as the equation for the Seiberg-Witten curve (6.6) if we identify $\sigma = v$ and $t = \tilde{\Lambda}^2$. That is, the ground states of the 2d sigma model that we studied in Sections 4.5.4 and 4.5.5 are determined by the same equation as the ground state of the 2d theory from the M2-brane ending at $t = \tilde{\Lambda}^2$ on the Seiberg-Witten curve (6.6). Furthermore, the choice of n for a ground state is translated on the M-theory side as the movement of the M2-brane endpoint on the t -plane, encircling n times around $t = 0$.

Here we will investigate the monodromy of the 2d BPS spectrum as we move the endpoint of the M2-brane around the puncture at $t = 0$ and relate it to the physics of the 2d θ -angle.

Let's first consider the case when we put t_s , the endpoint of the ground-state M2-brane, inside the wall and move t_s once around the circle of radius $|\tilde{\Lambda}|^2$ from $t = 0$, which is illustrated in Figure 6.13. Because the BPS spectrum consists of the states corresponding to the BPS strings $\gamma_{s_1} + p\gamma_f$ for $p \in \mathbb{Z}$, changing $\arg(t_s)$ by 2π just shifts each state by one

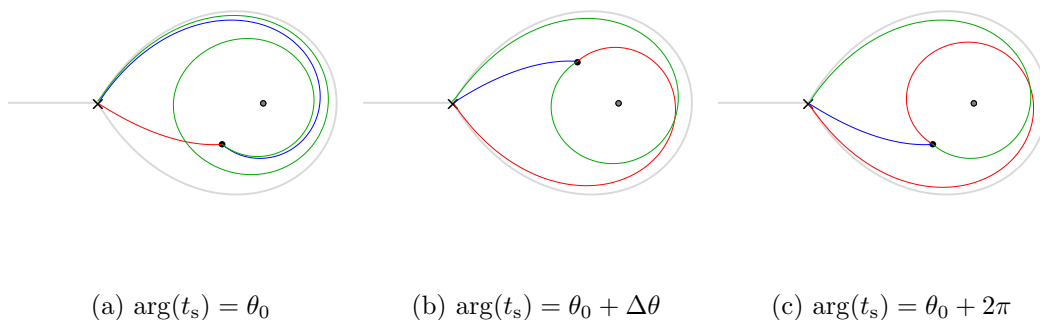


Figure 6.13

unit of γ_f , which does not change the spectrum because there are BPS states for every $p \in \mathbb{Z}$ [38].

It is interesting to think about the physics behind this phenomenon [56, 32, 31]. The potential energy of the 2d physics depends not on the 2d theta angle, but on the minimum value of $|\tilde{\theta}| = |\theta + 2\pi\mathbb{Z}|$. This is because the θ -angle induces a constant 2d electric field in the vacuum, and if the electric field is too strong, a pair creation can occur to reduce the field strength. As the supersymmetric ground states are the zeros of the potential energy, this implies that the ground states depend on $\tilde{\theta}$, not θ , and therefore so does the BPS spectrum.

Next, let's consider the case when t_s lies outside the wall. Again changing the value of $\arg(t_s)$ by 2π corresponds to moving the endpoint around $t = 0$ once. Here we have only two BPS solitons in the spectrum, and the BPS spectrum remains the same after moving the endpoint around $t = 0$ as shown in Figure 6.14, again suggesting that the 2d physics is invariant under the monodromy of t_s .

6.2.3 A light soliton in the 2d BPS spectrum

An interesting question is what happens when the endpoint of the ground-state M2-brane, $t = t_s$, lies exactly on the branch point at $t = t_b$, or away from it by an infinitesimal amount. What we have studied so far indicates that there will be a soliton, either γ_{s_1} or γ_{s_2} , becoming very light [19], while the masses of the other solitons remain finite.

One way to study the 2d physics with light degrees of freedom is taking the IR limit similar to that of a 4d $\mathcal{N} = 2$ theory toward its Argyres-Douglas fixed points [4]. That is, we take the limit of 2d gauge coupling $e \rightarrow \infty$, and at the same time zoom into the

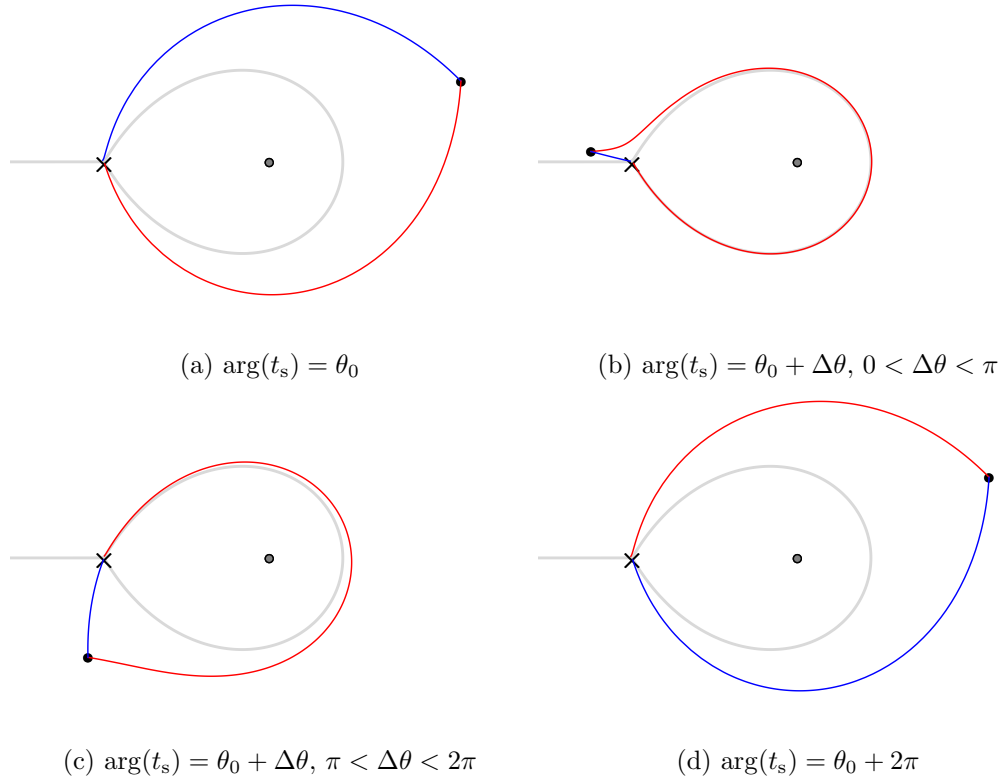


Figure 6.14

region near the branch point at $t = t_b$ by an appropriate scale so that only the light soliton remains in the BPS spectrum of the 2d IR theory and the other BPS states become massive in the IR limit.

To illustrate this procedure of taking an IR limit, let's consider the case when the M2-brane endpoint $t_s = \tilde{\Lambda}^2$ is on the 2d BPS wall and very close to the branch point, as shown in Figure 6.15. As the branch point is at $t_b = -m_1^2$, let's tune m_1 so that t_b is infinitesimally away from t_s ,

$$m_1 = i\tilde{\Lambda}(1 + \epsilon) \implies t_s = t_b - 2\tilde{\Lambda}^2\epsilon. \quad (6.12)$$

Then one of the two solitons, say γ_{s_1} , has the mass of

$$M(\gamma_{s_1}) = |Z(\gamma_{s_1})| = \left| \int_{t_b}^{t_s} \frac{v}{t} dt \right| \simeq |\tilde{\Lambda}| \epsilon^{3/2}, \quad (6.13)$$

which becomes very light in the limit of $\epsilon \rightarrow 0$. Because we have $Z(\gamma_{s_1}) + Z(\gamma_{s_2}) = 2m_1$, the mass of the other soliton should remain finite, $M(\gamma_{s_2}) \simeq 2|\Lambda|$. Although what we just

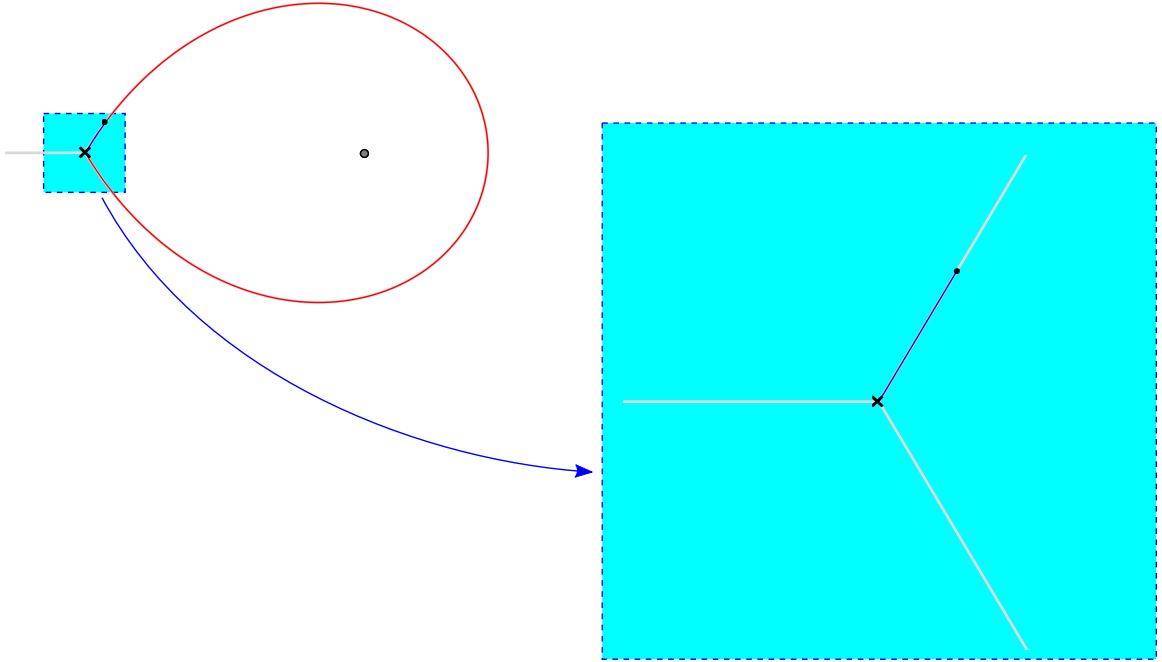


Figure 6.15

examined here is the case when t_s is on the 2d BPS wall, the fact that there is only one massless BPS state in the limit of $\epsilon \rightarrow 0$ should be true for any t_s satisfying $|t_s - t_b|/|\Lambda^2| \simeq \epsilon$. Then if we perform the following reparametrization,

$$t \rightarrow t_b + \frac{x}{\epsilon}, \quad (6.14)$$

$$v \rightarrow v(t_b) + \frac{y}{\sqrt{\epsilon}} = \frac{y}{\sqrt{\epsilon}}, \quad (6.15)$$

$$e \rightarrow \frac{e}{\sqrt{\epsilon}}, \quad (6.16)$$

where e is the dimensionfull 2d gauge coupling, then in the limit of $\epsilon \rightarrow 0$, we have $e \rightarrow \infty$, which indicates that we are taking the 2d IR limit, and the Seiberg-Witten curve (6.6) reduces to

$$t_b + \frac{t}{\epsilon} = \frac{v^2}{\epsilon} - m_1^2 + \mathcal{O}(\epsilon) \rightarrow t = v^2. \quad (6.17)$$

This curve has a single branch point at $t = 0$, and the spectral network from this curve has no finite \mathcal{S} -wall corresponding to a 4d BPS state [19]. There can be an \mathcal{S} -wall connecting the branch point and the endpoint of an M2-brane on the M5-brane wrapping this curve,

as we have seen in Section 6.1.1. This configuration corresponds to a 2d BPS soliton for the 2d theory from the M2-brane [40]. This shows that the procedure of sending $\epsilon \rightarrow 0$ indeed corresponds to zooming into the region near the branch point as illustrated in Figure 6.15. In the process we move the puncture with a simple mass pole to $t = \infty$ and at the same time make the mass infinite, which results in making the other BPS states massive and decoupling them from the 2d physics. This procedure and its generalization will be discussed in Section 7.1.1.

One thing to note is that, in this scaling or IR limit, we lose the monodromy information encoded in the massive BPS states [57], because we now see only a local structure of the Seiberg-Witten curve near the branch point, not a global one. However, if we instead think of starting from the IR fixed point of the 2d theory and increasing the scale to incorporate the massive BPS states one by one, which can be done by including the corresponding punctures with mass parameters to the IR Seiberg-Witten curve, in the end we can restore both the monodromy information and the full BPS spectrum.

From the analysis above we can expect that the 2d theory from the brane configuration we have been studying should always have a BPS state that becomes massless when the endpoint of the M2-brane coincides with a branch point. The occurrence of such a light degree of freedom is a signal that interesting physics happens in the 2d theory from such an M2-brane [30].

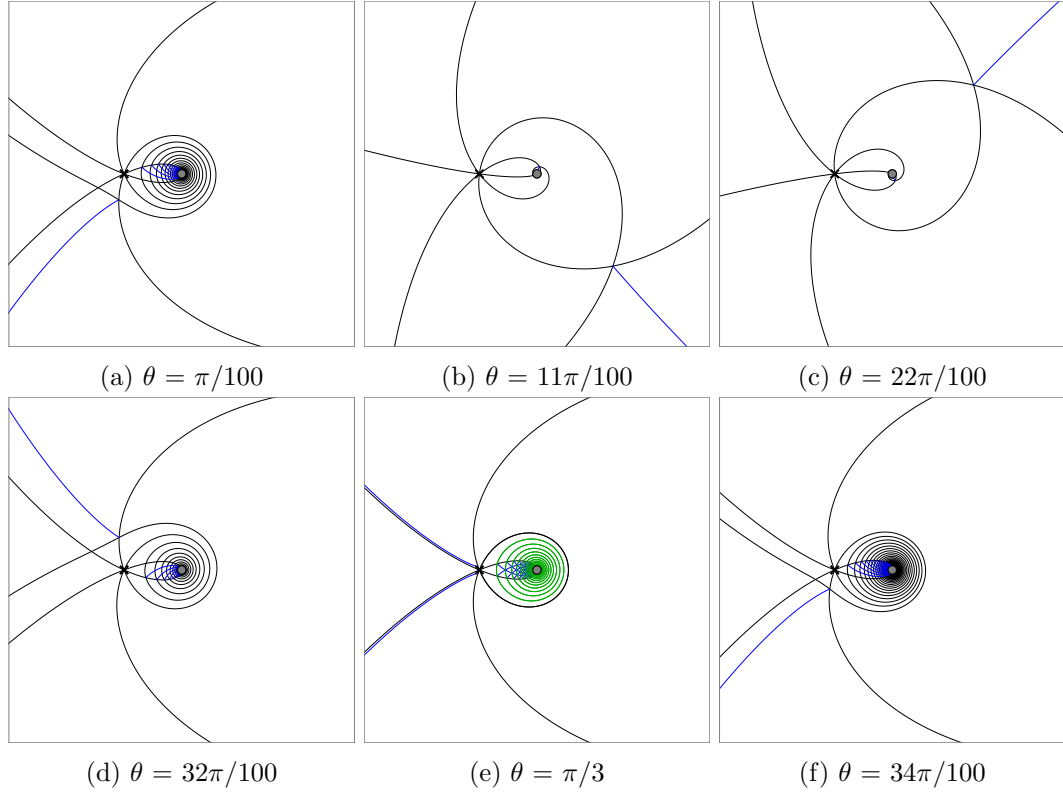
6.2.4 $N=3$

When $N = 3$, there are two independent mass parameters from the regular puncture at $z = 0$, and their values determine the types and the locations of branch points on the z -plane. When they are

$$m_1 = 1, \quad m_2 = \exp\left(\frac{2\pi}{3}\right), \quad m_3 = \exp\left(\frac{4\pi}{3}\right), \quad (6.18)$$

we have one branch point of ramification index 3, around which the spectral network looks like that of Section 6.1.2.1.

However, as the spectral network evolves away from the branch point, due to the existence of the regular puncture, it shows a different behavior, including the closed \mathcal{S} -walls similar to what we have observed in Section 6.2.1. Because we have mass parameters that

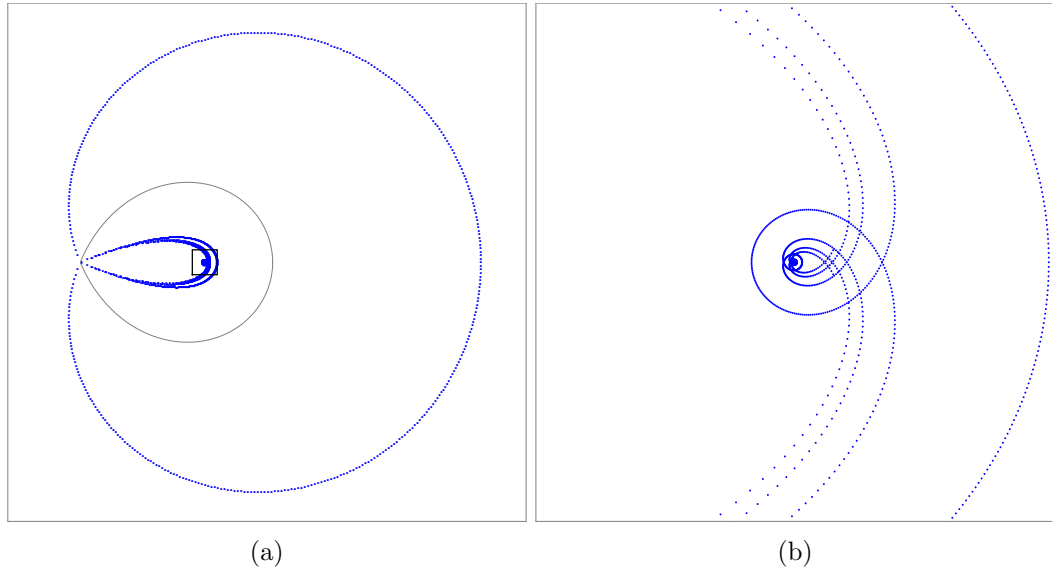
Figure 6.16: $N = 3$

have the same modulus and have phases that differ by $\pi/3$, we also have three values of θ_c between 0 and π that a family of closed \mathcal{S} -walls appear: $\theta_c = 0, \frac{\pi}{3}, \frac{2\pi}{3}$. Figure 6.16 shows the evolution of the spectral network around the second θ_c , $\theta_c = \frac{\pi}{3}$. At θ_c we have infinitely many closed \mathcal{S} -walls around the regular puncture, as shown in Figure 6.16e. But in this case each closed \mathcal{S} -wall form BPS joints with other \mathcal{S} -walls from the branch point, giving additional \mathcal{S} -walls that flow into the puncture.

Because we have three values of θ_c when $0 \leq \theta < \pi$, the evolution of the spectral network shown in Figure 6.16 is roughly 1/3 of the whole evolution of it as θ is increased from 0 to π . To see the animated version of the entire evolution, click [here](#), which shows the appearance of closed \mathcal{S} -walls three times.

Thanks to the BPS joints that appear in the higher-rank spectral networks, now the structure of the spectral network and the corresponding BPS spectrum is richer compared to the $N = 2$ case, and we can observe both kinds of 2d wall-crossing phenomena, one from BPS joints and another from closed \mathcal{S} -walls. These 2d BPS walls are shown in Figure 6.17.

In Figure 6.17a, the outmost wall is a 2d BPS wall from the BPS joint, similar to what

Figure 6.17: 2d BPS wall for $N = 3$

we found in Section 6.1. When the M2-brane endpoint ends outside the wall, the 2d theory has eighteen BPS states, corresponding to the three solitons that interpolate three vacua and their anti-states, each being a triplet of $SU(3)$ global symmetry: $\binom{3}{2} \times 2 \times 3 = 18$. This again agrees with the BPS spectrum of the 2d supersymmetric $\mathbb{C}P^2$ sigma model with zero twisted masses [48, 31].

The second wall, a gray one in Figure 6.17a, is the closed \mathcal{S} -wall from the branch point, which is shown in Figure 6.16e. When the M2-brane endpoint is between this wall and the outermost one, the 2d theory has six BPS states and their anti-state (therefore 12 states in total). The 2d spectrum lost three BPS states and their anti-states as we cross the first wall, and it does not have any BPS states from the closed \mathcal{S} -walls shown as green curves in Figure 6.16e.

Inside the second wall, as the M2-brane endpoint goes across each 2d BPS wall, shown in Figure 6.17b (which is a magnified view of the inset of Figure 6.17a), the 2d theory gains an additional BPS state and its anti-states.

The 2d BPS walls shown in Figure 6.17 illustrates that the analysis of spectral networks reproduces the BPS walls of $\mathcal{N} = (2, 2)$ classical $\mathbb{C}P^{N-1}$ sigma model described in [58, 59], where the walls are found from a field-theoretic viewpoint.

Chapter 7

2d $\mathcal{N} = (2, 2)$ SCFT and spectral networks

Consideration of multiple p -branes suspended between other branes is an effective way to study the dynamics of p -dimensional supersymmetric field theories [50, 7]. When we have multiple M5-branes ramified over a complex plane with a single ramification point, we can put M2-branes between the ramification point and another single, flat M5-brane, where all the branes share 2d spacetime and preserve four supercharges, leading to a 2d $\mathcal{N} = (2, 2)$ theory at low energy. In a certain limit where we decouple massive 2d degrees of freedom and flow the 2d theory to its IR fixed point, it is claimed in [30] that the 2d theory flows to a 2d SCFT described by a coset model of the type proposed by Kazama and Suzuki, which we will review in this chapter.

7.1 2d SCFT from the IR limit of the 2d $\mathcal{N} = (2, 2)$ theory from M-branes

Before going into the studies of the equivalences of various 2d $\mathcal{N} = (2, 2)$ theories claimed in [30], here we motivate why such equivalences are expected by studying an M-theory brane configuration corresponding to such a 2d theory and its spectral networks.

7.1.1 2d $\mathcal{N} = (2, 2)$ theory from 4d $\mathcal{N} = 2$ theory at an Argyres-Douglas fixed point

In [49], it was claimed that the 2d theory from the vortex string on the 4d theory at the Argyres-Douglas fixed point is described by a 2d $\mathcal{N} = (2, 2)$ theory with a Landau-Ginzburg

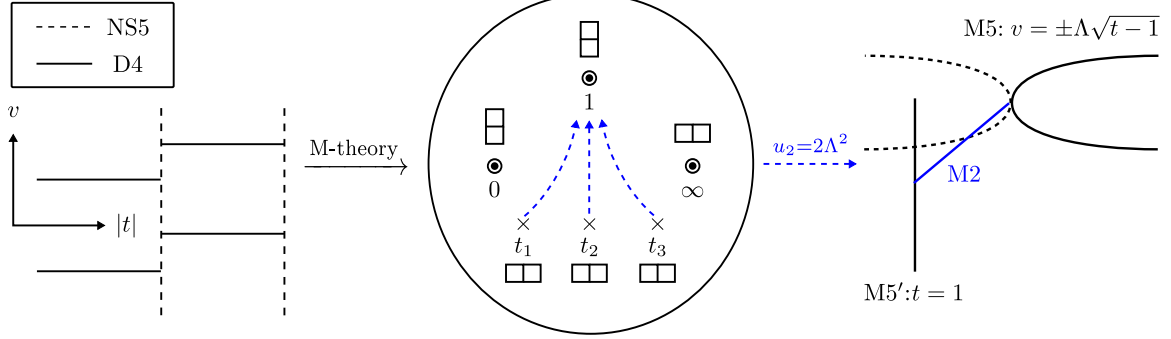


Figure 7.1

type twisted superpotential, which flows in the IR to the 2d $\mathcal{N} = (2, 2)$ minimal model SCFT. Here we will first observe that the brane configuration that the vortex string occurs is what we have studied in Section 4.5.2. And we will see that when the 4d theory is at its Argyres-Douglas fixed point, the brane configuration is exactly the case of an M2-brane ending at the ramification point of an M5-brane.

We start with an example of a 4d $\mathcal{N} = 2$ $SU(2)$ gauge theory with two hypermultiplets coming from the IIA brane configuration shown in the left of Figure 7.1. When we lift the brane configuration to M-theory, it becomes a Seiberg-Witten curve described by

$$f_2(t, v) = t^2 - (v^2 + u_2)t + \Lambda^2(v - m_1)(v - m_2). \quad (7.1)$$

When projected onto the t -plane, in addition to three punctures, there are three branch points [15]. We first tune the parameters of the 4d theory so that it is at the root of the baryonic Higgs branch, as we did in Section 4.5.2. This can be done by adjusting m_1 , m_2 , and u_2 such that they satisfy (4.36),

$$u_2 = m_1 m_2 + \Lambda^2 = -m_1^2 + \Lambda^2, \quad (7.2)$$

where we consider an $SU(2)$ flavor symmetry and therefore $m_1 + m_2 = 0$ is assumed. Then the original Seiberg-Witten curve factorizes into two curves,

$$f(t, v) \xrightarrow{(7.2)} (t - \Lambda^2) (t - (v^2 - m_1^2)). \quad (7.3)$$

Tuning the parameters to satisfy (7.2) corresponds to colliding two of the three branch

points at $t = \Lambda^2$ on the t -plane [15]. The curve represented by $t = \Lambda^2$ in (7.3) is from NS5' of Figure 4.2, which can be detached from the rest of the brane system when displaced along the direction perpendicular to both t and v .

In order to tune the 4d theory to be at an Argyres-Douglas fixed point, we collide the remaining third branch points with the other two at $t = 1$, which corresponds to taking the limit of

$$m_1 \rightarrow i\Lambda. \quad (7.4)$$

In this limit the Seiberg-Witten curve takes the form of

$$f(t, v) \xrightarrow{(7.4)} (t - \Lambda^2) (t - (v^2 + \Lambda^2)). \quad (7.5)$$

Now the M5-brane at $t = t_s = \Lambda^2$ is at the same location on the t -plane as the branch point at $t = t_b = -m_1^2 = \Lambda^2$. This is illustrated in the right of Figure 7.1. Between the two curves, we can put an M2-brane, which corresponds to the vortex string of [49]. Note that this M2-brane ends at the ramification point of the M5-branes from the IIA brane system.

After rotating the M5-brane at $t = \Lambda^2$ from (x^2, x^3) -plane into (x^8, x^9) -plane, we arrive at the same brane configuration as we have studied in Section 4.5.2. Then the s-rule applies for the M2-brane and the vortex string becomes massive along the (x^2, x^3) -plane, becoming a 2d defect from the viewpoint of the 4d physics. Now this is the same brane configuration that we have investigated in Section 6.2.3, where the 2d theory from the M2-brane and living on the 2d defect has in the IR limit only a massless soliton in its BPS spectrum.

Note that the IR limit corresponds to making the length of the D2-brane along the x^6 -direction in Figure 4.4 to be infinitesimal and placing NS5' very close to the other IIA brane system, and in this limit we recover the 4d $\mathcal{N} = 2$ SCFT at the Argyres-Douglas fixed point. Therefore it is plausible that the 2d physics embedded in this 4d physics would also be a SCFT in the IR limit.

We can generalize this to the case of $G = \text{SU}(N)$, $N_f = N$. Previously we described the Seiberg-Witten curve of the 4d theory at its root of the baryonic Higgs branch, (4.37).

$$f_N(t, v) = (t - \Lambda^N)(t - M_N), \quad M_N(v; m_j) = \prod_{k=1}^N (v - m_k). \quad (7.6)$$

Now let's tune the remaining parameters so that the 4d theory goes to an Argyres-Douglas fixed point. For general values of m_j , we have $N - 1$ branch points on the t -plane, and we expect that the 4d theory goes to an Argyres-Douglas fixed point if we collide them with each other at $t = \Lambda^N$. This is done by setting m_j as [49]

$$m_j = \Lambda \exp\left(\frac{2j+1}{N}\pi i\right). \quad (7.7)$$

Then M_N becomes

$$M_N(v; m_j) = v^N + \Lambda^N \quad (7.8)$$

and f_N becomes

$$f_N(t, v) = (t - \Lambda^N) [t - (v^N + \Lambda^N)]. \quad (7.9)$$

We again observe that the M5-brane corresponding to $t = \Lambda^N$ curve can be detached from the other M5-brane, and we can put an M2-brane between the M5-brane at $t = \Lambda^N$ and the ramification point of the M5-brane wrapping $t = v^N + \Lambda^N$. This M2-brane gives a vortex string in the 4d theory. Now if we rotate the M5-brane at $t = \Lambda^N$ from (x^2, x^3) -plane into (x^8, x^9) -plane, we again arrive at the brane configuration of Section 4.5.2.

In [49] it is claimed that the 2d theory on the vortex string is described by $\mathcal{N} = (2, 2)$ theory with a twisted superpotential

$$\mathcal{W} \propto \frac{\Sigma^{N+1}}{\Lambda^N}, \quad (7.10)$$

where the 4d theory has a gauge group $SU(N)$ and Λ is the scale of the 2d theory. As we have found the exact twisted superpotential in Section 4.5.5 and the exact BPS spectrum in Section 6.2.1 for $N = 2$, let's see how we can obtain (7.10) from the limit we explained in Section 6.2.3.

When the M2-brane ends exactly at the branch point, we have

$$t_s = t_b \Leftrightarrow \Lambda^2 = -m_1^2. \quad (7.11)$$

With $m_1 = i\Lambda$, we get from (4.59)

$$\mathcal{W}(y) = -\frac{i\pi}{2}m_1 - \frac{\sigma^3}{6\Lambda^2} + \mathcal{O}(y^5), \quad (7.12)$$

where we expanded \mathcal{W} around the ground state $\sigma(m_1 = i\Lambda) = 0$. Because the constant term does not affect the 2d physics we will disregard it. Then the cubic term is the leading-order term, and when we drop the higher-order terms this twisted superpotential agrees with (7.10). Note that, by discarding the higher-order terms we keep only the 2d BPS states that remain in the spectrum after taking the IR limit.

When the M2-brane endpoint is away from the branch point by

$$\frac{t_s - t_b}{\Lambda^2} = -\mu_2, \quad (7.13)$$

where $|\mu_2| \ll 1$, we can expand (4.59) both in $\sigma/\Lambda = y$ and in μ_2 to get

$$\mathcal{W}(y) = \frac{\Lambda}{2} \left(\pi - \frac{y^3}{3} + \mathcal{O}(y^5) \right) + \frac{\Lambda}{2} \left(\frac{\pi}{2} - y + \frac{y^3}{3} + \mathcal{O}(\sigma^5) \right) \mu_2 + \mathcal{O}(\mu_2^2). \quad (7.14)$$

The equation for the ground state is

$$-y^2 - \mu_2 + \dots = 2\pi i n, \quad (7.15)$$

where we collected only the leading-order terms. Choosing $n = 0$ and solving the equation gives us two ground states

$$y = \pm\sqrt{-\mu_2} \Leftrightarrow \frac{\sigma}{\Lambda} = \pm\sqrt{t_s - t_b} = \pm\sqrt{\Lambda^2 + m_1^2}, \quad (7.16)$$

and taking this into account we can rewrite the twisted superpotential, when we drop the σ -independent constant term, as

$$\mathcal{W} = -\frac{\Lambda}{2} \left(\frac{y^3}{3} + \mu_2 y \right) = -\frac{\sigma^3}{6\Lambda^2} + \frac{t_s - t_b}{2\Lambda^2} \sigma + \mathcal{O} \left[\left(\frac{t_s - t_b}{\Lambda^2} \right)^{5/2} \right]. \quad (7.17)$$

Therefore moving the M2-brane away from the branch point introduces the corresponding deformation of $\mathcal{O}(\sigma)$ into the twisted superpotential. For $N = 2$, this is all the deformation we can introduce in the 2d theory if we want to keep the $SU(2)$ flavor symmetry.

There is only a single ramification point in the Seiberg-Witten curve when $N = 2$ and that is why we can have only one deformation.

For $N > 2$, the twisted superpotential (7.10) comes from an M2-brane ending on the ramification point of an M5-brane with ramification index N , that is, N sheets of ramified M5-branes meeting at the point. We can introduce $N - 1$ deformations into the twisted superpotential [49],

$$\delta\mathcal{W}(y) = \sum_{j=2}^N \frac{\mu_j}{N+1-j} y^{N-j+1}, \quad \mathcal{W}(y) = \frac{\mu_0}{N+1} y^{N+1} + \delta\mathcal{W}(y). \quad (7.18)$$

When the deformations are introduced, the equation for the ground states is, with the choice of $n = 0$,

$$\frac{\partial\mathcal{W}}{\partial y} = \mu_0 y^N + \mu_2 y^{N-2} + \cdots + \mu_{N-1} y + \mu_N = \mu_0 \prod_{j=1}^N (y - \nu_j) = 0, \quad (7.19)$$

which is to be compared with (4.53) by identifying

$$\mu_1/\mu_0 = -(m_1 + \cdots + m_N)/\Lambda = 0 = -(\nu_1 + \cdots + \nu_N), \quad (7.20)$$

$$\mu_2/\mu_0 = (m_1 m_2 + \cdots + m_{N-1} m_N)/\Lambda^2 = \nu_1 \nu_2 + \cdots + \nu_{N-1} \nu_N, \quad (7.21)$$

$$\vdots \quad (7.22)$$

$$\mu_N/\mu_0 = (-1)^N (m_1 m_2 \cdots m_N)/\Lambda^N - 1 = (-1)^N \nu_1 \nu_2 \cdots \nu_N, \quad (7.23)$$

where m_j is deformed infinitesimally from (7.7) and therefore μ_j and ν_j are infinitesimal parameters.

Considering we identified (4.53) with the equation for the ground state M2-brane obtained from (4.37), μ_2, \dots, μ_N can be regarded as parametrizing $N - 1$ branch points of ramification index 2 on the t -plane. When we take the limit of all those μ_j to vanish, it corresponds to colliding all the branch points into the endpoint of the M2-brane, and the resulting 2d theory will have the twisted superpotential of (7.10).

7.1.2 2d $\mathcal{N} = (2, 2)$ theory from multiple M2-branes ending on a ramification point

So far we have studied the 2d theory from a single M2-brane ending on or near the ramification point of an M5-brane, whose IR limit is expected to be described by an $\mathcal{N} = (2, 2)$ SCFT with the twisted superpotential of Landau-Ginzburg type, (7.10), in a twisted chiral superfield Σ . The next question is, what is the 2d theory when we have multiple M2-branes instead of a single one.

Far away from a ramification point, the ramified M5-branes are well-separated, and we expect the 2d theory from multiple M2-branes ending on the M5-branes to be described by a supersymmetric sigma model whose target space is a Grassmannian $G(k, N)$ for k M2-branes ending at N M5-branes. This reduces to a \mathbb{CP}^{N-1} sigma model for a single M2-brane whose endpoint on the M5-brane is far away from the ramification point.

But when we put the M2-branes close to the ramification point, the sigma model coupling is too large and it is not a good perturbative description. What we are left with is the M-theoretic description, because it is valid at least for the quantities protected by supersymmetry. Here we will compare the brane configuration of our interest with a IIA brane configuration [42, 43] that gives a 4d $\mathcal{N} = 1$ theory with a superpotential of Landau-Ginzburg type and the M-theory lift of the brane configuration [60]. And we will argue from the similarity of the two brane configurations that we can learn about the twisted superpotential of the 2d theory from the description of the 4d theory.

Figure 7.2a shows a brane configuration that gives a 4d $\mathcal{N} = 1$ theory, where we have k D4-branes, N NS5-branes, and a single NS5'. All the branes fill the 4d space-time (x^0, x^1, x^2, x^3) where the 4d $\mathcal{N} = 1$ theory lives. The brane configuration of Figure 7.2a corresponds to a 4d theory with an $\mathcal{N} = 1$ hypermultiplet Φ , which is in the adjoint representation of $U(k)$ and infinitely massive.

Let's first consider the case $k = N$ and one D4-brane ending on each NS5-brane. Instead of having NS5-branes on top of each other, let's move them apart along $v = x^4 + ix^5$. When we label each location of an NS5-brane as v_j , $1 \leq j \leq N$, the superpotential $W(\Phi)$ satisfies [44]

$$\left. \frac{\partial W}{\partial \phi_i} \right|_{\phi_i=v} = s_0 \prod_{j=1}^N (v - v_j), \quad (7.24)$$

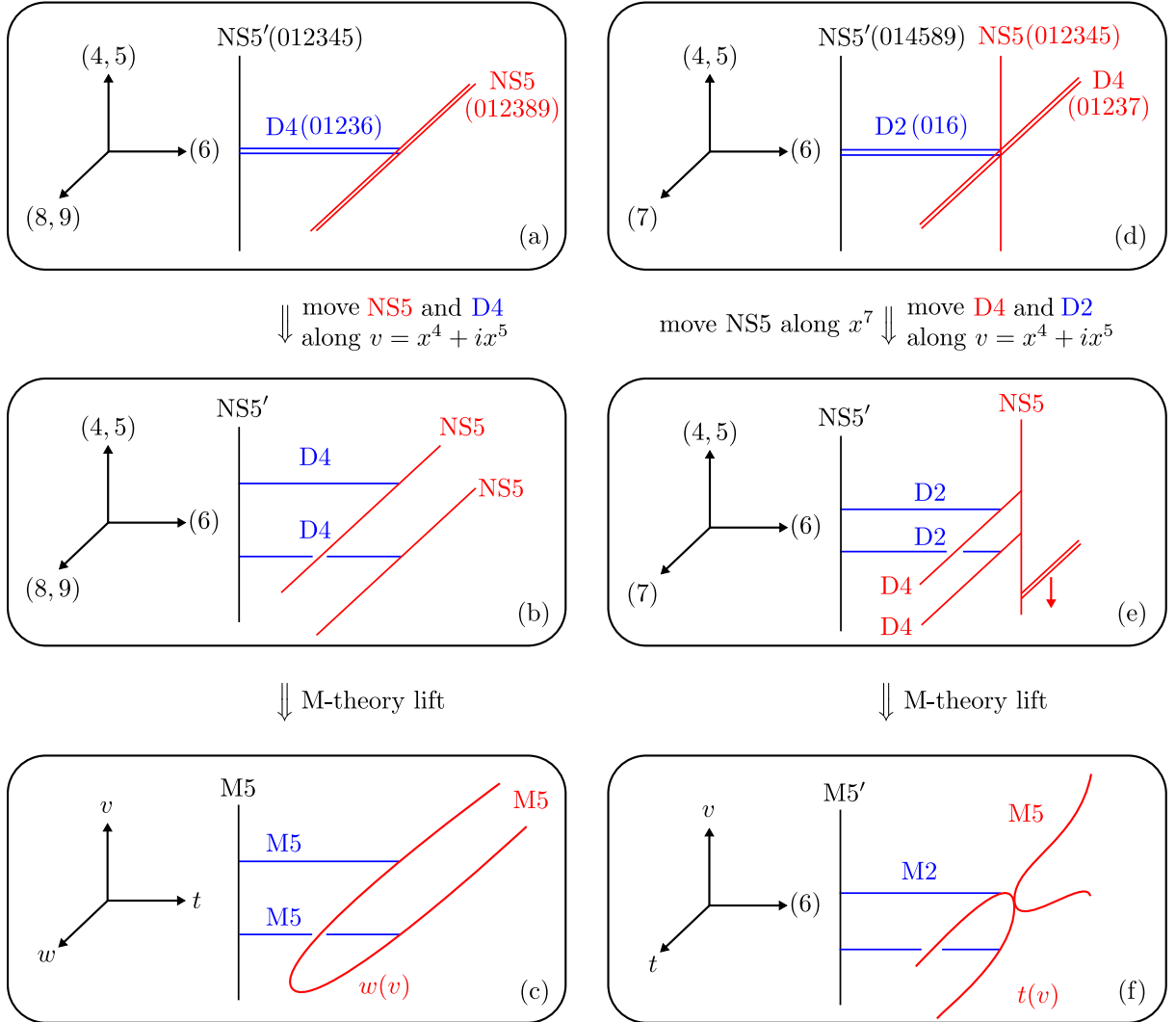


Figure 7.2: Brane configurations of 4d $\mathcal{N} = 1$ theory with a superpotential vs. those of 2d $\mathcal{N} = (2, 2)$ with a twisted superpotential.

where ϕ_i is a scalar component of the i -th diagonal element of Φ , representing the location of the i -th D4-brane on the v -plane, and s_0 should be infinitely large when we have NS5-branes rotated by $\pi/2$ from (x^4, x^5) to (x^8, x^9) . From this we get

$$W(\Phi) = \frac{s_0}{N+1} \text{Tr}(\Phi^{N+1}) + \frac{s_1}{N} \text{Tr}(\Phi^N) + \cdots + s_N \text{Tr}(\Phi) \quad (7.25)$$

$$= \sum_{j=0}^N \frac{s_j}{N+1-j} \text{Tr}(\Phi^{N+1-j}), \quad (7.26)$$

where s_j are related to v_j by

$$s_j/s_0 = (-1)^j e_j(v_1, v_2, \dots, v_N). \quad (7.27)$$

Here e_j is an elementary symmetric polynomial of j -th order, i.e.,

$$e_1 = v_1 + \cdots + v_N, \quad (7.28)$$

$$e_2 = v_1 v_2 + \cdots + v_{N-1} v_N, \quad (7.29)$$

$$\vdots \quad (7.30)$$

$$e_N = v_1 v_2 \cdots v_N. \quad (7.31)$$

From this, we can find the relations between s_j and the gauge-invariant Coulomb branch parameters $u_j = \langle \text{Tr}(\Phi^j) \rangle$ using the Newton's identities,

$$j s_j + \sum_{i=1}^j s_{j-i} u_i = 0. \quad (7.32)$$

When $k \neq N$, Φ is of the form

$$\Phi = \text{diag}(\underbrace{v_1, \dots, v_1}_{k_1}, \underbrace{v_2, \dots, v_2}_{k_2}, \dots, \underbrace{v_N, \dots, v_N}_{k_N}), \quad (7.33)$$

where $\sum_i k_i = k$. Note that when $N > k$ some $k_i = 0$, whereas when $N < k$ some $k_i > 1$.

So far we considered a IIA brane configuration that gives a 4d $\mathcal{N} = 1$ theory, which requires s_0 to be infinitely large. But we can lift this brane configuration to that of M-theory, where the NS5-branes and the D4-branes, as well as the NS5', become M5-branes. Then we can consider a superpotential with finite s_0 [60], and the M5-brane on the right of

Figure 7.2c wraps a complex curve $w(v)$,

$$w(v) = s_0 \prod_{j=1}^N (v - v_j) = \sum_{j=0}^N s_j v^{N-j}, \quad (7.34)$$

where $w = x^8 + ix^9$. When we compare this equation with (7.24), we can see why D4-branes ending on the M5-brane wrapping $w(v)$ correspond to a ground state of the 4d theory.

Figure 7.2d shows a brane configuration that gives a 2d $\mathcal{N} = (2, 2)$ theory. Here we have k D2-branes and N D4-branes. The 2d theory of the k coincident D2-branes suspended between two parallel NS5-branes spanning $(x^0, x^1, x^2, x^3, x^4, x^5)$ is described in Section 3.4 of [61] as $\mathcal{N} = (2, 2)$ $U(k)$ gauge theory with an adjoint matter Φ' , which represents the locations of the D2-branes in the (x^2, x^3) -plane and becomes massive when one of the two NS5-brane is rotated from (x^2, x^3) to (x^8, x^9) , as shown in Figure 7.2d. Therefore Φ' is integrated out for the brane configuration shown here because of the orientation of NS5' with respect to the other NS5-brane. The 2d twisted chiral multiplet Σ from the 2d gauge multiplet V is in the adjoint representation of $U(k)$. When Σ is diagonalized, its j -th diagonal element σ_j represents the location of the j -th D2-brane on the v -plane.

When we detach the D2-branes from the NS5-brane, put each of them to end at a different D4-brane, and move the NS5-brane away, we have the brane configuration shown in Figure 7.2e. Here the s-rule applies so there can be at most one D2-brane between NS5' and a D4-brane. Therefore each σ_j has a different value, which is the location of the j -th D2-brane and D4-brane on the v -plane. Each D4-brane crossing the NS5-brane can break at the NS5-brane in half and each of the two can be moved away from each other. When we move the semi-infinite D4-branes that do not have D2-branes ending on them away to infinity, it is the same brane configuration we have in Figure 4.4 except we now have more than one D2-brane here.

Now we lift the IIA brane configuration to M-theory, then we have multiple M2-branes between an M5-brane from the NS5' and another M5-brane wrapping the curve $t(v)$. This is shown in Figure 7.2f, and considering its similarity with Figure 7.2c, we can expect the 2d theory to have the twisted superpotential of the form

$$W(\Sigma) = \sum_{j=0}^N \frac{\mu_j}{N+1-j} \text{Tr} \left[\left(\frac{\Sigma}{\Lambda} \right)^{N+1-j} \right] = \sum_{j=0}^N \frac{\mu_j}{N+1-j} \text{Tr} [Y^{N+1-j}], \quad (7.35)$$

where Σ is in the adjoint representation of $U(k)$, $Y = \Sigma/\Lambda$, and μ_j are defined as

$$t(v) = \sum_{j=0}^N \mu_j \Lambda^j v^{N-j}. \quad (7.36)$$

Considering that the potential energy of the 2d theory contains a term proportional to

$$\mathrm{Tr} \left[\sigma, \sigma^\dagger \right]^2, \quad (7.37)$$

where σ is the lowest component of Σ , for this term to vanish we need σ to be diagonalizable, $\sigma = \mathrm{diag}(\sigma_1, \dots, \sigma_n)$. Then the twisted superpotential (7.35) becomes

$$\mathcal{W} = \frac{\mu_0}{N+1} \mathrm{Tr} [Y^{N+1}] + \frac{\mu_1}{N} \mathrm{Tr} [Y^N] + \dots \quad (7.38)$$

$$= \frac{\mu_0}{N+1} (y_1^{N+1} + \dots + y_k^{N+1}) + \frac{\mu_1}{N} (y_1^N + \dots + y_k^N) + \dots, \quad (7.39)$$

where $y_j = \sigma_j/\Lambda$, and the equation for the ground state of the i -th M2-brane is

$$\frac{\partial \mathcal{W}}{\partial y_i} = \sum_{j=0}^N \mu_j y_i^{N-j} = \mu_0 \prod_{j=1}^N (y_i - \nu_j). \quad (7.40)$$

Note that when $k = 1$, (7.35) and (7.40) reduce to (7.18) and (7.19), respectively. The contribution from the off-diagonal part of Y to the twisted superpotential is a constant term that is independent of y_i [62], so even after taking quantum correction into account (7.39) is still a valid description of the twisted superpotential.

To study the 2d theory from k M2-branes ending on a single ramification point of index N , we take the limit of $\mu_j \rightarrow 0$, $j = 2, \dots, N$. As was the case in Section 7.1.1, this corresponds to colliding $N - 1$ branch points on the t -plane to the point where k M2-branes end. Then the twisted superpotential for the 2d theory becomes

$$W(Y) = \frac{\mu_0}{N+1} \mathrm{Tr}(Y^{N+1}) = \frac{\mu_0}{N+1} (y_1^{N+1} + \dots + y_k^{N+1}). \quad (7.41)$$

When we define U_i as

$$U_i = \sum_{1 \leq l_1 < l_2 < \dots < l_i \leq k} y_{l_1} y_{l_2} \dots y_{l_i} = e_i(y_1, \dots, y_k), \quad i = 1, \dots, k, \quad (7.42)$$

they are gauge invariant superfields obtained from the gauge *covariant* superfield Y [35] via

$$\det[t - Y] = t^k + \sum_{i=1}^k (-1)^k t^{k-i} U_i, \quad (7.43)$$

and we can rewrite (7.41) in terms of U_i using [63]

$$-\log \left[\sum_{i=0}^n (-t)^i U_i \right] = \sum_{k=-n}^{\infty} t^{n+k+1} \mathcal{W}_{n,k}(U_i), \quad (7.44)$$

where

$$\mathcal{W}_{n,k}(y_1, \dots, y_k) = \frac{\mu_0}{n+k+1} (y_1^{n+k+1} + \dots + y_k^{n+k+1}). \quad (7.45)$$

Therefore we need to identify the 2d theory at the IR fixed point of the 2d $\mathcal{N} = (2, 2)$ Landau-Ginzburg model of twisted chiral superfields U_i with the twisted superpotential (7.41) to find out the IR limit of the 2d theory from the multiple M2-branes ending at a ramification point of an M5-brane.

7.2 SCFT from the IR limit of 2d $\mathcal{N} = (2, 2)$ theories

Let's summarize the brane configuration whose dynamics we want to analyze. We have multiple M2-branes suspended between two M5-branes in the following setup [31]. We use the coordinates $x^{0, \dots, 10}$, with a compactified x^{10} direction. Let us introduce complex combinations $v = x^4 + ix^5$ and $t = \exp(x^7 + ix^{10})$. Then we have, as summarized in Fig. 7.3,

- an M5-brane extending along $x^{0,1,2,3}$ and on the complex one-dimensional curve $t = t(v)$, at a fixed position $(x^6, x^8, x^9) = (L, 0, 0)$,
- an M5-brane (which we call the M5'-brane) extending along directions $x^{0,1,8,9}$ and v , at a fixed position $(x^2, x^3, x^6, t) = (0, 0, 0, 1)$, and
- k M2-branes extending along $x^{0,1}$ and suspended between the M5 and the M5' along the x^6 direction.

We are interested in the IR limit of the theory on k M2-branes.

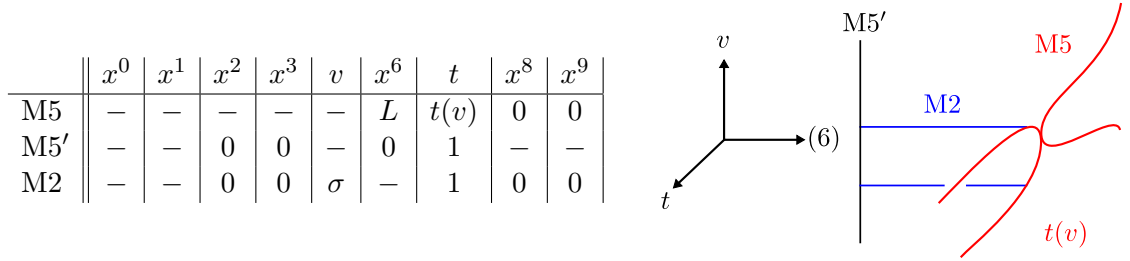


Figure 7.3: Configuration of branes. $v = x^4 + ix^5$ and $t = \exp(x^7 + ix^{10})$.

If we reduce the theory along the x^{10} direction, we have a system of k D2-branes suspended between one NS5-brane at $x^6 = 0$ and some configuration of branes at $x^6 = L$. This gives a 3d $U(k)$ gauge theory formulated on an interval with some boundary conditions at the two ends, which reduces to a 2d theory with $\mathcal{N}=(2, 2)$ supersymmetry at distances longer than the length L of the interval. We first assume that all solutions to the equation $t(v) = 1$ are non-degenerate. That is, if $\{v_i\}_{i \in I}$ denotes the set of solutions, then $t'(v_i) \neq 0$ for each $i \in I$. Then, from the M-theory description, the supersymmetric vacua are described by k M2-branes, separated along v directions, each at a fixed value of v being one of $\{v_i\}_{i \in I}$. The s-rule [50, 31] forbids that more than one M2-brane have the same value of v . This vacuum structure would arise if the low energy theory is the theory on the Coulomb branch with the twisted superpotential

$$\mathcal{W}_{\text{eff}} = \text{tr} P(\Sigma_T), \quad (7.46)$$

for the field strength superfield $\Sigma_T = \text{diag}(\Sigma_1, \dots, \Sigma_k)$ for the maximal torus $T \cong U(1)^k$, where the holomorphic function $P(v)$ is given by

$$\exp(P'(v)) = t(v). \quad (7.47)$$

Indeed, the vacuum equation is $t(\sigma_a) = 1$ for $a = 1, \dots, k$ and we expect that no supersymmetric vacuum is supported at the solutions with $\sigma_a = \sigma_b$ for $a \neq b$. Also, permutations of σ_a 's are gauge symmetry.

When $t(v)$ is a rational function, the M5 reduces to a number of D4-branes ending on an NS5-brane, and the 2d theory can be interpreted as a $U(k)$ gauge theory with a number

of fundamental and antifundamental chiral multiplets, possibly with twisted masses [31]. There are only finitely many solutions to $t(v) = 1$ and hence the number of supersymmetric vacua is finite. When $t(v)$ is such that $P'(v)$ in (7.47) is a polynomial, the 2d theory has a different type of interpretation: It is the $U(k)$ gauge theory without matter field and with the tree level twisted superpotential

$$\mathcal{W} = \text{tr}P(\Sigma) + \pi i(k+1)\text{tr}\Sigma, \quad (7.48)$$

where Σ is now the fieldstrength for the full $U(k)$ vector multiplet. The second term is the theta term with $\theta = \pi(k+1)$. It is non-trivial if and only if k is even since θ is a periodic parameter of period 2π . This is needed in order to have (7.46) as the effective twisted superpotential on the Coulomb branch [64]. The equation $t(v) = 1$ has infinitely many solutions, and correspondingly, there are infinitely many supersymmetric vacua in this gauge system.

Each vacuum has a mass gap when, as assumed above, all the solutions to $t(v) = 1$ are non-degenerate. Things would be more interesting if $t(v)$ is fine-tuned so that some of the solutions coincide, or equivalently, some of the solutions are degenerate. N solutions coincide, say at $v = 0$, when

$$t(v) = 1 + v^N + \dots \quad \text{or} \quad P(v) = v^{N+1} + \dots, \quad (7.49)$$

where the ellipses stand for possible terms of higher order in v . In such a case, we expect to have a non-trivial conformal field theory in the IR limit. In fact, for the case $k = 1$, it is argued in [49] that the vacuum at $v = 0$ is the same as the IR limit of the Landau-Ginzburg model with superpotential $W = X^{N+1}$, which is believed to be equivalent to the $\mathcal{N}=(2,2)$ superconformal minimal model of type A_{N-1} . For $k > 1$, we may have vacua where multiple M2 branes are at $v = 0$. We expect that all k of them can sit there as long as $N \geq k$. The question is, what is the IR limit of such a theory?

We will argue that the theory under question is equivalent to the IR limit of the Landau-Ginzburg model of k variables X_1, \dots, X_k , where the superpotential $W(X_1, \dots, X_k)$ is

$\text{tr}\Sigma_T^{N+1}$ written in terms of the elementary symmetric functions of $\Sigma_1, \dots, \Sigma_k$;

$$\sum_{a=1}^k \sigma_a^{N+1} = W(x_1, \dots, x_k), \quad (7.50)$$

$$x_b = \sum_{a_1 < \dots < a_b} \sigma_{a_1} \cdots \sigma_{a_b}, \quad b = 1, \dots, k \quad (7.51)$$

This model is believed to flow to the $\mathcal{N}=(2, 2)$ superconformal Kazama-Suzuki model [65, 66] of the coset type

$$\frac{\text{SU}(N)_1}{\text{S}[\text{U}(k) \times \text{U}(N-k)]}. \quad (7.52)$$

Thus, we claim that the answer to the question is this Kazama-Suzuki model.

The behaviour (7.49) is realized simply by $t(v) = 1 + v^N$ or $P(v) = v^{N+1}$. In the former case, the 2d theory is the $\text{U}(k)$ SQCD with N fundamental matter fields with fine tuned twisted masses [31, 49]. In the latter case, the 2d theory is the pure $\text{U}(k)$ gauge theory with the tree level twisted superpotential

$$\mathcal{W} = \text{tr}\Sigma^{N+1} + \pi i(k+1)\text{tr}\Sigma. \quad (7.53)$$

For $1 \leq k \leq N$, we shall argue that the theory has, among infinitely many others, a set of ground states supported at $\Sigma = 0$, and this “ $\Sigma = 0$ sector” flows to the superconformal field theory under question.

Thus, we have a purely field theoretical duality statement: for $1 \leq k \leq N$,

- the $\text{U}(k)$ SQCD with N fundamentals having fine tuned twisted masses,
- the $\Sigma = 0$ sector of the pure $\text{U}(k)$ gauge theory with superpotential (7.53), and
- the Landau-Ginzburg model with superpotential (7.50)

all flow to the IR fixed point given by the Kazama-Suzuki model (7.52).

To give evidence of the claims above, we compute the number of supersymmetric ground states and the chiral ring in the respective systems, and show that they agree. We also study the BPS spectrum of the brane system and compare it with the known field theoretical results. Superconformal points themselves are hard to analyze, and therefore we often make mass deformations. We also study the S^2 partition functions by using the recently-developed technique of exact computations [67, 68, 69, 70, 71] and show that they indeed

agree.

7.3 Supersymmetric Vacua

As the first check, we look at the supersymmetric vacua of the respective systems or compute the Witten index [72], and see if the results are consistent with the claimed duality.

7.3.1 Brane System

Let us first look at the brane system. As in the introduction, we denote the set of solutions to $t(v) = 1$ by $\{v_i\}_{i \in I}$ where we initially assume that each solution is non-degenerate $t'(v_i) \neq 0$. Supersymmetry requires each M2-brane to have a fixed position in (t, v) . The boundary at M5' fixes t to be 1 and allows v to be arbitrary, while the boundary at M5 requires the relation $t = t(v)$. Thus, each M2 must be at $t = 1$ and has $v = v_i$ for some $i \in I$. The s-rule requires different M2 branes to have different values of v . Therefore, a supersymmetric vacuum is specified by picking k distinct elements from this set:

$$V \subset \{v_i\}_{i \in I}, \quad |V| = k. \quad (7.54)$$

When $t(v)$ is a polynomial of order M , the equation $t(v) = 1$ has M roots. Generically, they are distinct and non-degenerate. Then, the number of supersymmetric vacua is 0 if $k > M$ and $\binom{M}{k}$ if $k \leq M$. We may also consider a special polynomial where some of the solutions coincide. In this situation we do not know how to identify the supersymmetric vacua. However, the Witten index [72], which does not change under continuous deformation, remains the same as in the non-degenerate case. When some number, say N , of the solutions are close to each other while others are far away, then, we may consider the “subsector” in which all k M2 branes are at one of these N solutions. In particular, when $N \geq k$ of them are at the same point, we expect to have a *single* infra-red theory whose Witten index is $\binom{N}{k}$. This discussion on subsectors and their Witten indices is applicable even when $t(v)$ is not a polynomial and the equation $t(v) = 1$ have infinitely many solutions.

7.3.2 Gauge Theory

Let us next consider the $U(k)$ gauge theory with the tree level twisted superpotential (7.48) determined by a polynomial $P(\sigma)$. The classical scalar potential takes the form

$$U = \frac{1}{4g^2} \text{tr}[\sigma, \sigma^\dagger]^2 + \frac{g^2}{2} \text{tr}(\text{Re}P'(\sigma))^2. \quad (7.55)$$

Vanishing of the first term requires σ to be diagonalizable,

$$\sigma = \text{diag}(\sigma_1, \dots, \sigma_k). \quad (7.56)$$

When all the eigenvalues are well separated, the value of σ breaks the gauge group $U(k)$ to its diagonal subgroup $T \cong U(1)^k$. In this Coulomb branch, we may integrate out the off-diagonal components of the vector multiplet. This induces a correction to the twisted superpotential. As explained in [64] following [62], the correction is given by πi times the sum of positive roots,

$$\Delta\mathcal{W} = \pi i \sum_{a < b} (\Sigma_a - \Sigma_b) \equiv \pi i (k+1) \sum_{a=1}^k \Sigma_a. \quad (7.57)$$

In the second equality, we used the periodicity $\theta_a \equiv \theta_a + 2\pi$ of the theta angle for the group T . This cancels the tree level theta term in (7.48) and hence the effective twisted superpotential is

$$\mathcal{W}_{\text{eff}} = \mathcal{W}|_T + \Delta\mathcal{W} = \sum_{a=1}^k P(\Sigma_a). \quad (7.58)$$

We denote the effective gauge coupling constant by $e_{ab}^2(\sigma)$. We know that it approaches $g^2\delta_{ab}$ in the limit where all σ_a are infinitely separated. We assume that it is positive definite in the region of σ we are looking at, and defines inner products, $\|y\|_{e^{-2}}^2 = (e^{-2})^{ab} y_a y_b$ and $\|x\|_{e^2}^2 = e_{ab}^2 x^a x^b$, on the Lie algebra of T and its dual. The effective potential is given by

$$U_{\text{eff}} = \frac{1}{2} \|\text{Re}\mathcal{W}'_{\text{eff}}(\sigma)\|_{e^2}^2 + \frac{1}{2} \|v_{01}\|_{e^{-2}}^2. \quad (7.59)$$

The first term, where $\text{Re}(\mathcal{W}'_{\text{eff}}(\sigma))^a = \text{Re}P'(\sigma_a)$, is the remnant of the classical potential (7.55). The second term is the electro-static energy [56, 32]. In the Hamiltonian formulation, see e.g. [45], $(e^{-2})^{ab} v_{b01} + \text{Im}(\mathcal{W}'_{\text{eff}}(\sigma))^a$ are regarded as the conjugate momenta for the

holonomy of T , each of which has period 1, and hence have eigenvalues in $2\pi\mathbb{Z}$. In other words,

$$v_{a01} = \sum_{b=1}^k e_{ab}^2(\sigma) \left(2\pi n^b - \text{Im}P'(\sigma_b) \right) \quad (7.60)$$

where $n^a \in \mathbb{Z}$. In the sector with definite n^a 's, the effective potential is

$$U_{\text{eff}} = \sum_{a,b=1}^k \frac{e_{ab}^2(\sigma)}{2} (P'(\sigma_a) - 2\pi i n^a) \overline{(P'(\sigma_b) - 2\pi i n^b)}. \quad (7.61)$$

Supersymmetric ground states must be at the zeroes of this potential. That is, each (σ_a, n^a) must satisfy

$$P'(\sigma) = 2\pi i n, \quad n \in \mathbb{Z}. \quad (7.62)$$

The above analysis is valid only when $\sigma_1, \dots, \sigma_k$ are separated. We do not know how to analyze the region near the diagonals where some of σ_a 's coincide. In many examples, however, it is found that no supersymmetric ground state is supported near the diagonals as long as the critical points of the effective twisted superpotential are all non-degenerate. See for example [73]. Here we assume that this applies to our system. Note also that solutions related by permutations of (σ_a, n^a) 's are related by the residual gauge transformations and must be identified. Thus, when $P''(\sigma) \neq 0$ at each solution to (7.62), a supersymmetric vacuum is specified by a choice of k unordered solutions $\{(\sigma_a, n^a)\}$ to (7.62) such that $\sigma_a \neq \sigma_b$ for $a \neq b$. We see that there are infinitely many supersymmetric vacua.

The equation (7.62) may be written simply as $\exp(P'(v)) = 1$. Then we see that the problem of finding supersymmetric vacua in this system is identical to that in the M2 brane system where the function $t(v)$ defining the M5 curve is given by (7.47).

Let us write

$$P_u(\sigma) = \frac{1}{N+1} \sigma^{N+1} + \sum_{j=1}^N \frac{\mu_j}{N+1-j} \sigma^{N+1-j}. \quad (7.63)$$

for which the equation (7.62) reads

$$\sigma^N + \sum_{j=1}^N \mu_j \sigma^{N-j} = 2\pi i n, \quad n \in \mathbb{Z}. \quad (7.64)$$

For a small but generic $\mu = (\mu_1, \dots, \mu_N)$, the equation with $n = 0$ has N distinct solutions close to $\sigma = 0$, while the equation with $n \neq 0$ has N separated solutions at $|v| \sim (2\pi n)^{1/N}$.

Our main interest will be the sector with $n^1 = \dots = n^k = 0$. The supersymmetric vacua must have σ_a values from the N solutions near 0. The number of such vacua is zero when $k > N$ and $\binom{N}{k}$ when $1 \leq k \leq N$. When we turn off u , the N solutions all go to $\sigma = 0$. If $1 \leq k \leq N$, we expect to have a single IR theory from the $n^1 = \dots = n^k = 0$ sector. Its Witten index is $\binom{N}{k}$.

7.3.3 Landau-Ginzburg Model

Finally, we consider the Landau-Ginzburg model. Let $W_u(X) = W_u(X_1, \dots, X_k)$ be the superpotential corresponding to $P_u(\sigma)$ of (7.63), that is, $\sum_{a=1}^k P_u(\Sigma_a)$ written in terms of the elementary symmetric functions of $\Sigma_1, \dots, \Sigma_k$.

When we turn off u , the superpotential $W_0(X)$ is the one (7.50) given in the introduction and is a quasi-homogeneous polynomial. When $N \geq k$, it has an isolated critical point at $X = 0$ and the Landau-Ginzburg model is believed to flow to a non-trivial superconformal field theory of central charge $c = 3k(N - k)/(N + 1)$. In fact the conformal field theory has been claimed to be equivalent to the Kazama-Sukuki supercoset of the type (7.52). See Appendix B. The space of supersymmetric ground states of the model is naturally identified with the representation $\wedge^k \mathbb{C}^N$ of $SU(N)$ [74]. Its dimension $\binom{N}{k}$ matches the Witten index of the M2 and the gauge systems.

The model with $\mu_j \neq 0$ can be regarded as a perturbation of this superconformal field theory by the chiral primary fields $\phi_j(X)$ corresponding to $\sum_{a=1}^k \sigma_a^{N+1-j}$. These have R-charges $2(N + 1 - j)/(N + 1)$ and conformal weights $(N + 1 - j)/(N + 1) < 1$ and hence the perturbation is relevant. In particular, the number of supersymmetric ground states remains the same, $\binom{N}{k}$. Moreover, for the particular deformation where all μ_j but μ_N vanish, the ground states are labelled by the weights of the representation $\wedge^k \mathbb{C}^N$ of $SU(N)$ mentioned above [75]. This picture matches with the one for the M2 and the gauge systems if we regard the roots of $\sigma^N + \mu_N = 0$ as the weights of the representation \mathbb{C}^N . This observation will be important when we compare the spectra of BPS solitons.

For a generic choice of u , the correspondence of the ground states with those of the gauge system can be seen more explicitly. The map $\sigma \mapsto x(\sigma)$, defined by the elementary symmetric functions $x_1(\sigma), \dots, x_k(\sigma)$ of $\sigma_1, \dots, \sigma_k$, is regular away from the diagonals, since

the Jacobi matrix has determinant

$$\det \left(\frac{\partial x_b}{\partial \sigma_a} \right)_{1 \leq a, b \leq k} = \prod_{1 \leq a < b \leq k} (\sigma_a - \sigma_b). \quad (7.65)$$

The singular values, i.e., the image of the diagonals, shall be called *the discriminant*. Let us write $f_u(\sigma_1, \dots, \sigma_k) = \sum_{a=1}^k P_u(\sigma_a)$. Then, we have

$$f_u(\sigma) = W_u(x(\sigma)). \quad (7.66)$$

Taking the first derivatives, we obtain

$$\frac{\partial f_u}{\partial \sigma_a}(\sigma) = \sum_{b=1}^k \frac{\partial x_b}{\partial \sigma_a}(\sigma) \frac{\partial W_u}{\partial x_b}(x(\sigma)). \quad (7.67)$$

This means that “off the diagonals” critical points of $f_u(\sigma)$ modulo permutations of σ_a ’s are in one-to-one correspondence with “off the discriminant” critical points of $W_u(x)$. Taking one more σ derivative and computing the determinant, one sees that the Hessian of $f_u(\sigma)$ vanishes if $x(\sigma)$ is a critical point of $W_u(x)$ on the discriminant. Therefore, if all the critical points of $f_u(\sigma)$ are non-degenerate, then, all the critical points of $W_u(x)$, if there exist, are off the discriminant and also non-degenerate. (Note however that $f_u(\sigma)$ may have a non-degenerate critical point on the diagonal that does not correspond to a critical point of $W_u(x)$.) This establishes a one-to-one correspondence between the supersymmetric ground states of the $n^1 = \dots = n^k = 0$ sector of the gauge system and those of the Landau-Ginzburg model, for a generic u so that $f_u(\sigma)$ is a Morse function. In particular, this is one way to see that the number of critical points of $W_u(X)$ is zero for $N < k$ and $\binom{N}{k}$ for $N \geq k$.

7.4 Chiral Rings

In this section, we shall study the chiral ring of the gauge system and compare the result with that of the Landau-Ginzburg model. We consider the $U(k)$ gauge theory with tree level twisted superpotential

$$\mathcal{W} = f(\Sigma) + \pi i(k+1)\text{tr}\Sigma \quad (7.68)$$

where $f(\Sigma)$ is an adjoint invariant polynomial of Σ . The effective twisted superpotential on the Coulomb branch is $\mathcal{W}_{\text{eff}} = f(\Sigma_T)$. We shall use the same notation $f(\sigma) = f(\sigma_1, \dots, \sigma_k)$ for that symmetric polynomial, and denote simply by $W(X)$ the corresponding superpotential, $f(\sigma) = W(x(\sigma))$. Just as in (7.67), we have

$$\frac{\partial f}{\partial \sigma_a}(\sigma) = \sum_{b=1}^k \frac{\partial x_b}{\partial \sigma_a}(\sigma) \frac{\partial W}{\partial x_b}(x(\sigma)). \quad (7.69)$$

We assume that $f(\sigma)$ is a Morse function. Then, $W(x)$ is also Morse, and supersymmetric ground states of the $n^1 = \dots = n^k = 0$ sector of the gauge system are in one-to-one correspondence with those of the Landau-Ginzburg model.

The chiral ring of the Landau-Ginzburg model is generated by the chiral variables x_1, \dots, x_k and the relations are generated by

$$0 \equiv \left\{ \mathbf{Q}_B, g^{a\bar{b}}(\bar{\psi}_{b-} - \bar{\psi}_{b+}) \right\} = \partial_{x_a} W(x), \quad a = 1, \dots, k. \quad (7.70)$$

Here \mathbf{Q}_B is the relevant supercharge, $g^{a\bar{b}}$ is the Kähler metric that appears in the kinetic term, and $\bar{\psi}_{b\pm}$ are the fermionic components of the antichiral multiplet \bar{X}_b . Hence the chiral ring is isomorphic to the Jacobi ring,

$$\text{Jac}(W) = \mathbb{C}[x_1, \dots, x_k] / (\partial_{x_1} W(x), \dots, \partial_{x_k} W(x)). \quad (7.71)$$

The twisted chiral ring of the gauge system is generated by gauge invariant polynomials of σ . In the low energy description on the Coulomb branch, they reduce to symmetric functions of $\sigma_1, \dots, \sigma_k$. To find the relations, we note that

$$\left\{ \mathbf{Q}_A, (e^{-2})^{ab}(\bar{\lambda}_{b-} - \lambda_{b+}) \right\} = (e^{-2})^{ab}(D_b + iv_{b01}) \quad (7.72)$$

where \mathbf{Q}_A is the relevant supercharge while $\bar{\lambda}_{b-}$, λ_{b+} and D_b are fermionic and auxiliary components of the twisted antichiral multiplet $\bar{\Sigma}_b$. The auxiliary fields D_b are constrained to be

$$(e^{-2})^{ab} D_b = -\text{Re} \partial_{\sigma_a} f(\sigma). \quad (7.73)$$

We also have equations like (7.60):

$$(e^{-2})^{ab} v_{b01} = -\text{Im} \partial_{\sigma_a} f(\sigma) + 2\pi n^a, \quad (7.74)$$

where n^a are integers labeling the momenta of the holonomy variables. Therefore the relations are $\partial_{\sigma_a} f(\sigma) \equiv 2\pi i n^a$. Our main interest is the $n^1 = \dots = n^k = 0$ sector. The relations are

$$\partial_{\sigma_a} f(\sigma) \equiv 0, \quad a = 1, \dots, k. \quad (7.75)$$

We shall also accept relations of the form

$$\sum_{a=1}^k \frac{F_a(\sigma)}{\Delta(\sigma)^\ell} \partial_{\sigma_a} f(\sigma) \equiv 0 \quad (7.76)$$

where $F_a(\sigma)$ are polynomials and $\Delta(\sigma)$ is the Vandermond determinant

$$\Delta(\sigma) := \prod_{1 \leq a < b \leq k} (\sigma_a - \sigma_b). \quad (7.77)$$

We allow division by $\Delta(\sigma)$ because σ_a 's are assumed to be separated from each other in the Coulomb branch. Let I_f be the ideal of the ring $\mathbb{C}[\sigma_1, \dots, \sigma_k]^{\mathfrak{S}_k}$ of symmetric polynomials consisting of polynomials that can be written in the form on the left hand side of (7.76). Then, the twisted chiral ring is

$$\mathbb{C}[\sigma_1, \dots, \sigma_k]^{\mathfrak{S}_k} / I_f. \quad (7.78)$$

When $f(\sigma)$ is generic so that $W(x)$ has only isolated and non-degenerate critical points, i.e., $W(x)$ is Morse, one can show that this is isomorphic to the Jacobi ring $\text{Jac}(W)$.

The proof goes as follows. First, we have an isomorphism $\mathbb{C}[x_1, \dots, x_k] \cong \mathbb{C}[\sigma_1, \dots, \sigma_k]^{\mathfrak{S}_k}$ given by $\phi(x) \mapsto \phi(x(\sigma))$. It is enough to show that the ideal $I_W = (\partial_{x_1} W, \dots, \partial_{x_k} W)$ is mapped precisely to I_f under this isomorphism. That I_W is mapped into I_f is obvious in view of (7.69) and the definition of I_f . To show that the map $I_W \rightarrow I_f$ is surjective, let $\phi(x)$ be a polynomial so that $\phi(x(\sigma))$ belongs to I_f . Then, $\phi(x(\sigma))$ vanishes on “off the diagonals” critical points of $f(\sigma)$. Here we recall from the previous section that $\sigma \mapsto x(\sigma)$ gives one-to-one correspondence between “off the diagonals” critical points of $f(\sigma)$ modulo

permutations and critical points of $W(x)$. Therefore, $\phi(x)$ vanishes on the critical points of $W(x)$. Since $W(x)$ is a Morse function, this means that $\phi(x)$ belongs to I_W . See [30] for the proof of the last statement.

7.5 BPS Solitons

In this section we analyze the spectrum of the BPS states from M2-branes, building on [31, 8, 9, 10, 39], and compare the results with the spectrum of BPS solitons in the Landau-Ginzburg model [34, 75].

In what follows, we are interested in M2-branes whose (t, v) values are confined into a small neighborhood of $v = 0$ and $t = 1$. Therefore, we write $t = e^z$ and regard z as a coordinate on a neighborhood of the origin of a complex plane \mathbb{C} . M5' is at $z = 0$ and we consider the M5-brane wrapped on the curve

$$z = v^N + \mu_1 v^{N-1} + \cdots + \mu_N. \quad (7.79)$$

Recall (7.54) that a supersymmetric ground state is specified for a choice of k distinct elements from the set $\{v_i\}_{i=1}^N$ of solutions to $v^N + \mu_1 v^{N-1} + \cdots + \mu_N = 0$. We are interested in solitonic M2-brane configurations that interpolate two different ground states.

7.5.1 A single M2-brane

Let us recall the basics of BPS solitons arising from a single M2-brane stretched between two M5-branes. This setup was originally studied in [31] and later in [39]. The system may be regarded as an $\mathcal{N}=(2, 2)$ supersymmetric field theory on $\mathbb{R}^2 = \{(x^0, x^1)\}$ with a chiral multiplet taking values in the space of paths $\phi : x^6 \in [0, L] \mapsto (z(x^6), v(x^6)) \in \mathbb{C}^2$ from the M5' at $z = 0$ to the M5 at (7.79). It has the superpotential [76]

$$\mathcal{W}[\phi] = \int_{C_{\phi, \phi_*}} \Omega, \quad \Omega := dz \wedge dv, \quad (7.80)$$

where C_{ϕ, ϕ_*} is a configuration that interpolates a reference path ϕ_* and ϕ . Note that

$$\frac{\delta \mathcal{W}}{\delta z(x^6)} = \partial_6 v(x^6), \quad \frac{\delta \mathcal{W}}{\delta v(x^6)} = -\partial_6 z(x^6). \quad (7.81)$$

In particular, the action includes the usual kinetic term of a theory on three dimensions (x^0, x^1, x^6) . A soliton is a configuration that approaches two vacua, say $\phi_j \equiv (0, v_j)$ and $\phi_i \equiv (0, v_i)$, as $x^1 \rightarrow -\infty$ and $x^1 \rightarrow +\infty$ respectively. The central charge of such a solitonic sector is

$$Z_{ij} = \mathcal{W}[\phi_i] - \mathcal{W}[\phi_j] = \int_{C_{\phi_i, \phi_j}} \Omega. \quad (7.82)$$

A soliton preserves a half of the supersymmetry if the configuration satisfies the BPS equation, $\partial_1 \phi = \zeta_{ij} \overline{\delta \mathcal{W} / \delta \phi}$ with $\zeta_{ij} := Z_{ij} / |Z_{ij}|$, i.e.,

$$\partial_1 z = \zeta_{ij} \partial_6 \bar{v}, \quad \partial_1 v = -\zeta_{ij} \partial_6 \bar{z}. \quad (7.83)$$

It follows that

$$\phi^* \omega = 0, \quad \bar{\zeta}_{ij} \phi^* \Omega = dx^1 \wedge dx^6 \cdot (\text{real positive}), \quad (7.84)$$

where $\omega := \frac{i}{2} dz \wedge d\bar{z} + \frac{i}{2} dv \wedge d\bar{v}$ is the Kähler form. This is equivalent [9] to the condition that the image of $\phi : \mathbb{R} \times [0, L] \rightarrow \mathbb{C}^2$ is a special Lagrangian submanifold.

One may also look at the usual supersymmetry condition [77, 8, 39]. Let η be the 11d spinor obeying $\eta = \Gamma_{012\dots 9,10} \eta$. Presence of the M5-branes imposes the condition $\eta = \Gamma_{014589} \eta = \Gamma_{012345} \eta = \Gamma_{01789,10} \eta$ from which we also have $\eta = \Gamma_{016} \eta$. Then, the BPS equation (7.83) is equivalent to the existence of a spinor η obeying

$$\eta = \frac{1}{2} \epsilon^{\alpha\beta} \Gamma_{0IJ} \partial_\alpha x^I \partial_\beta x^J \eta \quad (7.85)$$

(the summation over $I, J = 1, 4, 5, 6, 7, 10$ and $\alpha, \beta = 1, 6$ is assumed), in the limit

$$|\partial_{1,6} x^{4,5,7,10}| \ll 1 \quad (7.86)$$

where the eleven dimensional Planck length is set equal to one. The preserved supersymmetry is $(\zeta_{ij} \Gamma_{vz} + \bar{\zeta}_{ij} \Gamma_{\bar{v}\bar{z}}) \eta = \Gamma_{16} \eta$.

7.5.2 k M2-branes

We now consider the case of general k . Let us take two ground states specified by subsets V and V' of $\{v_i\}_{i=1}^N$ of order k . A soliton that interpolates V and V' is the superposition of k single M2-brane solitons, each of which approach $v_{i_a} \in V$ and $v_{i'_a} \in V'$ as $x^1 \rightarrow -\infty$ and

$x^1 \rightarrow +\infty$ respectively. The central charge of such a solitonic sector is the sum $\sum_{a=1}^k Z_{i'_a, i_a}$ while the mass is bounded below by $\sum_{a=1}^k |Z_{i_a, i'_a}|$. When μ_j are generic, Z_{ij} have different phases for different pairs (i, j) . Therefore, it saturates the BPS bound only when just one of the k M2-branes is a non-trivial soliton while the remaining $k - 1$ stay fixed at the vacua. This is possible only when $|V \cap V'| = k - 1$.

In the picture where $\{v_i\}_{i=1}^N$ is regarded as the set of weights of the fundamental representation \mathbb{C}^N of $SU(N)$, a BPS state for the k M2-brane system exists only if V and V' , which are regarded as weights of the representation $\wedge^k \mathbb{C}^N$, are connected by a root of $SU(N)$. This matches with the structure of the BPS spectrum of the Landau-Ginzburg model: In [34, 75], it was proposed that there is exactly one BPS soliton for each pair of vacua labelled by weights of $\wedge^k \mathbb{C}^N$ that differ by a root of $SU(N)$. Therefore, we would like to see that there is exactly one BPS soliton for any pair of v_i and v_j in the single M2-brane system.

Showing this seems to be a difficult problem to the authors. Instead of trying to find BPS configurations directly, we shall take a certain limit [10] that reduces the problem of finding BPS membranes to the problem of finding BPS geodesics [6], and then use the technique of spectral networks.

7.6 2d BPS spectrum from spectral networks

So far, we have been using the metric $ds^2 = |dz|^2 + |dv|^2$ in the $x^{4,5,7,10}$ directions. We now change it to

$$ds^2 = |dz|^2 + \beta^2 |dv|^2 \tag{7.87}$$

and take a small β limit. We also have

$$\omega = \frac{i}{2} dz \wedge d\bar{z} + \frac{i}{2} \beta^2 dv \wedge d\bar{v}, \quad \Omega = \beta dz \wedge dv. \tag{7.88}$$

The argument of [10] shows that, in the limit $\beta \rightarrow 0$, the projection of a BPS configuration $C_{ij} = C_{\phi_i, \phi_j}$ onto the z -plane is a real one-dimensional graph γ_{ij} , and the tangent directions Δz and Δv obey the constraint $\Delta z \cdot \Delta v = \zeta_{ij}$ (real number). Over a generic point z on the graph γ_{ij} , C_{ij} is a line segment from one solution v_l to another v_k of (7.79). Of course, $(k, l) = (i, j)$ near $z = 0$, but that may not be the case if z is far from $z = 0$. See Figure 7.4.

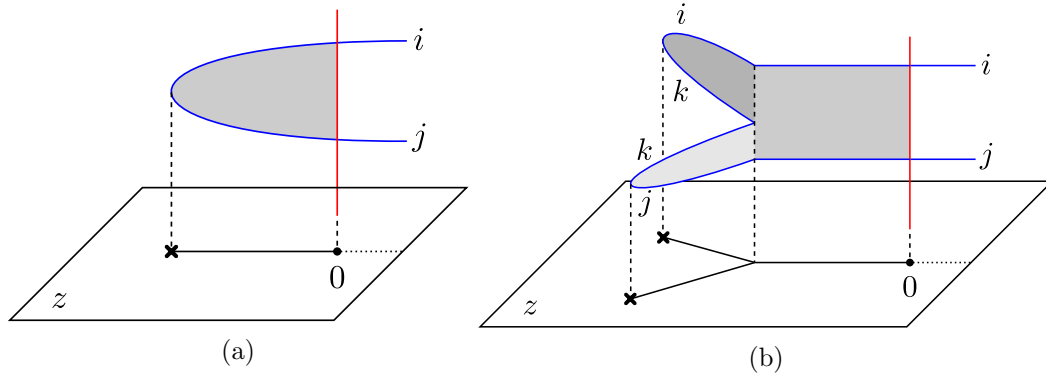


Figure 7.4: M2-brane solitons in the $\beta \rightarrow 0$ limit. Blue curves are parts of M5, and red lines are parts of M5'. The (z, v) images of the M2-brane solitons are shaded.

In a neighborhood of such a point, the graph γ_{ij} is a curve determined by the differential equation

$$\lambda_{kl}(z) \frac{\partial z}{\partial \tau} = \exp(i\vartheta_{ij}) = \frac{Z_{ij}}{|Z_{ij}|}, \quad (7.89)$$

where $\lambda_{kl} dz = (v_k(z) - v_l(z)) dz$ is the difference of $\lambda = v dz$ at the k -th sheet and at the l -th sheet of M5-branes, and τ is a real parameter along the curve γ_{ij} . Such a γ_{ij} is called a finite open web of BPS strings [37].

We would like to find a solution to (7.89) that starts from a branch point of the covering $v(z) \mapsto z$ and call it \mathcal{S}_{kl} . For a generic value of $\vartheta = \vartheta_{ij}$, it does not pass the endpoint of the ground-state M2-branes at $x = 0$ but goes to infinity, meaning that it does not correspond to any of the BPS states. These paths are called \mathcal{S} -walls. When two \mathcal{S} -walls \mathcal{S}_{ik} and \mathcal{S}_{kj} cross, another \mathcal{S} -wall, \mathcal{S}_{ij} , can emerge, when there is a supersymmetric junction of three M2-branes that satisfy $\lambda_{ik} + \lambda_{kj} = \lambda_{ij}$ [19, 37], like in Figure 7.4b. The collection of \mathcal{S} -walls is called a spectral network [37]. When there is an \mathcal{S} -wall \mathcal{S}_{ij} that passes $z = 0$, then this gives us a BPS object with a finite central charge.

7.6.1 Deformation by μ_N

Let us consider a particular deformation where the curve is

$$z = v^N + \mu_N. \quad (7.90)$$

The z -coordinate is zero when

$$v_j = (-\mu_N)^{1/N} \omega^j, \quad \text{where } \omega = e^{2\pi i/N}. \quad (7.91)$$

Hence, the vacua are depicted by the vertex of a regular polygon on the v -plane.

The curve has a branch point of ramification index N at $z = \mu_N$, and the differential equation that governs the behavior of each \mathcal{S}_{ij} on the z -plane is

$$\alpha_{ij}(z - \mu_N)^{1/N} \frac{\partial z}{\partial \tau} = \exp(i\vartheta), \quad (7.92)$$

where $\alpha_{ij} = \omega^i - \omega^j$. The solution is

$$z_{ij}(\tau) = \mu_N + c \left(\frac{N+1}{N} \frac{\tau}{\alpha_{ij}} \right)^{N/(N+1)} \exp\left(\frac{N}{N+1} i\vartheta\right) \quad (7.93)$$

where c is an $(N+1)$ -st root of unity. This is a straight line starting at the branch point $z = \mu_N$. When $\alpha_{ij} = \alpha_{i'j'}$ two S-walls can be on top of each other. As an example, Figure 7.5 shows the spectral network when $N = 4$ for $\vartheta = 0$. As can be seen there, \mathcal{S}_{12} and \mathcal{S}_{34} are coincident.

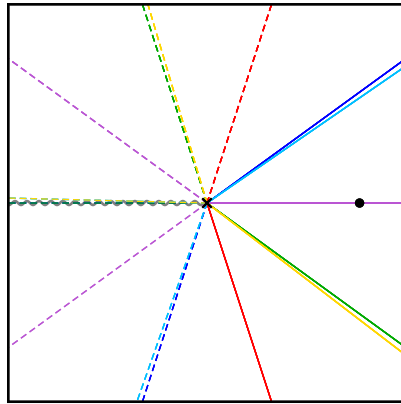


Figure 7.5: A spectral network around a branch point of ramification index $N = 4$.

When we change ϑ from 0 to 2π , the whole spectral network rotates by $2\pi N/(N+1)$, and the endpoint of the M2-brane meets $N(N-1)$ S-walls in the process, implying there are in total $N(N-1)$ BPS states in the BPS spectrum of this theory. Therefore, for each distinct i and j , there is one BPS state in the sector with the right boundary set to the vacuum i and the left boundary set to the vacuum j . It is easy to identify the value ϑ when

an \mathcal{S}_{ij} wall hits $x = 0$. There is one value of ϑ for each \mathcal{S}_{ij} .

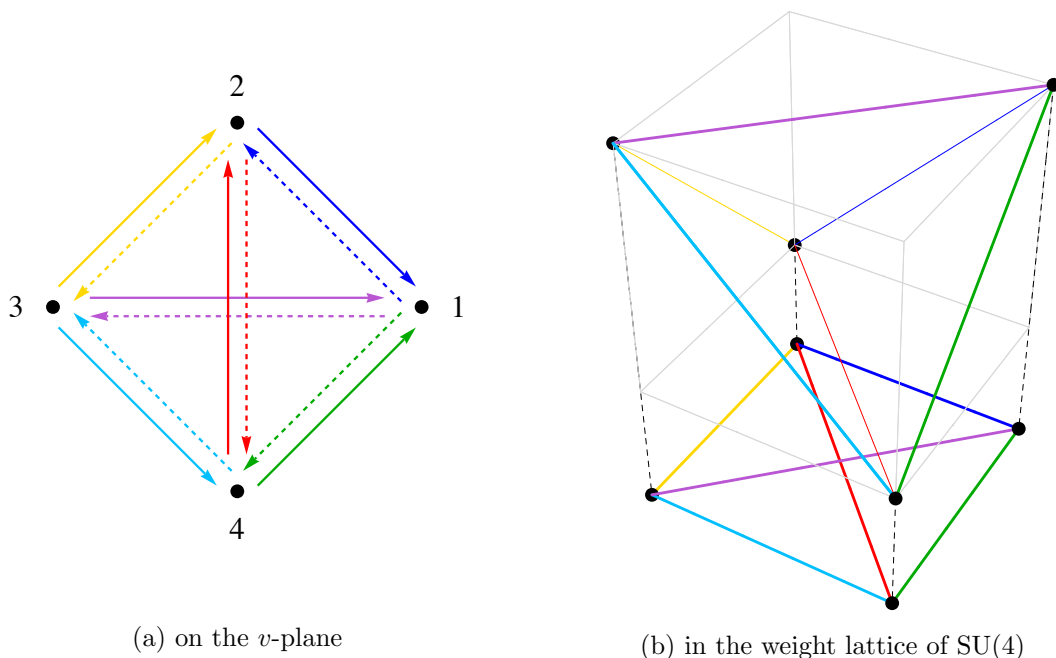
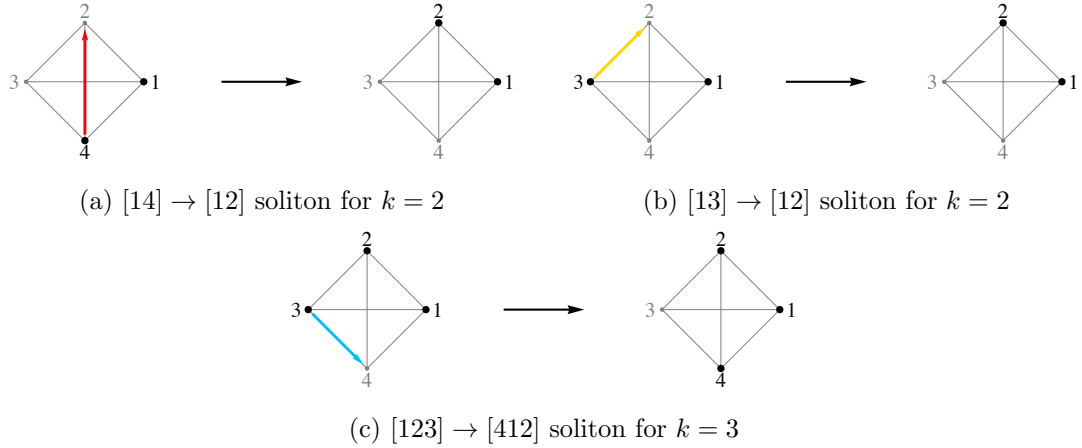


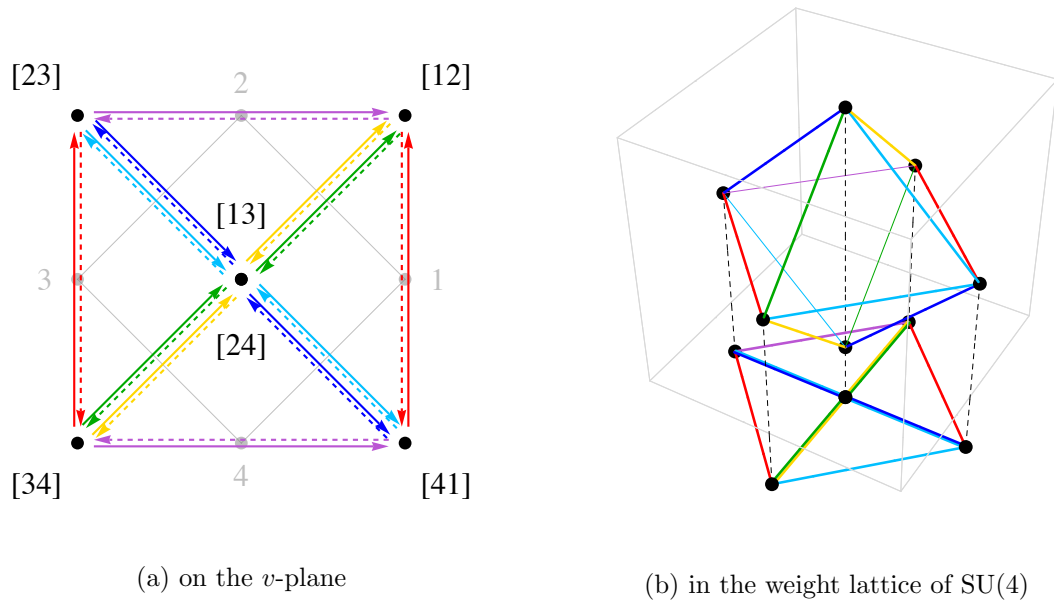
Figure 7.6: Vacua and solitons, $k = 1$.

On the v -plane, we can introduce a soliton of the $k = 1$ theory by a line connecting v_i and v_j . Let us illustrate the case $N = 4$. Figure 7.6a represents the four ground states and twelve solitons on the v -plane. We clearly see that $Z[\gamma_{12}]$ and $Z[\gamma_{34}]$ has the same phase, as was also reflected in the spectral network shown in Figure 7.5. Note that Figure 7.6a can be understood as obtained from the projection of the weights of the fundamental representation of $SU(4)$ and the roots connecting the weights, representing the ground states and the solitons respectively, as shown in Figure 7.6b. This structure of BPS solitons is the same as that of the corresponding Landau-Ginzburg model with a single chiral field, which has as its IR fixed point the $\mathcal{N}=2$ A_3 minimal model [34].

So far we discussed the case when there is just one M2-brane, $k = 1$. For general k , we need to choose k vertices out of N , and a soliton is obtained by moving one of the k vertices. In Figure 7.7, some representative examples of the solitons with $k = 2$ and $k = 3$ are shown. For $k = 2$, we see from Figures 7.7a and 7.7b that a $k = 1$ solitonic configuration can connect two $k = 2$ ground states. From this consideration we can represent $k = 2$ ground states and solitons as shown in Figure 7.8a. Again, we can understand this as obtained from the projection of the weights of the 2nd antisymmetric power of the fundamental representation

Figure 7.7: Examples of $k > 1$ solitons.

of $SU(4)$ and the roots connecting the weights, as shown in Figure 7.6b. The same structure of BPS solitons of the corresponding Landau-Ginzburg model is observed in [75], which is expected to flow in the IR to the Kazama-Suzuki model based on $SU(4)_1/S[U(2) \times U(2)]$.

Figure 7.8: Vacua and solitons, $k = 2$.

For $k = 3$, because choosing k ground states among N indistinguishable ones is the same as choosing $N - k$ ground state, the ground states and the solitons are represented by the same diagram as Figure 7.6a, thus we see the $k \leftrightarrow N - k$ duality.

7.6.2 General deformations

Now let us consider how the spectral networks look when the deformation parameters μ_j are general.

7.6.2.1 BPS spectrum with $z = v^3$

Now we consider the case where we have three M5-branes ramified over the z -plane:

$$z = v^3 + \mu_2 v + \mu_3. \quad (7.94)$$

For general μ_2 and μ_3 , we have two branch points of ramification index 2 on the z -plane as shown in Figure 7.9. In the figure, we chose $\mu_{2,3}$ so that a (12)-branch cut, a blue wavy line, comes out from the upper branch point, and (13)-branch cut, a green wavy line, from the lower branch point. From the (12)-branch point we have three \mathcal{S} -walls: two \mathcal{S}_{21} with solid blue line and one \mathcal{S}_{12} with a dashed blue line. Similarly, from the (13)-branch point, we have two \mathcal{S}_{13} with solid green line and one \mathcal{S}_{31} with dashed green line. We can see that one \mathcal{S}_{21} and one \mathcal{S}_{13} meet at a point, from which another \mathcal{S} -wall, \mathcal{S}_{23} , emerges.

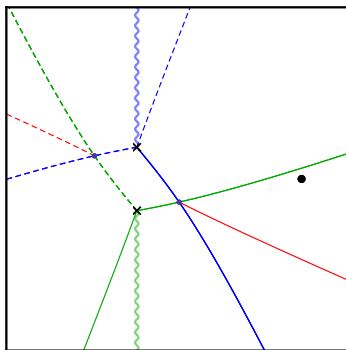


Figure 7.9: A spectral network with general μ_2 and μ_3 .

As we now have the full spectral network, let us rotate it by changing ϑ from 0 to 2π . Figure 7.10 shows spectral networks at various values of ϑ , $0 < \vartheta_{13} < \vartheta_{23} < \vartheta_{21} < \pi$. We see that there are γ_{13} , γ_{23} , and γ_{21} at ϑ_{13} , ϑ_{23} , and ϑ_{21} , respectively, between the branch point and the M2-brane endpoint. Therefore there are corresponding three BPS states for $0 < \vartheta < \pi$. There are another three BPS states for $\pi < \vartheta < 2\pi$, each of which has the central charge $Z[\gamma_{ji}] = -Z[\gamma_{ij}]$.

Now let us take the limit $\mu_2 \rightarrow 0$ so that the two branch points collide, see Figure 7.11.

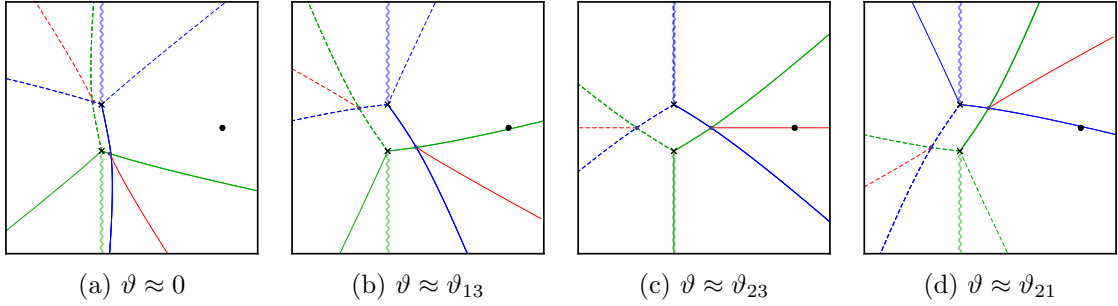


Figure 7.10: Rotation of a spectral network with general μ_2 and μ_3 .

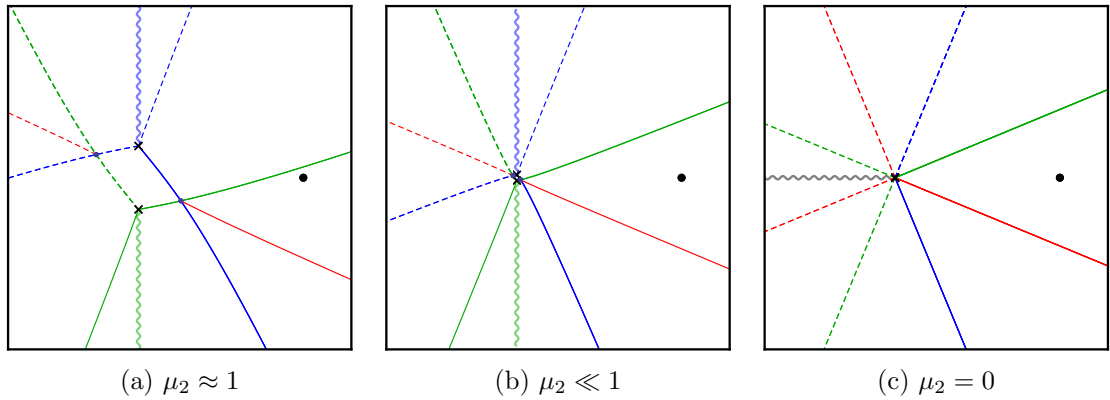


Figure 7.11: Evolution of the spectral network under the limit of $\mu_2 \rightarrow 0$.

Figure 7.11c shows the spectral network when $\mu_2 = 0$. There is only a single (123)-branch point and a single (123)-branch cut.¹ The whole spectral network rotates by $3\pi/4$ when we change ϑ from 0 to π continuously, and in the process we find three BPS strings connecting the branch point and the endpoint of the M2-brane, corresponding to three BPS states in $0 < \arg(Z) < \pi$.

7.6.2.2 BPS spectrum with $z = v^4$

Let us now consider the case $N = 4$, for more illustration.

Figure 7.12 shows the spectral network with $\mu_{2,3,4}$ chosen so that there is a (124)-branch point and a (34)-branch point. See the legend for the nature of walls represented by the colors and the styles.

Figure 7.13 shows the spectral network at various values of ϑ . At ϑ_{ij} there is γ_{ij} between one of the branch points and the endpoint of the M2-brane, and Figure 7.13 is arranged

¹The notation is that around the $(n_1 n_2 \cdots n_k)$ branch cut the sheets are exchanged in the order $n_1 \rightarrow n_2 \rightarrow \cdots \rightarrow n_k \rightarrow n_1$.

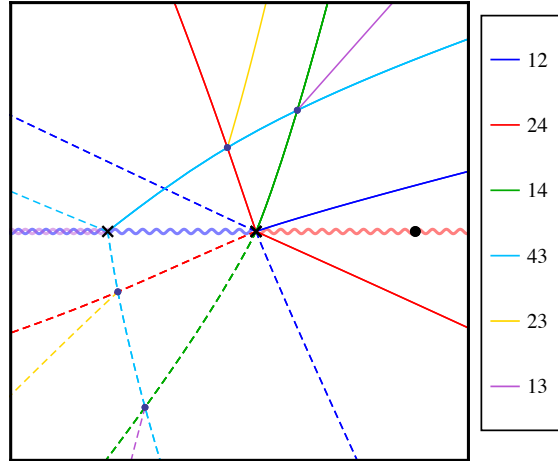


Figure 7.12: A spectral network with $\mu_{2,3,4} \neq 0$.

such that

$$0 < \vartheta_{13} < \vartheta_{43} < \vartheta_{12} < \vartheta_{42} < \vartheta_{41} < \vartheta_{34} < \pi. \quad (7.95)$$

That is, we can imagine the whole spectral network rotating anti-clockwise as we increase ϑ from 0 to π and in the course of the rotation we encounter six finite BPS strings. Therefore, we can expect this theory to have twelve BPS states in total. There are four vacua, so there is one BPS state for each boundary condition at the left and the right spatial infinity.

Let us consider what happens when we have just one branch point of ramification index 4. This limit corresponds to $\mu_2, \mu_3 \rightarrow 0$, and the evolution of the spectral network under the limit is depicted in Figure 7.14. Thus we see that the spectrum of the BPS states at general $\mu_{2,3,4} \neq 0$ is smoothly connected to the more symmetric situation analyzed in Sec. 7.6.1 with $\mu_{2,3} = 0$ and $\mu_4 \neq 0$.

7.7 S^2 partition functions

As a final check of our proposal, we show in this section that the partition function on S^2 of the 2d $\mathcal{N}=(2,2)$ $U(k)$ gauge theory with twisted superpotential $\mathcal{W} = \text{tr}P(\Sigma) + \pi i(k+1)\text{tr}(\Sigma)$ in the infrared limit agrees with that of the Landau-Ginzburg model with chiral fields X_1, \dots, X_k with appropriately chosen superpotential $W = W(X_1, \dots, X_k)$. We employ the localization methods recently developed in [67, 68, 69]. The derivation can be easily

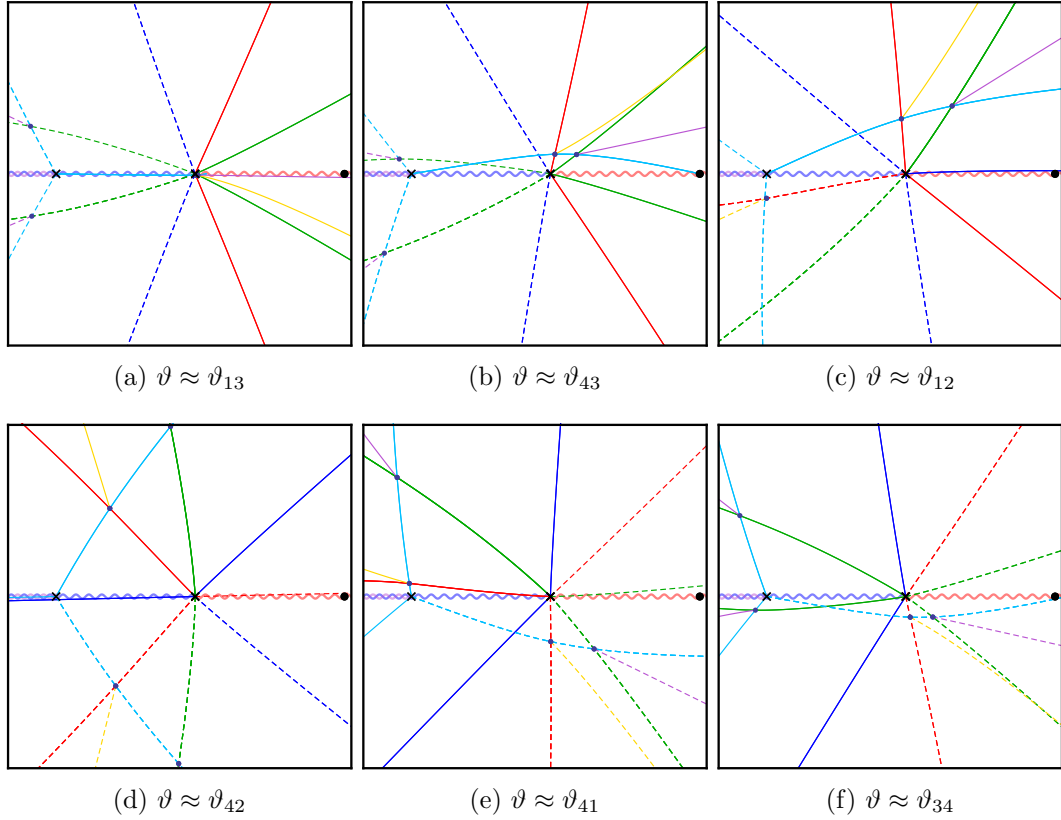


Figure 7.13: Rotation of the spectral network with $\mu_{2,3,4} \neq 0$.

generalized to arbitrary gauge group, and the quasihomogeneity of P and W is not required, either. The integrals below are only conditionally convergent. In this section we perform the comparison of the partition functions rather naively. The convergence issues are explained in [30].

The partition function of the Landau-Ginzburg model of k variables X_1, \dots, X_k with the superpotential $W(X_1, \dots, X_k)$ is given by [69]

$$Z_{\text{LG}} = (r\Lambda)^k \int_{\mathbb{C}^k} \prod_a dX_a d\bar{X}_a e^{-ir[W(X) + \bar{W}(\bar{X})]}, \quad (7.96)$$

where r is the radius of the sphere. The factor in front, $(r\Lambda)^k$, with Λ being a renormalization scale, was not in [67, 68, 69] but is noticed by the authors of these papers [78, 79]. The same applies to $(r\Lambda)^{-k^2}$ in (7.97) below. See [71] for a detailed explanation in a related context. When W is quasi-homogeneous, a rescaling of fields can absorb the r in the integrand and yields the expected behaviour $Z_{\text{LG}} \sim r^{\hat{c}}$ with \hat{c} being the expected central charge of the

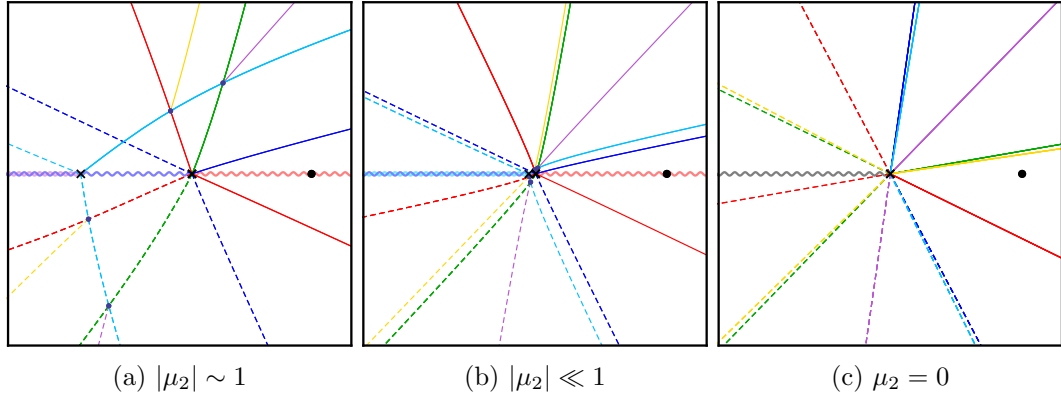


Figure 7.14: Evolution of the spectral network under the limit of $\mu_{2,3} \rightarrow 0$.

infra-red fixed point of the model [80, 81].

The partition function of the $\mathcal{N}=(2, 2)$ supersymmetric gauge theory was first computed in [67, 68] up to a sign factor which was later corrected in [70, 71]. The one for the theory with gauge group $U(k)$ and with the twisted superpotential $\mathcal{W}(\Sigma)$ is given by

$$Z_{\text{gauge}} = (r\Lambda)^{-k^2} \sum_{m \in \mathbb{Z}^k} \int_{\mathbb{R}^k} \prod_a d(r\tau_a) \prod_{a < b} \left(r^2(\tau_a - \tau_b)^2 + \frac{(m_a - m_b)^2}{4} \right) \times (-1)^{(k+1)\sum_a m_a} e^{-ir[\mathcal{W}(\Sigma) + \overline{\mathcal{W}}(\overline{\Sigma})]} \quad (7.97)$$

where

$$\Sigma = \text{diag}(\tau_1, \dots, \tau_k) + \frac{i}{2r} \text{diag}(m_1, \dots, m_k) \quad (7.98)$$

in the exponent.² For the twisted superpotential $\mathcal{W}(\Sigma) = \text{tr}P(\Sigma) + \pi i(k+1)\text{tr}(\Sigma)$, the formula (7.97) reads

$$Z_{\text{gauge}} = \Lambda^{-k^2} \sum_{m \in \mathbb{Z}^k} \int_{\mathbb{R}^k} \prod_a d\tau_a \prod_{a < b} \left((\tau_a - \tau_b)^2 + \left(\frac{m_a - m_b}{2r} \right)^2 \right) e^{-ir[\text{tr}P(\Sigma) + \text{tr}\overline{P}(\overline{\Sigma})]} \quad (7.99)$$

Now, look at the infra-red regime $r\Lambda \gg 1$. The sum $\sum_{m \in \mathbb{Z}^k}$ in (7.99) turns into an

²The sign factor $(-1)^{(k+1)\sum_a m_a}$ was not in [67, 68]. Its presence only changes the weight of the sum over the topological type of the $U(k)$ gauge bundle, only when k is even. Therefore such a factor is rather subtle. The presence is demanded for the factorization of the sphere partition function into two hemispheres [70, 71]. As we will see, its presence is also needed for the match with the partition function of the proposed Landau-Ginzburg model.

integral $(2r)^k \int_{\mathbb{R}^k} \prod_a dv_a$ for $v_a = \frac{m_a}{2r}$, and we have

$$Z_{\text{gauge}} \xrightarrow{r\Lambda \gg 1} \Lambda^{-k^2} r^k \int_{\mathbb{C}^k} \prod_a d\sigma_a d\bar{\sigma}_a \prod_{a < b} |\sigma_a - \sigma_b|^2 e^{-ir[\text{tr}P(\Sigma) + \text{tr}\bar{P}(\bar{\Sigma})]} \quad (7.100)$$

where $\sigma_a = \tau_a + iv_a$ and

$$\Sigma = \text{diag}(\sigma_1, \dots, \sigma_k). \quad (7.101)$$

Let us introduce variables X_a as the elementary symmetric polynomials of σ_a ; equivalently, let us take

$$\det(z - \Sigma) = \sum_a X_a z^{k-a}. \quad (7.102)$$

where z is a dummy variable. Then the Jacobian between the variables σ_a and the variables X_a are given as in (7.65),

$$\det \left(\frac{\partial X_b}{\partial \sigma_a} \right)_{1 \leq a, b \leq k} = \prod_{1 \leq a < b \leq k} (\sigma_a - \sigma_b). \quad (7.103)$$

Therefore, we see that the gauge partition function in the infrared, (7.100), agrees with the Landau-Ginzburg partition function (7.96), under the identification

$$P(\Sigma) = W(X_1, \dots, X_k). \quad (7.104)$$

We now have the equality of S^2 partition functions of the $U(k)$ theory with the twisted superpotential in the infrared limit and those of the Landau-Ginzburg theory. Two-point functions of BPS operators can be dealt with in the completely same way, by just inserting the operators in the integral. It is well-known that the resulting integral expressions suffer from subtleties: apparently spurious operators do not decouple and the choice of representatives of the (anti)chiral ring elements matters [82]. The agreement holds provided that the operators in the gauge system are identified with those in the Landau-Ginzburg model precisely via the isomorphism $\mathbb{C}[\sigma_1, \dots, \sigma_k]^{\mathfrak{S}_k} \cong \mathbb{C}[X_1, \dots, X_k]$.

Chapter 8

4d $\mathcal{N} = 2$ SCFT and spectral network

Recently, many superconformal field theories (SCFTs) of Argyres-Douglas type have been found and studied by making use of 6d $(2, 0)$ theoretic viewpoint of 4d $\mathcal{N} = 2$ theory [5, 19]: a topologically twisted compactification of a 6d $(2, 0)$ theory on a Riemann sphere with an irregular puncture leads to a 4d $\mathcal{N} = 2$ SCFT of Argyres-Douglas type [19, 83, 84, 85, 86, 87, 88, 89, 90]. In this chapter we will focus on the SCFTs obtained from 6d A_{N-1} $(2, 0)$ theories, each of whose Seiberg-Witten curves is an N -sheeted cover of the sphere.

The main tool we will use to find the BPS spectra of such a SCFT on the Coulomb branch is the spectral network of the theory [37, 91]. One merit of using spectral networks is that one can examine BPS spectra over the whole Coulomb moduli space of a theory of class \mathcal{S} and find various chambers depending on the moduli. These chambers are separated by codimension-one lines, called walls of marginal stability, across which the BPS spectrum is changed. In the chamber where the number of the BPS states are minimal, the spectrum of the SCFTs which we will study here is specified by the A - and the D -type Dynkin diagrams, agreeing with the results in [54, 83, 84, 85].

We study BPS spectra of various SCFTs obtained from the A_1 theory compactified on a punctured sphere. There are infinitely many theories depending on the singularity of the punctures. When the sphere has one irregular puncture, the theory corresponds to the maximal conformal point of the pure $SU(n)$ SYM theory, and when the sphere has two punctures with one being irregular and the other being regular, the theory corresponds to the maximal conformal point of the $SU(n)$ gauge theory with two flavors.

As pointed out in [83], the SCFTs from the A_1 theory discussed above have another

realization from the A_{N-1} theory, which can be expected from the fact that the “original” pure $SU(N)$ SYM theory and $SU(N)$ theory with two flavors can be constructed in the A_{N-1} theory framework. Using spectral networks, we study the BPS spectra of a 4d SCFT obtained from a higher rank 6d A_{N-1} theory ($N > 2$), whose spectral networks differ from those from the A_1 theory by the existence of a joint of multiple \mathcal{S} -walls.

We get strong evidence that each SCFT from the A_1 theory considered above is equivalent to an SCFT from the A_{N-1} theory on a sphere with one puncture of a particular singularity by showing that the equivalence of the chamber structure, minimal and maximal BPS spectra of the two when they have the maximal flavor symmetry, i.e., when all mass parameters vanish. We also see the enhancement of the flavor symmetry discussed in [92], by checking that the BPS states indeed form representations of the flavor symmetry when we set the associated mass parameters to vanish.

This chapter is organized as follows. Section 8.1 describes 4d SCFTs that we will consider in this chapter. In Sections 8.2 and 8.3 we study spectral networks of SCFTs on their Coulomb branch to see their minimal BPS spectra can be represented with A_n - and D_n -quivers, respectively, and propose the equivalence between the theories in each class. In Appendix C we describe in detail how to obtain various SCFTs at Argyres-Douglas fixed points starting from high-energy 4d $\mathcal{N} = 2$ theories.

8.1 SCFTs at Argyres-Douglas fixed points

8.1.1 $\mathcal{N} = 2$ SCFTs of class \mathcal{S}

By partially twisted compactification of the 6d A_{N-1} $(2, 0)$ theory on $\mathbb{R}^{1,3} \times \mathcal{C}$ where \mathcal{C} is a Riemann surface, we have a class of 4d $\mathcal{N} = 2$ SCFTs on $\mathbb{R}^{1,3}$, specified by the rank of A_{N-1} and by the Riemann surface \mathcal{C} [5, 19]. The Seiberg-Witten curve Σ which determines the low energy effective theory on the Coulomb branch is given by a curve in $(x, t) \in T^*\mathcal{C}$ where x and t are the coordinates of the fiber and the base respectively:

$$x^N + \sum_{k=2}^N \phi_k(t)x^{N-k} = 0. \quad (8.1)$$

The moduli of the k -th differentials ϕ_k on \mathcal{C} are identified with the Coulomb moduli. In terms of the Seiberg-Witten differential which is given in the coordinates as $\lambda = xdt$, the

central charge of a BPS state is calculated as

$$Z = \oint_{\gamma} \lambda, \tag{8.2}$$

where γ is a two-cycle in the curve (8.1). We will see a way to determine γ in the next subsection.

We allow the Riemann surface to have punctures, at which we place codimension-two defects in the $(2,0)$ theory. A puncture is associated with a flavor symmetry of the 4d theory obtained from the compactification of the 6d $(2,0)$ theory, and is classified into the following two types: regular where λ has a simple pole; irregular where λ has a higher order pole. Equipped with punctures, we denote the class of theories as $\mathcal{S}[A_{N-1}, \mathcal{C}; \mathcal{D}_1, \mathcal{D}_2, \dots]$ where \mathcal{D} represents a puncture or defect.

A_1 case Let us first focus on the rank one case, namely $\mathcal{S}[A_1, \mathcal{C}; \mathcal{D}]$. In this case the puncture is simply specified by the degree of the pole of the quadratic differential. When the degree is two, λ has a simple pole, thus it is regular. This is related with an $SU(2)$ flavor symmetry and denoted as \mathcal{D}_{reg} . When the degree is more than two, it is irregular. If all the punctures are regular, the 4d theory is a class of SCFTs. There are various weak coupling descriptions of this class associated with possible degeneration limits of \mathcal{C} , where all the $SU(2)$ gauge groups have vanishing one-loop beta functions. Thus, the only building block of this theory is a three-punctured sphere associated with four free hypermultiplets. Conversely, connecting two punctures corresponds to the gauging of the diagonal $SU(2)$ symmetry by an $\mathcal{N} = 2$ vector multiplet.

Allowing irregular punctures gives us two more building blocks: one is a one-punctured sphere with an irregular puncture; the other is a two-punctured sphere where one of them is regular and the other is irregular. The former is “isolated” in the sense that this cannot be used to construct a bigger theory. This is classified by the degree $n + 5$ ($n > 1$) of the pole of the quadratic differential at the puncture. Thus let us denote this puncture as \mathcal{D}_{n+5} . The 4d theory resulting from the compactification of the 6d theory on this sphere is indeed the nontrivial SCFT of Argyres-Douglas type: the maximal superconformal point of $SU(n + 1)$ pure SYM theory [87, 92]. (The central charges, a and c , have been computed in [93, 87, 94, 90].) We will denote this SCFT as $\mathcal{S}[A_1; \mathcal{D}_{n+5}]$. We omit \mathcal{C} here and below,

since we always consider the case where \mathcal{C} is a sphere.

The latter also corresponds to SCFTs of Argyres-Douglas type. We denote it as $\mathcal{S}[A_1; \mathcal{D}_{\text{reg}}, \mathcal{D}_{n+2}]$. Because of the existence of the regular puncture, this is not isolated in the sense mentioned previously. When $n = 1$, the theory is trivial. By gauging the diagonal $SU(2)$ flavor symmetry coming from the two regular punctures of two $\mathcal{S}[A_1; \mathcal{D}_{\text{reg}}, \mathcal{D}_3]$'s, we obtain the pure $SU(2)$ SYM theory. When $n = 2$, the theory is just two free hypermultiplets. When $n > 2$, we have the nontrivial SCFT which is the maximal superconformal point of $SU(n - 1)$ gauge theory with two flavors [86]. Indeed, for $n > 2$ the quadratic differential has moduli, indicating that the theory is nontrivial. Note that these SCFTs have at least an $SU(2)$ flavor symmetry associated with the regular puncture.

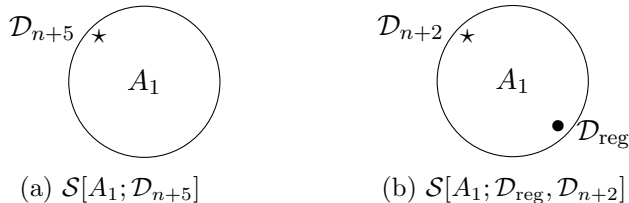


Figure 8.1: 4d SCFTs from 6d A_1 theory.

These two classes are the only possibilities which can be constructed in the A_1 theory on the sphere with the irregular puncture. We will elucidate how to obtain the BPS spectra of these two classes of SCFTs in Sections 8.2.1 and 8.3.1.

A_{N-1} case We then consider the higher rank theory $\mathcal{S}[A_{N-1}; \mathcal{D}]$. The 4d SCFTs of Argyres-Douglas type are again constructed by the compactification on the one-punctured sphere and on two-punctured sphere with one of them being regular. We will focus on the case with the regular puncture having an $SU(N)$ flavor symmetry. Let us denote this puncture as \mathcal{D}_{reg} .

There are various choices of the irregular puncture. Among them we will study the following three types of SCFTs in the subsequent sections. The first one is associated with the one-punctured sphere where the degree d_k of the pole of the differential ϕ_k is

$$(d_2, d_3, \dots, d_{N-1}, d_N) = (4, 6, \dots, 2N - 2, 2N + 2). \quad (8.3)$$

We will refer to this as \mathcal{D}_I . This type of SCFTs $\mathcal{S}[A_{N-1}; \mathcal{D}_I]$ can be obtained as the maximal conformal point of an $SU(N)$ pure SYM theory, as shown in Appendix C.1. Note

that we obtained $\mathcal{S}[A_1; \mathcal{D}_{N+4}]$ from the same 4d $\mathcal{N} = 2$ theory, so we propose that the two SCFTs are equivalent, though the constructions of these SCFTs are quite different. This equivalence was also proposed in [83].

The second type is associated with the one-punctured sphere with the following singularity

$$(d_2, d_3, \dots, d_{N-2}, d_{N-1}, d_N) = (4, 6, \dots, 2N - 4, 2N, 2N + 2), \quad (8.4)$$

which we will refer to as \mathcal{D}_{II} . This type of SCFTs, $\mathcal{S}[A_{N-1}; \mathcal{D}_{\text{II}}]$, can be obtained as the maximal conformal point of $\text{SU}(N)$ gauge theory with two flavors, as shown in Appendix C.2. Because we get $\mathcal{S}[A_1; \mathcal{D}_{\text{reg}}, \mathcal{D}_{N+3}]$ from the maximal conformal point of the same 4d theory, we propose that the two SCFTs are equivalent. Note that when $N = 3$, the singularity is $(d_2, d_3) = (6, 8)$.

The third type is the one associated with the sphere with one regular puncture and one irregular puncture. As an illustration of the inclusion of a regular puncture, here we consider only one example of SCFT from 6d A_2 theory with a regular puncture of the following singularity

$$(d_2, d_3) = (3, 5), \quad (8.5)$$

which we will denote as \mathcal{D}_{III} . We show in appendix C.3 that this is obtained from $\text{SU}(3)$ gauge theory with three flavors as the maximal superconformal point [89].

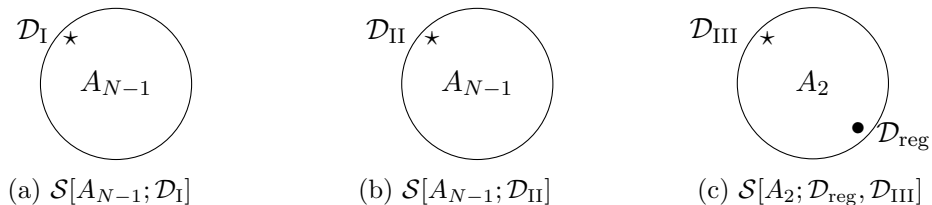


Figure 8.2: 4d SCFTs from 6d A_{N-1} theory.

The central charges and some properties of these SCFTs have been considered in [83, 94, 90], and the matching of the central charges of the SCFTs supports the proposed equivalences. Matching their BPS spectra provides more powerful evidence for the claims, and we will find the BPS spectra of these SCFTs in Sections 8.2.2, 8.3.2, and 8.3.3.

Equivalence classes of SCFTs One way to summarize the proposed equivalences of the SCFTs is to introduce a notion of equivalence classes of them. Because all the theories mentioned above that are proposed to flow to the same IR fixed point have the same minimal BPS spectrum, which in turn can be conveniently represented by a quiver based on a Dynkin diagram Γ , we will denote such an equivalence class of SCFTs as a Γ -class.

In Table 8.1 we summarized the SCFTs in the way that each row corresponds to SCFTs that are in the same class. Such theories have the same BPS spectrum and the same chamber structure. We also described in the table from which 4d $\mathcal{N} = 2$ gauge theories we can obtain the SCFT of each row.

Γ	6d A_1	6d A_{N-1}	UV 4d gauge theory
$A_{n=N-1}, N \geq 3$	$\mathcal{S}[A_1; \mathcal{D}_{n+5}]$	$\mathcal{S}[A_{N-1}; \mathcal{D}_I]$	pure $SU(N)$
$D_3 = A_3$	$\mathcal{S}[A_1; \mathcal{D}_8]$ $\mathcal{S}[A_1; \mathcal{D}_{\text{reg}}, \mathcal{D}_5]$	$\mathcal{S}[A_3; \mathcal{D}_I]$	$SU(2), N_f = 2$ (pure $SO(6)$) pure $SU(4)$
D_4	$\mathcal{S}[A_1; \mathcal{D}_{\text{reg}}, \mathcal{D}_6]$	$\mathcal{S}[A_2; \mathcal{D}_{II}]$ $\mathcal{S}[A_2; \mathcal{D}_{\text{reg}}, \mathcal{D}_{III}]$	$SU(3), N_f = 2$ (pure $SO(8)$) $SU(3), N_f = 3$
$D_{n=N+1}, N \geq 4$	$\mathcal{S}[A_1; \mathcal{D}_{\text{reg}}, \mathcal{D}_{n+2}]$	$\mathcal{S}[A_{N-1}; \mathcal{D}_{II}]$	$SU(N), N_f = 2$ (pure $SO(2N + 2)$)

Table 8.1: Various SCFTs from the 6d $(2, 0)$ A_1 and A_{N-1} theories in the same Γ -class.

8.1.2 Study of Argyres-Douglas fixed points via spectral networks

In Section 8.1.1 we have discussed which SCFTs from Argyres-Douglas fixed points we are interested in. Here we provide a schematic description of how to study the SCFTs using spectral networks.

The distances between branch points depend on the Coulomb branch parameters of the theory, and therefore the mass of the BPS states from finite \mathcal{S} -walls connecting those branch points vanish as we make the parameters to vanish. This could give the mutually nonlocal massless states required for an Argyres-Douglas fixed point. Therefore the limit of Coulomb branch parameters that results in the collisions of branch points are indications of interesting physics, especially for Seiberg-Witten theories from the 6d A_{N-1} $(2, 0)$ theory [15]. In general we have many complex parameters controlling the locations of the branch points, which in turn determine the shape of the Seiberg-Witten curve that is a multi-sheeted cover over a punctured Riemann surface. Studying BPS spectra when those parameters have

general values is an extensive, often practically impossible task. Instead, here we will pick a few choices of the parameters that are both physically interesting and practically less demanding.

First we maintain as much flavor symmetry as necessary. This makes mass parameters vanish and at the same time simplifies the analysis of spectral networks. When we maintain the maximal flavor symmetry it is easier to discuss an upper bound of the number of BPS states of the theory.

Next, to identify interesting points in the moduli space we consider the discriminant of the equation that describes the locations of the branch points on the t -plane. For a Seiberg-Witten curve $f(t, x; u_i)$, where u_i are Coulomb branch parameters, by eliminating x from the following equations

$$f(t, x) = 0, \quad \partial_t f(t, x) = 0, \quad (8.6)$$

we get a polynomial equation $g(t; u_i) = 0$, whose solutions are the locations of the branch points. Therefore the solutions of the discriminant of $g(t; u_i)$, $\Delta_t g(u_i)$, denotes the loci on the Coulomb branch where branch points collide. When we describe the Seiberg-Witten curve as a multi-sheeted cover, not all the choices correspond to singularities of the curve, however some of the choices can result in the collisions of the branch points that connect the same sheets, then it is exactly where we have the singularity of the curve and therefore it may result in a massless hypermultiplet. Even if a solution of the discriminant does not correspond to a singularity, it corresponds to having a branch point of higher ramification index, and as we have seen above it results in a more symmetric configuration of a spectral network which is easier to analyze.

8.2 4d SCFTs in A_n -class

8.2.1 $\mathcal{S}[A_1; \mathcal{D}_{n+5}]$ theories

Let us start studying the spectral networks of the $\mathcal{S}[A_1; \mathcal{D}_{n+5}]$ theories, which are in A_n -class. The Seiberg-Witten curve of (the deformation of) this theory is

$$x^2 = t^{n+1} + u_2 t^{n-1} + \cdots + u_{n+1}, \quad (8.7)$$

and the Seiberg-Witten differential is $\lambda = x dt$ which has one irregular puncture of degree $n + 5$ at $t = \infty$ and no regular puncture.

8.2.1.1 $\mathcal{S}[A_1; \mathcal{D}_7]$ in A_2 -class

The simplest theory is $\mathcal{S}[A_1; \mathcal{D}_7]$. This corresponds to the original example found in [4], and its spectral networks, which are studied in [19], are the building blocks of those of $n > 2$. The Seiberg-Witten curve is

$$x^2 = t^3 + c_2 t + v_2. \quad (8.8)$$

The parameters v_2 and c_2 are respectively the vev of the relevant deformation operator and its coupling constant with scaling dimensions $6/5$ and $4/5$. Thus v_2 is considered as the moduli of the theory. For a fixed value of c_2 , there is a single, closed BPS wall on the v_2 -plane encircling $v_2 = 0$ [19].

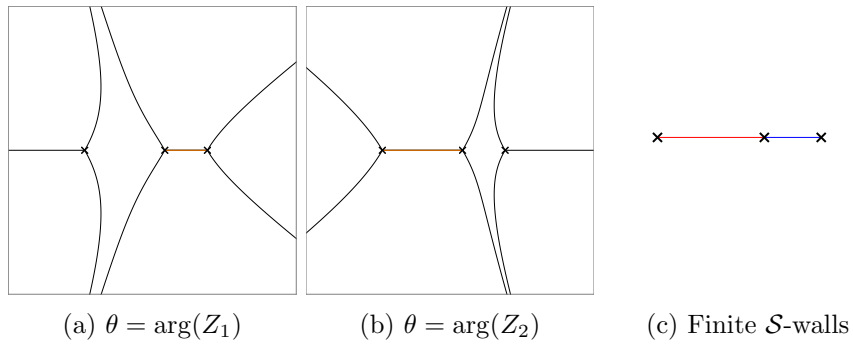


Figure 8.3: Spectral networks of $\mathcal{S}[A_1; \mathcal{D}_7]$ when the BPS spectrum is minimal.

Minimal BPS spectrum We first start inside the BPS wall, where the BPS spectrum is minimal. The spectral networks of $\mathcal{S}[A_1; \mathcal{D}_7]$ when c_2, v_2 are inside the BPS wall and when $\theta = \arg(Z_i)$ such that there is a finite \mathcal{S} -wall corresponding to a BPS state are shown in Figure 8.3. The animated version of Figure 8.3 can be found at [this website](#).

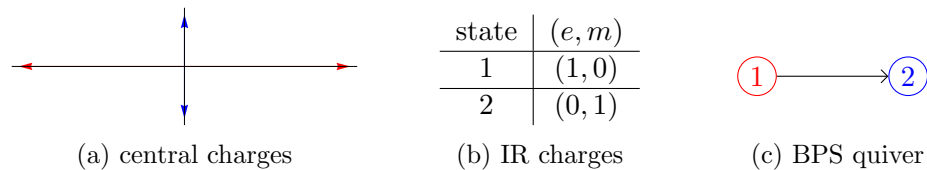


Figure and Table 8.4: Minimal BPS spectrum of $\mathcal{S}[A_1; \mathcal{D}_7]$.

To summarize the results from the spectral networks, let us collect the finite \mathcal{S} -walls and calculate the central charge of each BPS state from the corresponding finite \mathcal{S} -walls, which is shown in Figure 8.4a. One of the two \mathcal{S} -walls is an A-cycle of the Seiberg-Witten curve of $\mathcal{S}[A_1; \mathcal{D}_7]$, and the other is a B-cycle. Therefore the BPS spectrum of the theory has two BPS states, which is the minimal BPS spectrum of $\mathcal{S}[A_1; \mathcal{D}_7]$.

We can determine the low-energy U(1) charges of the BPS states from Figure 8.3 after picking up a suitable basis. If one chooses a branch cut along one of the finite \mathcal{S} -walls, say \mathcal{S}_1 , of Figure 8.3c, it is natural to define the cycle corresponding to that finite \mathcal{S} -wall as an A-cycle and the one corresponding to the other finite \mathcal{S} -wall, \mathcal{S}_2 , as a B-cycle. Their intersection number is $\langle \mathcal{S}_1, \mathcal{S}_2 \rangle = 1$ with a proper choice of orientations of the cycles, see Appendix 5.2.3 for the details. The IR charges of the BPS states are summarized in Table 8.4b and their anti-states have charges of opposite sign. Using the U(1) charges, this BPS spectrum can be represented with an A_2 quiver shown in Figure 8.4c, where the direction and the number of the heads of an arrow correspond to the inner product of the charges connected by the arrow.

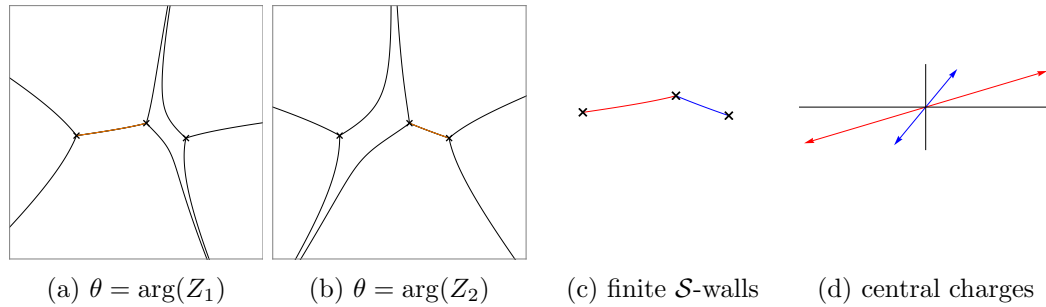


Figure 8.5: Spectral networks of $\mathcal{S}[A_1; \mathcal{D}_7]$ from different choices of parameters with minimal BPS spectrum. (c) and (d): finite \mathcal{S} -walls corresponding to two BPS states and their central charges.

When we deform v_2 a bit, as long as the parameters are inside the BPS wall, the number of BPS states does not change, which is shown in Figure 8.5. The animated version of Figure 8.5 can be found at [this website](#). Figure 8.5d describes the central charges of the BPS states. Now each BPS state has a different value of central charge from those in Figure 8.4a, however the U(1) charges are the same as shown in Table 8.4b and therefore the BPS spectrum is also represented by an A_2 quiver.

Maximal BPS spectrum When v_2 is further changed so that now the parameters are on the other side of the BPS wall, we observe a wall-crossing phenomenon of spectral networks [19] as shown in Figure 8.6, where we have an additional finite \mathcal{S} -wall. An animated version of the spectral network can be found at [this website](#).

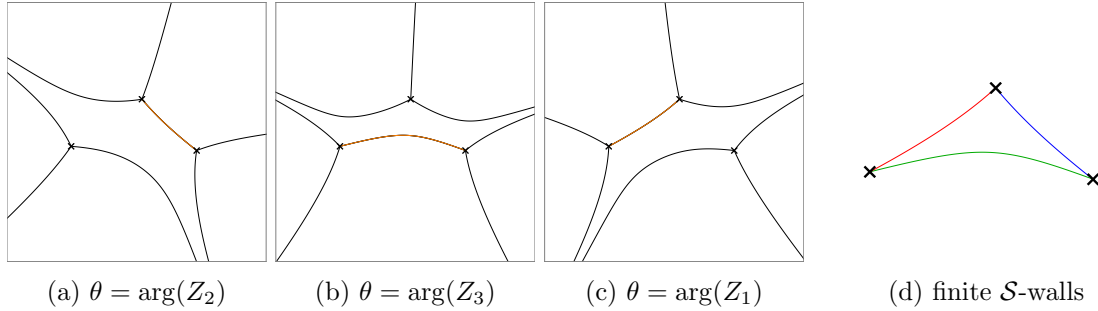


Figure 8.6: Spectral networks of $\mathcal{S}[A_1; D_7]$ with a maximal BPS spectrum.

The BPS spectrum of the theory after the wall-crossing is described in Figure 8.7a and Table 8.7b, where we have an additional BPS state from the third finite \mathcal{S} -wall. This is the maximal BPS spectrum of $\mathcal{S}[A_1; D_7]$.

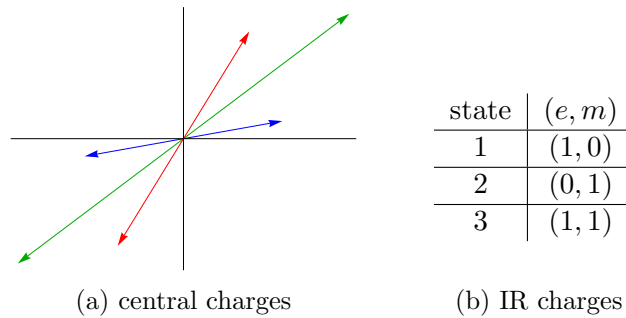
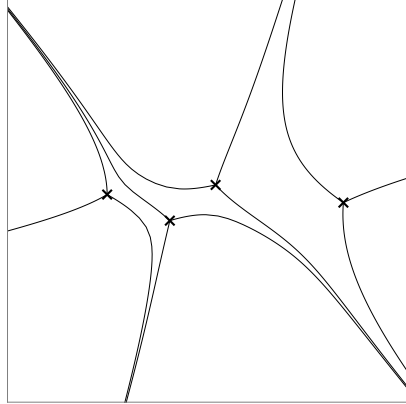


Figure and Table 8.7: Maximal BPS spectrum of $\mathcal{S}[A_1; D_7]$.

8.2.1.2 $\mathcal{S}[A_1; \mathcal{D}_{n+5}]$ in A_n -class, $n > 2$

Now we generalize the previous analysis to general n . The Seiberg-Witten curve of the $\mathcal{S}[A_1; \mathcal{D}_{n+5}]$ theory when $n = 2k$ is

$$x^2 = t^{2k+1} + c_2 t^{2k-1} + \cdots + c_{k+1} t^k + v_{k+1} t^{k-1} + \cdots + v_2 \quad (8.9)$$

Figure 8.8: A spectral network of $\mathcal{S}[A_1; \mathcal{D}_8]$.

with dimensions $\Delta(v_i) = 2 - \frac{2i}{2k+3}$ and $\Delta(c_i) = \frac{2i}{2k+3}$, and when $n = 2k - 1$ the Seiberg-Witten curve is

$$x^2 = t^{2k} + c_2 t^{2k-2} + \cdots + c_k t^k + c_{k+1} t^{k-1} + v_k t^{k-2} + \cdots + v_2 \quad (8.10)$$

with dimensions $\Delta(v_i) = 2 - \frac{i}{k+1}$, $\Delta(c_i) = \frac{i}{k+1}$, where $i = 2, \dots, k$, and $\Delta(c_{k+1}) = 1$. v_i and c_i ($i = 2, \dots, [n/2] + 1$) are the vevs of the relevant deformation operators and their couplings respectively. We can see that the Coulomb moduli space is $[n/2]$ -dimensional. When $n = 2k - 1$, λ has a nonzero residue at $t = \infty$, which is $\frac{1}{2}c_{k+1} + f(c_i)$, where $f(c_i)$ is a polynomial with $i \leq k$ and homogeneous of scaling dimension one [92].

Wall-crossing of $\mathcal{S}[A_1; \mathcal{D}_{n+5}]$ Studying the spectral networks of $\mathcal{S}[A_1; \mathcal{D}_8]$ gives us a good idea of the generalization to general $\mathcal{S}[A_1; \mathcal{D}_{n+5}]$. The Seiberg-Witten curve of $\mathcal{S}[A_1; \mathcal{D}_8]$ is

$$x^2 = t^4 + c_2 t^2 + c_3 t + v_2. \quad (8.11)$$

An example of its spectral network is shown in Figure 8.8. After analyzing the spectral networks for various values of the parameters, which is done in [19], we obtain the finite \mathcal{S} -walls and corresponding BPS spectra as shown in Figure 8.10.

The first row of Figure 8.10 shows finite \mathcal{S} -walls corresponding to three states in the BPS spectrum and the central charges of the states when the residue of λ at $x = \infty$ is not zero, i.e., $\frac{1}{2}c_3 + f(c_2) = \frac{1}{2}c_3 \neq 0$, where f is zero in this case. This is a minimal BPS spectrum of $\mathcal{S}[A_1; \mathcal{D}_8]$, but this does not have the $SU(2)$ flavor symmetry and we have three

BPS states of different central charges. This spectrum can be represented with a quiver diagram shown in Figure 8.9, which is based on an A_3 Dynkin diagram.



Figure 8.9: BPS quiver of the minimal BPS spectrum of $\mathcal{S}[A_1; \mathcal{D}_8]$.

As we change the value of v_2 while fixing c_i , we can observe three wall-crossings as shown in the bottom three rows of Figure 8.10. Each wall-crossing is similar to that of $\mathcal{S}[A_1; \mathcal{D}_7]$: each wall-crossing adds an additional BPS state to the spectrum, and at the end of the series of wall-crossings, we get the maximal BPS spectrum as shown in the last row of Figure 8.10, where we have a BPS state from an \mathcal{S} -wall connecting every pair of branch points as found in [54]. The IR gauge charges of the states in the maximal BPS spectrum is described in Table 8.2.

state	(e, m)
1	(1, 0)
2	(0, 1)
3	(1, 0)
4	(1, 1)
5	(1, 1)
6	(2, 1)

Table 8.2: IR charges of the BPS states in the BPS spectrum of $\mathcal{S}[A_1; \mathcal{D}_8]$.

We can generalize this to $n > 3$ using the fact that the spectral networks of $\mathcal{S}[A_1; \mathcal{D}_7]$ serve as the building blocks of those of $\mathcal{S}[A_1; \mathcal{D}_{n+5}]$. When $\mathcal{S}[A_1; \mathcal{D}_{n+5}]$ has a minimal BPS spectrum, its spectral network can be considered as a combination of $(n - 1)$ number of $\mathcal{S}[A_1; \mathcal{D}_7]$ spectral networks, where $(k - 1)$ -th, k -th, and $(k + 1)$ -th branch points of $\mathcal{S}[A_1; \mathcal{D}_{n+5}]$ are in the k -th building block. Starting from that configuration, the spectral network of $\mathcal{S}[A_1; \mathcal{D}_{n+5}]$ undergoes a series of the wall-crossing of $\mathcal{S}[A_1; \mathcal{D}_7]$ when the theory moves away from the minimal chamber in the Coulomb branch moduli space, at the end of which we get the maximal BPS spectrum having $\binom{n}{2}$ states.

Wall-crossing of $\mathcal{S}[A_1; \mathcal{D}_8]$ with an $SU(2)$ flavor symmetry Now let us consider the wall-crossing from the minimal BPS spectrum to the maximal one for $\mathcal{S}[A_1; \mathcal{D}_8]$ with the $SU(2)$ flavor symmetry, i.e., the residue of λ at $t = \infty$ vanishes: $c_3 = 0$. The first row of Figure 8.12 describes its BPS spectrum. Because of the vanishing residue, two of the

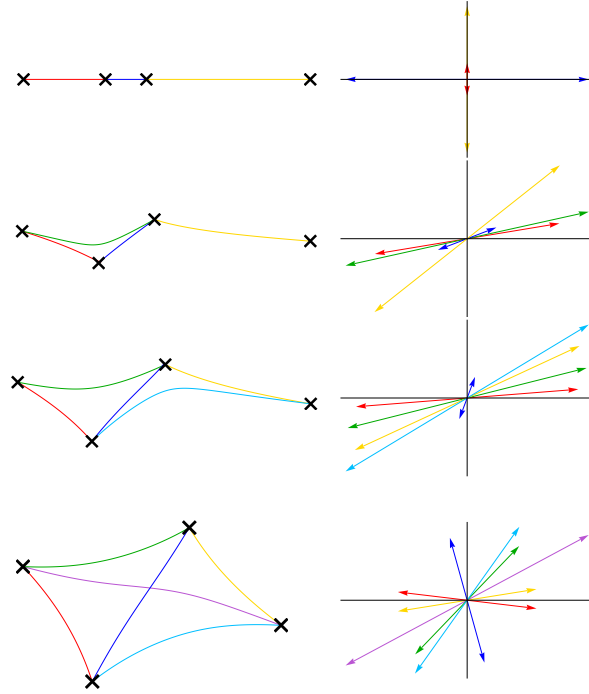


Figure 8.10: BPS spectra of $\mathcal{S}[A_1; \mathcal{D}_8]$ and their wall-crossings.

three BPS states form an $SU(2)$ doublet [92]: the two cycles of the Seiberg-Witten curve corresponding to the two red \mathcal{S} -walls are the same cycle when the residue vanishes. This is a minimal BPS spectrum of $\mathcal{S}[A_1; \mathcal{D}_8]$ with the $SU(2)$ flavor symmetry, which can be represented with a quiver of Figure 8.11.

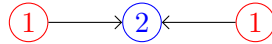


Figure 8.11: BPS quiver of the minimal BPS spectrum of $\mathcal{S}[A_1; \mathcal{D}_8]$ with an $SU(2)$ flavor symmetry. The left and the right nodes correspond to the BPS states forming the doublet of $SU(2)$.

Note that when c_3 vanishes, the Seiberg-Witten curve is $x^2 = t^4 + c_2 t^2 + v_2$, so for general values of c_2 and v_2 , we have four branch points where each pair is located symmetrically across $t = 0$. Because of the symmetry and the vanishing residue at $t = \infty$, we can see in Figure 8.12 that the three wall-crossings in Figure 8.10 happens now at the same time, after which we have three additional BPS states, two of them forming another doublet of the $SU(2)$ flavor symmetry. Note that maintaining the maximal flavor symmetry simplifies the analysis of wall-crossings of spectral networks: we have less number of free parameters, which constrains the motion of branch points and in the end we have one wall-crossing rather than three between the minimal and the maximal BPS spectrum. Figure 8.13 shows

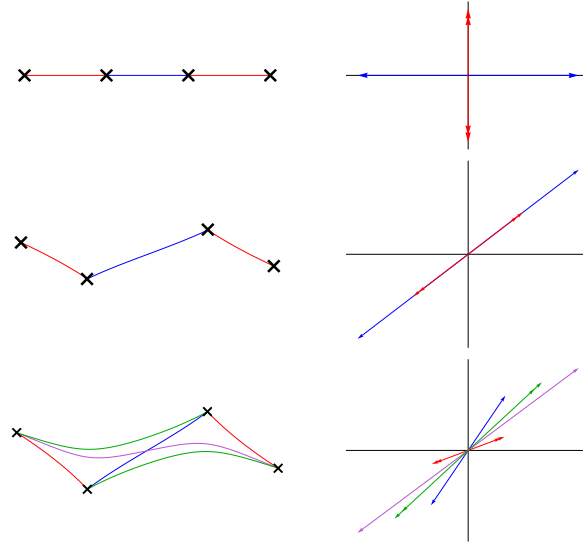


Figure 8.12: BPS spectra of $\mathcal{S}[A_1; \mathcal{D}_8]$ and their wall-crossings with an $SU(2)$ flavor symmetry.

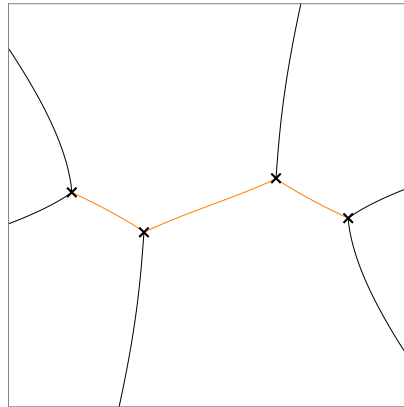


Figure 8.13: A spectral network of $\mathcal{S}[A_1; \mathcal{D}_8]$ with an $SU(2)$ flavor symmetry on the BPS wall.

the spectral network when the theory is on the BPS wall and θ has a value such that the finite \mathcal{S} -walls appear at the same time.

8.2.2 $\mathcal{S}[A_{N-1}; \mathcal{D}_1]$ theories

As we stated in section 8.1.1, this SCFT is obtained as the maximal conformal point of $SU(N)$ pure SYM theory. See appendix C.1 for the detailed derivation. We claim this SCFT is the same as $\mathcal{S}[A_1; \mathcal{D}_{N+4}]$.

The Seiberg-Witten curve of the SCFT is of canonical form $x^N + \sum_{i=2}^N \phi_i(t)x^{N-i} = 0$

where

$$\begin{aligned}\phi_i &= c_i, \quad (i = 2, \dots, [\frac{N+2}{2}]), \\ \phi_i &= v_{N-i+2}, \quad (i = [\frac{N+2}{2}] + 1, \dots, N-1), \quad \text{and} \quad \phi_N = t^2 + v_2,\end{aligned}\tag{8.12}$$

and the Seiberg-Witten differential is $\lambda = x dt$. The scaling dimensions are given by $\Delta(v_i) = 2 - \frac{2i}{N+2}$ and $\Delta(c_i) = \frac{2i}{N+2}$ for $i = 2, \dots, [\frac{N+1}{2}]$. When $N = 2k$, there is a mass parameter c_{k+1} with dimension 1. We can see that the dimensions of the operators are the same as those of $\mathcal{S}[A_1; \mathcal{D}_{N+4}]$.

We see that there is a singularity only at $t = \infty$ where the differentials ϕ_k have poles as described in (8.3). Note that from this curve we can obtain the curve of $\mathcal{S}[A_1; \mathcal{D}_{N+4}]$ by changing $t \rightarrow ix$ [37], which illustrates that this description boils down to how to project the complex one-dimensional curve living in a complex two-dimensional space onto a complex plane as either a 2-to-1 or an N -to-1 mapping. However, the Seiberg-Witten differentials for the two theories differ by an exact 1-form.

8.2.2.1 $\mathcal{S}[A_2; \mathcal{D}_I]$ in A_2 -class

The building blocks of the spectral networks of $\mathcal{S}[A_{N-1}; \mathcal{D}_I]$ are those of $\mathcal{S}[A_2; \mathcal{D}_I]$, which are studied in [37]. We will reproduce their result and provide a configuration of the spectral network that is useful in studying general N case. The Seiberg-Witten curve and the differential are

$$x^3 + c_2x + v_2 + t^2 = 0, \quad \lambda = x dt,\tag{8.13}$$

where $\Delta(c_2) = \frac{4}{5}$ and $\Delta(v_2) = \frac{6}{5}$.

Minimal BPS spectrum We first consider the case of $c_2 \neq 0$ and $v_2 = 0$, when the theory has a minimal BPS spectrum. This choice of parameters results in four branch points of index 2 at finite t and one branch point of index 3 at $t = \infty$, which is the location of the irregular puncture. A spectral network at a value of θ that contains a finite \mathcal{S} -wall is shown in Figure 8.14a. The animated version of the spectral network can be found at [this website](#). There will be another spectral network at $\pi - \theta$ that has the second finite \mathcal{S} -wall,

and both of the \mathcal{S} -walls are shown in Figures 8.14b.

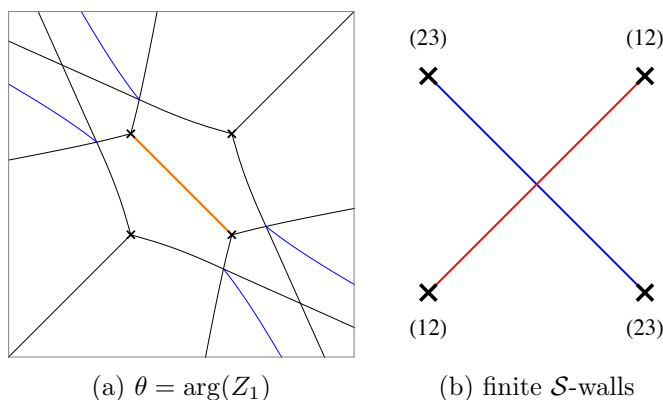


Figure 8.14: A spectral network of $\mathcal{S}[A_2; \mathcal{D}_1]$ with minimal BPS spectrum.

Figure 8.15a shows the central charges of the BPS states, and their low-energy $U(1)$ -charges are in Table 8.15b, which can be read out from the intersections of the cycles that are homologically equivalent to the \mathcal{S} -walls. This BPS spectrum can be represented by the BPS quiver shown in Figure 8.15c, which is an A_2 quiver. Note that this is exactly the same BPS spectrum as the minimal spectrum of $\mathcal{S}[A_1; \mathcal{D}_7]$, see Figure and Table 8.4.

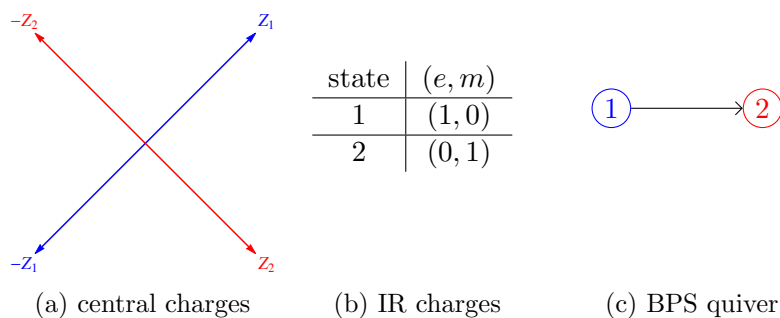
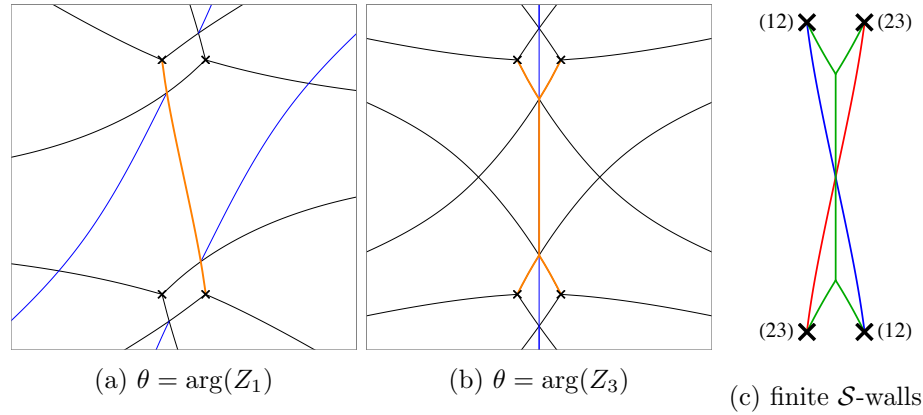


Figure and Table 8.15: Minimal BPS spectrum of $\mathcal{S}[A_2; \mathcal{D}_1]$.

Wall-crossing to a maximal BPS spectrum Now we fix c_2 and set v_2 to be nonzero. When v_2 is small, this deforms the previous configuration of spectral networks, but it does not cause a wall-crossing. After the value of v_2 is over a certain threshold, now the theory is on the other side of a BPS wall in the Coulomb branch moduli space.

Figure 8.16a shows a spectral network with a finite \mathcal{S} -wall that is similar to the one in Figure 8.14a. But in Figure 8.16b we have a finite \mathcal{S} -wall that appears only for A_{N-1} with $N > 2$ [37]. We can see there is a supersymmetric joint formed by three \mathcal{S} -walls, where $\lambda_{12} + \lambda_{23} = \lambda_{13}$ is satisfied. The animated version of Figure 8.16 can be found [at this](#)

Figure 8.16: Spectral networks of $\mathcal{S}[A_2; \mathcal{D}_1]$ with maximal BPS spectrum.

[webpage](#).

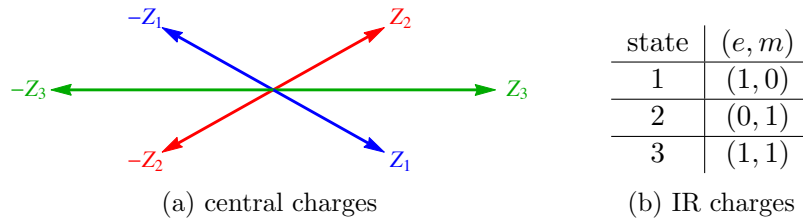
Figure and Table 8.17: Maximal BPS spectrum of $\mathcal{S}[A_2; \mathcal{D}_1]$.

Figure 8.16c shows the three finite \mathcal{S} -walls, and the central charges of the corresponding BPS states are shown in Figure 8.17a. When we compare it with Figure 8.15a, we see that Z_1 and Z_2 approach and cross over each other when the wall-crossing happens, resulting in the creation of Z_3 [37]. By considering the intersections of the cycles that are homologically equivalent to the finite \mathcal{S} -walls, we can find out the IR charges of the BPS states as in Table 8.17b. This maximal BPS spectrum is the same as that of $\mathcal{S}[A_1, \mathcal{D}_7]$, see Figure and Table 8.7.

Maximal, symmetric BPS spectrum We can collide two pairs of branch points of index 2 at finite values of t without causing a singularity, creating two branch points of index 3. This is obtained by setting $c_2 = 0$ and $v_3 \neq 0$, which gives us the maximal, symmetric BPS spectrum. Figure 8.18a shows a spectral network from the two branch points of index 3 when there is a finite \mathcal{S} -wall.

There are three finite \mathcal{S} -walls connecting the two (123) branch points for $0 \leq \theta < \pi$. The animated version of Figure 8.18a can be found [at this webpage](#). Figure 8.18b shows

the three finite \mathcal{S} -walls connecting the two branch points. Figure 8.19a and Table 8.19b describe the maximal symmetric BPS spectrum of $\mathcal{S}[A_2; \mathcal{D}_I]$, which can be identified with the symmetric maximal BPS spectrum of $\mathcal{S}[A_1; \mathcal{D}_7]$.

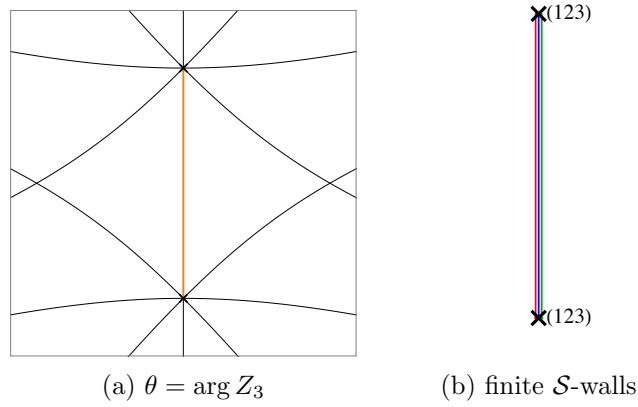
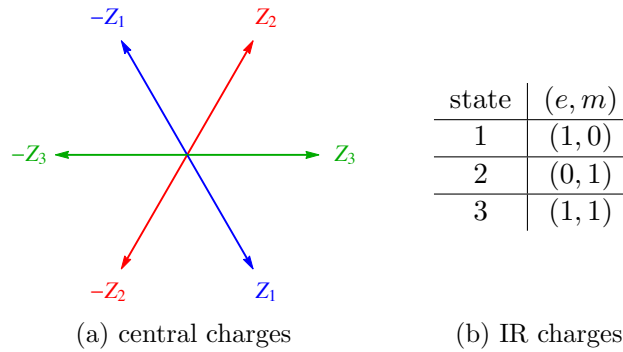


Figure 8.18: A spectral network of $\mathcal{S}[A_2; \mathcal{D}_I]$ with maximal, symmetric BPS spectrum.



state	(e, m)
1	(1, 0)
2	(0, 1)
3	(1, 1)

Figure and Table 8.19: Maximal, symmetric BPS spectrum of $\mathcal{S}[A_2; \mathcal{D}_I]$.

8.2.2.2 $\mathcal{S}[A_{N-1}; \mathcal{D}_I]$ in A_{N-1} -class, $N > 3$

Now we generalize the previous analysis to $\mathcal{S}[A_{N-1}; \mathcal{D}_I]$. We will compare its spectral networks with those of $\mathcal{S}[A_1; \mathcal{D}_{N+4}]$ to see that both SCFTs have the same minimal and maximal BPS spectra, and check for an example that the two theories have the same BPS chamber structure, which we expect to hold for general N and is therefore good evidence that both theories are in A_{N-1} -class.

Minimal BPS spectrum For general values of parameters, the Seiberg-Witten curve of $\mathcal{S}[A_{N-1}; \mathcal{D}_I]$ has $2(N-1)$ branch points of index 2 at finite t . In addition to that, when N

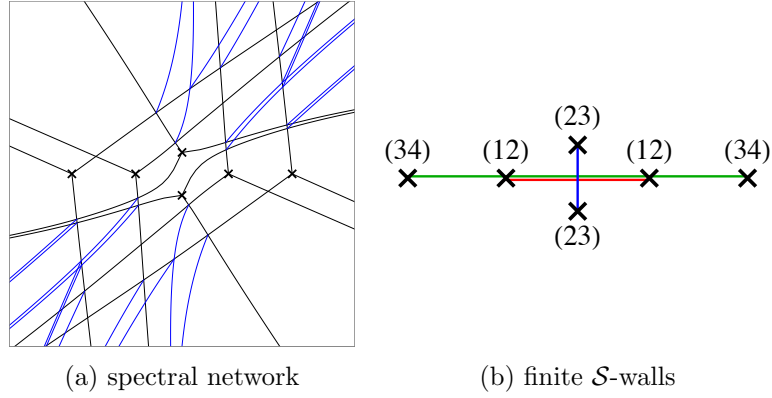


Figure 8.20: A spectral network of $\mathcal{S}[A_3; \mathcal{D}_I]$ with minimal BPS spectrum.

is odd, there is a branch point of index N at $t = \infty$, and by applying the Riemann-Hurwitz formula we get the genus of the Seiberg-Witten curve $g = (N - 1)/2$. When N is even, there are two branch points of index $N/2$ at $t = \infty$, and the genus of the Seiberg-Witten curve is $g = N/2 - 1$. We choose a branch cut between every branch point of finite t and the irregular puncture at $t = \infty$.

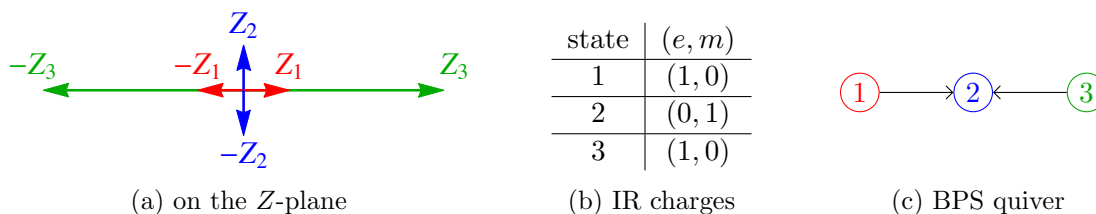
Having these configurations in mind, we can understand that when the theory has a minimal BPS spectrum, the configuration of its spectral networks has the branch points at finite t being aligned along two perpendicular lines. There is a finite \mathcal{S} -wall for every pair of branch points of the same kind, and none between the branch points of different kinds. This gives us the BPS spectrum that can be represented as an A_{N-1} quiver diagram.

The case of $N = 4$ is a useful example to understand the generalization. Its Seiberg-Witten curve is

$$x^4 + c_2 x^2 + mx + v_2 + t^2 = 0, \quad (8.14)$$

where $\Delta(c_2) = \frac{2}{3}$, $\Delta(m) = 1$, $\Delta(v_2) = \frac{4}{3}$. m is a mass parameter, and when it is zero we expect an $SU(2)$ doublet to appear. Figure 8.20a shows a spectral network at a general value of θ and Figure 8.20b shows finite \mathcal{S} -walls of $\mathcal{S}[A_3; \mathcal{D}_I]$ when it has a minimal BPS spectrum and when $m \neq 0$. When $m = 0$, (12)- and (34)-branch points are at the same location, resulting in an $SU(2)$ doublet of two finite \mathcal{S} -walls.

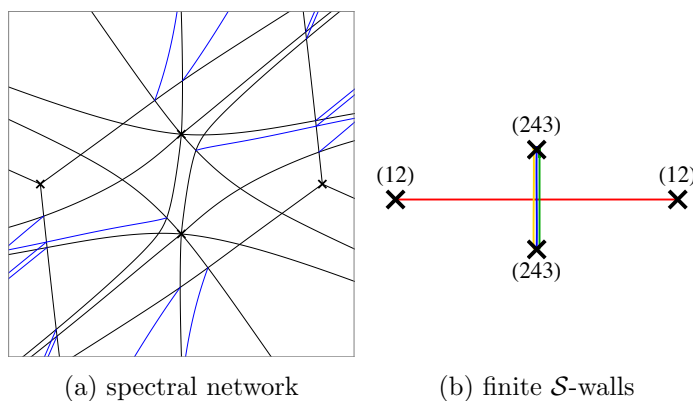
Figure 8.21a describes the central charges of the states in the minimal BPS spectrum of $\mathcal{S}[A_3; \mathcal{D}_I]$ when $m \neq 0$. When $m = 0$, we have an $SU(2)$ doublet with $Z_1 = Z_3$. Table 8.21b describes the IR $U(1)$ -charges of the states, from which we can construct a BPS quiver as

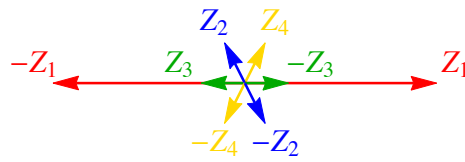
Figure and Table 8.21: Minimal BPS spectrum of $\mathcal{S}[A_3; \mathcal{D}_I]$.

shown in Figure 8.21c. This is the same BPS spectrum as the minimal BPS spectrum of $\mathcal{S}[A_1; \mathcal{D}_8]$, see Figures 8.9 and 8.10.

Wall-crossing to the maximal symmetric BPS spectrum From the minimal BPS spectrum of $\mathcal{S}[A_{N-1}; \mathcal{D}_I]$, when its parameters have general nonzero values, it undergoes one wall-crossing of $\mathcal{S}[A_2; \mathcal{D}_I]$ after another to reach the maximal BPS spectrum, where each wall-crossing adds a BPS state in the spectrum. Remember that each wall-crossing of $\mathcal{S}[A_1; \mathcal{D}_{N+4}]$ is that of $\mathcal{S}[A_1; \mathcal{D}_7]$, and from the minimal BPS spectrum after a series of such wall-crossings $\mathcal{S}[A_1; \mathcal{D}_{N+4}]$ reaches the chamber of the maximal BPS spectrum. This matching of both the BPS spectrum and its wall-crossings from the minimal chamber to the maximal one is good evidence for the equivalence of $\mathcal{S}[A_{N-1}; \mathcal{D}_I]$ and $\mathcal{S}[A_1; \mathcal{D}_{N+4}]$.

We illustrate this procedure with the example of $\mathcal{S}[A_3; \mathcal{D}_I]$. Starting from the configuration of Figure 8.20, we change the parameters such that two pairs of branch points of index 2 collide with each other to form two branch points of index 3 as shown in Figure 8.22. During the change we cross a BPS wall in the Coulomb branch moduli space, adding a BPS state in the spectrum.

Figure 8.22: A spectral network of $\mathcal{S}[A_3; \mathcal{D}_I]$ after one wall-crossing from the minimal BPS spectrum.



(a) central charges

state	(e, m)
1	$(1, 0)$
2	$(0, 1)$
3	$(1, 0)$
4	$(1, 1)$

(b) IR charges

Figure and Table 8.23: Next-to-minimal BPS spectrum of $\mathcal{S}[A_3; \mathcal{D}_1]$.

When we compare Figure 8.23a with Figure 8.21a, we see that as we collide the two branch points, Z_3 move across Z_2 when the BPS spectrum gains a BPS state with charge Z_4 . Analyzing the intersections of the cycles corresponding to the finite \mathcal{S} -walls shown in Figure 8.22b gives the IR charges of the BPS states in Table 8.23b. When we collide the two pairs of two branch points of different kinds, the BPS spectrum undergoes two additional wall-crossings, becoming a maximal symmetric BPS spectrum that we will see below.

Note that if we keep $m = 0$ throughout the whole process, then Z_1 and Z_3 should move on the Z -plane together because they form an $SU(2)$ doublet, and the wall-crossing from the minimal to the maximal BPS spectrum happens at once as the BPS spectrum of $\mathcal{S}[A_1; \mathcal{D}_8]$ with an $SU(2)$ flavor symmetry does, see Figure 8.12.

Maximal, symmetric BPS spectrum When $v_2 \neq 0$ and the other parameters are zero, a spectral network of $\mathcal{S}[A_{N-1}; \mathcal{D}_1]$ has two branch points of index N . It results in the maximal symmetric BPS spectrum that contains $2 \times \binom{N}{2} = N(N-1)$ states, including anti-states having $\pi \leq \arg(Z) \leq 2\pi$. Thanks to the symmetric configuration, the central charges of the BPS states can be identified with the projections of root vectors connecting every pair of weights of the fundamental representation of A_{N-1} in the weight space onto the Z -plane [30]. The maximal symmetric BPS spectrum of $\mathcal{S}[A_1; \mathcal{D}_{N+4}]$ has the same structure: the corresponding spectral network comes from a symmetric configuration of its branch points that form vertices of an N -polygon, and there is a finite \mathcal{S} -wall between every pair of the branch points.

Figure 8.24 shows spectral networks of $\mathcal{S}[A_3, \mathcal{C}; \mathcal{D}_1]$. Note that there is a value of θ that two \mathcal{S} -walls appear at the same time, corresponding to the $SU(2)$ doublet, as shown in Figure 8.24a. Although the two \mathcal{S} -walls are projected onto the same location on the t -plane, they are two distinct \mathcal{S} -walls. There are two values of θ between 0 and π that a doublet appears, and at the other two values of θ only a single finite \mathcal{S} -wall appears, thereby giving

6 BPS states and 6 anti-states.

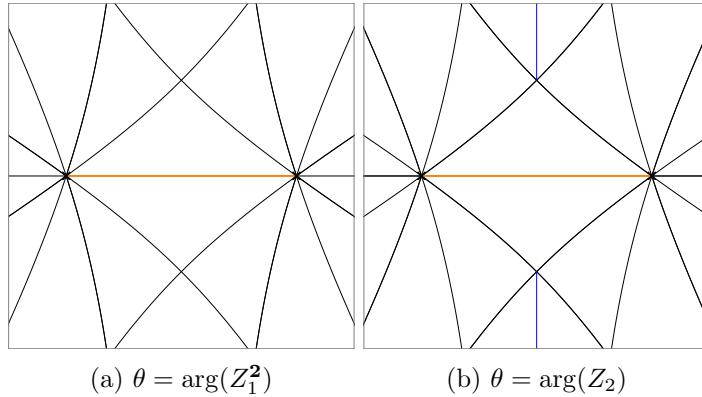


Figure 8.24: Spectral networks of $\mathcal{S}[A_3; \mathcal{D}_I]$ with maximal BPS spectrum.

Figure 8.25a and Table 8.25b describe the maximal symmetric BPS spectrum of $\mathcal{S}[A_3; \mathcal{D}_I]$, which can be identified with that of $\mathcal{S}[A_{N-1}; \mathcal{D}_8]$, see Figure 8.12 and Table 8.2.

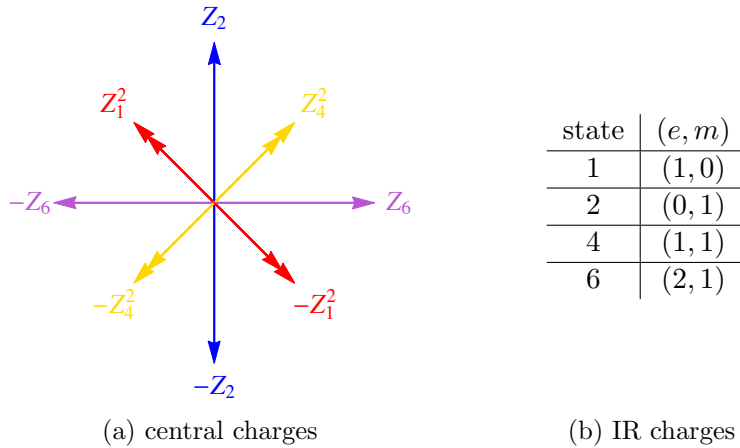


Figure and Table 8.25: Maximal, symmetric BPS spectrum of $\mathcal{S}[A_3, \mathcal{C}; \mathcal{D}_I]$

8.3 4d SCFTs in D_n -class

8.3.1 $\mathcal{S}[A_1; \mathcal{D}_{\text{reg}}, \mathcal{D}_{n+2}]$ theories

Let us next consider the SCFTs obtained from the A_1 theory on a sphere with the irregular puncture \mathcal{D}_{n+2} and the regular puncture \mathcal{D}_{reg} . This class of SCFTs $\mathcal{S}[A_1; \mathcal{D}_{\text{reg}}, \mathcal{D}_{n+2}]$ differs from $\mathcal{S}[A_1; \mathcal{D}_{n+5}]$ in that there is one regular puncture with a mass parameter. The Seiberg-

Witten curve is given by

$$v^2 = t^n + \sum_{i=1}^{n-1} s_{2i} t^{n-i} + m^2, \quad (8.15)$$

and the Seiberg-Witten differential $\lambda = \frac{v}{t} dt$, which has one regular puncture at $t = 0$ and one irregular puncture at $t = \infty$. The dimensions of the parameters are obtained as $\Delta(s_{2i}) = \frac{2i}{n}$. The parameter m with dimension one is associated with the global $SU(2)$ symmetry which is a subgroup of the full flavor symmetry.

8.3.1.1 $\mathcal{S}[A_1; \mathcal{D}_{\text{reg}}, \mathcal{D}_5]$ in D_3 -class

Let us first study the simplest example $\mathcal{S}[A_1; \mathcal{D}_{\text{reg}}, \mathcal{D}_5]$, whose Seiberg-Witten curve is

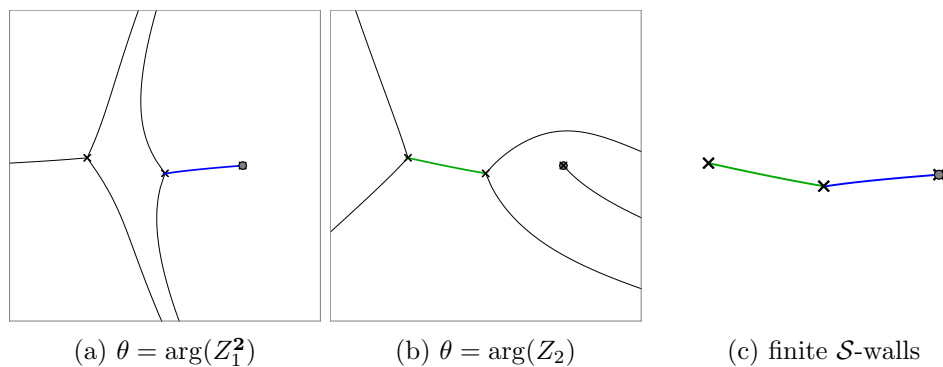
$$v^2 = t^3 + c_1 t^2 + v_1 t + m^2, \quad (8.16)$$

where we denoted the parameters as v_1 and c_1 in order to emphasize that v_1 is the vev of the relevant operator and c_1 is its coupling.

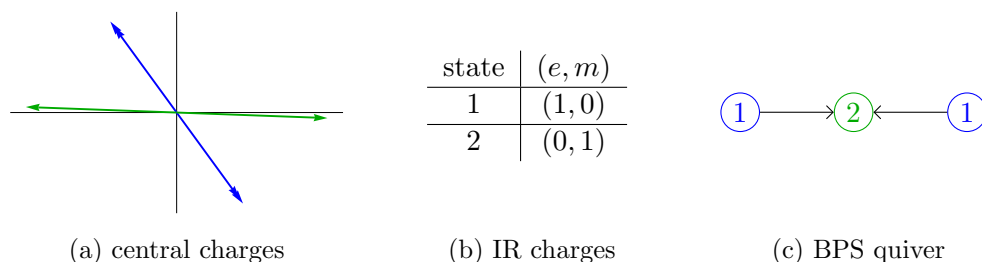
Here we describe how spectral networks can be used to show that $\mathcal{S}[A_1; \mathcal{D}_{\text{reg}}, \mathcal{D}_5]$ is in the same D_3 -class (= A_3 -class) as $\mathcal{S}[A_1; \mathcal{D}_8]$ and $\mathcal{S}[A_3; \mathcal{D}_1]$ are. We will see here in particular that when the three theories have the $SU(2)$ flavor symmetry they have the same BPS spectrum. However, the way that the $SU(2)$ doublet of $\mathcal{S}[A_1; \mathcal{D}_{\text{reg}}, \mathcal{D}_5]$ appears is different from the other two theories due to the existence of a regular puncture.

Minimal BPS spectrum When the parameters, c_1 , v_1 and m , have general values there are three branch points on the t -plane. When we take $m \rightarrow 0$, one of the three branch points now collides with the regular puncture at $t = 0$, as we discussed in Section 5.1.3, resulting in the spectral network shown in Figure 8.26, where we have a doublet of \mathcal{S} -walls from the branch point on the puncture along the same direction reaching another branch point (Figure 8.26a). For a different value of θ there is another \mathcal{S} -wall, now a singlet, connecting two branch points that are not on the puncture (Figure 8.26b).

From the finite \mathcal{S} -walls we get the corresponding BPS states. Figure 8.27a describes their central charges, where we denote a doublet as a double-headed arrow. Table 8.27b shows the IR $U(1)$ -charges of the states. This is a minimal BPS spectrum of $\mathcal{S}[A_1; \mathcal{D}_{\text{reg}}, \mathcal{D}_5]$,

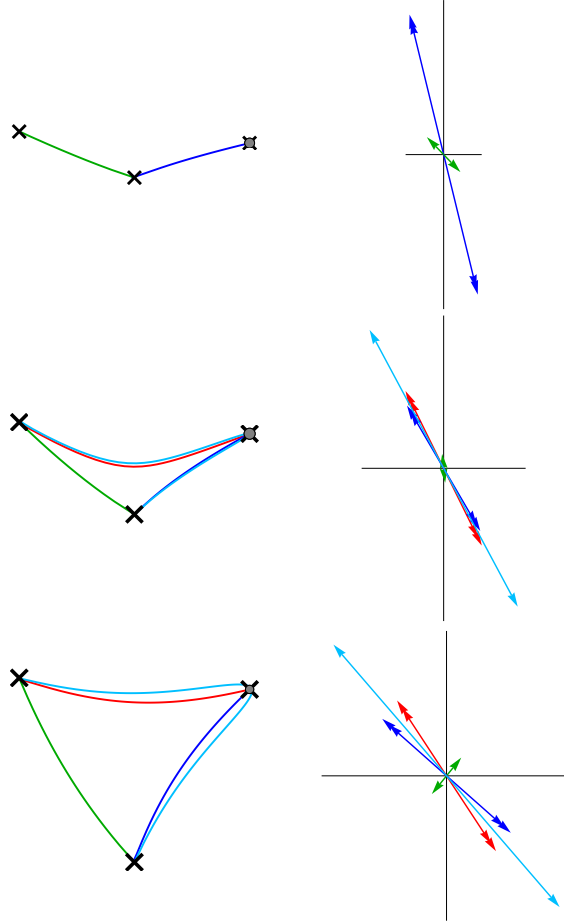
Figure 8.26: Spectral networks of $\mathcal{S}[A_1; \mathcal{D}_{\text{reg}}, \mathcal{D}_5]$ with minimal BPS spectrum.

which is represented by a $D_3 = A_3$ quiver shown in Figure 8.27c. In fact it is the same as the minimal BPS spectrum of A_3 -class theories with the $SU(2)$ flavor symmetry. For example, see Figure 8.11 and the first row of Figure 8.12 that illustrate the minimal BPS spectrum of $\mathcal{S}[A_1; \mathcal{D}_8]$.

Figure and Table 8.27: Minimal BPS spectrum of $\mathcal{S}[A_1; \mathcal{D}_{\text{reg}}, \mathcal{D}_5]$.

Wall-crossing to the maximal BPS spectrum Next we consider the wall-crossing of the BPS spectra of $\mathcal{S}[A_1; \mathcal{D}_{\text{reg}}, \mathcal{D}_5]$. This wall-crossing mechanism, in combination with that of $\mathcal{S}[A_1; \mathcal{D}_7]$, will form building blocks for the wall-crossings of $\mathcal{S}[A_1; \mathcal{D}_{\text{reg}}, \mathcal{D}_{n+2}]$. Figure 8.28 shows how a wall-crossing happens in $\mathcal{S}[A_1; \mathcal{D}_{\text{reg}}, \mathcal{D}_5]$ with the $SU(2)$ flavor symmetry as we move one of the branch points that is not on the puncture.

The second row of Figure 8.28 shows the finite \mathcal{S} -walls and the central charges of the corresponding BPS states right after a wall-crossing happens. Again it happens when the central charges of two BPS states move across each other on the Z -plane, see the first two rows of Figure 8.28, which show the central charge of a singlet BPS state going over that of the doublet. And similarly to the wall-crossing of $\mathcal{S}[A_1; \mathcal{D}_{n+5}]$ with the $SU(2)$ flavor symmetry, which is shown in Figure 8.12, when the wall-crossing happens we have another

Figure 8.28: Wall-crossing of $\mathcal{S}[A_1; \mathcal{D}_{\text{reg}}, \mathcal{D}_5]$.

doublet and an additional BPS state whose central charge is the sum of the central charges of two states from each doublet.

state	(e, m)
1	$(1, 0)$
2	$(0, 1)$
3	$(1, 1)$
4	$(2, 1)$

Table 8.3: IR charges of the states in the maximal BPS spectrum of $\mathcal{S}[A_1; \mathcal{D}_{\text{reg}}, \mathcal{D}_5]$.

To understand the wall-crossing involving a doublet, it is helpful to introduce an infinitesimal value of the mass parameter m to resolve each doublet into two states with infinitesimal difference in their central charges, as shown in Figure 8.29, where a series of three usual wall-crossings are illustrated. When $m \rightarrow 0$, the three wall-crossings happen at the same time, leading to the new wall-crossing phenomena shown in Figure 8.28.

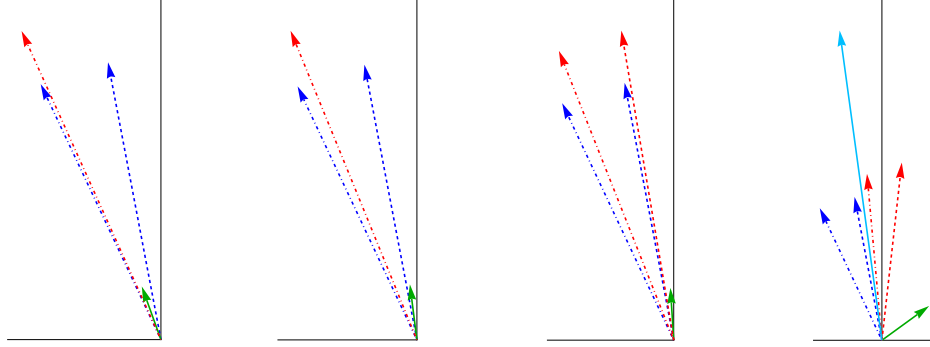


Figure 8.29: Wall-crossing of a doublet and a singlet.

The last row of Figure 8.28 shows the maximal BPS spectrum of $\mathcal{S}[A_1; \mathcal{D}_{\text{reg}}, \mathcal{D}_5]$ with the $SU(2)$ flavor symmetry, which consists of six BPS states with two doublets. This is the same as that of $\mathcal{S}[A_1; \mathcal{D}_8]$ with vanishing residue at infinity, see the last row of Figure 8.12.

Equivalence of $\mathcal{S}[A_1; \mathcal{D}_{\text{reg}}, \mathcal{D}_5]$ and $\mathcal{S}[A_1; \mathcal{D}_8]$ We have seen that the analysis of BPS spectra of $\mathcal{S}[A_1; \mathcal{D}_{\text{reg}}, \mathcal{D}_5]$ and $\mathcal{S}[A_1; \mathcal{D}_8]$ via spectral networks provides good evidence for the equivalence of the two SCFTs. Another piece of evidence comes from comparing the central charges of the SCFTs, which are $a = \frac{11}{24}$ and $c = \frac{1}{2}$. The central charge of $\mathcal{S}[A_1; \mathcal{D}_8]$ was computed in [54], see eq. (4.31) with $r = 1$. The central charge of the $\mathcal{S}[A_1; \mathcal{D}_{\text{reg}}, \mathcal{D}_5]$ theory was computed in some papers, e.g. [94], see $I_{2,1,F}$ in Table 3.

Actually, we can show the SCFTs have the same Seiberg-Witten curves when both of them have the $SU(2)$ flavor symmetry. Let us start with the curve of $\mathcal{S}[A_1; \mathcal{D}_8]$ with $c_3 = 0$,

$$x^2 = t^4 + c_2 t^2 + v_2, \quad (8.17)$$

where $\lambda = x dt$. Now we change variables: first we take $t \rightarrow \sqrt{\tilde{t}}$,

$$\lambda = x dt = \frac{1}{2} \sqrt{\tilde{t} + c_2 + \frac{v_2}{\tilde{t}}} d\tilde{t} = \tilde{x} d\tilde{t}, \quad (8.18)$$

and then define $v = \tilde{t}\tilde{x}$, after which we have $\lambda = (v/\tilde{t}) d\tilde{t}$ and

$$v^2 = \tilde{t}^3 + c_2 \tilde{t}^2 + v_2 \tilde{t}. \quad (8.19)$$

These are equivalent to the Seiberg-Witten differential and curve of $\mathcal{S}[A_1; \mathcal{D}_{\text{reg}}, \mathcal{D}_5]$. Therefore we expect the two theories to be fully equivalent.

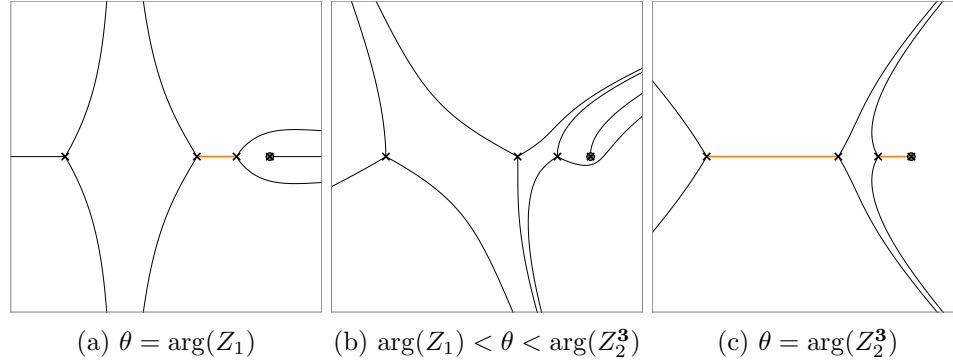


Figure 8.30: Spectral networks of $\mathcal{S}[A_1; \mathcal{D}_{\text{reg}}, \mathcal{D}_6]$ with an $SU(3)$ flavor symmetry and minimal BPS spectrum.

8.3.1.2 $\mathcal{S}[A_1; \mathcal{D}_{\text{reg}}, \mathcal{D}_6]$ in D_4 -class

The Seiberg-Witten curve of $\mathcal{S}[A_1; \mathcal{D}_{\text{reg}}, \mathcal{D}_6]$ is

$$v^2 = t^4 + c_1 t^3 + c_2 t^2 + v_1 t + m^2. \quad (8.20)$$

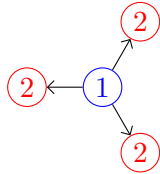
The residue of the Seiberg-Witten differential $\lambda = \frac{v}{t} dt$ at $t = \infty$ is $\frac{1}{8}(c_1^2 - 4c_2)$, which is associated with a $U(1)$ flavor symmetry. As in the previous case, the parameter m , which is the residue of the regular puncture at $x = 0$, is associated with an $SU(2)$ flavor symmetry. When both mass parameters vanish, we expect to have an enhanced $SU(3)$ flavor symmetry [92], which we will confirm here from the analysis of spectral networks. When only $m = 0$ but the residue of λ at $t = \infty$ is nonzero, it serves as a good stepping stone to understand the cases of general n , as we will see later.

Minimal BPS spectrum of $\mathcal{S}[A_1; \mathcal{D}_{\text{reg}}, \mathcal{D}_6]$ with an $SU(3)$ flavor symmetry When we set both $m = 0$ and $c_1^2 = 4c_2$ and set $v_1 = c_1^3/54 - \delta$, where δ is a small number, $\mathcal{S}[A_1; \mathcal{D}_{\text{reg}}, \mathcal{D}_6]$ has a spectral network shown in Figure 8.30. There are three BPS states of the same central charge Z_2^3 , which is represented as a three-headed arrow in the first row of Figure 8.32. This shows that when both the mass parameters vanish we indeed have an $SU(3)$ flavor symmetry, and that there is a triplet of the $SU(3)$.

We can determine the IR charges of BPS states from Figure 8.30 after picking up a suitable basis. If one chooses the two cuts along the triplet \mathcal{S} -walls at $\theta = \arg(Z_2^3)$ of the minimal spectrum in Figure 8.30c, we define the cycle corresponding to the singlet finite \mathcal{S} -wall at $\theta = \arg(Z_1)$, say \mathcal{S}_1 , as an A-cycle and one of the triplet finite \mathcal{S} -walls at

$\theta = \arg(Z_2^3)$, say \mathcal{S}_2 , as a B-cycle. Their intersection number is $\langle \mathcal{S}_1, \mathcal{S}_2 \rangle = 1$ with a proper choice of orientations of the cycles, and from this we get the IR charges as described in Table 8.31a. This BPS spectrum can be represented by a D_4 quiver as shown in Figure 8.31b.

state	(e, m)
1	$(1, 0)$
2	$(0, 1)$



(a) IR charges
(b) BPS quiver

Figure 8.31: Minimal BPS spectrum of $\mathcal{S}[A_1; \mathcal{D}_{\text{reg}}, \mathcal{D}_6]$ with an $SU(3)$ flavor symmetry.

Wall-crossing of $\mathcal{S}[A_1; \mathcal{D}_{\text{reg}}, \mathcal{D}_6]$ with an $SU(3)$ flavor symmetry When we maintain the maximal flavor symmetry of $\mathcal{S}[A_1; \mathcal{D}_{\text{reg}}, \mathcal{D}_6]$ during the wall-crossing, we observe that the BPS spectrum jumps from the minimal to the maximal one at once. Figure 8.32 illustrates such a wall-crossing.

When $\delta \rightarrow 0$, the singlet becomes massless and the BPS spectrum jump from the minimal one to the maximal one at once, and the result is as shown in the second row of 8.32, where now $v_1 = c_1^3/54 + \delta$. The last row of Figure 8.32 shows the case of $c_1 = c_2 = m = 0$ and $v_1 \neq 0$, which has the $SU(3)$ flavor symmetry and also symmetric arrangement of branch points and therefore a symmetric BPS spectrum. Under the same basis the charges of BPS states as we found to get Table 8.31a, states in the maximal BPS spectrum has IR charges as described in Table 8.4.

state	(e, m)
1	$(1, 0)$
2	$(0, 1)$
3	$(1, 3)$
4	$(1, 2)$
5	$(2, 3)$
6	$(1, 1)$

Table 8.4: IR charges of the states in the maximal BPS spectrum of $\mathcal{S}[A_1; \mathcal{D}_{\text{reg}}, \mathcal{D}_6]$ with an $SU(3)$ flavor symmetry.

Figure 8.33 provides an explanation of such a wall-crossing by resolving the triplet into three BPS states and considering a series of usual wall-crossings between a singlet and a

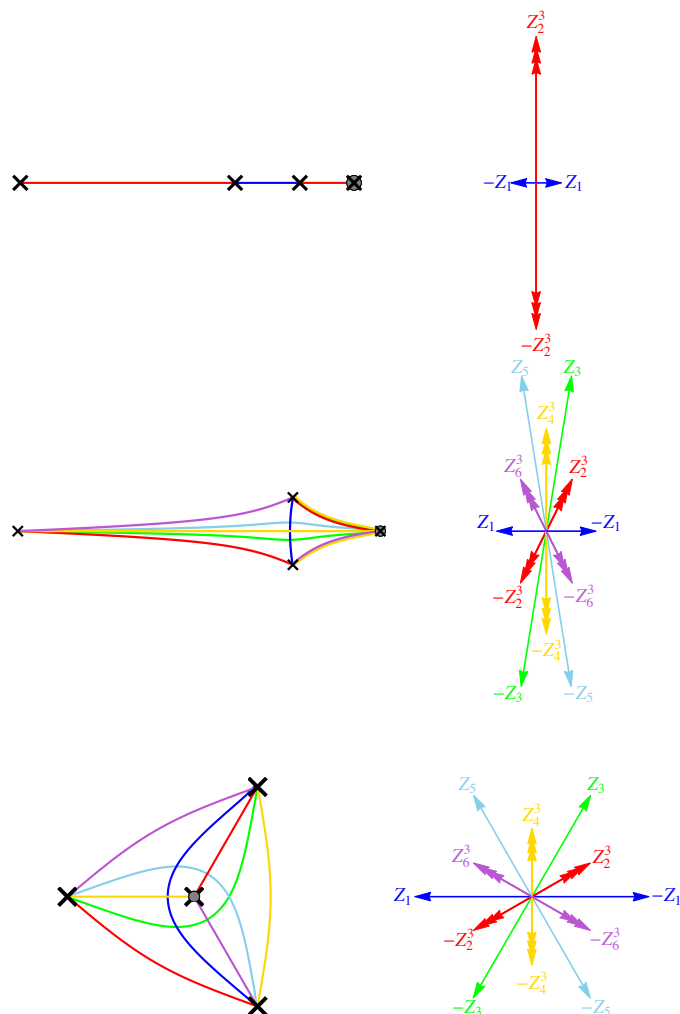


Figure 8.32: Wall-crossing of $\mathcal{S}[A_1; \mathcal{D}_{\text{reg}}, \mathcal{D}_6]$ with an $SU(3)$ flavor symmetry.

triplet, as we have resolved the doublet of $\mathcal{S}[A_1; \mathcal{D}_{\text{reg}}, \mathcal{D}_5]$ to understand the wall-crossing of its BPS spectrum, see Figure 8.29. In the limit of the three resolved BPS states becoming a triplet, these eight wall-crossings happen at the same time, resulting in two additional triplets and two additional singlets. We can also see that the structures of the triplets and the singlets suit well with what we have in Figure 8.32.

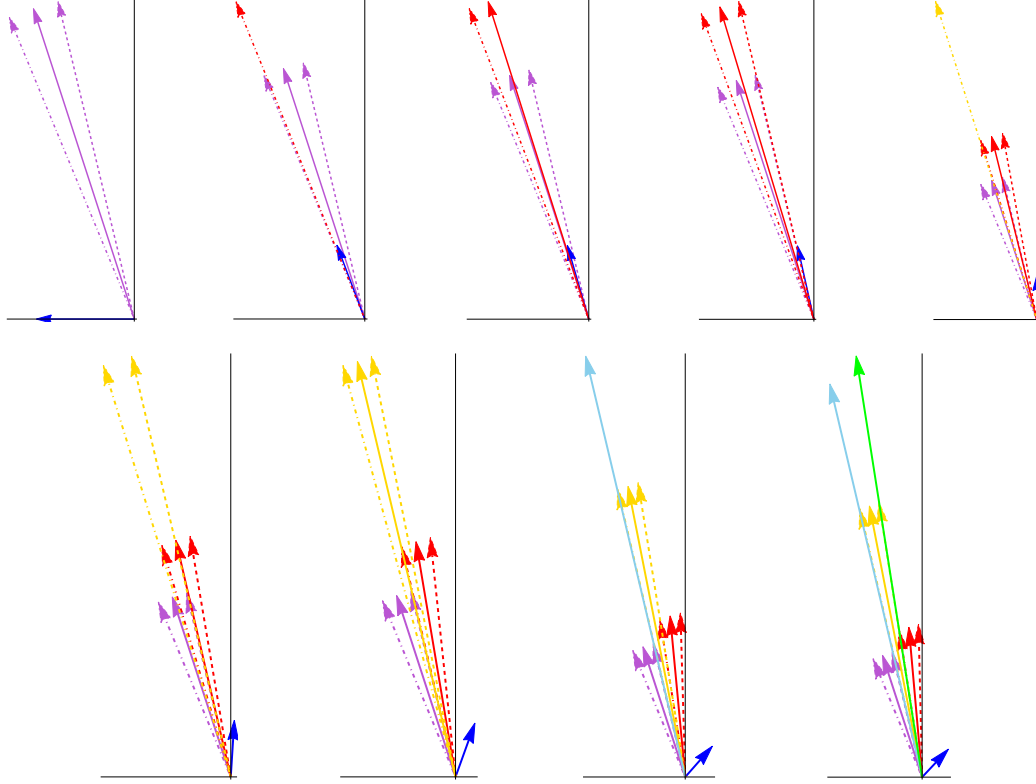


Figure 8.33: Wall-crossing of a singlet and a triplet.

8.3.1.3 $\mathcal{S}[A_1; \mathcal{D}_{\text{reg}}, \mathcal{D}_{n+2}]$ in D_n -class, $n \geq 4$

Now we consider $\mathcal{S}[A_1; \mathcal{D}_{\text{reg}}, \mathcal{D}_{n+2}]$ for a general n . When $n = 2k + 1$, the Seiberg-witten curve is

$$v^2 = t^{2k+1} + c_1 t^{2k} + \dots + c_k t^{k+1} + v_k t^k + \dots + v_1 t + m^2, \quad (8.21)$$

and when $n = 2k$ the Seiberg-Witten curve is

$$v^2 = t^{2k} + c_1 t^{2k-1} + \dots + c_{k-1} t^{k+1} + c_k t^k + v_{k-1} t^{k-1} + \dots + v_1 t + m^2. \quad (8.22)$$

We will focus on the case of $m = 0$, where the BPS spectrum has an $SU(2)$ flavor symmetry.

$\mathcal{S}[A_1; \mathcal{D}_{\text{reg}}, \mathcal{D}_{n+2}]$ with a minimal BPS spectrum & an $SU(2)$ flavor symmetry To consider the generalization, let us go back to the previous example and focus on the case with $m = 0$ and general values of c_1 , c_2 and v_1 where the flavor symmetry is $U(1) \times SU(2)$. Figure 8.34 shows a spectral network of $\mathcal{S}[A_1; \mathcal{D}_{\text{reg}}, \mathcal{D}_6]$ of the choice of the parameters. In

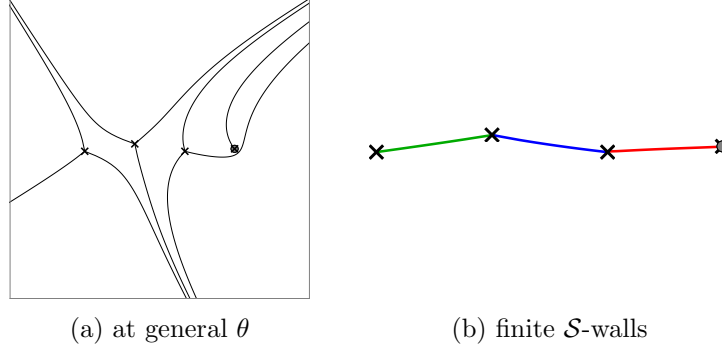


Figure 8.34: A spectral networks of $\mathcal{S}[A_1; \mathcal{D}_{\text{reg}}, \mathcal{D}_6]$ with an $U(1) \times SU(2)$ flavor symmetry and minimal BPS spectrum.

Figure 8.34b we have an $SU(2)$ doublet of the finite \mathcal{S} -walls connecting the puncture and one of the other branch point, as we have seen from the spectral network of $\mathcal{S}[A_1; \mathcal{D}_{\text{reg}}, \mathcal{D}_5]$.

We can see that the spectral network can be considered as a combination of an $\mathcal{S}[A_1; \mathcal{D}_7]$ spectral network and an $\mathcal{S}[A_1; \mathcal{D}_{\text{reg}}, \mathcal{D}_5]$ spectral network. This also applies for every $\mathcal{S}[A_1; \mathcal{D}_{\text{reg}}, \mathcal{D}_{n+2}]$ with $n > 4$, whose spectral network can be considered as a combination of an $\mathcal{S}[A_1; \mathcal{D}_{\text{reg}}, \mathcal{D}_5]$ spectral network and an $\mathcal{S}[A_1; \mathcal{D}_{n+3}]$ spectral network, which in turn consists of spectral networks of $\mathcal{S}[A_1; \mathcal{D}_7]$.

Figure 8.35a and Table 8.35b describe the minimal BPS spectrum of $\mathcal{S}[A_1; \mathcal{D}_{\text{reg}}, \mathcal{D}_6]$ with only the $U(1) \times SU(2)$ flavor symmetry. For general values of c_1 and c_2 , we have a nonzero residue of λ at $t = \infty$. Then the central charge of the doublet differs by the residue from the central charge of one of the other two BPS states, whose corresponding \mathcal{S} -wall is the same cycle of the elliptic curve from the Seiberg-Witten curve as the \mathcal{S} -wall for the doublet.

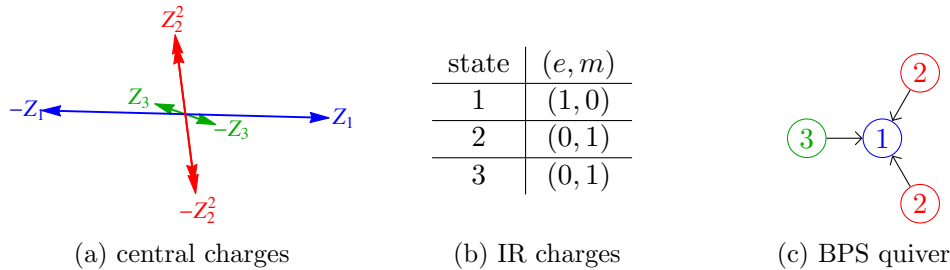


Figure and Table 8.35: Minimal BPS spectrum of $\mathcal{S}[A_1; \mathcal{D}_{\text{reg}}, \mathcal{D}_6]$ with an $U(1) \times SU(2)$ flavor symmetry.

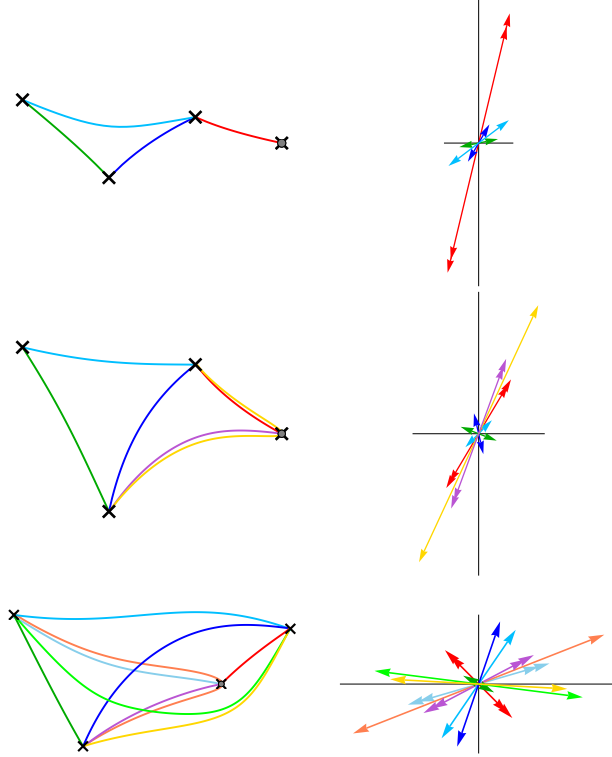


Figure 8.36: Wall-crossing of $\mathcal{S}[A_1; \mathcal{D}_{\text{reg}}, \mathcal{D}_6]$ with a $U(1) \times SU(2)$ flavor symmetry.

Wall-crossing of $\mathcal{S}[A_1; \mathcal{D}_{\text{reg}}, \mathcal{D}_{n+2}]$ with a $U(1) \times SU(2)$ flavor symmetry The wall-crossings of $\mathcal{S}[A_1; \mathcal{D}_{\text{reg}}, \mathcal{D}_6]$ consists of the wall-crossings from $\mathcal{S}[A_1; \mathcal{D}_7]$ and $\mathcal{S}[A_1; \mathcal{D}_{\text{reg}}, \mathcal{D}_5]$, as illustrated in Figure 8.36. Starting from the minimal BPS spectrum of Figures 8.34b and 8.35a, after an $\mathcal{S}[A_1; \mathcal{D}_7]$ wall-crossing we get the BPS spectrum at the first row of Figure 8.36. Between the first row and the second row is another $\mathcal{S}[A_1; \mathcal{D}_{\text{reg}}, \mathcal{D}_5]$ wall-crossing, and after two additional $\mathcal{S}[A_1; \mathcal{D}_{\text{reg}}, \mathcal{D}_5]$ wall-crossings we arrive at the last row of Figure 8.36, where we have the maximal number of BPS state, six BPS states and six anti-states.

Maximal BPS spectrum of $\mathcal{S}[A_1; \mathcal{D}_{\text{reg}}, \mathcal{D}_{n+2}]$ with a $U(1) \times SU(2)$ flavor symmetry

The configuration of a spectral network of $\mathcal{S}[A_1; \mathcal{D}_{\text{reg}}, \mathcal{D}_{n+2}]$ is a straightforward generalization of the previous discussions and the resulting minimal BPS spectrum has the BPS quiver of D_n . But its maximal BPS spectrum, which has $\binom{n}{2} \times 2$ states and their anti-states, is more complicated, so here we describe an example of the maximal BPS spectrum, having in mind that this will be used to analyze the equivalence of $\mathcal{S}[A_1; \mathcal{D}_{\text{reg}}, \mathcal{D}_{n+2}]$ and $\mathcal{S}[A_{n-2}; \mathcal{D}_{\text{II}}]$.

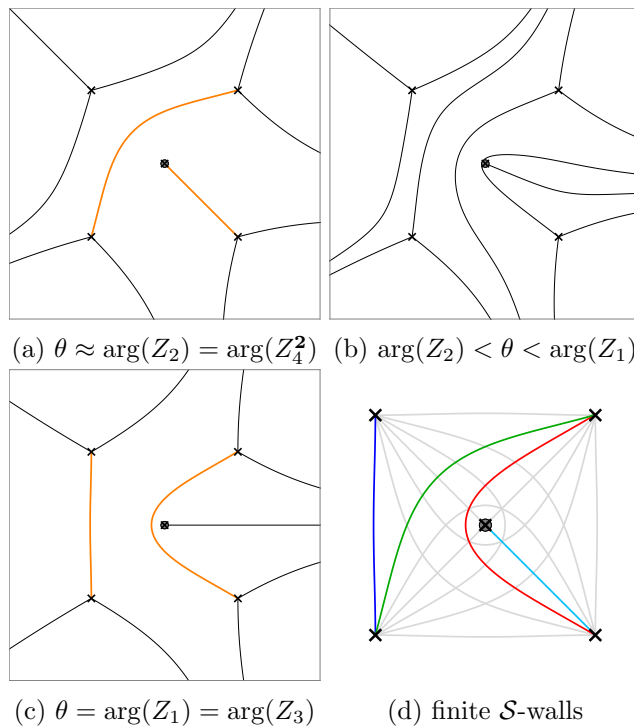


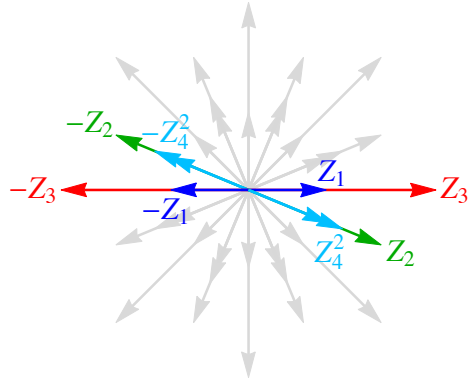
Figure 8.37: Spectral networks of $\mathcal{S}[A_1; \mathcal{D}_{\text{reg}}, \mathcal{D}_7]$ with maximal, symmetric BPS spectrum.

Consider $\mathcal{S}[A_1; \mathcal{D}_{\text{reg}}, \mathcal{D}_7]$. When only $v_1 \neq 0$ and all the other parameters vanish, we have a symmetric arrangement of branch points around the massless puncture, which results in the spectral networks shown in Figure 8.37. From the finite \mathcal{S} -walls shown in Figure 8.37d, we can find the maximal, symmetric BPS spectrum of $\mathcal{S}[A_1; \mathcal{D}_{\text{reg}}, \mathcal{D}_7]$, described in Figure & Table 8.38, where each state is labeled such that $Z_{i+4} = Z_i e^{i\pi/4}$. Between the minimal and the maximal BPS spectra there is a series of wall-crossings relating the two spectra.

8.3.2 $\mathcal{S}[A_{N-1}; \mathcal{D}_{\text{II}}]$ theories

Here we study the BPS spectrum of the SCFT associated with the sphere with one irregular puncture of degree (8.4).¹ We claim that this class of SCFTs is the same as $\mathcal{S}[A_1; \mathcal{D}_{\text{reg}}, \mathcal{D}_{N+3}]$, namely the maximal conformal point of $\mathcal{N} = 2$ $\text{SU}(N)$ gauge theory with two flavors. Indeed, as we will see in appendix C.2, starting from the N -sheeted cover form of the Seiberg-Witten curve of the latter theory we can obtain the irregular singularity as described above.

¹When $N = 3$, the degree of ϕ_2 at the irregular puncture is 6, so we have $\mathcal{C}_{(6,8)}$, which is an exception compared to $N > 3$.



(a) central charges

state	U(1) ₁	U(1) ₂
1	(1, 0)	(0, 0)
2	(0, 1)	(0, 0)
3	(1, 0)	(1, 0)
4	(0, 0)	(0, 1)
5	(1, 1)	(1, 0)
6	(2, 1)	(1, 0)
7	(3, 1)	(2, 2)
8	(1, 0)	(1, 1)
9	(1, 0)	(1, 2)
10	(2, 1)	(2, 2)
11	(3, 2)	(2, 2)
12	(2, 1)	(1, 1)
13	(1, 1)	(0, 0)
14	(2, 1)	(1, 2)
15	(1, 1)	(1, 2)
16	(1, 1)	(1, 1)

(b) IR charges

Figure and Table 8.38: Maximal BPS spectrum of $\mathcal{S}[A_1; \mathcal{D}_{\text{reg}}, \mathcal{D}_7]$.

The Seiberg-Witten curve of this theory is again of canonical form

$$x^N + \sum_{i=2}^N \phi_i x^{N-i} = 0, \quad (8.23)$$

where

$$\begin{aligned} \phi_i &= c_i, \quad (i = 2, \dots, \lfloor \frac{N+1}{2} \rfloor), \\ \phi_i &= v_{N-i+1}, \quad (i = \lfloor \frac{N+1}{2} \rfloor + 1, \dots, N-2), \\ \phi_{N-1} &= t^2 + v_2, \quad \phi_N = c_1 t^2 + C_2 t + v_1. \end{aligned} \quad (8.24)$$

The dimensions of the parameters are easily obtained as

$$\Delta(v_i) = 2 - \frac{2i}{N+1}, \quad \Delta(c_i) = \frac{2i}{N+1}, \quad \Delta(C_1) = \Delta(C_2) = 1, \quad (8.25)$$

for $i = 1, \dots, \lfloor N/2 \rfloor$, where $C_1 := c_{\lfloor (N+1)/2 \rfloor}$ with dimension-one exists only when N is odd. Note that the sum of dimensions of v_k and c_k is 2. This is the same set of operators as that of $\mathcal{S}[A_1; \mathcal{D}_{\text{reg}}, \mathcal{D}_{N+3}]$.

8.3.2.1 $\mathcal{S}[A_2; \mathcal{D}_{\text{II}}]$ in D_4 -class

We first study $\mathcal{S}[A_2; \mathcal{D}_{\text{II}}]$, which has a couple of interesting features because of its $\text{SU}(3)$ flavor symmetry. The curve is $x^3 + \phi_2 x + \phi_3 = 0$ with

$$\phi_2 = t^2 + C_1, \quad \phi_3 = c_1 t^2 + C_2 t + v_1, \quad (8.26)$$

where the scaling dimensions of the parameters are $\Delta(v_1) = \frac{3}{2}$, $\Delta(c_1) = \frac{1}{2}$ and $\Delta(C_1) = \Delta(C_2) = 1$. This is the same spectrum of operators as that of $\mathcal{S}[A_1; \mathcal{D}_{\text{reg}}, \mathcal{D}_6]$. Note that we can only see a $\text{U}(1)^2$ flavor symmetry whose mass parameters are combinations of C_1 , C_2 and c_1^2 . We propose that this is enhanced to $\text{SU}(3)$, which is the case of $\mathcal{S}[A_1; \mathcal{D}_{\text{reg}}, \mathcal{D}_6]$.

Each λ_{ij} has a residue at the irregular puncture $t = \infty$, which are of the form

$$\text{Res}(\lambda_{ij}(t), \infty) = \alpha_{ij} C_1 + \beta_{ij} C_2 + \gamma_{ij} c_1^2, \quad (8.27)$$

where α_{ij} , β_{ij} , and γ_{ij} are numerical coefficients. The residues are mass parameters for the $\text{SU}(3)$ flavor symmetry. By requiring the mass parameters to vanish, we find the relations between the three parameters

$$C_1 = -\frac{3}{4} c_1^2, \quad C_2 = 0, \quad (8.28)$$

which ensures the theory to have the maximal flavor symmetry. From now on we will fix C_1 and C_2 to satisfy the above relations.

Now we have two complex parameters c_1 and v_1 that can be changed. The discriminant of the equation that describes the branch points is

$$\Delta_t g(c_1, v_1) \propto \left(v_1 - \frac{c_1^3}{4}\right)^3 \left(v_1 + \frac{c_1^3}{4}\right) \left(v_1 + \frac{3}{4} c_1^3\right)^6. \quad (8.29)$$

The choice of $\frac{v_1}{c_1^3} = a_1 = \frac{1}{4}$ corresponds to the singularity where we have a massless triplet of the flavor $\text{SU}(3)$, whereas the choice of $\frac{v_1}{c_1^3} = a_2 = -\frac{1}{4}$ results in a massless singlet. The third choice, $\frac{v_1}{c_1^3} = a_3 = -\frac{3}{4}$ does not correspond to any singularity, but it gives us a branch point of index 3.

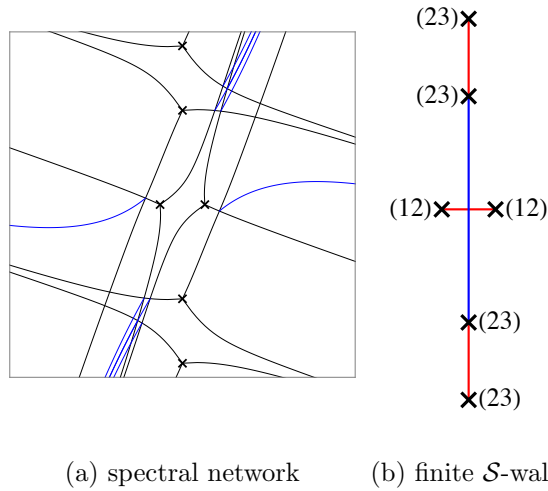
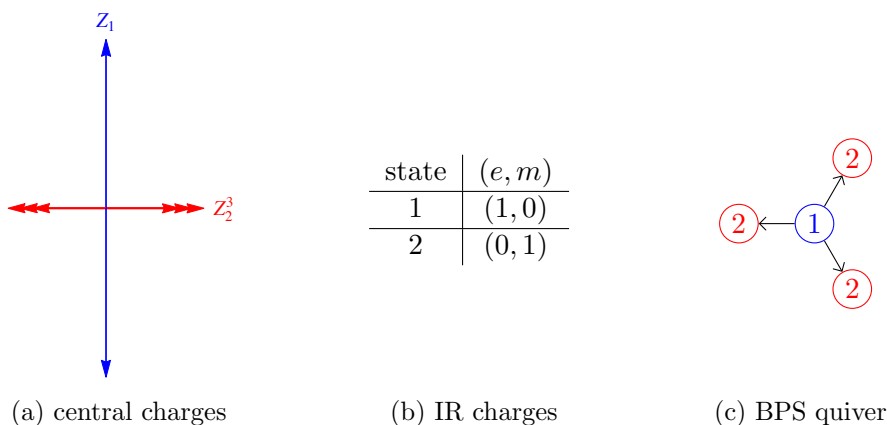
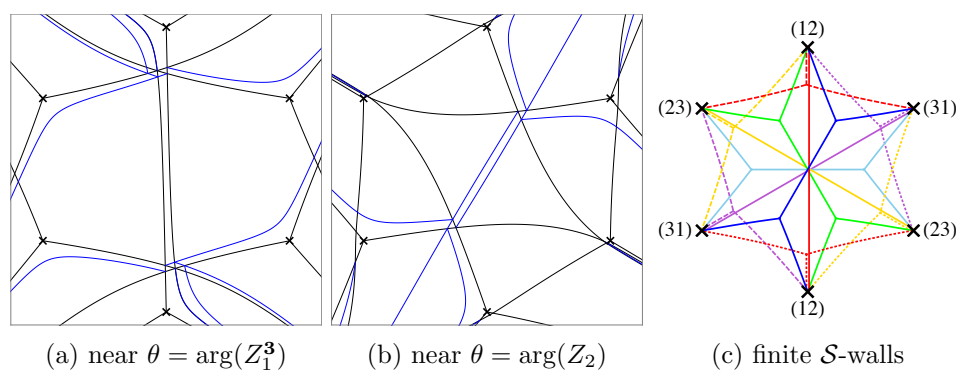


Figure 8.39: A spectral network of $\mathcal{S}[A_2; \mathcal{D}_{\text{II}}]$ with a minimal BPS spectrum.

Minimal BPS spectrum Let us first consider the case of $a_2 < \frac{v_1}{c_1^3} < a_1$, when the theory has its minimal BPS spectrum. Its spectral network at a general value of θ and the resulting finite \mathcal{S} -walls are shown in Figure 8.39.

There are six branch points of index 2. Because the irregular puncture at $t = \infty$ is not a branch point for this case, the (12)-branch cut should terminate at two (12)-branch points without intersecting two (23)-branch cuts connecting each pair of (23)-branch points. Thus we can figure out the intersections of the cycles corresponding to the finite \mathcal{S} -walls. The finite \mathcal{S} -walls corresponding to the BPS states of the triplet correspond to the same cycle, say A-cycle, of the Seiberg-Witten curve, which is a genus-1 curve in this case. The other finite \mathcal{S} -wall corresponding to the singlet is a B-cycle that has intersection number 1 with the A-cycle. This intersection corresponds to the IR $U(1)$ charges described in Table 8.40b, and we can represent this BPS spectrum with a BPS quiver of D_4 as shown in Figure 8.40c, which illustrates the $SU(3)$ flavor symmetry. This is the same BPS spectrum as that of the minimal BPS spectrum of $\mathcal{S}[A_1; \mathcal{D}_{\text{reg}}, \mathcal{D}_6]$, see Figure 8.31 and the first row of Figure 8.32.

Wall-crossing to the maximal BPS spectrum When $\frac{v_1}{c_1^3}$ approaches the value of a_1 , each pair of two branch points of the same indices collides, thereby giving a massless triplet. From the consideration of the wall-crossing of $\mathcal{S}[A_1; \mathcal{D}_{\text{reg}}, \mathcal{D}_6]$ with the $SU(3)$ flavor symmetry that we studied previously in Section 8.3.1.2, we expect $\mathcal{S}[A_2; \mathcal{D}_{\text{II}}]$ to have a maximal BPS spectrum as we go across the BPS wall. When the value of $\frac{v_1}{c_1^3}$ approaches

Figure and Table 8.40: Minimal BPS spectrum of $\mathcal{S}[A_2; \mathcal{D}_{II}]$.Figure 8.41: Spectral networks of $\mathcal{S}[A_2; \mathcal{D}_{II}]$ with a maximal & symmetric BPS spectrum.

a_2 , now it's the singlet that becomes massless, and again a similar wall-crossing will give us a maximal BPS spectrum after we go over the BPS wall. Therefore when we consider the plane of the value of $\frac{v_1}{c_1^3}$, there is one chamber of the minimal BPS spectrum and the rest is another chamber of the maximal BPS spectrum, and the BPS wall goes through $\frac{v_1}{c_1^3} = a_1$ and $\frac{v_1}{c_1^3} = a_2$.

Deep in the chamber of the maximal BPS spectrum is the point $c = C_1 = C_2 = 0, v \neq 0$, where we have a symmetric arrangement of branch points that leads to a symmetric BPS spectrum. Figure 8.41 shows two examples of its spectral networks, one near the value of θ for an $SU(3)$ triplet and the other for a singlet.

Figure 8.42a and Table 8.42b describe the maximal symmetric BPS spectrum that has three triplets and three singlets, which can be identified with the maximal, symmetric BPS spectrum of $\mathcal{S}[A_1; \mathcal{D}_{\text{reg}}, \mathcal{D}_6]$, see the last row of Figure 8.32. Upon suitable choice of A and B-cycles, the BPS states in the spectrum have the same electric and magnetic charges as

those in the maximal BPS spectrum of $\mathcal{S}[A_1; \mathcal{D}_{\text{reg}}, \mathcal{D}_6]$, compare Table 8.42b and Table 8.4.

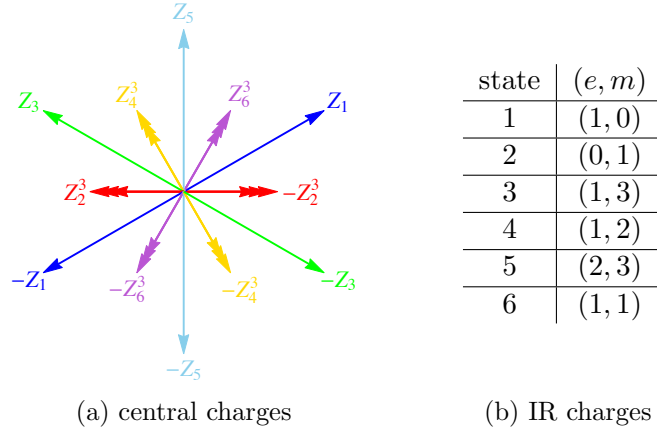


Figure and Table 8.42: Maximal & symmetric BPS spectrum of $\mathcal{S}[A_2; \mathcal{D}_{\text{II}}]$.

8.3.2.2 Exactly marginal deformation of $\mathcal{S}[A_2; \mathcal{D}_{\text{II}}]$

When and only when $N = 3$, we can add a marginal deformation to the theory at the fixed point. The corresponding curve is

$$\phi_2 = t^2 + C_1, \quad \phi_3 = t^3 + c_1 t^2 + C_2 t + v_1. \quad (8.30)$$

Compared to the previous curve of $\mathcal{S}[A_2, \mathcal{C}; \mathcal{D}_{\text{II}}]$ there is an additional t^3 term whose coefficient is dimensionless which we have fixed to 1. We claim this corresponds to an exactly marginal deformation by showing that the BPS spectrum of the SCFT and its wall-crossing is the same as those of the theory without the deformation.

By requiring the residue of λ_{ij} to vanish, we find the relations between the three parameters such that the theory has the maximal $\text{SU}(3)$ flavor symmetry are $C_1 = -\frac{3}{31}c_1^2$ and $C_2 = \frac{9}{31}c_1^2$. From now on we will fix C_1 and C_2 to satisfy the above relations. The discriminant for the given Seiberg-Witten curve is

$$\Delta_t g(c_1, v_1) \propto \left(v_1 - \frac{23c_1^3}{31^2} \right) \left(v_1 - \frac{c_1^3}{31} \right) \left(v_1 - \frac{3c_1^3}{31^2} (4\sqrt{93} - 31) \right) \left(v_1 + \frac{3c_1^3}{31^2} (4\sqrt{93} + 31) \right). \quad (8.31)$$

The choice of $\frac{v_1}{c_1^3} = a_1 = \frac{23}{31^2}$ corresponds to the singularity where we have a massless triplet of the flavor $\text{SU}(3)$, whereas the choice of $\frac{v_1}{c_1^3} = a_2 = \frac{1}{31}$ results in a massless singlet. The

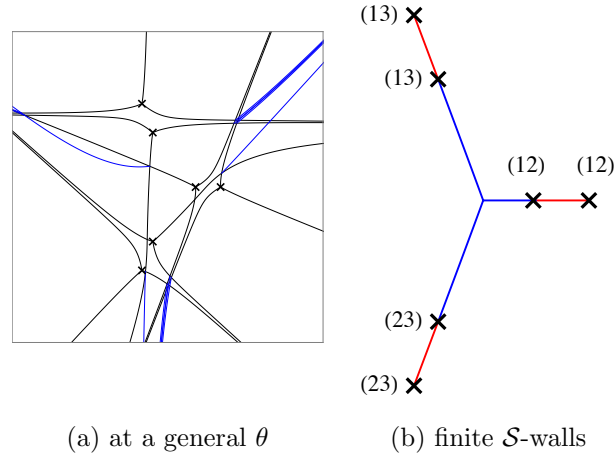


Figure 8.43: A spectral network of the deformation of $\mathcal{S}[A_2; \mathcal{D}_{II}]$ by a t^3 -term, with minimal BPS spectrum.

other two choices, $\frac{v_1}{c_1^3} = a_{\pm} = \pm \frac{3}{31^2}(4\sqrt{93} \mp 31)$ do not correspond to any singularity, but they give us a branch point of index 3. Therefore the singularity structure is the same as that of $\mathcal{S}[A_2, \mathcal{C}; \mathcal{D}_{II}]$, and we observe the same wall-crossing.

Minimal BPS spectrum Let us first consider the case of $a_2 < \frac{v_1}{c_1^3} < a_1$. An example of its spectral network and the resulting finite \mathcal{S} -walls are shown in Figure 8.43. Indeed the configuration of the spectral network and the \mathcal{S} -walls are different from what we had for $\mathcal{S}[A_2; \mathcal{D}_{II}]$ without the t^3 -term, but the BPS spectrum is the same, see Figure 8.44a and Table 8.44b. Its BPS quiver is again a D_4 quiver as shown in Figure 8.44c, which exhibits the $SU(3)$ flavor symmetry.

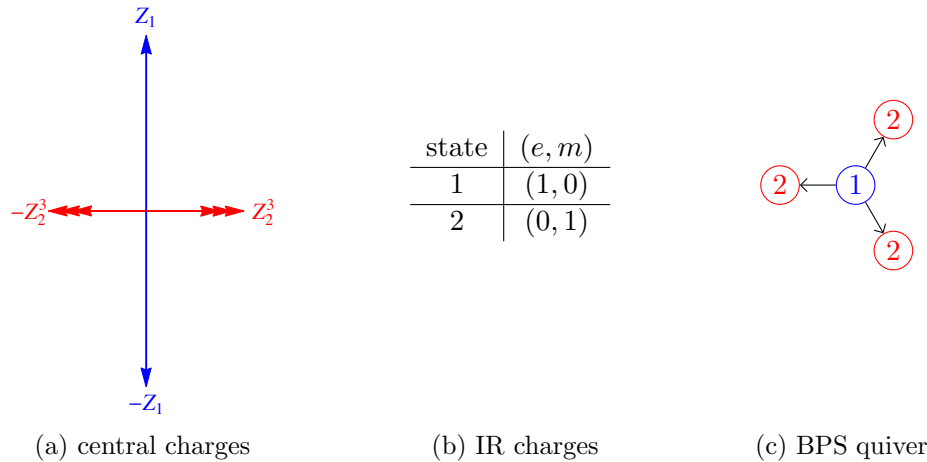


Figure 8.44: Minimal BPS spectrum of the deformation of $\mathcal{S}[A_2; \mathcal{D}_{II}]$ by a t^3 -term.

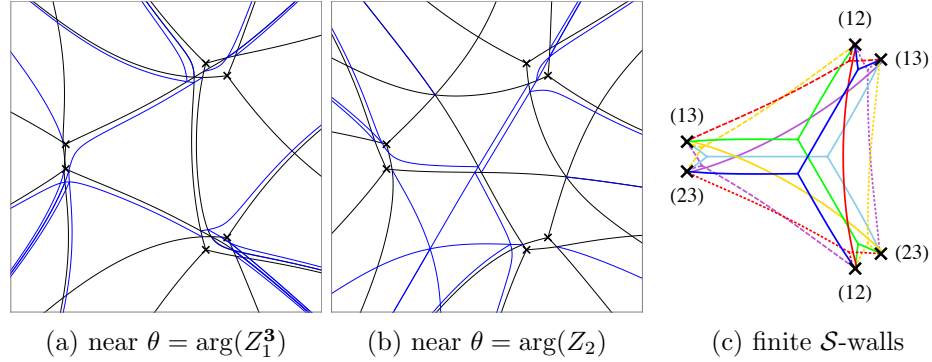


Figure 8.45: Spectral networks of the deformation of $\mathcal{S}[A_2; \mathcal{D}_{\text{II}}]$ by t^3 , with a maximal & symmetric BPS spectrum.

Wall-crossing to a maximal BPS spectrum When we change the value of v_1 from $(a_1 - \delta)c_1^3$ to $(a_1 + \delta)c_1^3$, where δ is a small positive real number, we are on the other side of the BPS wall in the Coulomb branch moduli space, where the triplet went through the phase of becoming massless.

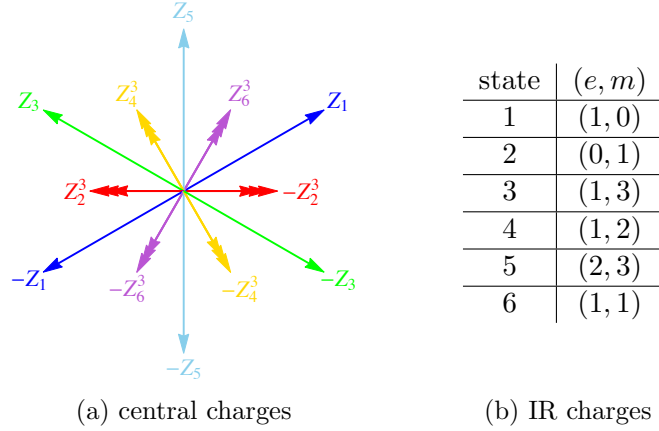
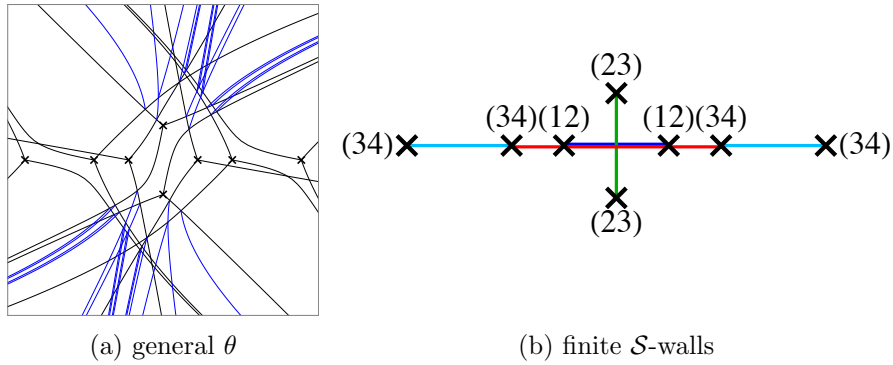
When $c_1 = C_1 = C_2 = 0$, $v_1 \neq 0$ the deformed theory has the maximal, symmetric BPS spectrum, as $\mathcal{S}[A_2; \mathcal{D}_{\text{II}}]$ did. Figures 8.45a and 8.45b show its spectral networks when θ is close to having a triplet and a singlet, respectively. Again, the spectral networks are different from those of the undeformed theory.

Figure 8.46a and Table 8.46b describe the BPS spectrum of the deformed theory, which can be identified with the maximal, symmetric BPS spectrum of $\mathcal{S}[A_2; \mathcal{D}_{\text{II}}]$, see Figure 8.42a and Table 8.42b. Although the two theories have different spectral networks, their BPS spectra agree and this is good evidence for the claim that t^3 -term corresponds to an exactly marginal deformation for the 4d SCFT.

8.3.2.3 $\mathcal{S}[A_{N-1}; \mathcal{D}_{\text{II}}]$ in D_{N+1} -class

Now we want to consider $\mathcal{S}[A_{N-1}; \mathcal{D}_{\text{II}}]$ with general N and show its BPS spectra and their wall-crossings are the same as those of $\mathcal{S}[A_1; \mathcal{D}_{\text{reg}}, \mathcal{D}_{N+3}]$. One difference from $N = 3$ case is that when $N > 3$ the maximal flavor symmetry is $\text{SU}(2)$ (or $\text{SU}(2) \times \text{U}(1)$ when N is odd), and we only have doublets rather than triplets of $\text{SU}(3)$ that exist in the BPS spectrum of $\mathcal{S}[A_2; \mathcal{D}_{\text{II}}]$.

Let us start with the minimal BPS spectrum. The configuration of a spectral network that provides the minimal BPS spectra of $\mathcal{S}[A_{N-1}; \mathcal{D}_{\text{II}}]$ has branch points of index 2 aligned

Figure and Table 8.46: Maximal & symmetric BPS spectrum of the deformed $\mathcal{S}[A_2; \mathcal{D}_{II}]$.Figure 8.47: A spectral network of $\mathcal{S}[A_3; \mathcal{D}_{II}]$ with minimal BPS spectrum.

along two perpendicular lines on the t -plane. Because the BPS spectrum is represented by a D_{N+1} quiver, which contains an A_{N-1} quiver in it, we expect the spectral network of $\mathcal{S}[A_{N-1}; \mathcal{D}_I]$ to be a part of that of $\mathcal{S}[A_{N-1}; \mathcal{D}_{II}]$ and it is indeed the case, see Figures 8.39 and 8.47, which represent $N = 3$ and $N = 4$ cases, respectively, and contain the spectral networks of $\mathcal{S}[A_2; \mathcal{D}_I]$ and $\mathcal{S}[A_3; \mathcal{D}_I]$, respectively, see Figures 8.14 and 8.20.

The Seiberg-Witten curve of $\mathcal{S}[A_{N-1}; \mathcal{D}_{II}]$ has two more branch points of index 2 in addition to those of the curve of $\mathcal{S}[A_{N-1}; \mathcal{D}_I]$. Remember that a trivialization of $\mathcal{S}[A_{N-1}; \mathcal{D}_I]$ is achieved by putting a branch cut between every branch point at finite t to $t = \infty$, where either there is a branch point of index N when N is odd, or there are two branch points of index $N/2$ when N is even. The two additional branch points are connecting the $(N-1)$ -th and N -th sheets. These branch points intercept two branch cuts from the other two branch points of the same kind, therefore at $t = \infty$ the curve of $\mathcal{S}[A_{N-1}; \mathcal{D}_{II}]$ has either a branch points of index $N-1$ when N is even, or two branch points of index $(N-1)/2$

when N is odd. Note that by applying the Riemann-Hurwitz formula we find the genus of the Seiberg-Witten curve to be $g = N/2$ when N is even and $g = (N - 1)/2$ when N is odd. With this trivialization of the curve of $\mathcal{S}[A_{N-1}; \mathcal{D}_{\text{II}}]$, and that we have two more finite \mathcal{S} -walls compared to $\mathcal{S}[A_{N-1}; \mathcal{D}_{\text{I}}]$ with minimal BPS spectrum, it is straightforward that the minimal BPS spectrum of $\mathcal{S}[A_{N-1}; \mathcal{D}_{\text{II}}]$ is equivalent to that of $\mathcal{S}[A_1; \mathcal{D}_{\text{reg}}, \mathcal{D}_{N+3}]$ and can be represented by a D_{N+1} quiver. Figure 8.48a and Table 8.48b describe the minimal BPS spectrum of $\mathcal{S}[A_3; \mathcal{D}_{\text{II}}]$, which can be represented with a D_5 quiver as shown in Figure 8.48c.

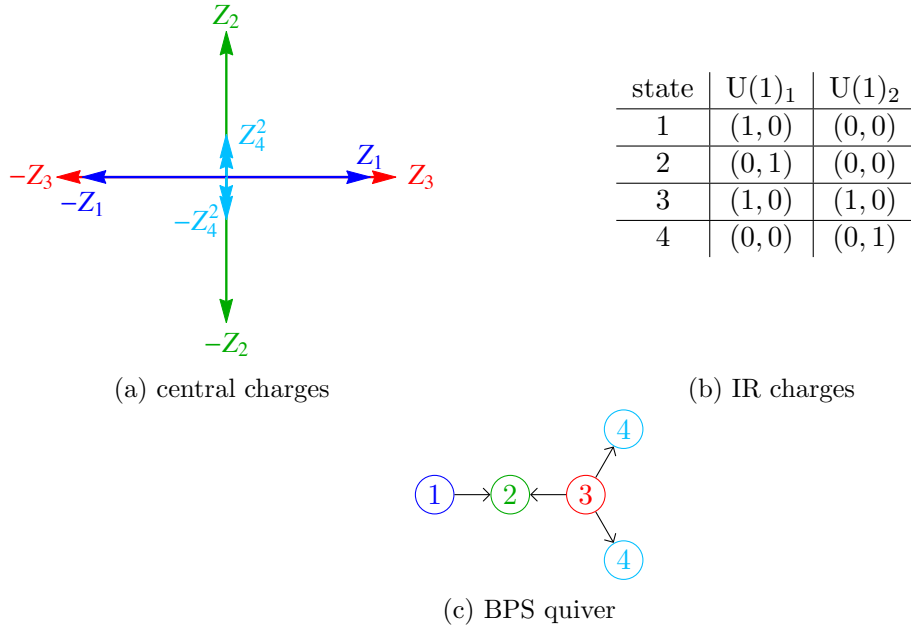


Figure and Table 8.48: Minimal BPS spectrum of $\mathcal{S}[A_3; \mathcal{D}_{\text{II}}]$.

To show that $\mathcal{S}[A_{N-1}; \mathcal{D}_{\text{II}}]$ is equivalent to $\mathcal{S}[A_1; \mathcal{D}_{\text{reg}}, \mathcal{D}_{N+3}]$, we also compare the maximal, symmetric BPS spectrum of the two. When only $v_1 \neq 0$ and all the other parameters vanish, $\mathcal{S}[A_{N-1}; \mathcal{D}_{\text{II}}]$ has a symmetric arrangement of branch points around $t = 0$. There are $2N$ branch points of index 2, each pair of them having the same indices and being located oppositely from $t = 0$. The indices of the first N branch points are $(12), (23), \dots, (N - 1, N), (N, 1)$, and each branch point is an end point of a branch cut that goes to $t = \infty$. When $N = 3$ this leads to no branch point at $t = \infty$ as we have seen previously. When $N > 3$, if N is even there is a branch point of index $N - 1$ at $t = \infty$, and if N is odd there are two branch points of index $(N - 1)/2$ at $t = \infty$.

This configuration leads to a symmetric, maximal BPS spectrum, where there are $N(N -$

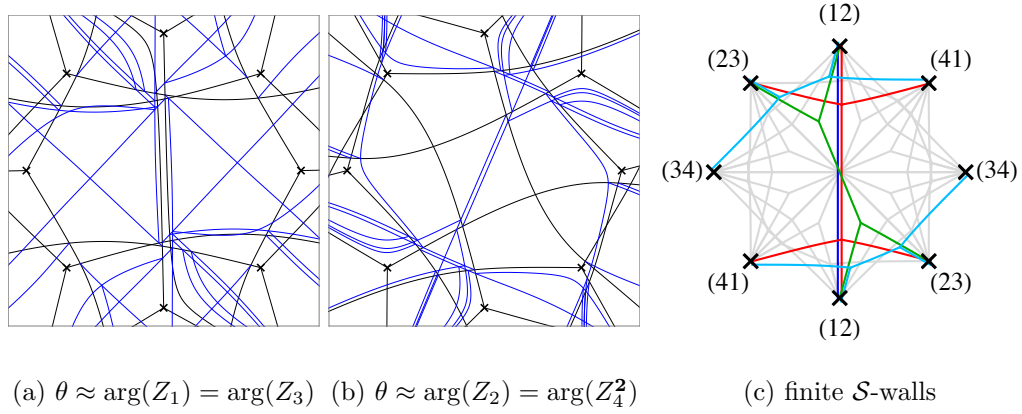
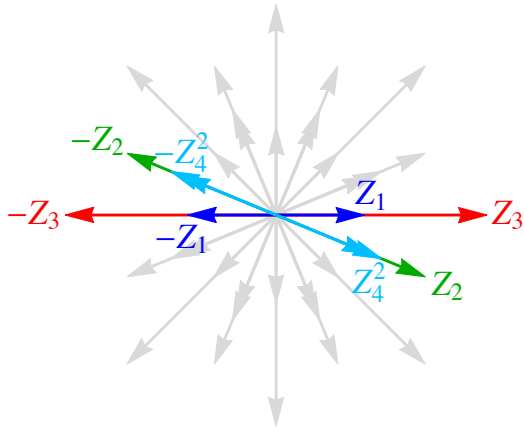


Figure 8.49: Spectral networks of $\mathcal{S}[A_3; \mathcal{D}_{II}]$ with maximal, symmetric BPS spectrum.

1) singlets and N doublets, including anti-states, which results in $N(N - 1) + 2 \times N = N(N + 1) = 2\binom{N+1}{2}$ states in the BPS spectrum, which is the same as the number of states in the maximal BPS spectrum of $\mathcal{S}[A_1; \mathcal{D}_{reg}, \mathcal{D}_{N+3}]$. An example of spectral networks for the $N = 4$ case is shown in Figure 8.49. The resulting BPS spectrum is described by Figure 8.50a and Table 8.50b, which is the same as the maximal symmetric BPS spectrum of $\mathcal{S}[A_1; \mathcal{D}_{reg}, \mathcal{D}_7]$, see Figure 8.38a and Table 8.38b.



(a) central charges

state	$U(1)_1$	$U(1)_2$
1	(1, 0)	(0, 0)
2	(0, 1)	(0, 0)
3	(1, 0)	(1, 0)
4	(0, 0)	(0, 1)
5	(1, 1)	(1, 0)
6	(2, 1)	(1, 0)
7	(3, 1)	(2, 2)
8	(1, 0)	(1, 1)
9	(1, 0)	(1, 2)
10	(2, 1)	(2, 2)
11	(3, 2)	(2, 2)
12	(2, 1)	(1, 1)
13	(1, 1)	(0, 0)
14	(2, 1)	(1, 2)
15	(1, 1)	(1, 2)
16	(1, 1)	(1, 1)

(b) IR charges

Figure and Table 8.50: Maximal, symmetric BPS spectrum of $\mathcal{S}[A_3; \mathcal{D}_{II}]$.

8.3.3 $\mathcal{S}[A_2; \mathcal{D}_{\text{reg}}, \mathcal{D}_{\text{III}}]$ theories

Here we will see an example of 4d SCFT from the 6d $(2,0)$ A_{N-1} theory with $N > 2$ compactified on a Riemann surface with both a regular puncture and an irregular one. The Seiberg-Witten curve is $v^3 + \tilde{\phi}_2 v + \tilde{\phi}_3 = 0$ with

$$\begin{aligned}\tilde{\phi}_2 &= ct + (C_2 - m_+^2/3), \\ \tilde{\phi}_3 &= t^2 - vt - \left(C_3 - \frac{C_2 m_+}{3} + \frac{2m_+^3}{27}\right),\end{aligned}\tag{8.32}$$

where the regular puncture is at $t = 0$ and the irregular puncture is at $t = \infty$. The Seiberg-Witten differential is $\lambda = \frac{v}{t} dt$. The dimensions of the parameters are

$$\Delta(C_3) = 3, \quad \Delta(C_2) = 2, \quad \Delta(m_+) = 1, \quad \Delta(c) = \frac{1}{2}, \quad \Delta(v) = \frac{3}{2}.\tag{8.33}$$

These are the same as those of the class 2 SCFT of $SU(3)$ with $N_f = 3$ in [95]. We will show that the BPS spectra of this theory and their wall-crossings are the same as those of $\mathcal{S}[A_1; \mathcal{D}_{\text{reg}}, \mathcal{D}_6]$ and $\mathcal{S}[A_2; \mathcal{D}_{\text{II}}]$, all three of which are in the same D_4 -class..

The irregular singularity at $t = \infty$ is a branch point of index 3 and has no residue. For general values of parameters, we have four branch points of index 2. When we set the values of C_2 and C_3 as

$$C_2 = \frac{m_+^3}{3}, \quad C_3 = \frac{m_+^3}{27},\tag{8.34}$$

two among the four branch points collide with the regular puncture at $t = 0$, forming a branch point of index 3. This choice corresponds to enhancing the flavor symmetry to $SU(3)$, and the puncture has two triplets of \mathcal{S} -walls coming out of it.

With values of C_i fixed as above, the discriminant of the equation of branch points is

$$\Delta_w g(c, v) \propto c^3 \left(v - \frac{c^3}{27}\right).\tag{8.35}$$

$v = c^3/27$ corresponds to the singularity where a singlet becomes massless. $c = 0$ does not correspond to a singularity but a collision of two branch points of index 2, forming a single branch point of index 3.

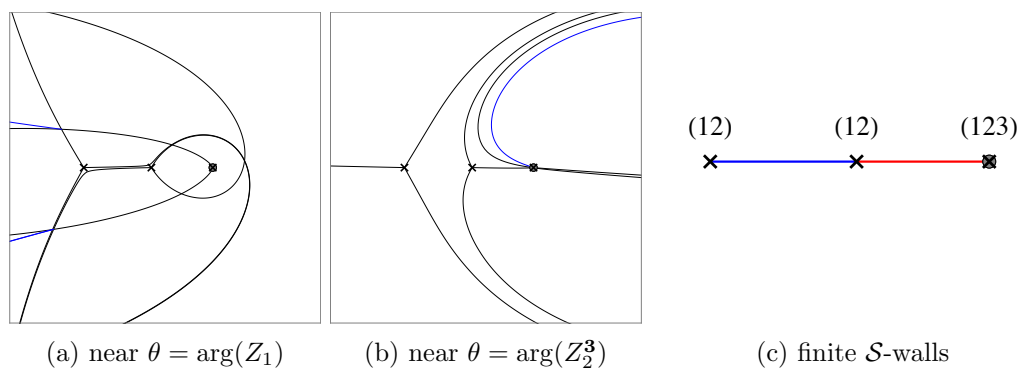


Figure 8.51: Spectral networks of $\mathcal{S}[A_2; \mathcal{D}_{\text{III}}]$ with minimal BPS spectrum.

Minimal BPS spectrum When c is fixed as a real number and $v = c^3/27 - \delta$, where δ is a small real number, we have two branch points of ramification index 2 in addition to the puncture of index 3, as shown in Figure 8.51, where finite \mathcal{S} -walls corresponding to BPS states are also depicted.

Note that, in addition to a finite \mathcal{S} -wall connecting the two branch points of index 2 that corresponds to a singlet, there is a triplet of \mathcal{S} -walls from the puncture, i.e., there are three coincident finite \mathcal{S} -walls connecting the puncture and one of the branch points of index 2, which gives us an $\text{SU}(3)$ triplet.

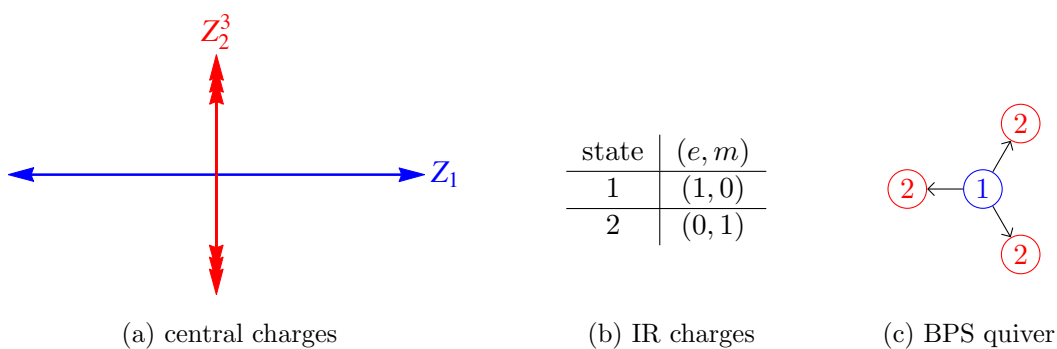


Figure and Table 8.52: minimal BPS spectrum of $\mathcal{S}[A_2; \mathcal{D}_{\text{III}}]$.

The intersections of the cycles corresponding to the \mathcal{S} -walls can be easily read out if we consider the trivialization of the Seiberg-Witten curve by introducing a branch cut between the two branch points of index 2 and another branch cut connecting the puncture and the branch point of index 3 at infinity. The resulting BPS spectrum, described in Figure 8.52a and Table 8.52b, is the same as the minimal BPS spectrum of $\mathcal{S}[A_1; \mathcal{D}_{\text{reg}}, D_6]$ (Figure 8.31) and $\mathcal{S}[A_2; \mathcal{D}_{\text{II}}]$ (Figure and Table 8.40), all of which can be represented with a D_4 quiver as shown in Figure 8.52c.

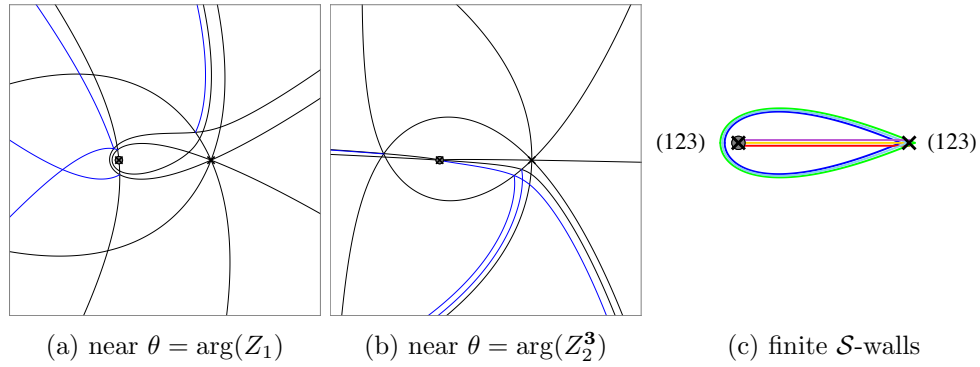
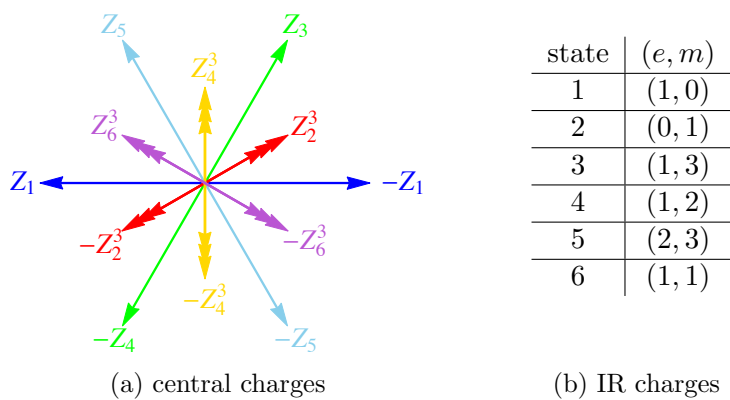


Figure 8.53: spectral networks of $\mathcal{S}[A_2, \mathcal{C}; D_{\text{III}}]$ with maximal BPS spectrum.

Wall-crossing to the maximal BPS spectrum As $\delta \rightarrow 0$, the two branch points of index 2 approach each other, corresponding to the BPS state from the \mathcal{S} -wall connecting the two becoming massless, and as we go across the wall at $\delta = 0$ the BPS spectrum undergoes a wall-crossing to the maximum BPS spectrum, which is similar to what we have observed for the other theories with a D_4 BPS spectrum and an $SU(3)$ flavor symmetry. Now we fix the value of v and take $c \rightarrow 0$, then the two branch points of index 2 move to the other side of the puncture, and one of the two branch points goes through the branch cut connecting the puncture and infinity, resulting in a branch point connecting different sheets.

When we eventually set $c = 0$, the two branch points collide to form a single branch point of index 3. This is a symmetric configuration of three branch points (including one at infinity), considering the locations of three points on a complex plane does not introduce any modulus. Figure 8.53 shows its spectral networks and finite \mathcal{S} -walls, from which we get the maximal, symmetric BPS spectrum of $\mathcal{S}[A_2; \mathcal{D}_{\text{III}}]$ described in Figure 8.54a and Table 8.54b. This spectrum can be identified with those of $\mathcal{S}[A_1; \mathcal{D}_{\text{reg}}, \mathcal{D}_6]$ (Figure 8.32 and Table 8.4) and $\mathcal{S}[A_2; \mathcal{D}_{\text{II}}]$ (Figure and Table 8.42), thereby providing good evidence for the equivalence of the three theories.

Figure and Table 8.54: Maximal BPS spectrum of $\mathcal{S}[A_2; \mathcal{D}_{III}]$.

Appendix A

Normalization of compactified Seiberg-Witten curves

A.1 Normalization of a singular algebraic curve

To understand how normalization works, let's try to normalize a curve with a singularity, $\bar{A} \subset \mathbb{CP}^2$. The left side of Figure A.1 illustrates how a singularity of \bar{A} is resolved when we normalize it to a smooth curve $\mathcal{A} = \sigma^{-1}(\bar{A})$ by finding a map σ . There are various kinds

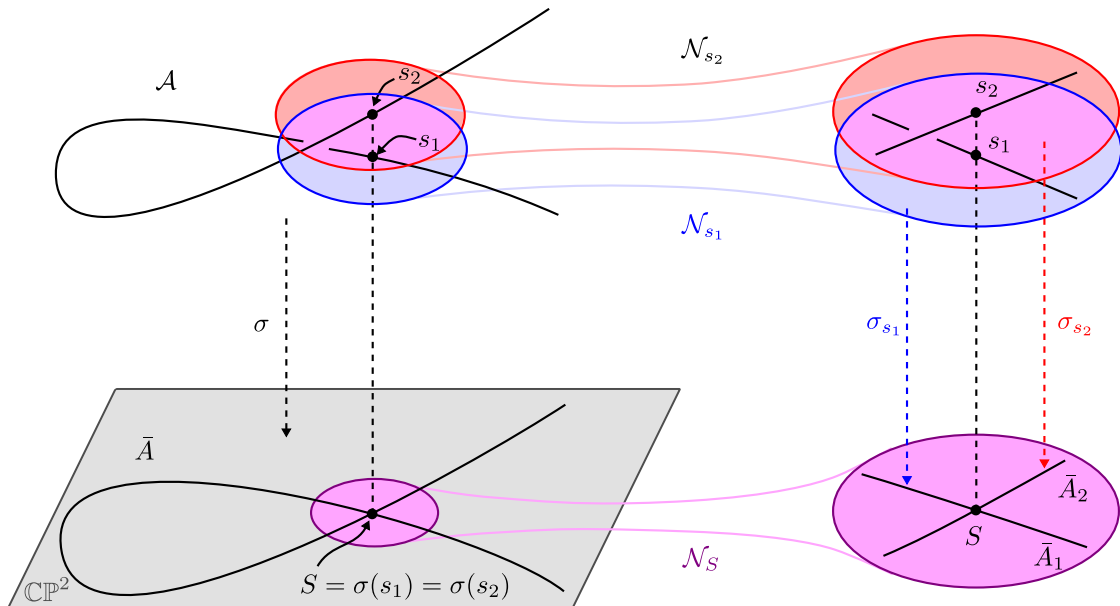


Figure A.1: Schematic description of the normalization of a singular curve.

of singular points, and the case illustrated here is that \bar{A} has two tangents at the singular point $S = \sigma(s_1) = \sigma(s_2)$, which corresponds to two different points $\sigma^{-1}(S) = \{s_1, s_2\}$ on

\mathcal{A} .¹ Without any normalization, \bar{A} is an irreducible curve that is singular at S . After the normalization we get a smooth irreducible curve \mathcal{A} .

Finding such σ that works over all \bar{A} will not be an easy job, especially because we don't know how to describe \mathcal{A} globally. However, if we are interested only in analyzing a local neighborhood of a point on \bar{A} , we do not need to find σ that maps the whole \mathcal{A} to the entire \bar{A} , but finding a local normalization [18] of \bar{A} near the point will be good enough for that purpose. What is good about this local version of normalization is that we know how to describe \mathcal{A} locally. That is, because \mathcal{A} is a Riemann surface, we can choose a local coordinate $s \in \mathbb{C}$ on \mathcal{A} such that $s_i = 0$. Then a local normalization is described by a map σ_{s_i} from the neighborhood of $s_i \in \mathcal{A}$ to the neighborhood of $S \in \bar{A}$.

$$\sigma_{s_i} : \mathcal{N}_{s_i} \rightarrow \mathcal{N}_S, \quad s \mapsto (x(s), y(s)),$$

where (x, y) is a coordinate system of $\mathbb{C}^2 \subset \mathbb{CP}^2$ such that $S = (0, 0)$. Or if we see σ_{s_i} as a map into a subset of \mathbb{CP}^2 when $S = [X_S, Y_S, Z_S] = [X_S/Z_S, Y_S/Z_S, 1]$,

$$\sigma_{s_i} : \mathcal{N}_{s_i} \rightarrow \mathcal{N}_S, \quad s \mapsto [X_S/Z_S + x(s), Y_S/Z_S + y(s), 1].$$

We can sew up the local normalizations to get a global normalization if we have enough of them to cover the whole curve.

Now let's get back to the case of Figure A.1 and find its local normalizations. Schematic descriptions of the local normalizations are shown in the right side of Figure A.1. When we zoom into the neighborhood \mathcal{N}_S of the singular point S on \bar{A} , we see a reducible curve, called the local analytic curve [18] of \bar{A} at S , with two irreducible components $\{\bar{A}_1, \bar{A}_2\}$, where each component \bar{A}_i is coming from a part of \mathcal{A} . By choosing \mathcal{N}_S as small as possible, we can get a good approximation of \bar{A} at S by the local analytic curve $f_S(x, y) = 0$. Because we have two irreducible component for the local analytic curve illustrated here, we can factorize $f_S(x, y)$ into its irreducible components $f_{s_i}(x, y)$, i.e., $f_S(x, y) = f_{s_1}(x, y)f_{s_2}(x, y)$, each giving us the local description of the component. Then we find a local normalization $\sigma_{s_i}(s) = (x(s), y(s))$ for each component defined as the zero locus of $f_{s_i}(x(s), y(s))$.

¹A similar kind of singularity occurs at $(z, w) = (0, 0)$ of a curve defined by $zw = 0$ in \mathbb{C}^2 , which can be lifted if we consider embedding the curve into \mathbb{C}^3 and moving $z = 0$ and $w = 0$ complex planes away from each other along the other complex dimension normal to both of them.

A.2 Calculation of local normalizations

Calculation of a local normalization of a curve near a point is done here by finding a Puiseux expansion [17] of the curve at the point. Puiseux expansion is essentially a convenient way to get a good approximation of a curve in \mathbb{CP}^2 around a point P on the curve. That is, for a local analytic curve defined as $f_P(x, y) = 0$, the solutions of the equation describe the different branches of the curve at P , and each of them is called a Puiseux expansion of the curve at P .

When the local analytic curve is irreducible, as we go around P the branches of the local analytic curve at P are permuted among themselves transitively. However, when it is reducible, for example into two components like the case we saw in Appendix A.1, the permutations happen only among the branches of each component.

A.2.1 SU(2) SCFT

We showed in Section 3.1 how to compactify the Seiberg-Witten curve of SU(2) SCFT. So let's start with the compactified curve, \bar{C}_{SW} , that is defined as the zero locus of

$$F(X, Y, Z) = (X - Z)(X - t_1 Z)Y^2 - uXZ^3$$

in \mathbb{CP}^2 . We want to get the local normalizations near

- (1) $\{p_i \in \mathcal{C}_{\text{SW}}\}$, where $\{\phi(p_i)\}$ are the points we add to \mathcal{C}_{SW} to compactify it,
- (2) $\{q_i \in \mathcal{C}_{\text{SW}} | dt(q_i) = 0\} \Leftrightarrow \{q_i \in \mathcal{C}_{\text{SW}} | (\partial f / \partial v)(t(q_i), v(q_i)) = 0\}$,
- (3) $\{r_i \in \mathcal{C}_{\text{SW}} | v(r_i) = 0\}$.

The corresponding points on \bar{C}_{SW} are

$$\begin{aligned}\sigma(p_1) &= [0, 0, 1], \\ \sigma(p_2) &= \sigma(p_3) = [0, 1, 0], \\ \sigma(p_4) &= [1, 0, 0]\end{aligned}$$

from (1). (2) and (3) do not give us any other candidate.

1. Near $\sigma(p_1) = [0, 0, 1]$, let's denote a small deviation from $[0, 0, 1]$ by $[x, y, 1]$. Along \bar{C}_{SW} x and y satisfy

$$F(x, y, 1) = (x - 1)(x - t_1)y^2 - ux = 0. \quad (\text{A.1})$$

From this polynomial we can get the corresponding Newton polygon. Here is how we get one. First we mark a point at $(a, b) \in \mathbb{Z}^2$ if we have in the polynomial a term $x^a y^b$ with nonzero coefficient. We do this for every term in the polynomial and get several points in the \mathbb{Z}^2 -plane. For instance, the polynomial (A.1) gives the points in Figure A.2, where the horizontal axis corresponds to the exponent of x and the vertical one to that of y for a term that is represented by a point. Now we connect some of the

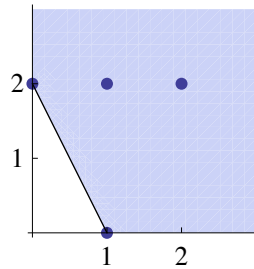


Figure A.2: Newton polygon of $F(x, y, 1)$.

points with lines so that the lines with the two axes make a polygon that contains all the points and is convex to the origin. This is the Newton polygon of the polynomial. Using this Newton polygon, we can find Puiseux expansions at $\sigma(p_1)$. Here we will describe just how we can get the Puiseux expansions using the data we have at hand. The underlying principle why this procedure works is illustrated in [17], for example. First we pick a line segment that corresponds to the steepest slope and collect the terms corresponding to the points on that edge to make a new polynomial. Then the zero locus of the polynomial is the local representation of \bar{C}_{SW} near $[0, 0, 1]$. In this case, the polynomial is

$$t_1 y^2 - ux.$$

The zero locus of this polynomial is an approximation of \bar{C}_{SW} at $x = y = 0$, i.e., the local analytic curve at $[0, 0, 1]$. We can get a better approximation by including

“higher-order” terms, but this is enough for now. The solutions of this polynomial,

$$y(x) = \pm \sqrt{\frac{ux}{t_1}},$$

are the Puiseux expansions of y in x at $x = y = 0$. We can see that there are two branches of $y(x)$, that the two branches are coming together at $x = y = 0$, and that the monodromy around $x = 0$ permutes the two branches with each other.

To get a local normalization near the point, note that

$$\sigma_{p_1} : s \mapsto [x, y, 1] = [s^2, a_0s, 1], \quad a_0 = \sqrt{u/t_1}$$

maps a neighborhood of $s = 0$ to the two branches. Therefore σ_{p_1} is a good local normalization when we consider s as a coordinate patch for \mathcal{C}_{SW} where p_1 is located at $s = 0$.

Now we have a local normalization σ_{p_1} near p_1 . Let’s use this to calculate the ramification index $\nu_{p_1}(\pi)$. Remember that the local description of $\pi : \mathcal{C}_{\text{SW}} \rightarrow C_B$ near p_1 is realized in Section 3.1 as

$$\pi_{p_1}(s) = \frac{X(s)}{Z(s)}.$$

Near $s = 0$,

$$\pi_{p_1}(s) - \pi_{p_1}(0) = \frac{x(s)}{1} - 0 = s^2.$$

The exponent of this map is the ramification index at $s = 0$. That is, $\nu_{p_1}(\pi) = 2$.

We can also calculate the degree of (ω) at p_1 using the local normalization. Remember that (ω) is the Seiberg-Witten differential pulled back by σ onto \mathcal{C}_{SW} .

$$\omega = \sigma^*(\lambda) = \sigma^* \left(\frac{Y/Z}{X/Z} d \left(\frac{X}{Z} \right) \right).$$

Near $s = 0$, this becomes

$$\omega_{p_1} = \frac{y(s)}{x(s)} d(x(s)) = \frac{a_0s}{s^2} \cdot d(s^2) = 2a_0ds.$$

Therefore ω has neither pole nor zero of any order at p_1 , which implies $\nu_{p_1}(\omega) = 0$.

2. Near $\sigma(p_2) = \sigma(p_3) = [0, 1, 0]$, let's denote a deviation from $[0, 1, 0]$ by $[x, 1, z]$. Then along \bar{C}_{SW} x and z satisfy

$$F(x, 1, z) = (x - z)(x - t_1 z) - uxz^3 = 0.$$

The Newton polygon of this polynomial is shown in Figure A.3. We collect the terms

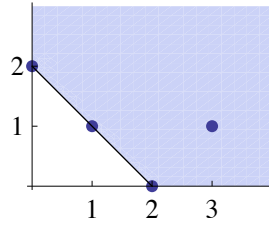


Figure A.3: Newton polygon of $F(x, 1, z)$.

corresponding to the points on the edge to get a polynomial

$$x^2 + xz(-1 - t_1) + z^2 t_1 = (x - z)(x - t_1 z),$$

whose zero locus is the local analytic curve of \bar{C}_{SW} at $[0, 1, 0]$. Note that this polynomial is reducible and has two irreducible components. This is the situation described in Figure A.1. Therefore we can see that $[0, 1, 0]$ has two preimages p_2 and p_3 on \mathcal{C}_{SW} by σ . However, this local description of the curve is not accurate enough for us to calculate R_π or (ω) . To see why this is not enough, let's focus on one of the two components, $x - t_1 z$. This gives us the following local normalization near p_3 .

$$\sigma_{p_3} : s \mapsto [x, 1, z] = [t_1 s, 1, s].$$

From this normalization we get

$$\pi_{p_3}(s) = \frac{x(s)}{z(s)} = t_1,$$

which maps the neighborhood of p_3 on \mathcal{C}_{SW} to a single point t_1 on C_B . Also,

$$\omega_{p_3} = \frac{1}{x(s)} d\left(\frac{x(s)}{z(s)}\right) = \frac{1}{t_1 s} d(t_1) = 0,$$

which does not make sense. The reason for these seemingly inconsistent results is because the local analytic curve we have now is not accurate enough to capture the true nature of $\bar{\mathcal{C}}_{\text{SW}}$. Therefore we need to include “higher-order” terms of the Puiseux expansion. To do this we first pick one of the two components that we want to improve our approximation. Let’s stick with $x - t_1 z$. The idea is to get a better approximation by including more terms of higher order. That is, we add to the previous Puiseux expansion

$$x(z) = t_1 z$$

one more term

$$x(z) = z(t_1 + x_1(z))$$

and then find such $x_1(z)$ that gives us a better approximation of the branch of $\bar{\mathcal{C}}_{\text{SW}}$. For that purpose we put this $x(z)$ into $F(x, 1, z)$. Then we get

$$F(z(t_1 + x_1), 1, z) = z^2 F_1(x_1, z),$$

where we factored out z^2 that is the common factor of every term in F . Now we draw the Newton polygon of $F_1(x_1, z)$ and do the same job as we have done so far. The Newton polygon is shown in Figure A.4. Collecting the terms on the line segment

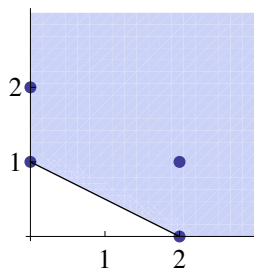


Figure A.4: Newton polygon of $F_1(x_1, z)$.

gives

$$(t_1 - 1)x_1 - ut_1z^2.$$

Setting this to zero gives $x_1(z)$, and by putting it back to $x(z)$, we get

$$x = z(t_1 + x_1(z)) = t_1z + \frac{t_1u}{t_1 - 1}z^3.$$

We now have an improved Puiseux expansion. If we want to do even better, we can iterate this process. However, as we will see below, this is enough for us for now, so we will stop here.

For the other irreducible component, $x - z$, we do a similar calculation and get the same Newton polygon and the following Puiseux expansion.

$$x = z(1 + x_1(z)) = z + \frac{u}{1 - t_1}z^3.$$

These expansions give us the following local normalizations

$$\sigma_{p_i} : s \mapsto [x, 1, z] = [b_0s + b_1s^3, 1, s],$$

where b_0 and b_1 are

$$b_0 = 1, \quad b_1 = \frac{u}{1 - t_1}$$

at p_2 and

$$b_0 = t_1, \quad b_1 = \frac{t_1u}{t_1 - 1}$$

at p_3 . From each of these local normalizations we get, near each p_i ,

$$\pi_{p_i}(s) - \pi_{p_i}(0) = \frac{x(s)}{z(s)} - b_0 \propto s^2 \Rightarrow \nu_{p_2}(\pi) = \nu_{p_3}(\pi) = 2,$$

and

$$\omega_{p_i} = \frac{1}{x(s)} d \left(\frac{x(s)}{z(s)} \right) \propto ds \Rightarrow \nu_{p_2}(\omega) = \nu_{p_3}(\omega) = 0.$$

3. Next, consider $\sigma(p_4) = [1, 0, 0]$. We start by denoting the deviations from $[1, 0, 0]$ as $[1, y, z]$. Then y and z satisfy

$$F(1, y, z) = (1 - z)(1 - t_1 z)y^2 - uz^3 = 0,$$

whose Newton polygon is shown in Figure A.5. This gives us a polynomial

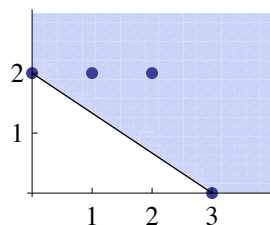


Figure A.5: Newton polygon of $F(1, y, z)$.

$$y^2 - uz^3,$$

whose zero locus is the local analytic curve of \bar{C}_{SW} at $[1, 0, 0]$. The corresponding local normalization is

$$\sigma_{p_4} : s \mapsto [1, y, z] = [1, c_0 s^3, s^2], \quad c_0 = \sqrt{u}.$$

Using this local normalization, we get

$$\frac{1}{\pi_{p_4}(s)} - \frac{1}{\pi_{p_4}(0)} = \frac{z(s)}{1} - \frac{1}{\infty} \propto s^2 \Rightarrow \nu_{p_4}(\pi) = 2,$$

where we took a reciprocal of $\pi_{p_4}(s)$ because $\pi_{p_4}(s = 0) = \pi(p_4) = \infty$. And we also find

$$\omega_{p_4} = y(s) d \left(\frac{1}{z(s)} \right) \propto ds \Rightarrow \nu_{p_4}(\omega) = 0.$$

As we have found out in Sections 3.1, for the Seiberg-Witten curve of SU(2) SCFT, $\{p_1, \dots, p_4\}$ are all the points that we need to investigate. Therefore we have all the local normalizations we need to construct R_π and ω . From the results of this subsection, we have

$$R_\pi = 1 \cdot [p_1] + 1 \cdot [p_2] + 1 \cdot [p_3] + 1 \cdot [p_4]$$

and

$$(\omega) = 0.$$

A.2.2 SU(2) \times SU(2) SCFT

The corresponding Seiberg-Witten curve C_{SW} is the zero locus of

$$f(t, v) = (t - 1)(t - t_1)(t - t_2)v^2 - u_1t^2 - u_2t.$$

We embed this into \mathbb{CP}^2 to compactify it to \bar{C}_{SW} , the zero locus of

$$F(X, Y, Z) = (X - Z)(X - t_1Z)(X - t_2Z)Y^2 - u_1X^2Z^3 - u_2XZ^4.$$

in \mathbb{CP}^2 . Now we want to get the local normalizations near

- (1) $\{p_i \in C_{\text{SW}}\}$, where $\{\phi(p_i)\}$ are the points we add to C_{SW} to compactify it,
- (2) $\{q_i \in C_{\text{SW}} | dt(q_i) = 0\} \Leftrightarrow \{q_i \in C_{\text{SW}} | (\partial f / \partial v)(t(q_i), v(q_i)) = 0\}$,
- (3) $\{r_i \in C_{\text{SW}} | v(r_i) = 0\}$.

The corresponding points on \bar{C}_{SW} are

$$\begin{aligned} \sigma(p_1) &= [0, 0, 1], \\ \sigma(p_2) &= \sigma(p_3) = \sigma(p_4) = [0, 1, 0], \\ \sigma(p_5) &= [1, 0, 0] \end{aligned}$$

from (1), and

$$\sigma(q) = [\rho, 0, 1], \quad \rho = -u_2/u_1$$

from (2). (3) does not give us any other candidate.

1. Near $\sigma(p_1) = [0, 0, 1]$, the Newton polygon of $F(x, y, 1)$ is shown in Figure A.6. This

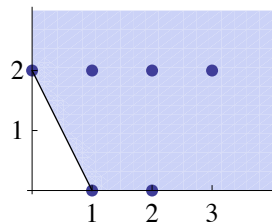


Figure A.6: Newton polygon of $F(x, y, 1)$.

gives us a polynomial

$$t_1 t_2 y^2 + u_2 x,$$

whose zero locus is the local analytic curve of \tilde{C}_{SW} at $[0, 0, 1]$. The local normalization near p_1 is

$$\sigma_{p_1} : s \mapsto [x, y, 1] = [s^2, a_0 s, 1], \quad a_0 = \sqrt{-u_2/(t_1 t_2)},$$

from which we can get

$$\begin{aligned} \pi_{p_1}(s) - \pi_{p_1}(0) &= \frac{x(s)}{1} - 0 \propto s^2 \Rightarrow \nu_{p_1}(\pi) = 2, \\ \omega_{p_1} &= \frac{y(s)}{x(s)} d(x(s)) \propto ds \quad \Rightarrow \nu_{p_1}(\omega) = 0. \end{aligned}$$

2. Near $\sigma(p_2) = \sigma(p_3) = \sigma(p_4) = [0, 1, 0]$, the Newton polygon of $F(x, 1, z)$ is shown in Figure A.7. This gives us

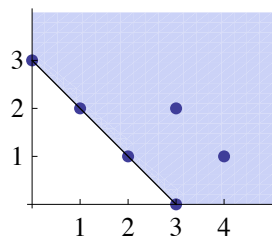


Figure A.7: Newton polygon of $F(x, 1, z)$.

$$x^3 + x^2z(-1 - t_1 - t_2) - z^3t_1t_2 + xz^2(t_1 + t_2 + t_1t_2) = (x - z)(x - t_1z)(x - t_2z),$$

whose zero locus is the local analytic curve of \bar{C}_{SW} at $[0, 1, 0]$. We see that it has three irreducible components, and that each component needs a higher-order term to calculate $\nu_{p_i}(\pi)$ and $\nu_{p_i}(\omega)$. We pick a component

$$x = b_0z.$$

By denoting the higher-order term as $x_1(z)$, now $x(z)$ is

$$x = z(b_0 + x_1(z)), \quad b_0 = \begin{cases} 1 & \text{at } p_2, \\ t_1 & \text{at } p_3, \\ t_2 & \text{at } p_4. \end{cases}$$

and by putting this back into $F(x, 1, z)$, we get

$$F(x, 1, z) = z^3F_1(x_1, z).$$

The Newton polygon of $F_1(x_1, z)$ is shown in Figure A.8. This gives us a polynomial

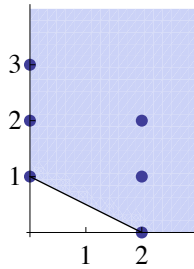


Figure A.8: Newton polygon of $F_1(x_1, z)$.

$$x_1 - b_1z^2, \quad b_1 = \begin{cases} \frac{u_1+u_2}{(1-t_1)(1-t_2)} & \text{at } p_2, \\ \frac{t_1(t_1u_1+u_2)}{(t_1-1)(t_1-t_2)} & \text{at } p_3, \\ \frac{t_2(t_2u_1+u_2)}{(t_2-1)(t_2-t_1)} & \text{at } p_4. \end{cases}$$

Therefore the Puiseux expansion at each p_i is

$$x = z(b_0 + x_1(z)) = b_0z + b_1z^3.$$

The local normalization near each p_i is

$$\sigma_{p_i} : s \mapsto [x, 1, z] = [b_0s + b_1s^3, 1, s],$$

from which we can get

$$\begin{aligned} \pi_{p_i}(s) - \pi_{p_i}(0) &= \frac{x(s)}{z(s)} - b_0 \propto s^2 \Rightarrow \nu_{p_i}(\pi) = 2, \\ \omega_{p_i} &= \frac{1}{x(s)} d\left(\frac{x(s)}{z(s)}\right) \propto ds \quad \Rightarrow \nu_{p_i}(\omega) = 0. \end{aligned}$$

3. Near $\sigma(p_5) = [1, 0, 0]$, the Newton polygon of $F(1, y, z)$ is shown in Figure A.9. This

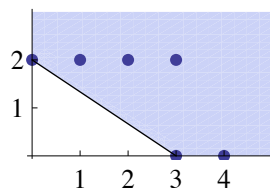


Figure A.9: Newton polygon of $F(1, y, z)$.

gives us

$$y^2 - u_1z^3$$

as the local analytic curve of \bar{C}_{SW} at $[1, 0, 0]$. The local normalization near p_5 is

$$\sigma_{p_5} : s \mapsto [1, y, z] = [1, c_0s^3, s^2], \quad c_0 = \sqrt{u_1},$$

from which we can get

$$\begin{aligned} \frac{1}{\pi_{p_5}(s)} - \frac{1}{\pi_{p_5}(0)} &= \frac{z(s)}{1} - \frac{1}{\infty} \propto s^2 \Rightarrow \nu_{p_5}(\pi) = 2, \\ \omega_{p_5} &= y(s)d\left(\frac{1}{z(s)}\right) \propto ds \quad \Rightarrow \nu_{p_5}(\omega) = 0. \end{aligned}$$

4. Near $\sigma(q) = [\rho, 0, 1]$, the Newton polygon of $F(\rho + x, y, 1)$ is shown in Figure A.10. This gives us a polynomial

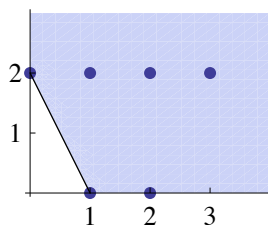


Figure A.10: Newton polygon of $F(\rho + x, y, 1)$.

$$u_2x - (\rho - 1)(\rho - t_1)(\rho - t_2)y^2,$$

whose zero locus is the local analytic curve of \bar{C}_{SW} at $[\rho, 0, 1]$. The local normalization near q is

$$\sigma_q : s \mapsto [\rho + x, y, 1] = [\rho + s^2, d_0s, 1], \quad d_0 = \sqrt{\frac{u_2}{(\rho - 1)(\rho - t_1)(\rho - t_2)}},$$

from which we can get

$$\begin{aligned} \pi_q(s) - \pi_q(0) &= \frac{\rho + x(s)}{1} - \rho \propto s^2 \Rightarrow \nu_q(\pi) = 2, \\ \omega_q &= \frac{d_0s}{\rho} d(x(s)) \propto s^2 ds \quad \Rightarrow \nu_q(\omega) = 2. \end{aligned}$$

From these results we can find out

$$\begin{aligned} R_\pi &= 1 \cdot [p_1] + 1 \cdot [p_2] + 1 \cdot [p_3] + 1 \cdot [p_4] + 1 \cdot [p_5] + 1 \cdot [q], \\ (\omega) &= 2 \cdot [q]. \end{aligned}$$

A.2.3 SU(3) SCFT

The Seiberg-Witten curve C_{SW} is the zero locus of

$$f(t, v) = (t - 1)(t - t_1)v^3 - u_2tv - u_3t.$$

We embed C_{SW} into \mathbb{CP}^2 to compactify it to \bar{C}_{SW} , which is the zero locus of

$$F(X, Y, Z) = (X - Z)(X - t_1 Z)Y^3 - u_2 X Y Z^3 - u_3 X Z^4$$

in \mathbb{CP}^2 . We want to get the local normalizations near

- (1) $\{p_i \in C_{\text{SW}}\}$, where $\{\phi(p_i)\}$ are the points we add to C_{SW} to compactify it,
- (2) $\{q_i \in C_{\text{SW}} | dt(q_i) = 0\} \Leftrightarrow \{q_i \in C_{\text{SW}} | (\partial f / \partial v)(t(q_i), v(q_i)) = 0\}$,
- (3) $\{r_i \in C_{\text{SW}} | v(r_i) = 0\}$.

The corresponding points on \bar{C}_{SW} are

$$\begin{aligned}\sigma(p_1) &= [0, 0, 1], \\ \sigma(p_2) &= \sigma(p_3) = [0, 1, 0], \\ \sigma(p_4) &= [1, 0, 0]\end{aligned}$$

from (1), and

$$\sigma(q_{\pm}) = [t_{\pm}, v_0, 1], \quad t_{\pm} = \frac{1 + t_1 + \rho}{2} \pm \sqrt{\left(\frac{1 + t_1 + \rho}{2}\right)^2 - t_1}, \quad \rho = \frac{(u_2/3)^3}{(u_3/2)^2}, \quad v_0 = -\frac{(u_3/2)}{(u_2/3)}$$

from (2). (3) does not give us any other candidate.

1. Near $\sigma(p_1) = [0, 0, 1]$, the Newton polygon of $F(x, y, 1)$ is shown in Figure A.11. This

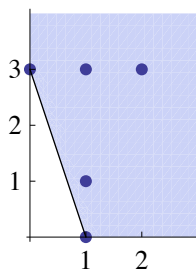


Figure A.11: Newton polygon of $F(x, y, 1)$.

gives us a polynomial

$$t_1 y^3 - u_3 x,$$

whose zero locus is the local analytic curve of \bar{C}_{SW} at $[0, 0, 1]$. The local normalization near p_1 is

$$\sigma_{p_1} : s \mapsto [x, y, 1] = [s^3, a_0 s, 1], \quad a_0 = \sqrt[3]{u_3/t_1},$$

from which we can get

$$\begin{aligned} \pi_{p_1}(s) - \pi_{p_1}(0) &= \frac{x(s)}{1} - 0 \propto s^3 \Rightarrow \nu_{p_1}(\pi) = 3, \\ \omega_{p_1} &= \frac{y(s)}{x(s)} d(x(s)) \propto ds \quad \Rightarrow \nu_{p_1}(\omega) = 0. \end{aligned}$$

2. Near $\sigma(p_2) = \sigma(p_3) = [0, 1, 0]$, the Newton polygon of $F(x, 1, z)$ is shown in Figure A.12. This gives us

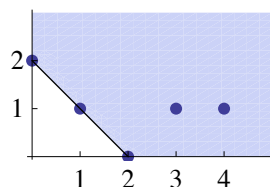


Figure A.12: Newton polygon of $F(x, 1, z)$.

$$x^2 - (1 + t_1)xz + t_1z^2 = (x - z)(x - t_1z),$$

whose zero locus is the local analytic curve of \bar{C}_{SW} at $[0, 1, 0]$. We see that it has two irreducible components, and that each component needs a higher-order term to describe \bar{C}_{SW} up to the accuracy to calculate $\nu_{p_1}(\pi)$ and $\nu_{p_1}(\omega)$. We pick a component

$$x = b_0 z, \quad b_0 = \begin{cases} 1 & \text{at } p_2, \\ t_1 & \text{at } p_3. \end{cases}$$

By denoting the higher-order term as $x_1(z)$, now $x(z)$ is

$$x = z(b_0 + x_1(z)),$$

and by putting this back into $F(x, 1, z)$, we get

$$F(x, 1, z) = z^2 F_1(x_1, z).$$

The Newton polygon of $F_1(x_1, z)$ is shown in Figure A.13. This gives us a polynomial

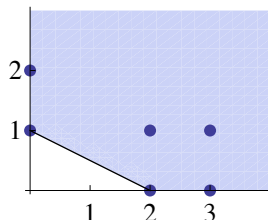


Figure A.13: Newton polygon of $F_1(x_1, z)$.

$$x_1 - b_1 z^2, \quad b_1 = \begin{cases} \frac{u_2}{1-t_1} & \text{at } p_2, \\ \frac{t_1 u_2}{t_1-1} & \text{at } p_3. \end{cases}$$

Therefore the Puiseux expansion at each p_i is

$$x = z(b_0 + x_1(z)) = b_0 z + b_1 z^3.$$

The local normalization near each p_i is

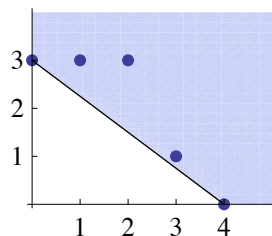
$$\sigma_{p_i} : s \mapsto [x, 1, z] = [b_0 s + b_1 s^3, 1, s],$$

from which we can get

$$\begin{aligned} \pi_{p_i}(s) - \pi_{p_i}(0) &= \frac{x(s)}{z(s)} - b_0 \propto s^2 \Rightarrow \nu_{p_i}(\pi) = 2, \\ \omega_{p_i} &= \frac{1}{x(s)} d \left(\frac{x(s)}{z(s)} \right) \propto ds \quad \Rightarrow \nu_{p_i}(\omega) = 0. \end{aligned}$$

3. Near $\sigma(p_4) = [1, 0, 0]$, the Newton polygon of $F(1, y, z)$ is shown in Figure A.14. This gives us

$$y^3 - u_3 z^4$$

Figure A.14: Newton polygon of $F(1, y, z)$.

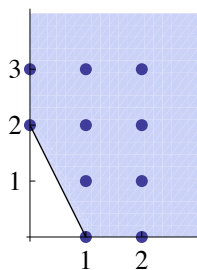
as the local analytic curve of \bar{C}_{SW} at $[1, 0, 0]$. The local normalization near p_4 is

$$\sigma_{p_4} : s \mapsto [1, y, z] = [1, c_0 s^4, s^3], \quad c_0 = \sqrt[3]{u_3},$$

from which we can get

$$\begin{aligned} \frac{1}{\pi_{p_4}(s)} - \frac{1}{\pi_{p_4}(0)} &= \frac{z(s)}{1} - \frac{1}{\infty} \propto s^3 \Rightarrow \nu_{p_4}(\pi) = 3, \\ \omega_{p_4} &= y(s)d\left(\frac{1}{z(s)}\right) \propto ds \quad \Rightarrow \nu_{p_4}(\omega) = 0. \end{aligned}$$

4. Near $\sigma(q_{\pm}) = [t_{\pm}, v_0, 1]$, the Newton polygon of $F(t_{\pm} + x, v_0 + y, 1)$ is shown in Figure A.15. This gives us a polynomial

Figure A.15: Newton polygon of $F(t_{\pm} + x, v_0 + y, 1)$.

$$\frac{1}{\rho} \left(\frac{1 + t_1 + \rho}{2} - t_{\pm} \right) x - \left(\frac{3t_{\pm}}{2v_0^2} \right) y^2,$$

whose zero locus is the local analytic curve of \bar{C}_{SW} at $[t_{\pm}, v_0, 1]$. The local normaliza-

tion near q_{\pm} is

$$\sigma_{q_{\pm}} : s \mapsto [t_{\pm} + x, v_0 + y, 1] = [t_{\pm} + s^2, v_0 + d_0 s, 1], \quad d_0 = v_0 \sqrt{\frac{2}{3\rho} \left(\frac{1 + t_1 + \rho}{2t_{\pm}} - 1 \right)},$$

from which we can get

$$\begin{aligned} \pi_{q_{\pm}}(s) - \pi_{q_{\pm}}(0) &= \frac{t_{\pm} + x(s)}{1} - t_{\pm} \propto s^2 \Rightarrow \nu_{q_{\pm}}(\pi) = 2, \\ \omega_{q_{\pm}} &= \frac{v_0}{t_{\pm}} d(x(s)) \propto s ds \quad \Rightarrow \nu_{q_{\pm}}(\omega) = 1. \end{aligned}$$

From these results we get

$$\begin{aligned} R_{\pi} &= 2 \cdot [p_1] + 1 \cdot [p_2] + 1 \cdot [p_3] + 2 \cdot [p_4] + 1 \cdot [q_+] + 1 \cdot [q_-], \\ (\omega) &= 1 \cdot [q_+] + 1 \cdot [q_-]. \end{aligned}$$

A.2.4 SU(3) pure gauge theory

The Seiberg-Witten curve C_{SW} is the zero locus of

$$f(t, v) = t^2 + (v^3 - u_2 v - u_3)t + \Lambda^6.$$

To avoid cluttered notations, let's rescale the variables in the following way:

$$\frac{t}{\Lambda^3} \rightarrow t, \quad \frac{v}{\Lambda} \rightarrow v, \quad \frac{u_k}{\Lambda^k} \rightarrow u_k. \quad (\text{A.2})$$

It is easy to restore the scale if needed, just reversing the direction of the rescaling. Then the equation that we start the usual analysis with is

$$f(t, v) = t^2 + (v^3 - u_2 v - u_3)t + 1 = tv^3 - u_2 tv + (t^2 - u_3 t + 1)$$

whose zero locus defines C_{SW} . We embed C_{SW} into \mathbb{CP}^2 to compactify it to \bar{C}_{SW} , the zero locus of

$$F(X, Y, Z) = XY^3 - u_2 XYZ^2 + (X^2 Z^2 - u_3 X Z^3 + Z^4).$$

in \mathbb{CP}^2 . We want to get the local normalizations near

- (1) $\{p_i \in \mathcal{C}_{\text{SW}}\}$, where $\{\phi(p_i)\}$ are the points we add to \mathcal{C}_{SW} to compactify it,
- (2) $\{q_i \in \mathcal{C}_{\text{SW}} | dt(q_i) = 0\} \Leftrightarrow \{q_i \in \mathcal{C}_{\text{SW}} | (\partial f / \partial v)(t(q_i), v(q_i)) = 0\}$,
- (3) $\{r_i \in \mathcal{C}_{\text{SW}} | v(r_i) = 0\}$.

The corresponding points on $\bar{\mathcal{C}}_{\text{SW}}$ are

$$\sigma(p_1) = [0, 1, 0],$$

$$\sigma(p_2) = [1, 0, 0]$$

from(1),

$$\sigma(q_{ab}) = [t_{2ab}, v_{2a}, 1], \quad a, b = \pm 1, \quad t_{2ab} = \left(v_{2a}^3 + \frac{u_3}{2}\right) + b\sqrt{\left(v_{2a}^3 + \frac{u_3}{2}\right)^2 - 1}, \quad v_{2a} = a\sqrt{\frac{u_2}{3}}.$$

from(2), and

$$\sigma(r_{\pm}) = [t_{3\pm}, 0, 1], \quad t_{3\pm} = \frac{u_3}{2} \pm \sqrt{\left(\frac{u_3}{2}\right)^2 - 1}$$

from(3).

1. Near $\sigma(p_1) = [0, 1, 0]$, the Newton polygon of $F(x, 1, z)$ is shown in Figure A.16. This

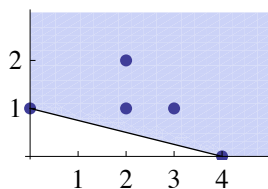


Figure A.16: Newton polygon of $F(x, 1, z)$.

gives us a polynomial

$$x + z^4,$$

whose zero locus is the local analytic curve of $\bar{\mathcal{C}}_{\text{SW}}$ at $[0, 1, 0]$. The local normalization

near p_1 is

$$\sigma_{p_1} : s \mapsto [x, 1, z] = [-s^4, 1, s],$$

from which we can get

$$\begin{aligned} \pi_{p_1}(s) - \pi_{p_1}(0) &= \frac{x(s)}{z(s)} - 0 \propto s^3 \Rightarrow \nu_{p_1}(\pi) = 3, \\ \omega_{p_1} &= \frac{1}{x(s)} d\left(\frac{x(s)}{z(s)}\right) \propto \frac{ds}{s^2} \Rightarrow \nu_{p_1}(\omega) = -2. \end{aligned}$$

2. Near $p_2 = [1, 0, 0]$, the Newton polygon of $F(1, y, z)$ is shown in Figure A.17. This

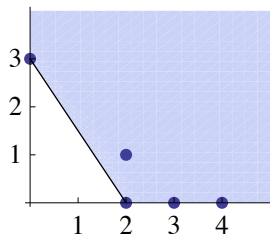


Figure A.17: Newton polygon of $F(1, y, z)$.

gives us

$$y^3 + z^2$$

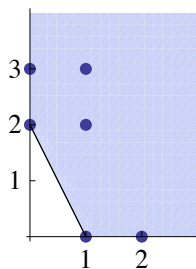
as the local analytic curve of \bar{C}_{SW} at $[1, 0, 0]$. The local normalization near p_2 is

$$\sigma_{p_2} : s \mapsto [1, y, z] = [1, -s^2, s^3],$$

from which we can get

$$\begin{aligned} \frac{1}{\pi_{p_2}(s)} - \frac{1}{\pi_{p_2}(0)} &= \frac{z(s)}{1} - \frac{1}{\infty} \propto s^3 \Rightarrow \nu_{p_2}(\pi) = 3, \\ \omega_{p_2} &= y(s) d\left(\frac{1}{z(s)}\right) \propto \frac{ds}{s^2} \Rightarrow \nu_{p_2}(\omega) = -2. \end{aligned}$$

3. Near $q_{ab} = [t_{2ab}, v_{2a}, 1]$, the Newton polygon of $F(t_{2ab} + x, v_{2a} + y, 1)$ is shown in Figure A.18. This gives us a polynomial

Figure A.18: Newton polygon of $F(t_{2ab} + x, v_{2a} + y, 1)$.

$$\left(2b\sqrt{\left(v_{2a}^3 + \frac{u_3}{2}\right)^2 - 1}\right)x + 3v_{2a}t_{2ab}y^2,$$

whose zero locus is the local analytic curve of \tilde{C}_{SW} at $[t_{2ab}, v_{2a}, 1]$. The local normalization near q_{ab} is

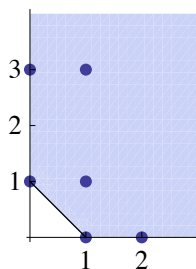
$$\begin{aligned} \sigma_{q_{ab}} : s &\mapsto [t_{2ab} + x, v_{2a} + y, 1] = [t_{2ab} + s^2, v_{2a} + c_0s, 1], \\ c_0 &= \sqrt{-\frac{2b}{3v_{2a}t_{2ab}}\sqrt{\left(v_{2a}^3 + \frac{u_3}{2}\right)^2 - 1}}. \end{aligned}$$

from which we can get

$$\begin{aligned} \pi_{q_{ab}}(s) - \pi_{q_{ab}}(0) &= \frac{t_{2ab} + x(s)}{1} - t_{2ab} \propto s^2 \Rightarrow \nu_{q_{ab}}(\pi) = 2, \\ \omega_{q_{ab}} &= \frac{v_{2a}}{t_{2ab}}d(x(s)) \propto sds \Rightarrow \nu_{q_{ab}}(\omega) = 1. \end{aligned}$$

4. Near $r_{\pm} = [t_{3\pm}, 0, 1]$, the Newton polygon of $F(t_{3\pm} + x, y, 1)$ is shown in Figure A.19.

This gives us a polynomial

Figure A.19: Newton polygon of $F(t_{3\pm} + x, y, 1)$.

$$2 \left(t_{3\pm} - \frac{u_3}{2} \right) x - u_2 t_{3\pm} y,$$

whose zero locus is the local analytic curve of \bar{C}_{SW} at $[t_{3\pm}, 0, 1]$. The local normalization near r_{\pm} is

$$\sigma_{r_{\pm}} : s \mapsto [t_{3\pm} + x, y, 1] = [t_{3\pm} + s, d_0 s, 1], \quad d_0 = \frac{1}{u_2} \left(2 - \frac{u_3}{t_{3\pm}} \right).$$

from which we can get

$$\begin{aligned} \pi_{r_{\pm}}(s) - \pi_{r_{\pm}}(0) &= \frac{t_{3\pm} + x(s)}{1} - t_{3\pm} \propto s \Rightarrow \nu_{r_{\pm}}(\pi) = 1, \\ \omega_{r_{\pm}} &= \frac{y(s)}{t_{3\pm}} d(x(s)) \propto s ds \quad \Rightarrow \nu_{r_{\pm}}(\omega) = 1. \end{aligned}$$

From these results we can find out

$$\begin{aligned} R_{\pi} &= 2 \cdot [p_1] + 2 \cdot [p_2] + 1 \cdot [q_{++}] + 1 \cdot [q_{+-}] + 1 \cdot [q_{-+}] + 1 \cdot [q_{--}], \\ (\omega) &= -2 \cdot [p_1] - 2 \cdot [p_2] + 1 \cdot [q_{++}] + 1 \cdot [q_{+-}] + 1 \cdot [q_{-+}] + 1 \cdot [q_{--}] + 1 \cdot [r_+] + 1 \cdot [r_-]. \end{aligned}$$

Appendix B

On Kazama-Suzuki models and their Landau-Ginzburg descriptions

The Kazama-Suzuki model [65] is a coset model G_k/H where G is a compact simple simply connected Lie group, H is its closed subgroup of the same rank as G such that the space G/H of left cosets is Kähler; k is a positive integer. It can be realized as a gauge theory [96]: the gauge group is H and the matter theory is the direct product of the G_k Wess-Zumino-Witten model and the $\mathfrak{g}/\mathfrak{h}$ -valued free fermion, where H acts on G and $\mathfrak{g}/\mathfrak{h}$ by the conjugation. The models relevant for us are a subclass of

$$\frac{\mathrm{SU}(m+n)_k}{\mathrm{S}[\mathrm{U}(m) \times \mathrm{U}(n)]} \quad (\mathrm{B}.1)$$

with the central charge

$$\hat{c} = \frac{c}{3} = \frac{kmn}{k+m+n}. \quad (\mathrm{B}.2)$$

This model is invariant under permutations of k, m, n [65]. The model with $m = n = 1$, i.e., $\mathrm{SU}(2)_k/\mathrm{U}(1)$, is equivalent to the $\mathcal{N} = 2$ A_k minimal model [97]. The model with $m = 1$, $n = N - k$, i.e.,

$$\frac{\mathrm{SU}(N)_1}{\mathrm{S}[\mathrm{U}(k) \times \mathrm{U}(N-k)]}, \quad (\mathrm{B}.3)$$

is believed [74, 63] to be equivalent to the IR fixed point of a Landau-Ginzburg model with a superpotential $W(x_1, \dots, x_k)$ which is chosen so that

$$W(x_1, \dots, x_n) = \sum_{b=1}^k \sigma_b^N, \quad (\text{B.4})$$

where σ_b are auxiliary variables such that x_b are their elementary symmetric polynomials:

$$x_b = \sum_{1 \leq l_1 < l_2 < \dots < l_b \leq k} \sigma_{l_1} \sigma_{l_2} \cdots \sigma_{l_b}. \quad (\text{B.5})$$

One piece of evidence of the equivalence comes from computing the central charge and the spectrum of the operators on each side and matching them. In addition, when $k > N - k$, we can re-express everything in terms of $N - k$ chiral fields, which implies $k \leftrightarrow N - k$ duality [63]. Another nontrivial evidence comes from the calculation of elliptic genera in the two descriptions, which yields agreement [98, 99].

Appendix C

SCFTs of Argyres-Douglas type

C.1 $\mathcal{S}[A_{N-1}; \mathcal{D}_I]$ theories from $SU(N)$ pure SYM

The M-theory curve of $\mathcal{N} = 2$ $SU(N)$ pure SYM theory is

$$\Lambda^N t^2 + P_N(v)t + \Lambda^N = 0, \quad (\text{C.1})$$

where $P_N = v^N + \sum_{i=2}^N u_i v^{N-i}$ and u_i are the Coulomb moduli parameters. By setting $v = xt$, we get the following form of the curve:

$$x^N + \sum_{i=2}^N \phi_i(t) x^{N-i} = 0, \quad (\text{C.2})$$

where

$$\phi_i = \frac{u_i}{t^i}, \quad (i = 2, \dots, N-1), \quad \text{and} \quad \phi_N = \frac{\Lambda^N}{t^{N+1}} + \frac{u_N}{t^N} + \frac{\Lambda^N}{t^{N-1}}. \quad (\text{C.3})$$

The Seiberg-Witten differential is $\lambda = x dt$. This denotes that there are two irregular singularities at $t = 0$ and $t = \infty$.

The maximal conformal point is at $u_i = \pm 2\Lambda^{2N} \delta^{iN}$ (we choose the minus sign here), at which the curve becomes

$$x^N + \frac{\Lambda^N}{t^{N+1}} (t-1)^2 = 0. \quad (\text{C.4})$$

To consider the small deformation from this point, let us define the parameters as $u_i =$

$\hat{u}_i - 2\Lambda^{2N}\delta^{iN}$ by which the curve is

$$x^N + \frac{\Lambda^N}{t^{N+1}}(t-1)^2 + \sum_{i=2}^N \frac{\hat{u}_i}{t^i} x^{N-i} = 0. \quad (\text{C.5})$$

Let us look at the region close to $t = 1$. To do this, we introduce the new coordinate $\tilde{t} = (t-1)\Lambda^a$ with $a > 0$ and take the limit $\Lambda \rightarrow \infty$. This is written as $t = 1 + \frac{\tilde{t}}{\Lambda^a}$. The SW differential is now written as $\lambda = \frac{x}{\Lambda^a} d\tilde{t}$, so we define $\tilde{x} = \frac{x}{\Lambda^a}$ such that the differential is of canonical form. The curve in terms of these coordinates is written as

$$\tilde{x}^N + \Lambda^{N-(2+N)a}\tilde{t}^2 + \sum_{i=2}^N \frac{\hat{u}_i}{\Lambda^{ia}(1 + \mathcal{O}(\Lambda^{-a}))^i} \tilde{x}^{N-i} = 0. \quad (\text{C.6})$$

We want to keep the second term finite which means $a = \frac{N}{N+2}$. In order for the deformation terms to be finite, we also have

$$\hat{u}_i = \Lambda^{\frac{N}{N+2}i} c_i, \quad (\text{C.7})$$

where $i = 2, \dots, N$. We can easily see that the scaling dimension of c_i is $\frac{2i}{N+2}$. Let us define $v_i = c_{N-i+2}$ for $i = 2, \dots, [\frac{N+1}{2}]$ such that the dimensions are

$$\Delta(v_i) = 2 - \frac{2i}{N+2}, \quad \Delta(c_i) = \frac{2i}{N+2}. \quad (\text{C.8})$$

for $i = 2, \dots, [\frac{N+1}{2}]$. Note that they satisfy $\Delta(v_i) + \Delta(v_i) = 2$. When $N = 2k$, there is a mass parameter c_{k+1} with dimension 1. The final form of the curve is

$$\tilde{x}^N + \sum_{i=2}^N \phi_i(t) \tilde{x}^{N-i} = 0, \quad (\text{C.9})$$

where

$$\begin{aligned} \phi_i &= c_i, \quad (i = 2, \dots, [\frac{N+2}{2}]), \\ \phi_i &= v_{N-i+2}, \quad (i = [\frac{N+2}{2}] + 1, \dots, N-1), \quad \text{and} \quad \phi_N = \tilde{t}^2 + v_2. \end{aligned} \quad (\text{C.10})$$

C.2 $\mathcal{S}[A_{N-1}; \mathcal{D}_{\text{II}}]$ from $\text{SU}(N)$ with $N_f = 2$

The Seiberg-Witten curve of $\text{SU}(N)$ gauge theory with two flavors with masses $m_{1,2}$ is

$$\Lambda^{N-1}(v - m_1)t^2 + P_N(v)t + \Lambda^{N-1}(v - m_2) = 0. \quad (\text{C.11})$$

The most singular point of this curve is at

$$u_k = \pm 2\Lambda^{N-1}\delta_{k,N-1}, \quad m_1 = m_2 = 0. \quad (\text{C.12})$$

Indeed the curve is factorized at this point into

$$x^N + x\Lambda^{N-1}\frac{(t \pm 1)^2}{t^N} = 0, \quad (\text{C.13})$$

where $v = xt$.

We parameterized the parameters as $u_k = -2\Lambda^2 + \hat{u}_k$ and the coordinate as $\Lambda^a(t-1) = \tilde{t}$. The SW differential is $\lambda = x dt = \tilde{x} d\tilde{t}$ where $\tilde{x} = \frac{x}{\Lambda^a}$. By substituting these into the curve we obtain $a = \frac{N-1}{N+1}$ in order to keep the second term in (C.13) finite. Therefore we obtain the curve of the form (C.9) where

$$\begin{aligned} \phi_i &= c_i, \quad (i = 2, \dots, [\frac{N+1}{2}]) \\ \phi_i &= v_{N-i+1}, \quad (i = [\frac{N+1}{2}] + 1, \dots, N-2) \\ \phi_{N-1} &= \tilde{t}^2 + v_2, \quad \phi_N = c_1\tilde{t}^2 + C_2\tilde{t} + v_1, \end{aligned} \quad (\text{C.14})$$

where the last terms have been obtained from the expansion of x^0 terms

$$\frac{1}{\Lambda^{Na}} \left(-\frac{m_2\Lambda^{N-1}}{(1 + \tilde{t}/\Lambda^a)^{N+1}} + \frac{\hat{u}_N}{(1 + \tilde{t}/\Lambda^a)^N} - \frac{m_1\Lambda^{N-1}}{(1 + \tilde{t}/\Lambda^a)^{N-1}} \right). \quad (\text{C.15})$$

The dimensions of the parameters are easily obtained as

$$\Delta(v_i) = 2 - \frac{2i}{N+1}, \quad \Delta(c_i) = \frac{2i}{N+1}, \quad \Delta(C_1) = \Delta(C_2) = 1, \quad (\text{C.16})$$

for $i = 1, \dots, [N/2]$, where $C_1 := c_{[(N+1)/2]}$ with dimension-one exists only when N is odd.

C.3 $\mathcal{S}[A_2; \mathcal{D}_{\text{reg}}, \mathcal{D}_{\text{III}}]$ from SU(3) with $N_f = 3$

Let us next consider the AD point of SU(3) with $N_f = 3$. The Seiberg-Witten curve is given by

$$\begin{aligned}\phi_2 &= -\frac{m_+^2}{3(t-1)^2} + \frac{C_2}{t^2} + \frac{u_2}{t^2(t-1)}, \\ \phi_3 &= \frac{2m_+^3}{27(t-1)^3} + \frac{\Lambda^3}{t^4} + \frac{C_3 - \frac{2C_2m_+}{3}}{t^3} + \frac{u_3}{t^3(t-1)} - \frac{u_2m_+}{3t^2(t-1)^2}.\end{aligned}\quad (\text{C.17})$$

There are a simple regular puncture at $t = 1$ and a full regular puncture at $t = \infty$. The puncture at $t = 0$ is irregular of $\{2, 4\}$, which corresponds to no hypermultiplet.

We first consider ϕ_2 whose expansion is, by setting $t = \Lambda^a w$,

$$\Lambda^{2a} \left(\frac{C_2 - m_+^2/3}{\Lambda^{2a} w^2} + \frac{u_2 - 2m_+^2/3}{\Lambda^{3a} w^3} + \frac{u_2 - m_+^2}{\Lambda^{4a} w^4} + \dots \right).\quad (\text{C.18})$$

Let m_+ be finite parameter here. It follows that the second term can be kept finite by $u_2 = \Lambda^a v$ and the higher order terms are suppressed. So, we get

$$\phi_2 = \frac{C_2 - m_+^2/3}{w^2} + \frac{v}{w^3}.\quad (\text{C.19})$$

We next consider ϕ_3 whose expansion is

$$\Lambda^{3a} \left(\frac{C_3 - \frac{C_2m_+}{3} + \frac{2m_+^3}{27}}{\Lambda^{3a} w^3} + \frac{\frac{2m_+^3}{9} + \Lambda^3 + u_3 - \frac{u_2m_+}{3}}{\Lambda^{4a} w^4} + \frac{\frac{4m_+^3}{9} + u_3 - \frac{2u_2m_+}{3}}{\Lambda^{5a} w^5} + \dots \right).\quad (\text{C.20})$$

Since m_+ is finite and $u_2 \sim \Lambda^a$, in order to have $1/w^5$ term we need to set $u_3 = -\Lambda^3 + \Lambda^{3/2} v_2$ and $a = 3/2$. By this, we get

$$\phi_3 = \frac{C_3 - \frac{C_2m_+}{3} + \frac{2m_+^3}{27}}{w^3} + \frac{v_2}{w^4} - \frac{1}{w^5}.\quad (\text{C.21})$$

The dimensions of the parameters are

$$\Delta(C_3) = 3, \quad \Delta(C_2) = 2, \quad \Delta(m_+) = 1, \quad \Delta(v_1) = \frac{3}{2}, \quad \Delta(v_2) = \frac{1}{2}.\quad (\text{C.22})$$

These are the same as those of the class 2 SCFT of SU(3) with $N_f = 3$ in [95].

In terms of a Riemann surface, this AD point corresponds to a sphere with one regular full puncture at $t = \infty$ and one irregular puncture of $\{3, 5\}$. Note that these degrees are lower than those of the two hypermultiplets, which is $\{4, 6\}$.

By the transformation $w \rightarrow 1/w$, the Seiberg-Witten curve is

$$\begin{aligned}\phi_2 &= \frac{v}{w} + \frac{C_2 - m_+^2/3}{w^2}, \\ \phi_3 &= \frac{1}{w} - \frac{v_2}{w^2} - \frac{C_3 - \frac{C_2 m_+}{3} + \frac{2m_+^3}{27}}{w^3}\end{aligned}\tag{C.23}$$

where the regular puncture is at $t = 0$ and the irregular puncture is at $t = \infty$. The Seiberg-Witten differential is $\lambda = x dw$, where $x^3 + \phi_2 x + \phi_3 = 0$.

Bibliography

- [1] N. Seiberg, *Supersymmetry and Nonperturbative beta Functions*, *Phys.Lett.* **B206** (1988) 75.
- [2] N. Seiberg and E. Witten, *Monopoles, duality and chiral symmetry breaking in $N=2$ supersymmetric QCD*, *Nucl. Phys.* **B431** (1994) 484–550, [[hep-th/9408099](#)].
- [3] N. Seiberg and E. Witten, *Monopole Condensation, And Confinement In $N=2$ Supersymmetric Yang-Mills Theory*, *Nucl. Phys.* **B426** (1994) 19–52, [[hep-th/9407087](#)].
- [4] P. C. Argyres and M. R. Douglas, *New phenomena in $SU(3)$ supersymmetric gauge theory*, *Nucl. Phys.* **B448** (1995) 93–126, [[hep-th/9505062](#)].
- [5] D. Gaiotto, *$N=2$ dualities*, [arXiv:0904.2715](#).
- [6] A. Klemm, W. Lerche, P. Mayr, C. Vafa, and N. P. Warner, *Self-Dual Strings and $N=2$ Supersymmetric Field Theory*, *Nucl. Phys.* **B477** (1996) 746–766, [[hep-th/9604034](#)].
- [7] E. Witten, *Solutions of Four-Dimensional Field Theories via M-theory*, *Nucl. Phys.* **B500** (1997) 3–42, [[hep-th/9703166](#)].
- [8] A. Fayyazuddin and M. Spalinski, *The Seiberg-Witten differential from M-theory*, *Nucl. Phys.* **B508** (1997) 219–228, [[hep-th/9706087](#)].
- [9] M. Henningson and P. Yi, *Four-dimensional BPS spectra via M theory*, *Phys.Rev.* **D57** (1998) 1291–1298, [[hep-th/9707251](#)].
- [10] A. Mikhailov, *BPS states and minimal surfaces*, *Nucl. Phys.* **B533** (1998) 243–274, [[hep-th/9708068](#)].

- [11] A. Karch, D. Lust, and D. J. Smith, *Equivalence of geometric engineering and Hanany-Witten via fractional branes*, *Nucl. Phys.* **B533** (1998) 348–372, [[hep-th/9803232](#)].
- [12] H. Ooguri and C. Vafa, *Two-Dimensional Black Hole and Singularities of CY Manifolds*, *Nucl. Phys.* **B463** (1996) 55–72, [[hep-th/9511164](#)].
- [13] D. Tong, *NS5-branes, T-duality and worldsheet instantons*, *JHEP* **07** (2002) 013, [[hep-th/0204186](#)].
- [14] J. A. Harvey and S. Jensen, *Worldsheet instanton corrections to the Kaluza-Klein monopole*, *JHEP* **10** (2005) 028, [[hep-th/0507204](#)].
- [15] C. Y. Park, *Ramification Points of Seiberg-Witten Curves*, *JHEP* **07** (2011) 068, [[arXiv:1102.0288](#)].
- [16] P. C. Argyres and N. Seiberg, *S-duality in $N=2$ supersymmetric gauge theories*, *JHEP* **12** (2007) 088, [[arXiv:0711.0054](#)].
- [17] F. Kirwan, *Complex Algebraic Curves*. Cambridge University Press, 1992.
- [18] P. A. Griffiths, *Introduction to Algebraic Curves*. American Mathematical Society, 1989.
- [19] D. Gaiotto, G. W. Moore, and A. Neitzke, *Wall-crossing, Hitchin Systems, and the WKB Approximation*, [arXiv:0907.3987](#).
- [20] T. J. Hollowood, *Strong coupling $N = 2$ gauge theory with arbitrary gauge group*, *Adv. Theor. Math. Phys.* **2** (1998) 335–355, [[hep-th/9710073](#)].
- [21] P. C. Argyres, M. R. Plesser, N. Seiberg, and E. Witten, *New $N=2$ Superconformal Field Theories in Four Dimensions*, *Nucl. Phys.* **B461** (1996) 71–84, [[hep-th/9511154](#)].
- [22] P. C. Argyres and A. E. Faraggi, *The vacuum structure and spectrum of $N=2$ supersymmetric $SU(n)$ gauge theory*, *Phys. Rev. Lett.* **74** (1995) 3931–3934, [[hep-th/9411057](#)].

- [23] A. Klemm, W. Lerche, S. Yankielowicz, and S. Theisen, *Simple singularities and $N=2$ supersymmetric Yang-Mills theory*, *Phys. Lett.* **B344** (1995) 169–175, [[hep-th/9411048](#)].
- [24] P. C. Argyres, M. R. Plesser, and A. D. Shapere, *The Coulomb phase of $N=2$ supersymmetric QCD*, *Phys. Rev. Lett.* **75** (1995) 1699–1702, [[hep-th/9505100](#)].
- [25] A. Hanany and Y. Oz, *On the Quantum Moduli Space of Vacua of $N = 2$ Supersymmetric $SU(N_c)$ Gauge Theories*, *Nucl. Phys.* **B452** (1995) 283–312, [[hep-th/9505075](#)].
- [26] U. H. Danielsson and B. Sundborg, *The Moduli space and monodromies of $N=2$ supersymmetric $SO(2r+1)$ Yang-Mills theory*, *Phys. Lett.* **B358** (1995) 273–280, [[hep-th/9504102](#)].
- [27] A. Brandhuber and K. Landsteiner, *On the monodromies of $N=2$ supersymmetric Yang-Mills theory with gauge group $SO(2n)$* , *Phys. Lett.* **B358** (1995) 73–80, [[hep-th/9507008](#)].
- [28] P. C. Argyres and A. D. Shapere, *The Vacuum Structure of $N=2$ SuperQCD with Classical Gauge Groups*, *Nucl. Phys.* **B461** (1996) 437–459, [[hep-th/9509175](#)].
- [29] E. J. Martinec and N. P. Warner, *Integrable systems and supersymmetric gauge theory*, *Nucl. Phys.* **B459** (1996) 97–112, [[hep-th/9509161](#)].
- [30] K. Hori, C. Y. Park, and Y. Tachikawa, *2d SCFTs from M2-branes*, [arXiv:1309.3036](#).
- [31] A. Hanany and K. Hori, *Branes and $N = 2$ theories in two dimensions*, *Nucl. Phys.* **B513** (1998) 119–174, [[hep-th/9707192](#)].
- [32] E. Witten, *Phases of $N=2$ theories in two-dimensions*, *Nucl.Phys.* **B403** (1993) 159–222, [[hep-th/9301042](#)].
- [33] E. Witten and D. I. Olive, *Supersymmetry Algebras That Include Topological Charges*, *Phys.Lett.* **B78** (1978) 97.

- [34] P. Fendley, S. Mathur, C. Vafa, and N. Warner, *Integrable deformations and scattering matrices for the $N=2$ supersymmetric discrete series*, *Phys.Lett.* **B243** (1990) 257–264.
- [35] S. Cecotti and C. Vafa, *On classification of $N=2$ supersymmetric theories*, *Commun.Math.Phys.* **158** (1993) 569–644, [[hep-th/9211097](#)].
- [36] A. D’Adda, A. Davis, P. Di Vecchia, and P. Salomonson, *An Effective Action for the Supersymmetric CP^{n-1} Model*, *Nucl.Phys.* **B222** (1983) 45.
- [37] D. Gaiotto, G. W. Moore, and A. Neitzke, *Spectral networks*, [arXiv:1204.4824](#).
- [38] N. Dorey, *The BPS spectra of two-dimensional supersymmetric gauge theories with twisted mass terms*, *JHEP* **9811** (1998) 005, [[hep-th/9806056](#)].
- [39] N. Dorey, T. J. Hollowood, and D. Tong, *The BPS spectra of gauge theories in two-dimensions and four-dimensions*, *JHEP* **9905** (1999) 006, [[hep-th/9902134](#)].
- [40] D. Gaiotto, G. W. Moore, and A. Neitzke, *Wall-Crossing in Coupled 2d-4d Systems*, [arXiv:1103.2598](#).
- [41] J. Barbon, *Rotated branes and $N=1$ duality*, *Phys.Lett.* **B402** (1997) 59–63, [[hep-th/9703051](#)].
- [42] S. Elitzur, A. Giveon, and D. Kutasov, *Branes and $N=1$ duality in string theory*, *Phys.Lett.* **B400** (1997) 269–274, [[hep-th/9702014](#)].
- [43] S. Elitzur, A. Giveon, D. Kutasov, E. Rabinovici, and A. Schwimmer, *Brane dynamics and $N=1$ supersymmetric gauge theory*, *Nucl.Phys.* **B505** (1997) 202–250, [[hep-th/9704104](#)].
- [44] A. Giveon and D. Kutasov, *Brane dynamics and gauge theory*, *Rev.Mod.Phys.* **71** (1999) 983–1084, [[hep-th/9802067](#)].
- [45] K. Hori, S. Katz, A. Klemm, R. Pandharipande, R. Thomas, et al., *Mirror symmetry*. the American Mathematical Society, 2003.
- [46] J. H. Brodie, *Two-dimensional mirror symmetry from M theory*, *Nucl.Phys.* **B517** (1998) 36–52, [[hep-th/9709228](#)].

- [47] D.-E. Diaconescu and N. Seiberg, *The Coulomb branch of (4,4) supersymmetric field theories in two-dimensions*, *JHEP* **9707** (1997) 001, [[hep-th/9707158](#)].
- [48] E. Witten, *Instantons, the Quark Model, and the 1/n Expansion*, *Nucl.Phys.* **B149** (1979) 285.
- [49] D. Tong, *Superconformal vortex strings*, *JHEP* **0612** (2006) 051, [[hep-th/0610214](#)].
- [50] A. Hanany and E. Witten, *Type IIB superstrings, BPS monopoles, and three-dimensional gauge dynamics*, *Nucl. Phys.* **B492** (1997) 152–190, [[hep-th/9611230](#)].
- [51] A. Hanany and D. Tong, *Vortex strings and four-dimensional gauge dynamics*, *JHEP* **0404** (2004) 066, [[hep-th/0403158](#)].
- [52] N. A. Nekrasov and S. L. Shatashvili, *Supersymmetric vacua and Bethe ansatz*, *Nucl.Phys.Proc.Suppl.* **192-193** (2009) 91–112, [[arXiv:0901.4744](#)].
- [53] N. A. Nekrasov and S. L. Shatashvili, *Quantization of Integrable Systems and Four Dimensional Gauge Theories*, [arXiv:0908.4052](#).
- [54] A. D. Shapere and C. Vafa, *BPS structure of Argyres-Douglas superconformal theories*, [hep-th/9910182](#).
- [55] D. Gaiotto, G. W. Moore, and A. Neitzke, *Framed BPS States*, [arXiv:1006.0146](#).
- [56] S. R. Coleman, *More About the Massive Schwinger Model*, *Annals Phys.* **101** (1976) 239.
- [57] A. Ritz, *Superconformal R-charges and dyon multiplicities in N=2 gauge theories*, *Phys.Rev.* **D75** (2007) 085008, [[hep-th/0612077](#)].
- [58] P. A. Bolokhov, M. Shifman, and A. Yung, *2D-4D Correspondence: Towers of Kinks versus Towers of Monopoles in N=2 Theories*, *Phys.Rev.* **D85** (2012) 085028, [[arXiv:1202.5612](#)].
- [59] N. Dorey and K. Petunin, *On the BPS Spectrum at the Root of the Higgs Branch*, *JHEP* **1205** (2012) 085, [[arXiv:1202.5595](#)].
- [60] J. de Boer and Y. Oz, *Monopole condensation and confining phase of N=1 gauge theories via M theory five-brane*, *Nucl.Phys.* **B511** (1998) 155–196, [[hep-th/9708044](#)].

- [61] D. Tong, *TASI lectures on solitons: Instantons, monopoles, vortices and kinks*, [hep-th/0509216](#).
- [62] E. Witten, *The Verlinde algebra and the cohomology of the Grassmannian*, [hep-th/9312104](#).
- [63] D. Gepner, *Scalar Field Theory And String Compactification*, *Nucl.Phys.* **B322** (1989) 65.
- [64] K. Hori, *Duality In Two-Dimensional (2,2) Supersymmetric Non-Abelian Gauge Theories*, [arXiv:1104.2853](#).
- [65] Y. Kazama and H. Suzuki, *New $N=2$ Superconformal Field Theories and Superstring Compactification*, *Nucl.Phys.* **B321** (1989) 232.
- [66] Y. Kazama and H. Suzuki, *Characterization of $N=2$ Superconformal Models Generated by Coset Space Method*, *Phys.Lett.* **B216** (1989) 112.
- [67] F. Benini and S. Cremonesi, *Partition functions of $N=(2,2)$ gauge theories on S^2 and vortices*, [arXiv:1206.2356](#).
- [68] N. Doroud, J. Gomis, B. Le Floch, and S. Lee, *Exact Results in $D=2$ Supersymmetric Gauge Theories*, [arXiv:1206.2606](#).
- [69] J. Gomis and S. Lee, *Exact Kahler Potential from Gauge Theory and Mirror Symmetry*, [arXiv:1210.6022](#).
- [70] D. Honda and T. Okuda, *Exact Results for Boundaries and Domain Walls in 2D Supersymmetric Theories*, [arXiv:1308.2217](#).
- [71] K. Hori and M. Romo, *Exact Results In Two-Dimensional (2,2) Supersymmetric Gauge Theories With Boundary*, [arXiv:1308.2438](#).
- [72] E. Witten, *Constraints on Supersymmetry Breaking*, *Nucl.Phys.* **B202** (1982) 253.
- [73] K. Hori and D. Tong, *Aspects of Non-Abelian Gauge Dynamics in Two-Dimensional $N=(2,2)$ Theories*, *JHEP* **0705** (2007) 079, [[hep-th/0609032](#)].
- [74] W. Lerche, C. Vafa, and N. P. Warner, *Chiral Rings in $N=2$ Superconformal Theories*, *Nucl.Phys.* **B324** (1989) 427.

- [75] W. Lerche and N. Warner, *Polytopes and solitons in integrable, $N=2$ supersymmetric Landau-Ginzburg theories*, *Nucl.Phys.* **B358** (1991) 571–599.
- [76] E. Witten, *Branes and the dynamics of QCD*, *Nucl.Phys.* **B507** (1997) 658–690, [[hep-th/9706109](#)].
- [77] K. Becker, M. Becker, and A. Strominger, *Five-branes, membranes and nonperturbative string theory*, *Nucl.Phys.* **B456** (1995) 130–152, [[hep-th/9507158](#)].
- [78] J. Gomis, Private communication. March 1-3, 2013.
- [79] S. Lee, talks at *Geometry and Physics of the Gauged Linear Sigma Model*, Univ. Michigan, March 4-8, 2013 and at *Strings 2013*, Seoul, June 24-28, 2013.
- [80] E. J. Martinec, *Algebraic Geometry and Effective Lagrangians*, *Phys.Lett.* **B217** (1989) 431.
- [81] C. Vafa and N. P. Warner, *Catastrophes and the Classification of Conformal Theories*, *Phys.Lett.* **B218** (1989) 51.
- [82] S. Cecotti and C. Vafa, *Topological antitopological fusion*, *Nucl.Phys.* **B367** (1991) 359–461.
- [83] S. Cecotti, A. Neitzke, and C. Vafa, *R-Twisting and $4d/2d$ Correspondences*, [arXiv:1006.3435](#).
- [84] S. Cecotti and C. Vafa, *Classification of complete $N=2$ supersymmetric theories in 4 dimensions*, *Surveys in differential geometry, vol 18* (2013) [[arXiv:1103.5832](#)].
- [85] M. Alim, S. Cecotti, C. Cordova, S. Espahbodi, A. Rastogi, et al., *BPS Quivers and Spectra of Complete $N=2$ Quantum Field Theories*, [arXiv:1109.4941](#).
- [86] G. Bonelli, K. Maruyoshi, and A. Tanzini, *Wild Quiver Gauge Theories*, *JHEP* **1202** (2012) 031, [[arXiv:1112.1691](#)].
- [87] D. Xie, *General Argyres-Douglas Theory*, *JHEP* **1301** (2013) 100, [[arXiv:1204.2270](#)].
- [88] S. Cecotti and M. Del Zotto, *Infinitely many $N=2$ SCFT with ADE flavor symmetry*, *JHEP* **1301** (2013) 191, [[arXiv:1210.2886](#)].

- [89] H. Kanno, K. Maruyoshi, S. Shiba, and M. Taki, *W_3 irregular states and isolated $N=2$ superconformal field theories*, *JHEP* **1303** (2013) 147, [[arXiv:1301.0721](#)].
- [90] S. Cecotti, M. Del Zotto, and S. Giacomelli, *More on the $N=2$ superconformal systems of type $D_p(G)$* , [arXiv:1303.3149](#).
- [91] D. Gaiotto, G. W. Moore, and A. Neitzke, *Spectral Networks and Snakes*, [arXiv:1209.0866](#).
- [92] P. C. Argyres, K. Maruyoshi, and Y. Tachikawa, *Quantum Higgs branches of isolated $N=2$ superconformal field theories*, *JHEP* **1210** (2012) 054, [[arXiv:1206.4700](#)].
- [93] A. D. Shapere and Y. Tachikawa, *Central charges of $N=2$ superconformal field theories in four dimensions*, *JHEP* **0809** (2008) 109, [[arXiv:0804.1957](#)].
- [94] D. Xie and P. Zhao, *Central charges and RG flow of strongly-coupled $N=2$ theory*, *JHEP* **1303** (2013) 006, [[arXiv:1301.0210](#)].
- [95] T. Eguchi, K. Hori, K. Ito, and S.-K. Yang, *Study of $N=2$ superconformal field theories in four-dimensions*, *Nucl.Phys.* **B471** (1996) 430–444, [[hep-th/9603002](#)].
- [96] E. Witten, *The N matrix model and gauged WZW models*, *Nucl.Phys.* **B371** (1992) 191–245.
- [97] J. H. Schwarz, *Superconformal Symmetry and Superstring Compactification*, *Int.J.Mod.Phys.* **A4** (1989) 2653.
- [98] E. Witten, *On the Landau-Ginzburg description of $N=2$ minimal models*, *Int.J.Mod.Phys.* **A9** (1994) 4783–4800, [[hep-th/9304026](#)].
- [99] P. Di Francesco and S. Yankielowicz, *Ramond sector characters and $N=2$ Landau-Ginzburg models*, *Nucl.Phys.* **B409** (1993) 186–210, [[hep-th/9305037](#)].